Order Number 9405565

ON- and OFF-inputs to transient amacrine cells and the effects of light modulation depth: An experimental and theoretical study in catfish retina

Naylor, David Earl, Ph.D.

City University of New York, 1993

U·M·I
300 N. Zeeb Rd.
Ann Arbor, MI 48106

ON- AND OFF- INPUTS TO TRANSIENT AMACRINE CELLS AND THE EFFECTS OF LIGHT MODULATION DEPTH: AN EXPERIMENTAL AND THEORETICAL STUDY IN CATFISH RETINA

by

DAVID E. NAYLOR

A dissertation submitted to the Graduate Faculty in Biomedical Sciences in partial fulfillment of the requirements for the degree of Doctor of Philosophy, The City University of New York

1993

This manuscript has been read and accepted for the Graduate Faculty in Biomedical Sciences in satisfaction of the dissertation requirements for the degree of Doctor of Philosophy.

Aug 31, '93 — Craig J. Benham
Date — Signature — Craig Benham, PhD, Chair of Examining Committee

August 31, 1993 — Terry Krulwich, PhD, Executive Officer
Date — Signature

Daniel Tranchina, PhD

Michael Lacker, MD PhD

Scott Brodie, MD PhD

Supervisory Committee

THE CITY UNIVERSITY OF NEW YORK

PREFACE

I would like to express my deep gratitude to Daniel Tranchina whose keen analytic mind, judgement, and regard for students earned my utmost respect. Special thanks to Ken-Ichi Naka, one of my mentors, for taking me in and training me to be an experimentalist as well as a theorist. Finally, thanks to a fellow graduate student, Eric Reifsnider, for his time and assistance in helping me to prepare my figures - there are a lot of them.

The work involved with this thesis was compressed within a three year period and limited time was allowed for revisions prior to deposit, due to the sudden imposition of a deadline for deposit with sundry financial penalties attached. Consequently, some of the corrections were made in haste and the reader may encounter an occasional difficulty. My apologies.

TABLE OF CONTENTS

LISTS OF TABLES

LISTS OF FIGURES

I. SUMMARY

Signal processing measured in bipolar cells is highly linear and was modelled as a bandpass filter of the form: $B_1^{on}(\omega) = k_1(1+i\omega\tau_1)(1+i\omega\tau_2)^{-1}(1+i\omega\tau_3)^{-10}$, $k_1 > 0$. $B_1^{off}(\omega) = k_2(1+i\omega\tau_1')(1+i\omega\tau_2')^{-1}(1+i\omega\tau_3')^{-10}$, $k_2 < 0$ was of similar form but had different kinetics and opposite polarity. The complete transfer functions which represent processing by bipolars that is conveyed to transient C amacrines were $L_1^{on}(\omega) \equiv B_1^{on}(\omega)B_2(\omega)$ and $L_1^{off}(\omega) \equiv B_1^{off}(\omega)B_2(\omega)$. $B_2(\omega) = (1+i\omega\tau_1'')(1+i\omega\tau_2'')$ is designed to represent pre-synaptic filtering in bipolar terminals and is identical for ON- and OFF-bipolar pathways. Each of the parallel pathways then is assumed to have a static-nonlinearity, generally represented as a 4th order polynomial, which intervenes between the bipolar terminals and the post-synaptic ligand gated conductance in the C cell. Finally, linear filtering occurs post-synaptically in the amacrine membrane: $L_2(\omega) = k_3(1+i\omega\tau_1''')(1+i\omega\tau_2''')^{-1}(1+i\omega\tau_3''')^{-10}$, $k_3 > 0$.

This scheme enabled the prediction of analytic forms for the 1st and 2nd order Wiener kernels which incorporated the ON- and OFF-bipolar and amacrine filter parameters into a parallel form L_1-N-L_2 model. These parameters were adjusted successfully so as to fit simultaneously the actual 1st order kernel and diagonal of the 2nd order Wiener kernels obtained from 22 C amacrine cells. The same parameter values subsequently were able to reconstruct the entire 2nd order kernel as a further support for the model. Fits of the actual time series responses of transient amacrines to white noise and step inputs helped characterize the parameters of the static-nonlinearity and offered more definitive support for the model.

Several conclusions emerged from the results. First, a great deal of variation in the shape of the 1st order Wiener kernels was suggestive of cancellation between ON- and OFF-pathways and could be accounted for only by the parallel form of the model. As the linear and other odd order components tend to cancel between the pathways, while the even order components tend to summate, the highly nonlinear nature of the C amacrines and their strong 2nd order kernels are explained. Although $B_2(\omega)$ and $L_2(\omega)$ could not be measured directly, they were justified indirectly by inspection of the 1st order and diagonal of 2nd order kernel waveforms. Model results suggest kinetic differences between the ON- and OFF-bipolars with the inverse transform of L_1^{on} showing a slower peak response time (PRT) and a more biphasic waveform than the inverse transform of L_1^{off}. In addition, the static-nonlinearity along the ON-pathway was generally not as monotonic as the OFF-pathway, suggesting further differences between ON- and OFF-pathways at the amacrine synapse, possibly related to a difference of receptor subtypes or of input range to a receptor.

The responses of the C cells to decreasing modulation depths of light were recorded and the Wiener kernels showed changes in shape as well as an increase in scale, or sensitivity, that was inversely related to the decrease in modulation level. Relative to the 1st order kernel, the 2nd order kernel showed much greater scaling, suggesting that bipolar inputs (which precede the nonlinearity) are a primary focus of adjustment to changes in modulation level. The shape changes were consistent with an increased dominance of the OFF-pathway at lower modulation levels and were most apparent in the 1st order kernels. In addition new features, such as

oscillations, emerged at lower modulation levels and occurred later along the time axis of kernels. Their time course and behavior were inconsistent with an origin from centripetal bipolar inputs, but, instead, were compatible with a proposed circuitry that involves feedbacks from ON- and OFF- ganglion cells. The feedback inputs are postulated to be more linear than the bipolar inputs and, consequently, were expected to become more prominent at lower modulation levels. The parallel L_1-N-L_2 model, which does not account for feedback, performed less well at the lower modulations due to the appearance of these late features. However, three select cells, which did not demonstrate strong late features, were analysed with the present model and showed a slowing in ON- and OFF-pathways by a few msec. No significant change in the shape of the static-nonlinearities was observed in these few cells with decreasing modulation levels. A scaling increase of bipolar inputs to transient amacrines at the presynapse, probably via feedback from the inner retina, is consistent with the results and can explain the increased sensitivity of C cells at low modulation levels.

II. INTRODUCTION

This thesis embodies an attempt to clarify how visual stimuli are encoded and processed by the retina. The task involved the collection of experimental data with subsequent theoretical analysis (via mathematical models and computer simulations). Mathematics is an essential component of this project. The retina is a highly complex neural network whose cell interactions consist of extensive syncytial and chemical contacts (Sakai & Naka, 1988c). The sophisticated spatial and dynamic processing of this network cannot be understood without rigorous analytic methods. Thus, mathematics provides insights into retinal function not available from other methods.

The general approach to modelling is to choose a circumscribed subsystem of the retina for study that has well defined anatomy and physiology and make a prudent guess at a circuit architecture. Mathematics then allows the fusion of observations and hypotheses into a single, compact and testable model whose responses can be simulated on the computer. The aim of a rigorous model is to reproduce the full range of behavior of the original subsystem. The logical progression is then to expand the smaller successful model into a larger or more versatile model that includes additional features of the original system.

The retina is quite suitable for this sort of piecemeal modelling. While there is a fair amount of feedback and lateral processing, the pervasive amount of processing in the retina is in the forward direction; lateral interactions are even less of a consideration for models involving spatially uniform light inputs. This provides

an axis of orientation for signal propagation that can be used to simplify the design and expansion of models by removing the need to consider signal flows from all directions. For instance, the successfully modelled output of one subsystem now becomes the input to a model of a more centrally located subsystem - in this case, starting with the outer retina and gradually working towards the inner layers. In addition, the lack of essential centrifugal input from higher centers of the brain makes the retina a nice, isolated and tractable system for study. Furthermore, the ability to control precisely the temporal and spatial quality of the light input makes the retinal eye-cup preparation suitable for the type of circuit analysis used in electrical engineering, whereby an input/output couple is used to define the "black box" in between. All these features aid the goal of constructing a successful model for retinal function.

The particular emphasis of this study was to define, via a mathematical model, the functional properties of amacrine cells in the inner retina. This also involves some collateral study of other cells with respect to their interactions with amacrine cells. This project focused on experiments involving light inputs that were spatially uniform in order to simplify the modelling efforts. Nonetheless, amacrine cells can exhibit quite complex responses with such spatially bare stimuli or even without light stimulation at all. For example, while cells proximal to the inner retina behave quite linearly, nonlinear behaviors emerge in the amacrines. These include a frequency doubling property of transient amacrine cells and the occurrence of spontaneous oscillations in sustained amacrines. As a great deal of information on the physiology and anatomy of the inner retina of the catfish has been accumulated, reasonable

models are constructed that begin to explain the complex nonlinear behaviors in these amacrine cells.

Modelling of the amacrine cells of the inner retina promises to provide insights into visual processing for several reasons. First, these cells demonstrate very complex processing. For example, some amacrine cells are observed to respond to stimuli of preferred orientation in catfish (Naka, 1980), and preferred direction in the salamander (Werblin, 1970; Werblin & Copenhagen, 1974). In addition, amacrines have strong nonlinear components to their behavior; yet inputs from more distal cells are highly linear. This offers a unique opportunity to study the origination of important nonlinearities. Such nonlinear systems are interesting because they tend to involve sophisticated processing that does not merely mimic the stimulus in some fashion. And, although nonlinear systems are more difficult to study than linear ones, traits such as a lack of complex color interactions in catfish makes the modelling task more manageable.

One prominent nonlinearity, the frequency doubling property of the transient cells, is believed to arise from inputs by both ON- and OFF-bipolars (Kujiraoka *et al.*, 1988). Thus, transient cells provide a striking example of the convergence of ON- and OFF-pathways. Modelling of the simultaneous effects of each pathway on the transient cells reveals important dynamic relations between ON- and OFF-channels and provides some new insights into a basis for segregation of visual input into ON- and OFF-pathways.

Another nonlinear behavior of interest is the oscillations of sustained amacrines (Sakai & Naka, 1990b). Oscillations are also characteristic of many other

cells in the central nervous system. Oscillations have been observed in areas such as the cortex (Llinas, 1988) and hippocamus (Traub *et al.*, 1989). In general, oscillations can be generated by intracellular mechanisms due to changes in membrane conductance or, alternatively, they can result through network interactions of cells. It is proposed in this project that they arise from network connections involving a fast positive feedback followed by a delayed polysynaptic negative feedback.

The purpose of oscillations in the nervous system is a mystery. Oscillations may function to synchronize or coordinate network behavior (Cohen, 1987), provide for network resonance tuning and sensory gating (Wiener, 1961), or serve as a means of setting global states or linking global features (Crick, 1984). Alternatively, their occurrence simply may be a network epiphenomenon stemming from the existence of both positive and negative feedbacks between cells. The present project suggests their origin in the catfish retina and offers some clues as to their function. Future modelling of these oscillations may have broad implications for oscillations elsewhere in the nervous system.

The results from this project supplement the modelling efforts in the cat that have described a mechanism of 'contrast gain control' (Victor & Shapley, 1979a). This phenomenon was characterized and modelled at the level of the ganglion cells but is believed to involve amacrine cells (Victor, 1988). Recording from other retinal cells is extremely difficult in the cat which makes further experiments aimed at studying the cells involved with contrast gain control quite difficult. Unlike the retina of higher vertebrates, obtaining recordings from all of the cell types in the catfish

retina is relatively easy. Thus, studies in the catfish have provided the unique opportunity to add to the cat findings and investigate cell interactions that contribute to the contrast gain phenomenon. The present work aimed study of the contrast gain effect at transient amacrine cells and provides valuable insight into the underlying mechanisms of contrast gain control.

The retina is a very good system for studying the properties of sensory processing in general. Light stimuli can be controlled much more precisely than inputs to other sensory modalities. In addition, visual processing can be studied by treating the retina as an isolated preparation. This is not the case for other modes of sensory processing. Furthermore, mechanisms have been observed in the retina that may apply to other sensory systems. For example, the response sensitivity of the retina is adjusted to the mean level of light input and to the modulation depth (contrast) around that mean (Shapley & Enroth-Cugell, 1984). It makes sense that other sensory systems should behave similarly. Indeed, amacrine cells in the olfactory bulb have notable similarities with those in the retina, including reciprocal synapses, oscillatory behavior and intimate interactions with the spiking output cells of the bulb, the mitral cells (Freeman, 1972, 1974a, 1974b; Getchell & Shepherd, 1975; Shepherd, 1972).

III. BACKGROUND

A. Structure, Circuitry, and Pharmacology

The retina is a complex network of neurons consisting of five principal cell types organized into layers (fig. 1; Kandel & Schwartz, 1985). These cells communicate primarily via slow, graded potentials. Although single refractory spikes are observed in amacrine cells (Eliasof *et al.*, 1987; Barnes & Werblin, 1986), frequency coding of signals as action potentials does not occur in the retina except in the ganglion cells of the inner retina. These ganglion cells contain the axons which leave the retina and communicate to higher centers in the brain.

In the outermost layer are the photoreceptors, the rods and cones, which detect photons. In the catfish, there are only red cones, eliminating the need for consideration of the color attributes of cells. The photoreceptors release transmitter tonically in the dark. Hyperpolarization by light diminishes transmitter release. The process underlying this behavior can be explained in biochemical terms. First, light activates rhodopsin, a photosensitive pigment. The excited form of rhodopsin then interacts with transducin, a G-protein like complex. Subsequently, an activated subunit of this complex, T_{α}, excites a phosophodiesterase (PDE) enzyme which in turn cleaves cGMP to form GMP. cGMP, produced by guanylate cyclase, opens a Na^{+}/Ca^{++} channel that results in depolarization of the photoreceptor cell. Thus, the cleavage of cGMP due to the excitation of rhodopsin by light results in cell hyperpolarization (Kandel & Schwartz, 1985).

The voltage response to a very short light pulse is generally monophasic in the receptor cells under dark adapted conditions. For linear regime stimuli superimposed on a spatially uniform background, the receptive field of these cells is also monophasic and has a radius of .1 mm (fig. 3a; Sakai & Naka, 1988c). The photoreceptors provide inputs to the bipolar and the horizontal cells.

There are two classes of bipolar cells, the ON- and the OFF-bipolar cells. They are so categorized according to whether they depolarize to a step from background illumination of light increment or decrement, respectively. This segregation into two pathways persists throughout the retina as information is relayed to more central cells such as the amacrine and ganglion cells. The ON-bipolar cells have a sign-inverting, "invaginated" synapse with the receptors (i.e. a hyperpolarization in the receptors, as with light input, leads to a depolarization in the ON-bipolar cell). The OFF-bipolar and the horizontal cells receive sign-preserving, "flat" synapses from the photoreceptors. The horizontal cells are monophasic (integrative) like the receptors and also have a monophasic receptive field that spans .5mm for the horizontal somas (fig. 3a). This large receptive field results from numerous syncitial contacts between horizontal cells that essentially allow them to function as a broad conducting sheet or S-space (Krausz & Naka, 1980).

At all stages of light adaptation, the bipolar cells have much more biphasic (differentiating) 1st order kernels[1] than receptor or horizontal cells (fig. 2). These biphasic kernels have much greater variablilty in response dynamics than the

---

[1]For linear behaving cells such as bipolar cells, the 1st order kernel can be interpreted as a "brief-flash" response.

monophasic horizontal or receptor kernels (Sakuranaga & Naka, 1985a). The bipolar cells also have biphasic receptive fields. Contributions from horizontal cells are most likely responsible for the biphasic kernels and receptive fields.

This contention is supported by the observation that current injection into horizontal cells produces monophasic responses in bipolars (fig. 2; Sakuranaga & Naka, 1985a). This contrasts sharply with the biphasic responses of bipolars observed to light inputs and is most likely attributed to a lack of direct receptor input. The responses to current injection were sign-preserving in ON-bipolars and sign-inverting in OFF-bipolars (fig. 2). Thus, the inputs from horizontal cells to bipolars oppose those from the receptors (fig. 5a). Consequently, in response to light inputs, the slower kinetics of the horizontal cells and the faster kinetics of the receptors appear to superpose in an antagonistic manner at the bipolar cell to contribute to the biphasic nature of the bipolar impulse response.[2] Similarly, the broad receptive field of the horizontal cell opposes the much narrower field of the receptors to help create a center (excitatory) - surround (inhibitory) biphasic field in bipolar cells (fig. 3b). The schematic of fig. 5a can account for the horizontal cell interactions and is consistent with the view that in the catfish, as with the turtle (Tranchina *et al.*, 1983), horizontal cell feedback to receptors does not appear to be as significant as forward processing to bipolars (Sakai & Naka, 1987b).

Unlike the bipolar and horizontal cells, amacrine cells are axonless. They receive inputs from bipolar cells. There is also morphological and physiological

---

[2]equivalent to a 1st order kernel for linear cells

evidence that horizontal cell axons may provide inputs to amacrines, but their significance is unclear and will not be considered further (Sakai & Naka, 1985). At the level of amacrine cells in the inner plexiform layer, a new division of cells appears. Cells can now be categorized as sustained or transient based on their responses to a step of light from darkness. In catfish, there are three general classifications of amacrine cells; the 'sustained' N cells which can be ON (NA) or OFF (NB) and the 'transient' C cells (fig. 4).

The NA, NB, and C cells have an organized location in the inner plexiform layer. Sublamina a in the outermost portion of this layer is where the OFF-cells - the OFF-bipolar (BB), NB, and GB - make contacts. More proximally, the ON-bipolar, NA and GA cells make their contacts in sublamina b. The C cells lie inbetween and send processes to both sublamina a and sublamina b. (Sakai & Naka, 1988c) The N cells are believed to receive excitatory input from their corresponding ON- or OFF-bipolar type. These N cells often have elliptical receptive fields of .5 mm oriented along the horizontal axis and have been observed to exhibit orientation specific responses with preference for vertically moving stimuli (Naka, 1980).

While the N cells primarily receive bipolar input from only the matching ON- or OFF-type, the C cells are thought to receive inputs from both ON- and OFF-bipolar types (Kujiraoka *et al.*, 1988). For example, whereas a step of light resulted in depolarization transients at both the increment and decrement in luminance (fig. 4c), a current step into an ON-bipolar produced a transient response only at the increment (Sakai, personal communication). This result implies that the OFF-bipolar is responsible for the transient at step decrement.

Similar to the horizontal cells, the C cells are characterized by numerous syncitial contacts. These gap junctions are a distinguishing feature of transient amacrine cells. For example, in carp, transient ON/OFF cells have dendritic tip to tip appositions that allow for substantial dye coupling between homologous cells. In sustained amacrines the coupling is not as strong (Teranishi *et al.*, 1984, Negishi *et al.*, 1991, Negishi & Teranishi, 1990, Yazulla & Zucker, 1988). In goldfish, transient cells are also conspicuous for the extensive gap junctions they possess (Marc *et al.*, 1988). The electrical coupling of transient cells can allow them to function as spatial integrators and explains their very broad receptive field, on the order of 1 mm (Sakai & Naka, 1988c).

The syncitial space of C cells is characterized as having a high membrane resistance, but low internal resistance, which allows for significant spatial spread and preservation of step signals (Naka & Christensen, 1981). Therefore, it is unlikely that the transient responses observed in the C cells are due to an inherent quality of the C cell itself to remove DC. In addition, after blocking synaptic transmission, transretinal current pulses can elicit a sustained response in transient amacrine cells of the carp retina (Kujiraoka *et al.*, 1988). This provides further evidence that transient cells do not behave in a highly differential manner towards membrane polarizations. Since bipolar cells very often have a sustained component to their voltage response to light steps while C cells do not, some form of a high-pass filter must intervene to remove the DC of bipolars before it is delivered to the transient C cells.

A mechanism has been proposed for the tiger salamander that can account for the transient responses of amacrine cells. Subpopulations of bipolars are described that have pre-synaptic $GABA_B$ receptors at bipolar-amacrine synapses. In the tiger salamander, the sustained amacrine cells are chiefly GABAergic whereas the transient amacrines are often glycinergic. GABA from sustained cells is postulated to act at the presynaptic $GABA_B$ receptor of some bipolars, subsequently modulating an L-type calcium channel (Maguire *et al.*, 1989b). Consequently, while the bipolar cell voltage may remain depolarized, Ca^{++} influx and hence transmitter release is curtailed, yielding a transient post-synaptic response. AVA, a $GABA_B$ antagonist, can block the GABA effects of sustained amacrines on these bipolar cells, thereby transforming the post-synaptic response of the transient cells into a more sustained depolarization (Werblin *et al.*, 1988). A network scheme consistent with these observations is shown in fig. 5b.

The effects of inhibitory neurotransmitters on bipolars are established in many other species. In patch clamp recordings from solitary bipolar cells of goldfish, for example, GABA sensitivity is observed primarily at the axon terminals. GABA sensitivity is observed in 98% of rod dominant ON-bipolar terminals, but in only 52% of other types of bipolar terminals. Thus, the existence of subpopulations, similar to the salamander, is suggested. However, unlike the tiger salamander, the inhibition is mediated by $GABA_A$ receptors which interact with chloride channels (Tachibana & Kaneko, 1988; Kaneko & Tachibana, 1987). In addition, a third type of GABA receptor modulates Ca^{++} currents in a GTP-dependent manner, similar to the $GABA_B$ receptor but not sensitive to baclofen (Heidelberger & Matthews, 1991).

GABA is not the only inhibitory transmitter that mediates pre-synaptic inhibition in bipolars. In the mudpuppy, the light responses of OFF-bipolar cells are more glycine than GABA sensitive whereas the responses of ON-bipolar cells are more GABA than glycine sensitive (Miller *et al.*, 1981a). GABA reduced and bicuculline (a $GABA_A$ antagonist) enhanced the light evoked response of ON-bipolars in a preferential manner, whereas glycine reduced and strychnine (a glycine antagonist) enhanced the light evoked response of OFF-bipolars in a preferential manner. These results suggest pharmacological distinctions between the ON- and the OFF-pathways of the mudpuppy.

In the ON/OFF transient amacrine cells of mudpuppy, GABA caused a greater inhibition of the ON- as compared to OFF-response to light steps whereas glycine inhibited the OFF-response more (Miller *et al.*, 1981b). Thus, the population of bipolars that are susceptible to presynaptic inhibition provides inputs to transient cells. Furthermore, the step response shows a DC elevation when bicuculline was added to the preparation and a DC depression when strychnine was added. The result can be attributed to a sustaining and enhancing effect of bicuculline on the ON-bipolar cells with a similar effect by strychnine on the OFF-bipolar cells. This offers additional evidence, along with the AVA effects observed for salamander, that the effects of inhibitory neurotransmitters at the presynaptic terminals of bipolars are responsible for the filtering that leads to transient responses in the ON/OFF amacrines.

Sustained amacrines in the inner retina are presumed to be the source of both types of inhibitory neurotransmitters. The findings in goldfish that GABA is

accumulated by amacrines in sublamina b of the inner plexiform layer whereas glycine is accumulated in sublamina a supports the existence of two separate pharmacological classes of amacrines for ON- and OFF-pathways (Marc & Lam, 1981), although in goldfish, the glycinergic amacrines rarely make contacts with bipolars (Muller & Marc, 1990). In turtle also, glycinergic amacrines, which constitue 50% of amacrine cells, are found mostly in sublamina a (Eldred & Cheung, 1989).

A great deal of variation exists between species with respect to the pharmacology of the amacrine/bipolar interactions. In goldfish, for example, solitary bipolars do not show glycine sensitivity at the axon terminals (Tachibana & Kaneko, 1988). In fact, extensive inputs to bipolars in sublamina a are shown to be GABAergic, indicating that feedback from amacrines to both ON- and OFF-bipolars is predominantly GABAergic in goldfish (Muller & Marc, 1990). Likewise, glycine has no effect on either type of bipolar, and glycinergic amacrines are not observed to contact bipolar cells in carp (Kondo & Toyoda, 1983). Unlike the goldfish, though, GABA appears to effect the ON- but not OFF-bipolars in carp. Interestingly, isolated bipolars from mice demonstrated sensitivity to both GABA and glycine at the axon terminals. The GABA effects were antagonized by bicuculline, but not baclofen, and the glycine effects were antagonized by strychnine (Suzuki *et al.*, 1990). Thus, while the ON-bipolar terminals generally are perceived to have GABA sensitivity, the OFF-bipolar terminals are observed to show sensitivity to glycine (mudpuppy), to GABA (goldfish), to both glycine and GABA (mouse), and to neither glycine nor GABA (carp).

A morphological basis for the interaction between amacrines and bipolars has been observed by EM. In the rabbit retina, for example, a dyad synapse between amacrine and rod bipolars has been characterized. Bipolar cells can be presynaptic to two types of amacrine cells, but only the more sustained amacrine has reciprocal synapses onto the bipolar terminals. Presumably these types of bipolars belong to the B^t population (fig. 5b), with the more sustained amacrines receiving inputs from B^s bipolars as well. The lack of particle aggregates typically associated with the excitatory synapses suggests that the amacrine cell is inhibitory to the bipolar cell at the dyad synapse (Raviola & Dacheux, 1987). Sustained amacrines can make reciprocal synapses with bipolars in many other vertebrates, including catfish (Sakai, personal communication; Tachibana & Kaneko, 1988; Yazulla *et al.*, 1987).

The amacrine and the bipolar cells provide inputs to the ganglion cells, whose myelinated axons exit the retina. These are the first cells capable of repetitive spiking, although amacrine cells in the salamander can generate a single spike but become refractory thereafter due to an inability to remove Na^+ channel inactivation (Barnes & Werblin, 1986; Eliasof *et al.*, 1987). In the catfish, spiking is not observed in type N neurons (Naka, 1977). As was the case with the amacrine cells, there are three general categories of ganglion cells - GA,GB,GC. The GA cells show ON-type behavior, the GB cells OFF-, and the GC cells show transient behavior to ON- or OFF-type inputs (Sakai & Naka, 1987a). The ganglion cells should not be perceived solely as post-synaptic output neurons as there are numerous interconnections between bipolar, amacrine and ganglion cells. Sakai and Naka have attempted to probe this complex network of the inner retina with light stimuli such as steps and

white noise, as well as through current injection/recording couples of various cell pairings. They compiled a vast amount of data from such recordings. The bulk of the rest of this section is devoted towards organizing the discrete results that they obtained into a consistent scheme that can be represented as a functional circuit architecture. The fairly comprehensive circuit schematic derived in this thesis (fig. 5d and 5e) then will be used to motivate modelling efforts and provide possible explanations for many of the present results from experiments studying contrast effects.

A basic framework for the connections between the different types of amacrine and ganglion cells can be constructed based on these cells' responses to light inputs. First, comparison of the Wiener kernels from the different types of retinal cells can provide some insight into the circuitry. Wiener analysis is an effective technique for studying nonlinear systems. Comparable to the expansion of a function into a power series, Wiener analysis expands a functional (an operator on a function, e.g. an integral) into a series sum of functionals (see appendix C-i). The Wiener kernels, h_n, are the analogues of the power series coefficients.[3] The 1st order kernel, h_1, is familiar as the impulse response of linear signal analysis so that the functional, G_1, is a convolution. The theoretical methods section provides more thorough discussion of Wiener analysis.

The receptors, horizontal cells, and bipolar cells can be adequately characterized as linear. For example, the linear approximation usually gives a MSE

---

[3]Actually, a more accurate comparsion is between the orthogonal Hermite terms and Wiener functionals. The Taylor coefficients are more complementary to Volterra kernels, in fact.

of <10% for horizontal cells and <20% for bipolar cells (Sakai & Naka, 1987b). The amacrine cells, however, have a significant non-linear component to their responses. In the NA and NB cells, the linear 1st order kernel accounts for 40-60% of the response while the 2nd order kernel can account for 20-30% of the response (Sakuranaga & Naka, 1985b). With the C cells, the 1st order kernel accounts for approximately 10% of the response to light whereas the 2nd order kernel represents 40-60% (Sakuranaga & Naka, 1985c). Since a strongly odd-ordered or monotonic nonlinearity at a synapse is more realistic physiologically than a synaptic nonlinearity that contains dominant even-order powers, a model of the C cell should be able to account for this cells strong 2nd order component using synaptic inputs that behave primarily in a odd-ordered manner. The model of fig. 21b presents the C cell as receiving parallel inputs from ON- and OFF-bipolar cells. The convergence of the two opposing pathways allows for rectification or cancellation which can generate strong even-ordered nonlinearities. As the N cells are not believed to receive significant parallel inputs from ON- and OFF-bipolars, the most reasonable explanation for their strong 2nd order components is that they receive input either directly or indirectly from C cells. The recent observation that the N cells only show strong nonlinear responses if a large area of retinal surface is stimulated further supports the premise that the 1st and 2nd order kernels of N cells arise from different inputs. Presumably, the 1st order kernel originates from bipolar inputs, the 2nd order from the spatially broad C cell inputs (Sakai & Naka, 1992).

The resemblance of the N cell 2nd order kernel shape to that of the C cell tends to substantiate this assumption as well (fig. 4). In particular, the 2nd order

kernel of a N cell can be obtained by application of a band-pass filter to the C cell responses (Sakai & Naka, 1987b). By comparing the polarity of the NA and the NB 2nd order kernels with the "four-eyed" C cell kernel, C cells are postulated to communicate to NA cells in a sign-inverting manner, whereas C to NB communication is sign-preserving. However, the NA 2nd order kernel tends to be much more variable than that of the NB. This may relate to the inhibitory nature of the C to NA input, since inhibitory inputs often decrease the resistance of the resting membrane without any change in the membrane potential. In fact, Toyoda *et al.* (1987) suggested that the chloride equilibrium of amacrines was close to the resting potential, allowing application of the inhibitory transmitters GABA or glycine to even cause slight depolarizations of the amacrine cell membrane at times. Alternatively, other unique features of the C to NA path (perhaps less direct than C to NB) may contribute to the 2nd order kernel variablity. In addition, Sakai has observed a sign preservation in the three C to NA pairs stable enough to record from, but notes that the responses where much more biphasic (differentiating) than is observed with the C to NB responses (personal communication). Nonetheless, much more of a sign-inverting quality characterizes the C to NA than C to NB interactions. Current kernels for C to GA and C to GB pairs show a similar result (fig. 10).

In most cases, the 1st and 2nd order kernels of the GA and GB cells (as well as the responses to light steps) bear an extremely close resemblance to the response properties of the NA and NB cells, respectively (fig. 6). This was true for 22 of 26 GA cells and 92 of 97 GB cells (catfish retina is OFF-cell dominated) (Sakai &

Naka, 1987a). Thus, apart from some direct contributions from bipolar cells, the GA and GB cells maintain a close adherence to N cell behavior. The results for light input experiments have been summarized in fig. 5c.

The results from current injection experiments can add new details to this basic scheme. In a set of experiments involving current injections into amacrine cells and recordings in ganglion cells, two distinct conduction speeds were observed. The fast 1st order kernel for current inputs is mono- or biphasic and has a peak response time (PRT) of approximately 6 msec (fig. 7). The slower kernel is triphasic and has a PRT of approximately 21 msec (fig. 8). Interestingly, both of these types of kernels are observed in injection couples involving the same cell type pairings. For example, NA to GA transmission can be either fast or slow for any given couple. Sakai and Naka (1988a) concluded that the fast responses are monosynaptic and the slower ones are polysynaptic (probably at least trisynaptic).

Certain patterns are observed for the cell interactions. The fast responses from amacrines to ganglion cells are always sign-preserving. The slow responses recorded in GA cells are sign-inverting regardless of injection cell type. Conversely, the slow responses of GB cells are sign-preserving. In addition, any couple that involves cells of opposite polarity (e.g. NB to GA) always yields a slow response (Sakai & Naka, 1988a).

If the slow response kernels in GA cells are generated by signals that eventually travel via the C to NA to GA path (postulated for the light inputs), then the sign-inverting characteristic of the slow GA kernels is consistent with the C to NA sign-inversion. Similarly, the sign-preserving nature of the GB slow kernels is

consistent with conduction via the C to NB to GB path. This scheme portrays the C cell as a central hub and assumes that the signal from the injected cell is sign-preserved prior to reaching the C cell (nearly all fast responses couples recorded in the inner retina have been sign-preserving). The apparent absence of disynaptic inputs for N to G couples as evidenced by the clear demarcation of kernels as either fast (PRT=4-8 msec) or slow (PRT=19-22 msec) (fig. 11; table 4) fits with a scheme of signal conduction that involves passage through a central relay such as a C cell. In addition, the broad syncitial spread of the C cell, as well as its central location between sublamina a and sublamina b, makes it ideal as a center for convergence of signals.

The 1st order kernels for interactions between ganglion cells also are classified as fast or slow (Sakai & Naka, 1988b). GA to GA couples are fast and sign-preserving in 75% of the cases, and slow and sign-inverting in the remaining 25%. GB to GA couples are always slow and sign-inverting. GB to GB pairs are, like the GA cells, fast and sign-preserving in 75% of recordings, but are also sign-preserving for the slow responses. Signals are sign-preserving for the slow GA to GB pairs also. The polarities of the fast and slow kernels of G to G couples are very similar to those observed with the N to G couples (fig. 9). However, the occurrence of slow responses is more common than fast for injection into N cells.

These observations for G to G interactions are compatible with the scheme of fig. 5c if GA to C and GB to C interactions are permitted and considered to be sign-preserving. In fact, distal dendrites greater than 100 μm from the soma of ganglion cells often make presynaptic connections with amacrine cells in the catfish

(Sakai *et al.*, 1986a). Furthermore, Matsumota reported that optic nerve stimuli can depolarize the transient amacrine cells of the frog retina. Based on careful analysis of the latency of amacrine responses to repetitive ganglion spikes, he concluded that ganglion cell dendrites, not direct efferent spike innervation, provide the route of innervation (Matsumoto, 1975). However, myelinated fibers are observed to coarse near amacrine cell somas in the catfish on occasion (Sakai & Naka, 1986b).

The sustained amacrine cells also are depolarized by ganglion cells. Fast responses from GA to NA and from GB to NB are easily elicited and sign-preserving (Sakai & Naka, 1990a). Slow responses from GA to NA or from GB to NB are much less frequently observed than fast (9% of the couples) and are sign-inverting for the NA responses and sign-preserving for the NB responses. In addition, GB to NA responses (always slow) are sign-inverting, while GA to NB responses are sign-preserving (Sakai, personal communication). The predicted paths for these responses are GA (or GB) to C to NA or, alternatively, GB (or GA) to C to NB. The above results are consistent with the circuit schematic shown in fig. 5d.

The inclusion of G to C feedback of ganglion cells can provide a more complete path for the NA to GA, NA to GB, NB to GB, and NB to GA slow responses. For example, the NA to GB path could be NA to GA to C to NB to GB. A more straightforward path might seem to be NA to C to NB to GB. However, Sakai has indicated that, while recording from the C cell is delicate in general, detection of fast responses in C cells by injection into N cells is especially difficult. Hence, a direct N to C synapse is not included in this circuit model at present.

The circuit diagram is also compatible with responses for GA to NA and GB to NB pairings involving injections of 10 msec current pulses (fig. 12, fig. 13; Sakai & Naka, 1990a). Both the responses had a very short latency. A particularly salient feature is the occurrence of a much more robust oscillation in the GA to NA pair than in the GB to NB pair. Based on the schematic of fig. 5d, a possible explanation is that positive feedback between GA and NA cells leads to a strong and fast depolarization in the NA cell from injection into the GA cell. Concomitantly, the injected GA cell depolarizes C cells which then provide either direct or indirect inhibitory feedback to the NA cell via the C to NA sign-inversion. The damped oscillation, then, results from initial positive feedback followed by delayed polysynaptic negative feedback. The initial peak of the damped oscillation at approximately 8-10 msec and a second peak at approximately 20-30 msec matches well with the PRTs for fast and slow responses, respectively. For the GB to NB couples, the sign-preserving quality of the C to NB synapse in the circuit scheme precludes the possibility of negative feedback.

An interesting observation is that the NA to GA pulse injection does not produce as robust of a damped oscillation in the GA cell as the GA to NA injection produces in the NA cell. Perhaps this stems from the fact that the negative feedback is more direct for the GA to NA couple, involving an initial GA to NA positive interaction that is quickly opposed by a GA to C to NA contribution. On the contrary, for the NA to GA couple, the initial excitement from the direct NA to GA interaction is opposed by negative feedback that has to course the longer NA to GA to C to NA to GA pathway.

A rather intriguing phenomenon in the inner retina is the occurrence of oscillations in both NA and NB cells. A current pulse of 10 msec duration injected into an NA cell can induce several cycles of oscillation lasting up to 200 msec in an NB cell (fig. 15; Sakai & Naka, 1990b). There is a latency of nearly 20 msec in the NB response, which has an initial depolarization. The 1st order kernel of the NA to NB pair is highly oscillatory as would be expected, with a peak frequency at 30 Hz (fig. 16; Sakai & Naka, 1990b). It accounts for 75% of the NB response. By contrast, the 1st order kernel for NB to NA pairs has one twentieth of the amplitude of the NA to NB kernel and is quite short-lived. It has an initial hyperpolarization. Hence, the NA cell is able to drive the NB cell, but not the reverse. This phenomenon is supported by the schematic in fig. 5d. The NA cell excites the GA cell which in turn excites the C cell. The C cell then excites the NB cell (initial positivity), but also inhibits the NA cell. This inhibition is then spread via the same NA to GA to C to NB path, but now the C cell disinhibits the NA cell. This initiates, yet again, another round of the cycle. The 30 Hz frequency of oscillation (period of 33 msec) correlates well with the slow GA to GA kernel which has a PRT of 18 msec (a half period in this model).

Sinusoidal current has also been used to probe NA to NB interactions (fig. 17; Sakai & Naka, 1990b). Quite expected is the observation of a very strong NB response for 35 Hz injections as this is near the resonance frequency of the neural circuitry of fig. 5d. Current injections of 20 Hz resulted in a frequency doubling of the input in the NB response, with every other oscillatory peak slightly diminished in peak amplitude. If the input is considered to drive the natural frequency of the

circuitry at every other peak, but to antagonize the natural response between peaks (being approximately half the resonant frequency), the observed response is predictable from the model of fig 5d.

The 30 Hz oscillations of the sustained amacrine cells are so robust that they are very often observed in the dark. The NA and NB cells oscillate at the same frequency, but are nearly 180 degrees out of phase (fig. 18, fig. 19; Sakai & Naka, 1990b). Although light input may change the response amplitude, the frequency remains very constant. Since the rate of propagation of signals through a hard-wired cell network would be expected to remain fairly constant regardless of stimulus amplitude, a fixed frequency is consistent with the network model. This would be especially true for a network whose individual components behave quite linearly, as has been observed for the current injection couples of the catfish inner retina. On the contrary, polarization of the membrane by light input might be expected to change the frequency of oscillations that were generated through intracellular mechanisms by affecting the voltage gated properties of the channels involved. Indeed, studies of neuroblastoma cells indicate that the frequency properties of the cells are dependent on their membrane voltage levels (Moore *et al.*, 1988; Yoshii *et al.*, 1988).

The cell interactions of the inner retina have been described as very linear, and linear circuits tend to be very stable. Spontaneous oscillations in the dark such as those seen in the NA and NB cells are very unusual for such linear systems. However, linear systems can be made to oscillate with an external driving force. The source of such an external force may be related to spiking from ganglion cells. The

GA cells (which fire spontaneously in the dark) may be able to drive the oscillations through spread of waves to their distal dendrites. The tonic release of transmitter in the dark may contribute to the spontaneous spiking of the GA cells. The GB cells do not demonstrate the robust spontaneous firing seen in GA cells.

A distinguishing feature of the circuitry proposed in fig. 5d,e is that transient C cells are proposed to make inhibitory inputs to NA cells but excitatory inputs to NB cells. Such mutually excitatory and inhibitory cells have been reported elsewhere. Starburst amacrine cells in the rabbit retina, for example, are found to uptake and co-release acetylcholine and GABA (Massey *et al.*, 1991). K^+ induced depolarizations cause the release of both transmitters, but only acetylcholine showed noticeable release to light inputs. The acetylcholine release involves Ca^{++} dependent exocytosis, but GABA release involves a Ca^{++} independent cotransport mechanism (O'Malley *et al.*, 1992; Miller, 1989).

These cholinergic amacrines, in fact, are transient cells. While a resting release of acetylcholine does occur in dark, it is very small compared to the release triggered by light stimuli (Masland & Cassidy, 1987). A flashing light caused a continual high rate of acetylcholine release into the superfusate that returned to baseline with cessation of the stimulus, whereas a steady light step resulted in a burst of acetylcholine release at increment or decrement. Uptake of the tritiated acetylcholine occurred in two bands in the inner plexiform layer. Both bands became progressively more faint as the acetylcholine was released, but administration of APB prevented depletion of acetylcholine from the proximal band (sublamina b) (Masland *et al.*, 1984). The segregation of the starburst amacrines into the two bands is

consistent with the finding by Famiglietti (Famiglietti, 1983) of a mirror-symmetric organization of the cholinergic amacrines in sublamina a and sublamina b. The starburst morphology of the cholinergic amacrines is very similar to the morphology of transient amacrine cells in lower vertebrates. However, unlike the transient cells of the catfish - which have processes extending to both sublamina b and sublamina a that receive inputs from both ON- and OFF-bipolars, respectively (Sakai & Naka, 1988c) - the transient amacrine cells of the rabbit are divided into the two symmetric groups. These are the type b (displaced) and type a starburst amacrines which respond to ON- and OFF-inputs, respectively.

Despite the difference in anatomical arrangement, the morphological and physiological similarities of the cholinergic amacrines of the rabbit with the transient amacrines of lower vertebrates suggest a strong functional identity between the two. In fact, pharmacological correlates have been observed in lower vertebrates. For example, cholinergic amacrines that mediate interactions between ON- and OFF-channels have been reported in the frog (Jardon *et al.*, 1992), and excitatory responses to acetylcholine have been observed in amacrines of the carp (Toyoda *et al.*, 1987). Also, a bistratified transient amacrine cell in goldfish that has dendritic projections to sublamina a and sublamina b, and contains gap junctions, has been established as GABAergic (Muller & Marc, 1990).

In addition, glycinergic transient amacrine cells have been described in the mudpuppy (Frumkes *et al.*, 1981) and Tiger salamander (Belgum *et al.*, 1984). More than one type of transient ON/OFF amacrine may function in the retina, though. For instance, two types of transient ON/OFF amacrines are described in the

mudpuppy. One type exhibits a large spatial summation and no surround inhibition. A second type has a suppressive surround and responds best to focal stimulation. These two types of ON/OFF amacrines are proposed to use different inhibitory neurotransmitters based on the isolation of two distinct ON/OFF effects that are differentially sensitive to GABAergic and glycinergic pharmacological agents (Frumkes *et al.*, 1981). Hence, the type of transient amacrine that has a large spatial summation (probably indicative of syncitial coupling via gap junctions) may be GABAergic, whereas the ON/OFF cell with suppressive surround may be glycinergic. This categorization is supported by the fact that transient amacrine cells of the Tiger salamander are presumed to be glycinergic (Belgum *et al.*, 1987), do not stain for anti-GABA (Werblin *et al.*, 1988), and glycinergic amacrines show mutual synaptic lateral inhibition and no syncitial coupling (Barnes & Werblin, 1987).

This is in strong contradistinction to the syncitial nature of the transient cells of goldfish, carp, and catfish (Muller & Marc, 1990; Negishi *et al.*, 1991; Sakai, 1988c). Perhaps the two types of ON/OFF amacrines subserve very different functions. In fact, the transient glycinergic amacrines of the Tiger salamander have been implicated in a mechanism for the detection of motion and directional selectivity (Werblin *et al.*, 1988; Weblin, 1991; Maguire *et al.*, 1989b), whereas the syncitial C cells of catfish may function as spatial summators for a mechanism of contrast gain control (Victor & Shapley, 1979b; Victor, 1988). It is worth noting that both mechanisms are involved in the detection of change.

According to the scheme of fig. 5d, the transient C cells might be expected to provide cholinergic inputs to NB cells but GABAergic inputs to NA cells. The

findings in frog that amacrines containing glycine have muscarinic cholinergic binding sites is supportive of this. Glycine has been implicated as an inhibitory transmitter that mediates amacrine to bipolar negative feedback for the OFF-pathway (Miller *et al.*, 1981a), and these acetylcholine sensitive cells may be the counterparts of the NB cells of catfish. The finding in carp that OFF-amacrines are much less sensitive to GABA than ON-amacrines provides some additional support for the mechanism that the transient cells provide excitatory cholinergic inputs to sustained OFF-amacrines but inhibitory GABAergic inputs to sustained ON-amacrines. In addition, the observation that the reduction of the light evoked response of ON-amacrines to GABA perfusion often was not accompanied by a membrane hyperpolarization (sometimes even a depolarization was observed) suggests that GABA inhibition primarily causes a shunting type of conductance change (Toyoda *et al.*, 1987). This type of silent inhibition is described in the amacrine cells of mudpuppy as well, but is not characteristic of the ganglion cells (Miller *et al.*, 1981b). As discussed above, perhaps the greater variablitiy of the 2nd order kernels of NA cells (as opposed to NB cells) can be attributed to a shunting inhibition from C cells.

While the effects of acetylcholine on sustained OFF-amacrines do cause membrane depolarizations, the depolarizations are much weaker than those caused by glutamate (Toyoda *et al.*, 1987). However, the potency of cholinergic inputs may extend beyond direct effects on membrane conductance. For example, acetylcholine was found to potentiate responses of rat hippocampal cells to NMDA. The effect was mediated via the inositol-diacylglycerol pathway and involved an amplification of the response, especially for small signals, and an increase in the duration of the

response. This enhancement of small signals suggests a possible mechanism that may contribute to contrast gain control and is consistent with the finding of regulatory protein kinase sites on NMDA receptors (Miller & Oliva, 1992). Thus, the cholinergic amacrines may also modulate the excitatory amino acid inputs to sustained OFF-amacrines from OFF-bipolars.

Several reports, taken together, support the contention that sustained OFF-amacrines receive cholinergic inputs from ON/OFF amacrines and are also part of a negative feedback loop to the ON/OFF amacrines via OFF-bipolar cells (fig. 5e). Several notable effects consistent with this negative feedback loop become apparent after perfusion with APB, an ON-channel inhibitor. First, as expected, APB increases the OFF-response of ON/OFF ganglion cells in the frog (Jardon *et al.*, 1992). Application of ethylcholine mustard arizidinium (ECMA), a toxin highly specific for cholinergic cells, also increases the OFF-response of transient ganglion cells, but without suppressing ON-responses. If APB is added as well, the ON-response is abolished, but no detectable effect is observed on the already enhanced OFF-response. This suggests that the APB effect on ON/OFF ganglion cells is mediated by cholinergic cells which correlates well with the observation that APB partly blocks the release of acetylcholine from the starburst amacrines of rabbit (Massey & Redburn, 1983; Masland *et al.*, 1984; Neal *et al.*, 1981). The ECMA result also indicates that a general reduction in choline release, whether or not it is due to a decreased ON-channel input to cholinergic amacrines, results in enhancement of the OFF- but not ON-responses.

The APB effect on transient ganglions was abolished by perfusion with atropine (a choline antagonist at muscarinic receptors) or strychnine in the frog (Jardon *et al.*, 1989). In addition, administration of glycine totally suppresses the OFF-response but only mildly decreases the ON-response. Since glycine can act at the OFF-bipolar pre-synaptic terminals that provide excitatory inputs to transient cells, the identical effects observed by the application of either atropine or strychnine result from the disruption of the same feedback loop, but at different synapses within that loop. The relatively mild effects of strychnine on the ON-response can probably be attributed to the preferential sensitivity of ON-bipolar terminals for GABA over glycine (Miller *et al.*, 1981a).

The observation that APB can increase the light responses of OFF-bipolars in mudpuppy by an indirect mechanism (Arkin & Miller, 1987; Miller & Slaughter, 1986) is quite consistent with the feedback loop: the decreased release of choline from transient amacrine cells removes excitatory inputs from sustained OFF-amacrines which results in disinhibition of the OFF-bipolars. This same neuronal loop can explain why perfusion of the rabbit eyecup with: 1) atropine caused a doubling of the light evoked acetylcholine release; 2) muscarine (a muscarinic agonist) reduced the light evoked release by 50%; and 3) strychnine blocked both effects (Cunningham *et al.*, 1983). It is worth noting that this feedback loop appears to act as a homeostatic device since removal of input to the loop by treatment of the retina with APB or ECMA results in a readjustment of the gain of that loop so as to cause a compensatory increase in the OFF-response. Interestingly, no such gain is observed for the ON-response of the transient ganglions with application of ECMA

(Jardon *et al.*, 1992). But, the inputs from transient ganglions to sustained ON-amacrines are postulated to be inhibitory and GABAergic (fig. 5d). As a consequence, the loop is not a simple feedback loop as is the cholinergic/glycinergic loop of the OFF-pathway and should not be expected to exhibit similar behavior.

B. Retinal Sensitivity Control:Light Adaptation and Contrast Gain

The retina can respond to a range of 10 log units in light intensity - from starlight to broad daylight. However, the range of receptor responses, from noise to full saturation, is only 2 log units (Shapley & Enroth-Cugell, 1984). The process of light adaptation results in a decrease in retinal sensitivity to changes in the level of absolute light quanta as the mean light intensity, I, is increased. This allows the neurons to respond to changes related to the contrast, $\Delta I/I$ rather than to changes in absolute quanta of light, ΔI, and assures that changes in light level remain within neural response ranges. Tranchina and his coworkers have modelled light adaptation as a biochemical modulation of the phototransduction process in turtle cones, whereby an increase in intracellular Ca^{++} inhibits guanylate cyclase. This results in a decrease of cGMP, consequent channel closing, and less influx of Ca^{++} (Tranchina *et al.*, 1991).

Unlike light adaptation, which adjusts retinal sensitivity to the mean luminance of the visual field, contrast gain control adjusts retinal dynamics to the level of modulation, or variance, around that mean luminance. This phenomenon has been described in cat X and Y ganglion cells (Shapley & Victor, 1978). They observed that by varying the modulation depth (contrast) of a sum of eight temporal sinusoids which modulated the contrast of a standing spatial sine grating, the shape of the 1^{st} and 2^{nd} order frequency kernels could be adjusted. In particular, the kernels became more tuned to higher frequencies and were more phase advanced at these higher frequencies with an increase in modulation depth of the light input.

This effect was much more pronounced in the non-linear Y cells than the linear X cells. The ability to change the shape of the kernels was strong indication that the contrast gain control behaved in a dynamically nonlinear fashion.

In fact, a mechanism that adjusts gain according to variations in contrast about a mean luminance would be expected to involve an even order nonlinearity, since such a mechanism would detect the absolute value of deviations from the mean and not necessarily the direction of such deviations. By observing the total change in power of different orders of response in Y cells to an increase in contrast, the even order terms (especially the second) were indeed the most dramatically enhanced (Victor & Shapley, 1979b).

The observed effects of contrast gain control are independent of the temporal or spatial phase of the grating. The response of a cell with a center/surround receptive field would vary greatly with spatial phase; a slight shift in stimulus position could move a bar from over the excitatory center to over the inhibitory surround. The lack of phase dependence implies that there are many subunits (estimated at 100; Victor & Shapley, 1979b) contributing to the contrast effect on a ganglion cell, so that a shift that diminishes the response in one subunit is equally as likely to enhance the response in another. Furthermore, an increase in the area of light stimulation over a broad region has essentially the same effect as a comparable increase in the contrast over the smaller original area (Shapley & Victor, 1981). Hence, contrast detection involves significant spatial summation and pooling. This subunit pooling is postulated to occur after the even order non-linearity. Otherwise, cancellation could occur between subunits as they are pooled.

The Y ganglion response to contrast was modelled using a L_1-N-L_2 sandwich structure (see Methods; fig. 21, appendix C). Each L consisted of a n-stage low-pass filter followed by a single stage high-pass filter. After fitting the parameters of this L_1-N-L_2 structure to Y cell kernels, L_1 was found to demonstrate spatial tuning, reflective of a center/surround organization of its receptive field (Victor & Shapley, 1979b). This result implicates bipolar cells as likely candidates for the single subunit represented by L_1. In addition, L_1 was found to be band-pass in nature, again reflective of bipolar cell behavior. L_2, then, represents the spatial pooling after the non-linearity. The transient amacrine C cells are likely anatomical correlates for L_2, as they have strong 2nd order kernels suitable for contrast detection and have wide spatial pooling due to their syncytial nature and low internal resistance (Naka & Christensen, 1981). Subunit pooling in C cells is also consistent with the presence of a monotonic receptive field in these cells, lacking a center/surround antagonism (Davis & Naka, 1980; Sakai & Naka, 1992). In addition, the gentle high-pass nature of L_2 and its fairly even amplitude at low frequencies is consistent with C cell behavior observed in the present study (fig. 24h).

The static-nonlinearity is postulated to occur at the bipolar to amacrine synapse. It was probed by gradually increasing contrast and carefully observing how the response amplitude changed. It was characterized by this method as a rectifier, $|X|^{\alpha}$ with $\alpha = .82$ (Victor & Shapley, 1979b).

Fits of the L_1-N-L_2 model to responses at various contrasts revealed that adjustments were made primarily at the high-pass stages of L_1 and also L_2. These filters would become more high-pass in nature (decreasing the time constants and

increasing the gains) as contrast was increased. The low-pass stages remained remarkably uniform despite rather large variations in contrast. By comparison of the filter parameters for model fits of the linear X cells (treated as a filter, L) and Y cells (treated as L_1-N-L_2), the L_1 filter of Y cells was found to have significantly greater high-pass strength than the L filter of X cells. Assuming that both X and Y cells share similar bipolars, then the nonlinear path of the Y cells must contain additional high-pass filtering that occurs before the nonlinearity, N, presumed to act at the bipolar to amacrine synapse (Victor, 1988). This finding is consistent with the scheme (Maguire *et al.*, 1989a,b) that describes a population of bipolars containing $GABA_B$ receptors that can be made to release transmitter transiently, in a high-pass manner, to C-like amacrine cells (fig. 5b).

For the X cell, Victor modelled the changes to contrast successfully as a dynamic feedback that adjusted the parameters of the high-pass stage. The feedback involved a rectification of the output of the L filter (Victor, 1987). If the population of bipolars with pre-synaptic GABAergic receptors are the targets of such feedback, and the transient amacrine cell is the contrast detector, then a feedback pathway from C amacrines to bipolars exists. As the sustained cells in salamander are GABAergic and suspected of regulating transmitter release from some bipolars, the sustained N cells in catfish might mediate feedback. A C to N pathway would complete the route from C cells to bipolars. The observation that the 2^{nd} order kernel of N cells has a monotonic receptive field similar to that of C cells (unlike the 1^{st} order kernel, which demonstrates the center/surround antagonism characteristic of bipolar cells) tends to support the existence of such a pathway (Sakai & Naka,

1992). Alternatively, numerous synapses have been observed between pre-synaptic C cells and bipolars in the catfish, providing a more direct route for feedback (Sakai, personal communication).

The effects of modulation depth on 1st order kernels has been recorded in N cells and some G cells in the catfish retina. An increase in contrast decreased the amplitude of the kernel and caused some changes in dynamics. Thus, these cells were more sensitive to inputs of lower modulation depths. This contrast effect was not seen in more distal cells such as bipolars, horizontals and photoreceptors, even for large variations in modulation depth on the order of 20 db (Sakai & Naka, 1987b).

IV. METHODS

A. EXPERIMENTAL

The experiments were peformed on the eyecup preparation from the channel catfish (*Ictalurus punctatus*). The eyecup was drained of vitreous and then placed in an unperfused chamber, aerated with oxygen, and held at room temperature (air-conditioning). The first eye was removed from a fish anesthetized with (MS222; 3-aminobenzoic acid ethyl ester); the second, from the sacrificed fish. (No physiological distinctions were apparent between the two eyes). The fish were approximately 30 cm in length and weighed about 1lb. Intracellular recordings were made from glass microelectrodes (Grass, pulled on a Kopf) that were placed inverted in a well of sodium citrate (2M) and then vaccuum filled. The resistance of the electrodes was approximately (100MΩ). Extracellular electodes were made of tungsten, had their tips etched in acid (KNO_2), were plated in gold, then platinum, and then insulated with EPO-TEK 301-2 epoxy (Epoxy Technology Incorporated). Prior to recording the tip epoxy was breached by a current jolt. The impedance of the extracellular electrodes was .5MΩ at 1 kHz. The intracellular and, if present, the extracellular electrodes were positioned with hydraulic manipulators (Narishige Science Instruments, Tokyo). The extracellular signals were preamplified 1000x. Additional amplification, both for intra- and extracellular recordings, was 100x.

The light stimuli used for the experiment included step flashes in darkness, white noise, steps from a mean, and sinusoids. Occasionally, the retina was held in

steady darkness or at a steady mean for several minutes in order to record spontaneous neural activity. The light was generated by a red LED (Stanley Electric, Tokyo) at a wavelength of 640 nm and detected via photodiode (Hammer Matsu Photoelectronics). The step flashes from darkness had a luminance of 30 $\mu W/cm^2$ over the retinal surface and were 300 ms in duration. The mean or background luminance for the other stimuli was 30 $\mu W/cm^2$. The white noise stimuli were generated on a 1360 Random Noise Generator (CNF Electronics, Tokyo) with a bandwidth from DC to 50 Hz and recorded on a Teac RD-101 PCM data recorder. At least three, and, if the stability of the cell recording permitted, four, different modulation depths of white noise stimuli were presented to a given cell (see fig. 25). The highest variance was a quarter of the mean luminance (level 1), and each succeeding modulation level was half of the variance of the previous level (*i.e.*, level 2, 3, 4 are 1/2, 1/4, and 1/8 of the initial level 1 variance, respectively). Each was delivered for a period of from 30 to 120 sec, depending on the stability of the recording. An attempt would always be made to return to a previously presented modulation level in order to provide a control for that cell. The step and sinusoid inputs were generated by a computer that was programmed to deliver a prefabricated stimulus regimen. The computer interfaced with a digital/analog card, and the voltage outputs from this card were used to drive the light source. The step increments and decrements from the mean varied in luminance change from 1/2 to 1/32 of the mean luminance. Likewise, the amplitude of the sinusoids varied from a luminance of 1/4 to 1/32 of the mean luminance.

Neurons were identified by their responses to the light flashes in darkness, by the 1st and 2nd order Wiener kernels (see Methods - Theoretical) generated from the white noise analysis (Naka *et al.*, 1975; Naka, 1977), and, less so, by the relative depth of the electrode in the retina. The response voltages of the neurons and the photodiode detected light stimuli were stored on four channel digital tape (DAT). Subsequently, the data were digitized at a rate of 500 Hz and transferred off-line to a VAX 11/780 computer (Digital Equipment, Maynard, MA). The 1st and 2nd order kernels and MSEs for the kernel contributions to the response power were generated off-line through the use of a software analysis package, STAR. This software ran on the VAX 11/780 with the aid of an AP120B array processor (Floating Point Systems, Portland, OR). The data files stored on the VAX 11/780 for the Wiener kernels and the digitized time series were transferred to a SUN (SUN microsystems) for further theoretical analysis, mathematical modelling, and computer simulations.

B. THEORETICAL

1. LINEAR ANALYSIS

i). General Theory

Linear systems have the key property of superposition. This property can be demonstrated as follows. Given an input, $x_i(t)$, whose response is $y_i(t)$, the summation of various inputs expressed as $\Sigma_{i=1}^{n} a_i x_i(t)$ (where a_i is a scaling factor) will lead to the system response $\Sigma_{i=1}^{n} a_i y_i(t)$.

The approach for applying this property to complex inputs is to define a very basic input, $x_i(t)=\delta(t-t_i)$. Then, a more complex input, x(t), is treated as the summation and scaling of this basic input. The Dirac delta function, $\delta(t-t_i)$, can be defined as a pulse input of unit area such that $\delta(t-t_i)$ equals zero everywhere except at $t=t_i$. It can result from taking

$$\delta(t-t_i) = \begin{cases} 1/\Delta t \text{ for } t_i < t < t_i+\Delta t \\ 0 \quad \text{elsewhere} \end{cases}$$

and allowing $\Delta t \rightarrow 0$. According to this definition,

$$\int_{-\infty}^{\infty} x(t)\delta(t-t_i)dt = x(t_i).$$

This is known as the 'sifting' property of the Dirac delta function and will be used quite frequently. The system response to $\delta(t)$ is appropriately known as the 'impulse response', h(t).

Now consider each t_i to be equally spaced such that t_i equals $i\Delta t$. Then, the complex input x(t) from $t=-\infty$ to $t=+\infty$ can be approximated as a sum of rectangles of width Δt and height $x(i\Delta t)$. The approximation improves as $\Delta t \rightarrow 0$. Defining $x^*(t)$ as the function obtained by replacing each rectangular pulse with a δ function of equal area, then

$$x^*(t) \cong \Sigma_{i=-\infty}^{\infty} x(i\Delta t)\delta(t-i\Delta t)\Delta t$$

which, by superposition, gives

$$y(t) \cong \Sigma_{i=-\infty}^{\infty} x(i\Delta t)h_i(t-i\Delta t)\Delta t$$

where h_i is the impulse response for the $i\Delta t$ impulse. If the system is time invariant, the impulse response does not depend on i. Taking the limit as $\Delta t \rightarrow 0$ and letting $i\Delta t=\tau$ gives

$$\begin{aligned} y(t) &= \int_{-\infty}^{\infty} x(\tau)h(t-\tau)d\tau \\ &= \int_{-\infty}^{\infty} x(t-\tau)h(\tau)d\tau \text{ by change of variable.} \end{aligned}$$

This is known as the convolution integral (Oppenheim *et al.*, 1983). If the linear system being studied is causal, then an impulse response cannot occur before the impulse so that $h(\tau)$ is zero for $\tau<0$. Also, if the input, x(t), is zero before $t=0$, then

$$y(t) = \int_0^t x(t-\tau)h(\tau)d\tau.$$

A linear time invariant system can be defined entirely by the impulse response function. Bipolar, horizontal, and photoreceptor cells behave very linearly and can be modelled in this manner (Sakai & Naka, 1987b). Fig. 22a shows a 1st order Wiener kernel (equivalent to a linear impulse response function) for a bipolar cell.

ii). Fourier Analysis

A theorem proposed by Fourier allows the expression of a very large class of time domain signals as a sum of sinusoids of various amplitudes, frequencies, and phases (Oppenheim *et al.*, 1983). This can apply to signals that are periodic or aperiodic. The constraints on the class of signals that can be converted to the frequency domain representation are:

i) x(t) must be absolutely integrable for aperiodic signals (have finite energy):

$$\int_{-\infty}^{\infty} |x(t)|\,dt < \infty$$

ii) x(t) has a finite number of finite discontinuities, maxima, and minima within any finite interval

Both of these conditions are met for stable physical systems.

The Fourier transform converts aperiodic signals from the time domain to the frequency domain and is of the form:

$$X(\omega) = \int_{-\infty}^{\infty} x(t)\exp(-i\omega t)dt.$$

The inverse Fourier transform converts from frequency to time domains and is of the form

$$x(t) = \frac{1}{2\pi}\int_{-\infty}^{\infty} X(\omega)\exp(i\omega t)d\omega.$$

The primary reason to convert signals to the frequency domain is that several operations that are quite tedious to perform in the time domain are quite easy to perform in the frequency domain. The approach, then, is to use the Fourier

transform to convert to the frequency domain, to perform certain operations, and then convert back to the time domain with the inverse Fourier transform.

One useful property is the convolution property. If

$$y(t) = \int_{-\infty}^{\infty} x(t-\tau)h(\tau)d\tau ,$$

then

$$\begin{aligned} Y(\omega) &= \int_{-\infty}^{\infty}[\int_{-\infty}^{\infty} x(t-\tau)h(\tau)d\tau]\exp(-i\omega t)dt \\ &= \int_{-\infty}^{\infty} h(\tau)[\int_{-\infty}^{\infty} x(t-\tau)\exp(-i\omega t)dt]d\tau . \end{aligned}$$

Letting $t'=t-\tau$ gives

$$\begin{aligned} Y(\omega) &= \int_{-\infty}^{\infty} h(\tau)[\int_{-\infty}^{\infty} x(t')\exp(-i\omega(t'+\tau))dt']d\tau \\ &= \int_{-\infty}^{\infty} h(\tau)\exp(-i\omega\tau)d\tau X(\omega) \\ &= H(\omega)\cdot X(\omega) . \end{aligned}$$

A convolution integral in the time domain is reduced to a multiplication in the frequency domain. $H(\omega)$, the Fourier transform of $h(t)$, is known as a transfer function. $H(\omega)=Y(\omega)/X(\omega)$ and can be viewed as an operation relating the output to the input. As a consequence of this multiplicative property, a cascade (series of transfer functions in which the output of one serves as the input to another) can be treated as a product of all the transfer functions. For parallel paths, the transfer functions of each path are just added. The operation of addition is equivalent in both time and frequency domains.

Another useful property is the derivative property.

$$\frac{dx(t)}{dt} = \frac{1}{2\pi}\int_{-\infty}^{\infty} i\omega X(\omega)\exp(i\omega t)d\omega$$

so that $i\omega X(\omega)$ is the equivalent operation in the frequency domain for the derivative operation in the time domain.

iii). Applications to Circuits

Analysis of the simple RC circuit shown in fig. 20 can provide a good example of the application of the methods of signal analysis (Oppenheim *et al.*, 1983).

a) single stage low pass filter:

Let $v_S(t)$ be the input voltage and $v_C(t) = v_2(t)-v_3(t)$ be the response voltage measured across the capacitor. By physics, the capacitor charge, $Q = Cv_C(t)$ so that the current, $I=C(dv_C(t)/dt)$. By the voltage law of Kirchoff,

$$R[C(dv_C(t)/dt)] + v_C(t) = v_S(t)$$

Taking the Fourier transform of each side

$$[i\omega RC+1]V_C(\omega) = V_S(\omega) \text{ so that } H_C(w)=V_C(\omega)/V_S(\omega)=1/[1+i\omega RC]$$

The transfer function, $H_C(\omega)$, acts as a low-pass filter, preserving the DC and low frequencies of input, while dampening higher frequencies. This function is consistent with the ability of capacitors to store charge and, hence, preserve DC inputs. The time constant, $\tau=RC$, determines the cutoff region of the filter (see fig. 20b).

b) single stage high pass filters:

Let the system response voltage be measured across the resistor.

$v_R(t)=v_1(t)-v_2(t)$ and $v_S(t)=v_R(t)+v_C(t)$.

$$I = v_R(t)/R = C(dv_C(t)/dt) = C(d[v_S(t)-v_R(t)]/dt).$$

Therefore,

$$RCdv_R(t)/dt + v_R(t) = RCdv_S(t)/dt$$

and

$$[i\omega RC+1]V_R(\omega) = i\omega RCV_S(\omega) \text{ and } H_R(\omega)=i\omega RC/(1+i\omega RC)$$

The transfer function, $H_R(\omega)$, acts as a high-pass filter, damping out the lower frequencies while preserving the passage of the higher frequencies (fig. 20c). Another type of high-pass filter occasionally used may be represented as $H_{high}(\omega)=k(1+i\omega\tau')/(1+i\omega\tau)$ with $\tau'>\tau$ so that the filter is not constrained to be zero at $\omega=0$.

c) band pass filters

More complex filters such as band pass filters can be expressed as a cascade of n of the discrete filters above. A bandpass filter used in a model of bipolar cells involves n-stages of low pass filtering and a single high-pass stage (e.g. B_{Ion}, appendix C-iii). This discrete n-stage filtering is an approximation to the continuous filtering that would occur as a signal propagates along a real membrane. A good way to estimate the number of stages needed to fit an experimentally measured transfer function is to look at the overall phase lead or lag at higher frequencies, ω. A single stage low pass filter has a phase lag of $\pi/2$, whereas a single stage high pass filter has a phase advance of $\pi/2$ (fig. 20b,c). Thus, the number of high pass stages minus the number of low pass stages then multiplied by $\pi/2$ should correspond roughly to the empirical phase at large ω. Alternatively, one can look at the slope of the gain curve in the Bode plot.

2. NONLINEAR ANALYSIS

i). General Theory

Unlike linear systems, the principle of superposition does not hold for nonlinear systems. Hence, such systems cannot be characterized neatly with a transfer function the way linear systems can. However, the white noise method of nonlinear signal analysis can be applied to a broad class of nonlinear systems. These include systems that are time-invariant and that have a finite memory. Systems that oscillate do not have a finite memory and are not directly approachable by these methods.

Nonlinearity emerges from the ability of inputs to influence each other via "cross-talk" in such a manner that the inputs no longer act independently of each other. For example, consider two separate pulse inputs where:

$x_1(t) = \delta(t-t_1)$ and $x_2(t) = \delta(t-t_2)$ t_1 may equal t_2

with corresponding outputs, $y_1(t)$ and $y_2(t)$. The response for the combined inputs, $x_{1,2}(t)$, is

$$y_{1,2}(t) = y_1(t) + y_2(t) + w_{1,2}(t).$$

$w_{1,2}(t)$ represents the effect of the cross-talk interaction between the two pulses on the response at time t. If there were no interaction between the two inputs, $w_{1,2}(t)$ would equal 0 and superposition would hold. Thus, superposition implies the independence of inputs.

If another pulse, $x_3(t)$, is added, more cross-talk terms must be considered. These now include the possible pairings $w_{1,2}(t)$, $w_{1,3}(t)$, and $w_{2,3}(t)$ as well as the triplet $w_{1,2,3}(t)$. In general, this process can be expanded to include any number of input impulses. For n impulses, the response becomes

$$y_{1,2,\ldots,n}(t) = \Sigma_{i=1}^{n} y_i(t) + \Sigma_{j=i}^{n}\Sigma_{i=1}^{n} w_{i,j}(t) + \Sigma_{k=j}^{n}\Sigma_{j=i}^{n}\Sigma_{i=1}^{n} w_{i,j,k}(t) + \ldots$$

If any number of impulses are allowed now, but they occur in discrete time intervals of Δt, the response is

$$y(t) = \Sigma_{i=1,..} f_1(t-n_i\Delta t) +$$

$$\Sigma_{i=1,..}\Sigma_{j=1,..} f_2(t-n_i\Delta t, t-n_j\Delta t) +$$

$$\Sigma_{i=1,..}\Sigma_{j=1,..}\Sigma_{k=1,..} f_3(t-n_i\Delta t, t-n_j\Delta t, t-n_k\Delta t) + \ldots$$ where $f_1()$ represents the linear contribution of a single pulse and $f_i()$ for $i > 1$ is a function that represents the crosstalk interactions for pairs, triplets and so on. The resemblance of this formula in the discrete case with the Volterra kernels for the continuous case can now begin to be appreciated:

$$y(t) = \int_0^{\infty} k_1(t_1)x(t-t_1)dt_1 +$$

$$\int_0^{\infty}\int_0^{\infty} k_2(t_1,t_2)x(t-t_1)x(t-t_2)dt_1dt_2 +$$

$$\int_0^{\infty}\int_0^{\infty}\int_0^{\infty} k_3(t_1,t_2,t_3)x(t-t_1)x(t-t_2)x(t-t_3)dt_1dt_2dt_3 + \ldots.$$

where $k_m()$ are known as the Volterra kernels.

The Volterra series can be viewed as an extension of a Taylor series for a function of greater than one variable. The Taylor series of such a function expanded around 0 is

$$F(z_1,z_2,z_3,\ldots,z_k) = \Sigma_{n1=0}^{\infty}\Sigma_{n2=0}^{\infty}\Sigma_{n3=0}^{\infty}\ldots\Sigma_{nk=0}^{\infty} C_{n1n2..nk} z_1^{n1} z_2^{n2} .. z_k^{nk}$$

where

$$C_{n1n2\ldots nk} = \frac{1}{(n_1!n_2!\cdots n_k!)} \frac{\partial^{n1}}{\partial_{z1}{}^{n1}} \frac{\partial^{n2}}{\partial_{z2}{}^{n2}} \ldots \frac{\partial^{nk}}{\partial_{zk}{}^{nk}} [F(z_1,z_2,\ldots,z_k)]|_{z1=z2=\cdots=zk}$$

and $z_j = x^*(t_j)\Delta t$ where $x^*(t_j)$ is the average value of x(t) between t_j and t_{j+1}. If $n_1+n_2+\ldots n_k = m$, for m=2 the terms are 2nd order for pair interactions. For m=3, the terms are 3rd order for triplet interactions, and so on. Now, if the discrete values $z_1,z_2,\ldots z_k$ are allowed to approach the values of a continuous function x(t) defined over some interval, a functional (operation on a function) - F(x(t)) - now appears on the left-hand side of the equation. In this case, all the terms $C_{n1n2\ldots nk}$ for which $\Sigma_{i=1}{}^{k} n_i = m$ now contribute to the Volterra kernel, k_m, and the sums of discrete variables are now sums of integrals, forming the Volterra series above. The kernels $k_m(t_1,t_2,..,t_m)$ now represent the cross-talk contributions for the group of input values occurring at times $t_1,t_2,..,t_m$ before the response time, t (*i.e.* $x(t-t_i)$). For a system that is time-invariant, has finite memory, and is analytic, the series expression defined by Volterra relating the system input (x(t)) to the output (y(t)) is applicable (Marmarelis & Marmarelis, 1978).

ii). White Noise Method of Wiener

Unfortunately, no straight-forward, computationally efficient method is available for the calculation of the Volterra kernels. However, Wiener was able to adapt the Volterra method so as to make the calculation of Wiener kernels, h_m, very direct. His method required the use of Gaussian white noise as the input, x(t), and the construction of the Wiener functionals of various orders m as being mutually orthogonal.

Gaussian white noise has its amplitudes distributed in a Gaussian manner and has a constant power spectrum for all frequencies. In the experimental, non-ideal situation, the spectrum dips at lower frequencies because of finite record lengths and at higher frequencies because of finite energy reqirements. These deviations are not significant as long as the band-width of the input signal is much greater than the band-width of the system being analyzed.

Wiener's method of orthogonalization is very similar to a Gram-Schmidt method using the expectation, E{ }, as the inner product. Basically, if the average (expectation) of the product of two different terms of a series sum of functionals (see appendix C-ii) is equal to 0, then those two terms are orthogonal in the Wiener sense:

$E\{G_m[h_m;x(t)]\cdot G_n[h_n;x(t)]\} = 0$ for $m \neq n$ given that x(t) is Gaussian.

As an example, the first three functional terms of the Wiener series - G_0, G_1, G_2 - can be shown to be orthogonal by this definition.

(a) $E\{G_0[h_0;x(t)]\cdot G_1[h_1;x(t)]\} = E\{h_0 \cdot \int_0^\infty h_1(\tau)x(t-\tau)d\tau\}$

$$= h_0 \cdot \int_0^\infty h_1(\tau) E\{x(t-\tau)\} d\tau$$

$$= 0$$

since the expectation of the product of an odd number of Gaussian distributed variables of zero mean (e.g. $x(t-\tau)$) is 0 (see Appendix A).

(b) $E\{G_1[h_1;x(t)] \cdot G_2[h_2;x(t)]\}$

$$= E\{\int_0^\infty h_1(\tau)x(t-\tau)d\tau \cdot \int_0^\infty \int_0^\infty h_2(t_1,t_2)x(t-t_1)x(t-t_2)dt_1dt_2\}$$

$$- E\{\int_0^\infty h_1(\tau)x(t-\tau)d\tau \cdot P\int_0^\infty h_2(t_1,t_1)dt_1\}$$

$$= \int_0^\infty \int_0^\infty \int_0^\infty h_1(\tau)h_2(t_1,t_2)E\{x(t-\tau)x(t-t_1)x(t-t_2)\}d\tau dt_1dt_2\}$$

$$- P\int_0^\infty \int_0^\infty h_1(\tau)h_2(t_1,t_1)E\{x(t-\tau)\}d\tau$$

= 0 since each term involves an odd product of Gaussians

(c) $E\{G_0[h_0;x(t)] \cdot G_2[h_2;x(t)]\}$

$$= E\{h_0 \cdot \int_0^\infty \int_0^\infty h_2(t_1,t_2)x(t-t_1)x(t-t_2)dt_1dt_2\}$$

$$- h_0 \cdot P\int_0^\infty h_2(t_1,t_1)dt_1$$

$$= h_0 \cdot \int_0^\infty \int_0^\infty h_2(t_1,t_2)E\{x(t-t_1)x(t-t_2)\}dt_1dt_2\}$$

$$- h_0 \cdot P\int_0^\infty h_2(t_1,t_1)dt_1$$

but $E\{x(t-t_1)x(t-t_2)\}$ is the autocorrelation function, $\Phi_{xx}(t_1-t_2)$. Since x(t) is a Gaussian of mean zero, $\Phi_{xx}(t_1-t_2) = P\delta(t_1-t_2)$. Therefore, the left-side of the equation now is:

$$= h_0 \cdot \int_0^\infty \int_0^\infty h_2(t_1,t_2)P\delta(t_1-t_2)dt_1dt_2 - h_0 \cdot P\int_0^\infty h_2(t_1,t_1)dt_1$$

= 0 since $\delta(t_1-t_2)$ is 0 except when $t_1 = t_2$

Hence, the first three terms of the Wiener series are orthogonal given x(t) is a white-noise input. (Lee & Schetzen, 1965). A significant difference of the orthogonal functionals of the Weiner series from the functionals of the original Volterra series

is the dependence of the Weiner functionals for systems with greater than 2nd order nonlinearity on P, the power of the white-noise input. The Volterra functionals are independent of input in this regard.

Orthogonality also assures that the truncated sum of Wiener functionals up to order m will be the best approximation of the response, y(t), for that order (for white noise input with the same power density used to define the functionals). And, addition of higher terms will not affect the contribution to the response from the lower terms. This mutual orthogonality of the terms is also very useful in the explicit calculation of the kernels, h_m.

The cross-correlation method of Wiener kernel calculation outlined by Lee and Schetzen (1965) involves multiplying the measured response, y(t), by a product of input values that have various delays, t_i. Lastly, this response/input product is averaged over time, giving the cross-correlation:

$$\Phi_{yx1\cdots xn}(t_1,t_2,..,t_n) = E\{y(t)x(t-t_1)..x(t-t_n)\}$$

$$= E\{\Sigma_{m=0}^{\infty} G_m[h_m;x(t)]\cdot x(t-t_1)..x(t-t_n)\}$$

The basis for this approach is that the product $x(t-t_1)..x(t-t_n)$ is a functional of order n. Hence, the Wiener functionals, G_m, contributing to y(t) that are of order $m > n$ can be ignored in the average due to their orthogonality. The zeroth order kernel, h_0, is simply $E\{y(t)\}$, or the DC contribution of the response.

For computation of the 1st order kernel, y(t) is multiplied by a single input term (i.e. $n=1$), $x(t-t_1)$. The functional terms $m > 1$ for y(t) can be ignored. With $m=0$, $E\{G_0[h_0;x(t-t_1)]\} = E\{h_0x(t-t_1)\} = 0$ since x(t) has mean 0.

So, up to $m=1$,

$$\Phi_{yx}(t_1) = E\{[\int_0^\infty h_1(\tau_1)x(t-\tau_1)d\tau_1]\cdot x(t-t_1)\}$$
$$= \int_0^\infty h_1(\tau_1)E\{x(t-\tau_1)x(t-t_1)\}d\tau_1$$
$$= \int_0^\infty h_1(\tau_1)P\delta(\tau_1-t_1)d\tau_1$$
$$= Ph_1(t_1)$$

Therefore, $h_1(t_1) = \Phi_{yx}(t_1)/P$, showing that the power of the input is an important consideration in Wiener kernel estimation.

With the 2nd order kernel computation, the functionals $G_m[h_m;x(t)]$ for m > 2 can be ignored, since y(t) is multiplied by $x(t-t_1)x(t-t_2)$ (i.e. n=2). For m=0,

$$E\{G_0[h_0;x(t)]\cdot x(t-t_1)x(t-t_2)\} = E\{h_0x(t-t_1)x(t-t_2)\}$$
$$= h_0P\delta(t_1-t_2)$$

The average for m=1 is:

$$E\{G_1[h_1;x(t)]\cdot x(t-t_1)xt-t_2)\} = E\{[\int_0^\infty h_1(\tau_1)x(t-\tau_1)d\tau_1]\cdot x(t-t_1)x(t-t_2)\}$$
$$= \int_0^\infty h_1(\tau_1)E\{x(t-\tau_1)x(t-t_1)x(t-t_2)\}d\tau_1$$
$$= 0$$

since the average involves an odd number of Gaussian variables.

Finally, for m=2,

$$E\{G_2[h_2;x(t)]\cdot x(t-t_1)x(t-t_2)\}$$
$$= E\{[\int_0^\infty\int_0^\infty h_2(\tau_1,\tau_2)x(t-\tau_1)x(t-\tau_2)d\tau_1d\tau_2]\cdot x(t-t_1)x(t-t_2)\}$$
$$- E\{[P\int_0^\infty h_2(\tau_1,\tau_1)d\tau_1]\cdot x(t-t_1)x(t-t_2)\}$$
$$= \int_0^\infty\int_0^\infty h_2(\tau_1,\tau_2)E\{x(t-\tau_1)x(t-\tau_2)x(t-t_1)x(t-t_2)\}d\tau_1d\tau_2$$
$$- P\int_0^\infty h_2(\tau_1,\tau_1)d\tau_1\cdot E\{x(t-t_1)x(t-t_2)\}$$

Since $E\{x_1x_2x_3x_4\} = E\{x_1x_2\}E\{x_3x_4\} + E\{x_1x_3\}E\{x_2x_4\} + E\{x_1x_4\}E\{x_2x_3\}$

(see Appendix A)

$$= \int_0^\infty \int_0^\infty h_2(\tau_1,\tau 2)P^2[\ \delta(\tau_1-\tau_2)\delta(t_1-t_2) + \delta(\tau_1-t_1)\delta(\tau_2-t_2)$$

$$+ \delta(\tau_1-t_2)\delta(\tau_2-t_1)\ ]d\tau_1 d\tau_2 - P\int_0^\infty h_2(\tau_1,\tau_1)d\tau_1 \cdot P\delta(t_1-t_2)$$

$$= P^2[(\delta(t_1-t_2)\int_0^\infty h_2(\tau_1,\tau_1)d\tau_1) + h_2(t_1,t_2) + h_2(t_2,t_1)$$

$$- \delta(t_1-t_2)\int_0^\infty h_2(\tau_1,\tau_1)d\tau_1]$$

$$= 2P^2 h_2(t_1,t_2)$$

noting that $h_2(t_1,t_2)=h_2(t_2,t_1)$, since all h_m are symmetric.

Therefore, summing the averages for the first three functionals;

$$\Phi_{yxx}(t_1,t_2) = 2P^2 h_2(t_1,t_2) + h_0 P\delta(t_1-t_2)$$

The second term on the right side can be removed by a slight manipulation of the equation. Recall that this term is from the G_0 contribution to the response. By subtracting h_0 from y(t) before cross-correlating with $x(t-t_1)x(t-t_2)$, this term can be removed from the equation. Thus, for $y'(t)=y(t)-h_0$ (removal of the DC):

$$h_2(t_1,t_2) = \Phi_{y'xx}(t_1,t_2)/2P^2$$

This same general method can be applied for the estimation of higher order kernels as well.

The great strength of this white-noise method is that Wiener kernel computation involves the very simple numerical process of cross-correlation. However, in order for this technique of cross-correlation to be applicable, an assumption of ergodicity must be made. Ergodicity implies that, given an ensemble of equal events occurring at time t_0, the probability distribution of outcomes of these events (products of y(t) and $x(t-\tau_i)$'s in this case), is the same as the probability distribution of different outcomes for a single event followed over time. Basically, a cross-correlation such as

$$\Phi_{yx}(\tau) = \frac{1}{R}\int_0^R y(t)x(t-\tau)dt$$

takes a sampling of events over time, sums them and divides by the number of such events (a time interval, R, in this case) in order to make a statistical assessment of the expectation, which is the predicted average of an ensemble based on its theoretical probability distribution.

iii). Analytic Models of Wiener Kernels - the L_1-N-L_2 Sandwich

The Wiener kernels can be very useful for testing a nonlinear model. A common nonlinear model involves processing of x(t) by a linear filter, L_1, followed by processing with a static-nonlinearity, N, and subsequent additional filtering by L_2. This is the L_1-N-L_2 sandwich model. The static-nonlinearity has no memory and depends only on the current output of L_1, z(t). Examples of static-nonlinearities are $e^{z(t)}$ or $z^2(t)$.

Since z(t) is the output of a linear filter operating on a Gaussian of zero mean (x(t)), it also is a Gaussian of zero mean (Schetzen, 1980). A linear filter may change the spectrum of the input so that it is no longer white noise (uniform spectrum), but z(t) will still have a Gaussian distribution of amplitudes. This is shown by the fact that z(t) has characteristics that are unique to a Gaussian process. In particular, all moments of z(t) are those of a Gaussian process, and by probability theory it follows that z(t) must be Gaussian (Cramer, 1949).

Specifically, since $z(t)=\int_0^\infty l_1(\tau)x(t-\tau)d\tau$ where $l_1(\tau)$ is the impulse response corresponding to $L_1(\omega)$, the n^{th} moment of z(t) is:

$$E\{z(t-t_1)z(t-t_2)\cdots z(t-t_n)\}$$

$$= \int_0^\infty \int_0^\infty \cdots \int_0^\infty l_1(\tau_1)\cdots l_1(\tau_n)E\{x(t-t_1-\tau_1)x(t-t_2-\tau_2)\cdots x(t-t_n-\tau_n)\}d\tau_1\cdots d\tau_n$$

Thus, for n odd, the n^{th} moment of z(t) is zero since the expectation of an odd number of input Gaussians, x(t), is zero (see Appendix A). So, all of the odd moments of z(t) behave as a Gaussian. For the even n,

$$E\{z(t-t_1)z(t-t_2)\cdots z(t-t_n)\}$$

$$= \int_0^\infty \int_0^\infty \cdots \int_0^\infty l_1(\tau_1) \cdots l_1(\tau_n) E\{x(t-t_1-\tau_1)x(t-t_2-\tau_2)\cdots x(t-t_n-\tau_n)\} d\tau_1 \cdots d\tau_n$$

$$= \int_0^\infty \int_0^\infty \cdots \int_0^\infty l_1(\tau_1) \cdots l_1(\tau_n) [\Sigma\prod E\{x(t-t_i-\tau_i)x(t-t_j-\tau_j)\}] d\tau_1 \cdots d\tau_n$$

where the term in [ ] is the sum of all possible distinct products of 2nd moment pairings of the n terms. For example, for n=4:

$$E\{x_1x_2x_3x_4\} = E\{x_1x_2\}E\{x_3x_4\} + E\{x_1x_3\}E\{x_2x_4\} + E\{x_1x_4\}E\{x_2x_3\}.\text{(Appendix A)}$$

Continuing,

$$= \Sigma\prod[\int_0^\infty \int_0^\infty l_1(\tau_i) l_1(\tau_j) E\{x(t-t_i-\tau_i)x(t-t_j-\tau_j)\} d\tau_i d\tau_j]$$

$$= \Sigma\prod[E\{\int_0^\infty l_1(\tau_i)x(t-t_i-\tau_i)d\tau_i \cdot \int_0^\infty l_1(\tau_j)x(t-t_j-\tau_j)\} d\tau_j\}]$$

$$= \Sigma\prod[E\{z(t-t_i)z(t-t_j)\}]$$

Therefore, the even moments of z(t) also behave as Gaussians. Consequently, since all moments of z(t) behave Gaussian, z(t) must also be Gaussian.

Hermite polynomials are most suitable for expanding into a series the nonlinear function, N(z(t)). This is because the input, z(t), is a Gaussian variable and the terms of the Hermite series are orthogonal for Gaussian inputs (Wiener, 1958).

This stems from the fact that the mean of a function, F, is given by $E\{F(z^*)\} = \int_{-\infty}^{\infty} F(z^*)Q(z^*)dz^*$ where $Q(z^*)$ is the probability density function of the random variable, z^*. If z^* is Gaussian of zero mean,

$$Q(z^*) = \frac{1}{\sqrt{2\pi\sigma^2}} \exp(-(z^*)^2/(2\sigma^2)).$$

Then, if $F(z^*)$ is a product of two terms of the Hermite series;

$$E\{H_j(z^*)H_k(z^*)\} = \frac{1}{\sqrt{2\pi\sigma^2}} \int_{-\infty}^{\infty} H_j(z^*)H_k(z^*)\exp(-(z^*)^2/(2\sigma^2))dz^*$$

$$= 0 \text{ for } j \neq k$$

Thus, the orthogonality of these polynomials depends on z^* being a Gaussian distributed variable. The equation

$$\frac{1}{\sqrt{2\pi\sigma^2}} \int_{-\infty}^{\infty} (z^*)^m H_n(z^*) \exp(-(z^*)^2/(2\sigma^2)) dz^*$$

$$= 0 \text{ for } m < n$$

can be integrated by parts to provide an integral involving $(z^*)^{m+1}$ and reveal a recursion relation for the Hermite terms involving $H_n(z^*)$ and its derivative (Schetzen, 1980):

$H_{n+1}(z^*) = z^* H_n(z^*) - PH_n'(z^*)$. Starting with $H_0(z^*)=1$ gives:

$$H_1(z^*) = z^*$$

$$H_2(z^*) = z^* z^* - P$$

$$H_3(z^*) = z^* z^* z^* - 3Pz^*$$

...

P is the variance, σ^2, for this single variable Hermite series. It is derived from $E\{z^*_i z^*_j\} = P\delta_{ij}$, where z^*_i and z^*_j are two independent Gaussian variables of zero mean and $\delta_{ij} = \begin{cases} 1 & i=j \\ 0 & i \neq j \end{cases}$. For i=j, this gives $P=\sigma^2$. There is a multivariate Hermite series that is of the form

$$H^{[0]}=1$$

$$H^{[1]}(z^*_i) = z^*_i$$

$$H^{[2]}(z^*_i, z^*_j) = z^*_i z^*_j - P\delta_{ij}$$

$$H^{[3]}(z^*_i, z^*_j, z^*_k) = z^*_i z^*_j z^*_k - P[z^*_i \delta_{jk} + z^*_j \delta_{ik} + z^*_k \delta_{ij}]$$

... (Ogura, 1972; Grad, 1949; Imamura *et al.*, 1965)

For i = j = k, the multivarite series yields the single-variable Hermite series. The multivariate series for discrete Gaussians, z^*_i, can be converted in a straightforward manner into a form that applies to a Gaussian function, $z^*(t)$. Let z^*_i be a Gaussian variable with zero mean and variance P. Then, a discrete autocorrelation can be used to define the Kronecker delta function, δ_{ij}:

$$\frac{1}{2N}\sum_{i=-N+1}^{N} z^*_i z^*_{i+k} = P\delta_{ij} \text{ for } z^* \text{ ergodic as } N \rightarrow \infty, \text{ where } j = i + k.$$

Now, let $N = L/\Delta t$ and $z^*_i = \int_{-\infty}^{\infty} z^*(t)q(t_i-t)dt$ where $t_i = i\Delta t$ and

$$q(t^*) = \begin{cases} 1/\Delta t & 0 < t^* < \Delta t \\ 0 & \text{everywhere else} \end{cases}$$

(*i.e.* discrete z^*_i is an average of continuous $z^*(t)$ over a small interval).

This gives

$$\frac{1}{2L}\sum_{i=-N+1}^{N} \left[\int_{-\infty}^{\infty} z^*(t)q(t_i-t)dt \cdot \int_{-\infty}^{\infty} z^*(t')q(t_{i+k}-t')dt'\right] \Delta t$$

for the left side of the equation above. Setting t_i ($=i\Delta t$) equal to t and t_{i+k} ($=(i+k)\Delta t$) equal to $t+\tau$ and allowing $\Delta t \rightarrow 0$, $q(t^*)$ behaves like a Dirac delta function, $\delta(t^*)$. Then, using the 'sifting property' of $\delta(t^*)$ on the two integrals within brackets gives the integral

$$\frac{1}{2L}\int_{-L}^{L} [z^*(t)z^*(t+\tau)]dt$$

which is recognizable as the autocorrelation function, $\Phi_{z^*z^*}(\tau)$, in the limit as $L \rightarrow \infty$. For an ideal Gaussian white noise signal, $z^*(t)$, the Fourier transform of the autocorrelation function (spectrum) is defined to be a constant, P, for all frequencies, and, hence, the signal has infinite energy. This yields the result that $\Phi_{z^*z^*}(\tau) = P\delta(\tau)$ which (for $\tau = 0$) shows that $z^*(t)$ has an infinite variance. By comparing the results

for the discrete and continuous cases, the Kronecker delta function, δ_{ij}, for discrete Gaussians is interchangeable with the Dirac delta function, $\delta(\tau)$, in the continuous situation. For example, the 2nd order Hermite term above becomes;

$$H^{[2]}(z^*(t-t_1),z^*(t-t_2)) = z^*(t-t_1)z^*(t-t_2) - P\delta(t_1-t_2).$$

The multivariate series is related to the single variable series by

$$H_n(z(t)) = H_n(\int_0^\infty l_1(t_1)x(t-t_1)dt_1)$$

$$= \int_0^\infty \int_0^\infty \cdots \int_0^\infty l_1(t_1)\cdots l_1(t_n)H^{[n]}(x(t-t_1),x(t-t_2),\cdots x(t-t_n))dt_1\cdots dt_n$$

(Sakuranaga *et al.*, 1986)

For example, in the 2nd order case, this can be seen from

$$H_2(z(t)) = z(t)z(t) - E\{z(t)z(t)\}$$

$$= \int_0^\infty \int_0^\infty l_1(t_1)l_1(t_2)x(t-t_1)x(t-t_2)dt_1dt_2$$

$$- E\{\int_0^\infty \int_0^\infty l_1(t_1)l_1(t_2)x(t-t_1)x(t-t_2)dt_1dt_2\}$$

$$= \int_0^\infty \int_0^\infty [l_1(t_1)l_1(t_2)x(t-t_1)x(t-t_2)$$

$$- E\{l_1(t_1)l_1(t_2)x(t-t_1)x(t-t_2)\}]dt_1dt_2$$

$$= \int_0^\infty \int_0^\infty l_1(t_1)l_1(t_2)[x(t-t_1)x(t-t_2) - E\{x(t-t_1)x(t-t_2)\}]dt_1dt_2$$

$$= \int_0^\infty \int_0^\infty l_1(t_1)l_1(t_2)H^{[2]}(x(t-t_1),x(t-t_2))dt_1dt_2$$

The static-nonlinearity can be expanded as a single-variable Hermite polynomial whose mutually orthogonal terms are:

$$N(z(t)) = c_0H_0(z(t)) + c_1H_1(z(t)) + c_2H_2(z(t)) + \ldots$$

where, by Parseval's:

$$c_n = (1/(P^n n!))E\{N(z(t))H_n(z(t))\} \quad \text{(Sakuranaga } \textit{et al.}\text{, 1986)}$$

$$z(t) = \int_0^\infty l_1(t_1)x(t-t_1)dt_1$$

An analytic form for the 1st order part of the response results from treating the 1st order term of N(z(t)) as the input to the post filter, L_2:

$$y_1(t) = \int_0^\infty l_2(t_1)\{c_1 H_1[z(t-t_1)]\}dt_1$$

$$= \int_0^\infty l_2(t_1)\{c_1 H_1[\int_0^\infty l_1(t_2)x((t-t_1)-t_2)dt_2]\}dt_1$$

$$= \int_0^\infty l_2(t_1)\{c_1 \int_0^\infty l_1(t_2)H^{[1]}[x((t-t_1)-t_2)]dt_2\}dt_1$$

$$= c_1 \int_0^\infty \int_0^\infty l_2(t_1)l_1(t_2)x(t-(t_1+t_2))dt_2dt_1 \quad \text{let } \tau = t_1 + t_2, \text{ then}$$

$$= c_1 \int_0^\infty [\int_0^\infty l_2(\tau-t_2)l_1(t_2)dt_2]x(t-\tau)d\tau$$

$d\tau = dt_2$ as t_1 is held constant over that integral

But, $y_1(t)$ is only $G_1[h_1;x(t)]$, and by comparison with the equation for $G_1[h_1;x(t)]$ (appendix C-i), $h_1(\tau) = \int_0^\infty l_2(\tau-t_2)l_1(t_2)dt_2$.

Similarly, for the 2nd order part of the response the 2nd order term of N(z(t)) is treated as the input to L_2:

$y_2(t)$

$$= \int_0^\infty l_2(\tau)\{c_2 H_2[z(t-\tau)]\}d\tau$$

$$= \int_0^\infty l_2(\tau)\{c_2 H_2[\int_0^\infty l_1(t_1)x((t-\tau)-t_1)dt_1]\}d\tau$$

$$= \int_0^\infty l_2(\tau)\{c_2 \int_0^\infty \int_0^\infty l_1(t_1)l_1(t_2)H^{[2]}[x(t-t_1-\tau)x(t-t_2-\tau)]dt_1dt_2\}d\tau$$

$$= c_2 \int_0^\infty l_2(\tau)\{\int_0^\infty \int_0^\infty l_1(t_1)l_1(t_2)[x(t-t_1-\tau)x(t-t_2-\tau)-P\delta(t_1-t_2)]dt_1dt_2\}d\tau$$

$$= c_2 \int_0^\infty l_2(\tau)\{\int_0^\infty \int_0^\infty l_1(t_1)l_1(t_2)x(t-t_1-\tau)x(t-t_2-\tau)dt_1dt_2$$

$$-\int_0^\infty \int_0^\infty l_1(t_1)l_1(t_2)P\delta(t_1-t_2)dt_1dt_2\}d\tau \qquad \text{let } \tau_1 = t_1+\tau \quad \tau_2 = t_2+\tau$$

$$= c_2 \int_0^\infty \int_0^\infty [\int_0^\infty l_2(\tau)l_1(\tau_1-\tau)l_1(\tau_2-\tau)d\tau]x(t-\tau_1)x(t-\tau_2)d\tau_1d\tau_2$$

$$-P\int_0^\infty [\int_0^\infty l_2(\tau)l_1(\tau_1-\tau)l_1(\tau_1-\tau)d\tau]d\tau_1$$

But, $y_2(t)$ is only $G_2[h_2;x(t)]$, and by comparison with the equation for $G_2[h_2;x(t)]$, $h_2(\tau_1,\tau_2) = \int_0^\infty l_2(\tau)l_1(\tau_1-\tau)l_1(\tau_2-\tau)d\tau_1d\tau_2$.

Some very useful consequences result from modelling a nonlinear system via fits to its Wiener kernels, $h_n(\tau_1,\tau_2,..,\tau_n)$. First, two or more kernels can be fit simultaneously to improve accuracy. But more importantly, only the linear filters, $L_1(w)$ and $L_2(w)$, are characterized through such fits, since the nonlinear terms, c_1 and c_2, are absorbed as scaling factors. This can reduce significantly the number of parameters to be fit. In addition, no *a priori* assumptions need be made about the form of the nonlinearity. Later, the nonlinearity can be characterized by fits to the actual system response; after the linear parameters have been defined fairly well.

iv). A Model of C Cells Applying the L_1-N-L_2 Sandwich

ON- and OFF-bipolar contacts are presumed to provide the principal inputs to the transient C cells. The anatomical sketch of fig. 21a depicts the transient cell as receiving parallel inputs from ON- and OFF-bipolar pathways. Fig. 21b shows a proposed circuit architecture which is considered to be the electrical analog of the retinal anatomy and physiology. Each of the parallel pathways representing bipolar inputs serves as a separate linear filter of the initial light input - L_1^{on},L_1^{off}. The interaction of each of these pathways with the amacrine cell is represented by two parallel static-nonlinearities which intervene between bipolar terminals and post-synaptic ligand-gated conductances, g_{on} and g_{off}. Finally, linear filtering (L_2) occurs post-synaptically in the amacrine cell membrane, acting on the summated effects of the convergent bipolar inputs.

Based on this scheme, analytic forms for the 1st order kernel and the diagonal of the 2nd order kernel of the amacrine cell can be predicted (appendix C-ii, see Methods). Basically, the representation of the Wiener functionals for the parallel path circuit of fig. 21b simply involves the summation of two Wiener functionals - one for each pathway - that each correspond to a L_1-N-L_2 sandwich. An analytic function used in the model for the bipolar cell 1st order kernel was obtained by fitting the Fourier transform of the experimentally measured ON-bipolar kernel with a quotient of polynomials in $i\omega$ of the form B_1^{on} (appendix C-iii; fig. 22a). A corresponding B_1^{off} was presumed to have a similar analytic form, but opposite polarity. L_1^{on} and L_1^{off} consist of a cascade of B_1^{on} with B_2 and B_1^{off} with B_2,

respectively. B_2 is a lead-lag filter designed to represent pre-synaptic filtering in the bipolar terminals and, for simplicity, is treated as identical along each pathway (appendix C-iii).

The 1st and 2nd order kernels were used in the present study to test the feasibility of the postulated circuit achitecture for transient cells (fig. 21b). In this regard, the kernels served as templates to optimize the parameters on the computer and initially assess the merit of the amacrine cell model. Subsequently, more rigorous evaluation of the model involved fitting of the actual response of the C cells to white noise and step inputs.

Parameter adjustment of the τ's to simultaneously fit both the 1st order kernel (fig. 24a) and the diagonal of the 2nd order kernel (fig. 24b, fig. 23 for orientation) was accomplished by the simplex method (NAG subroutine - E04CCF). The weighting of importance of the diagonal fit over that of the 1st order fit was set at one to one. While the relative power contributed by the 2nd order kernel to the cell response can be up to six times that of the 1st order kernel, very significant features are conveyed in the 1st order kernels that often can serve as more important constraints in guiding the numerical algorithm to the most appropriate solution. Therefore, the fit of the 1st order kernel was given significantly more weight than its relative contribution to the response power of the cell. The fits to the kernels were evaluated both in the time and the frequency domain, weighting particular portions of each. Placing emphasis on early events in the time domain fits while eliminating certain bands for the frequency domain fits allowed the algorithm consistently to converge to good fits of the kernels. Then, using the best-fit parameters, predicted

slices for the 2nd order kernel (generally at 34 msec and 66 msec) were generated and compared to data as a further check of the model (fig. 24c,d, fig. 23 for orientation). A good match of the generated slices with the actual kernel slices provided strong indication that the filter parameters obtained from fits of the 1st order kernel and diagonal of the 2nd order kernel subsequently were able to reconstruct the entire 2nd order kernel.

While fitting the kernels can specify the filter parameters of the model, such fits cannot provide sufficient information on the parameter values of the intervening static-nonlinearity, especially for complex functions containing nonlinearities of order greater than two. Therefore, fits of the model to actual time series responses of the C cells are necessary in order to characterize the parameters of the static-nonlinearities in this model. For the kernel fits, the nonlinearity is absorbed as a scaling factor and, hence, obscured by the other scaling factors. As a consequence, a change in the form of the static-nonlinearity results in a scaling adjustment of the kernels. It does not result in a change of shape of the kernels. In a L_1-N-L_2 model, adjustment of the filter parameters is necessary for shape changes to occur.

For the time series fits, the scaling factors of the linear filters are absorbed as part of the function which represents the static-nonlinearity. Quartic Hermite polynomials were the functions used for most of the time domain fits. Since the input to the polynomials was a filtered version of a Gaussian input, which is also Gaussian, the choice of Hermite polynomials (which are orthogonal for Gaussian inputs) is reasonable. Occasionally some other functions such as saturating exponentials or rectifier functions were employed (Appendix C-iii).

The filter parameters obtained from the Wiener kernel fits were initially treated as constrained variables of the model for time domain fits involving white noise inputs. The C cell response used in the model fits was filtered to remove DC and frequencies greater than 50 Hz.[4] This obviated the need to include a constant coefficient as part of the quartic polynomials since such a term would only contribute to the DC component of the response. Thus, a reduction in the number of parameters was achieved. Once an adequate solution for the static-nonlinearity was achieved, the filter parameters were allowed to vary while the parameters of the static-nonlinearity were held fixed. Then, the static-nonlinearity was allowed to vary while the new values for the filter parameters were held fixed. This boot-strap process was repeated until convergence to the best solution occurred. Eleven filter parameters and eight static-nonlinearity parameters are contained in the model. Allowing all nineteen parameters to vary at once would have reduced greatly the efficiency of the numerical algorithm and, hence, the alternate boot-strap approach was used. Fixing all the parameters, additional white noise and step stimuli were used in order to verify that the model could predict the response of C cells to novel time series inputs.

Attempts were made to reduce the mean square error by treating the amacrine cell membrane in a more realistic manner. So far the model has corresponded to the circuit architecture of fig. 21b. A more accurate portrayal of the amacrine cell membrane is in fig. 21c. Fig. 21b is a linearized version of fig. 21c and

---

[4]No filtering was done on the white noise input, nor on cell responses to step inputs.

corresponds to the circuit of fig. 21c if the two variable conductance pathways involving g_{on} and g_{off} are replaced by current sources. For example, assuming the C cell voltage fluctuates around zero, Kirchoff's current law for the circuit of fig. 21c gives

$$C\frac{dV_{ama}}{dt} + \frac{V_{ama}}{Z} + g_{on}\cdot(V_{ama}-E_{on}) + g_{off}\cdot(V_{ama}-E_{off}) = 0.$$

If the fluctuations in g_{on}, g_{off} and V_{ama} are small then

$$g_{on} \approx \epsilon\cdot g_{on}', \quad g_{off} \approx \epsilon\cdot g_{off}', \quad \text{and } V_{ama} \approx \epsilon\cdot V_{ama}'$$

which gives after substitution, division by ϵ and letting $\epsilon \rightarrow 0$

$$C\frac{dV_{ama}'}{dt} + \frac{V_{ama}'}{Z} + g_{on}'\cdot(-E_{on}) + g_{off}'\cdot(-E_{off}) = 0.$$

This is a linear differential equation with current source $g_{on}\cdot(-E_{on})$ along one parallel branch and current source $g_{off}\cdot(-E_{off})$ along the other. Thus, the current source approximation corresponds to the physical situation in which the fluctuations in voltage and conductances are small. Models that employed the differential equation for the full nonlinear representation are applicable to a broader range of inputs.

Another adaptation of the original L_1-N-L_2 model was to include another nonlinearity, N_2, consisting of a quadratic polynomial after the L_2 filter. This constitutes a L_1-N_1-L_2-N_2 model. The model includes parallel paths through N_1, but a single path thereafter. While the physiological relevance of the additional nonlinearity is not well defined, N_2 may endow some features characteristic of voltage gated properties to the model and represents a preliminary move in that direction. For example, the adaptation to the sandwich model would offer more flexibility and

sharpness to the response peak heights, qualities often attributed to voltage gated behavior.

V. RESULTS

A. EXPERIMENTAL

1. C CELLS

I recorded from twenty-six C cells in the eye-cup preparation of the catfish (Table 1); eleven in conjunction with extracellular recordings from ganglion cells. Primarily, intracellular results will be discussed. An example of an intracellular recording from a C cell responding to white noise light inputs of constant mean but at three different variance levels is shown in fig. 25 (along with the responses of a NA, a NB, and a horizontal cell for comparison). Corresponding distribution functions of the responses from the four cell types are also included. Note that the amacrine cells are able to adjust their sensitivity relative to the modulation depth whereas the horizontal cell cannot. Comparison of the horizontal response distribution with the distributions from the C, NA, and NB cells of the inner retina is very revealing. This contrast gain phenomenon is not observed in intracellular recordings from outer plexiform cells including horizontal and bipolar cells (Sakai & Naka, 1987b), whereas it is quite prominent in the amacrine and ganglion cells of the inner retina. Both the 1^{st} order kernel and 2^{nd} order kernel diagonals of C cells (calculated from white noise records) demonstrated marked changes in shape, amplitude, and kinetics with the adjustment in depth of modulation (*e.g.* fig. 29a,b).

The 1st order kernel, which would usually account for between 5% to 25% of the cell's response across different modulation levels, was highly variable in shape both between cells at the same modulation depth and within the same cell at different modulation depths. For some cells, the 1st order kernel would appear to change only its shape but maintain roughly the same amplitude with each new modulation level (*e.g.* fig. 32a), whereas for other cells the 1st order kernel would maintain a similar shape but demonstrate a continual and proportional increase in amplitude as modulation depth decreased (*e.g.* fig. 35a). Yet other cells showed a blend of these two possibilities (*e.g.* fig. 36a). There was no instance for a C cell where the 1st order kernel was invariant - without change in shape or amplitude - across modulation levels (as has been observed for cells in the outer retina such as the horizontal and bipolar cells) (fig. 25).

A general trend observed across all C cells was that the 1st order kernel would appear more OFF-bipolar in character at lower modulations (*e.g.* fig. 40a). With decreasing modulation level, the transition from a bicuspid negativity (with the first negativity at around 30 msec and the second at 50 msec) to a larger single negativity at near 50 msec (with the disappearance of the first negativity) was a frequent observation among cells (*e.g.* fig. 40a). In general, the peak response time of the 1st order kernels was between 30 and 40 msec but slowed with decreasing modulation level. For those 1st order kernels that tended to scale their amplitude without much change in shape, the peak response was consistently found to show a gradual slowing by five to eight msec as the modulation level was changed to lower levels (*e.g.* fig. 35a).

MSE's almost universally decrease for the 1st order kernel contribution as modulation depth decreases as seen by Table 1 (indicating greater linearity at lower modulation levels). The cell of fig. 32 is a remarkable exception in that there was a gradual rise from an MSE of 79% at highest modulation to 90.3% at the lowest modulation, but this can probably be attributed to the highly unusual shape of this kernel at low modulation, including oscillatory features that will be described below. The cell of fig. 42 is more typical as its MSE for the 1st order kernel went from 93% at the highest modulation level to 71% at the lowest. In a few instances, the MSE did not decrease monitonically but actually increased at the second highest modulation level before decreasing as one proceeded to lower modulation levels. The cell in fig. 41 is a good example; with decreasing modulation, the MSE went from 86.6% to 95.4%, finally having a value of 77.6% at the lowest modulation level. This progression paralleled the transition in 1st order kernel shape from an ON-bipolar shaped kernel, to a more-bicuspid structure, then to an OFF-bipolar form at the lowest modulation. While making the assertion that the C cell becomes more OFF-like at lower modulations is difficult since the 1st order kernel usually only accounts for 10-20% of the response power (and the 2nd order kernel will not help distinguish ON from OFF as a result of squaring), the step response of C cells does show a much stronger response to step offset than onset at lower step heights (*e.g.* fig. 40c).

The 2nd order kernels of C cells showed much less variablity in shape for different modulation depths. Instead, a smooth scaling in amplitude of the kernels was observed that was roughly inversely proportional to the modulation level of the

light input. The basic shape of these kernels was a three- or four-eyed symmetric structure (fig. 23). The diagonal of the four-eyed kernels places the two positive peaks at approximately 35 and 55 msec, consistent with a frequency doubling property of a squarer device applied to a biphasic bipolar input (fig. 33c). Note that the diagonal completes a full cycle with two peaks for the one bipolar peak. This frequency doubling property is seen in the frequency domain of the 2nd order kernel diagonal as a sharp peak from 20 to 40 Hz (*e.g.* fig. 29c).

A very intriguing phenomenon that sometimes became apparent in C cell kernels at low modulation levels was the emergence of oscillations. They were observed in 12 of the 26 cells and, in the cells that showed oscillations, they became more conspicuous at the low modulation levels (fig. 33a, fig. 32a, fig. 35a, fig. 43a). These oscillations generally occurred later along the time axis (after 55 msec); after the response peaks that occurred at higher modulation levels. Occasionally, the oscillations appeared to ride on a depolarizing plateau (fig. 36a).

Oscillations tended to be more striking in the 1st order kernel than in the diagonal of 2nd order kernel (fig. 33a,b). Sometimes, oscillations were prominent in both 1st and 2nd order kernels (fig. 34a,b). In two instances, they were more evident in the 2nd order kernel diagonal (fig. 29a,b; fig. 31a,b). The 2nd order kernels that tended to demonstrate oscillations also tended to account for much less of the response power (approximately 15% to 20%) than the normal power contribution of 40-50% attributed to them, especially at higher modulation depths. Only one C cell with a 2nd order kernel power contribution in the amount of 30% demonstrated oscillations, demonstrating them in both the 1st and 2nd order kernels. Notably,

ganglion cells from the same retina showed significant spontaneous firing at both a dark and a mean level of luminance (retinas whose ganglion cells demonstrate a strong degree of spontaneous firing are also disposed to robust oscillations as observed intracellularly - see discussion). Excluding this exceptional C cell (fig. 43a,b), the other eight cells that had oscillations in the 2nd order kernel generally showed the amplitude of these oscillations to be small for 2nd order kernels with large power contributions. Along the diagonal of the oscillatory kernels, the initial two peaks attributed to frequency doubling were separated by approxiamtely 20 msec (at 35 and 55 msec), whereas the subsequent peaks after 55 msec were separated by 30 to 35 msec (fig. 29b).

The oscillation was generally evident as a 30 Hz peak in the frequency domain of the 1st order kernel. This was quite conspicuous in the power spectrums of 1st order kernels which normally do not show such a peak at the higher modulation depths (fig. 33d). For the Fourier transform of the diagonal of 2nd order kernels, the peak observed at 20 to 40 Hz (attributable to the squaring property applied to the bipolar inputs) may obscure a 30 Hz oscillatory peak in the frequency domain (fig. 29c). However, oscillations are observed occasionally at twice the usual 30 Hz frequency. Fig. 36c shows the emergence of a sharp peak at 60 Hz in the frequency domain of a 2nd order kernel diagonal at low modulation level. As can be seen in the time domain, this 60 Hz peak occurred along with and in-phase (or precisely out-of-phase) with a more dominant oscillation at half its frequency (fig. 36a,b).

Another phenomenon that became apparent in kernels at low modulation levels was a strong, broad depolarization hump (often with double dimples) that

began to appear in the kernels (usually the 1st order kernel) at 70-80 msec (fig. 38a, 37a). These broad depolarizations had a duration of 30 to 40 msec and were often preceded by a hyperpolarizing peak response at around 50 msec. The humps were not apparent at the highest modulation depth but became more apparent at each successive modulation decrease, apparently scaling their amplitude inversely to the decrease in modulation depth. The humps were quite common. In fact, humps occurred in all the cells which did not display oscillatory behavior (14 of 26 cells), implying that the one phenomenon may have precluded somehow the occurrence of the other. Table 1 comments on which cells demonstrated the oscillations (O) or the hyperpolarizations followed by depolarization plateaus (H).

2. NA AND NB CELLS

Seven NA and NB cells were analyzed for comparison with C cells with respect to the contrast gain effects at different modulation depths. Much less variation in shape of the kernels was observed with adjustment of modulation depth. Instead, a smooth and progressive scaling increase in amplitude is seen with decreasing levels of modulation. This scaling was more pronounced for some peaks of the 1st order kernel and the diagonal of the 2nd order kernel. In particular, the peak at around the 60 to 70 msec mark was much more profoundly increased for a given drop in modulation depth than the other peaks. For both the 1st and 2nd order kernels, this involves a negative peak for the NA cells and a positive peak for the NB cells (fig. 47a,b; fig. 48a,b; respectively).

The 2nd order kernel diagonal invariably had oscillations after the more pronounced 70 msec peak. In fact, these oscillations became quite pronounced at lower modulations in a similar manner as was observed for the C cells. Unlike the C cells, the oscillations along the diagonals were observed in all the N cells and were much more pronounced. They occurred much less frequently in the 1st order kernels. This is the reverse of what was observed with the C cells, whose oscillations tended to be more pronounced in the 1st order kernels. Interestingly, whereas the 1st order kernel generally accounts for between 5-25% in C cells (maybe more at the lowest modulation level), the 1st order kernel in N cells can account for 50% or greater of the cell's response. Conversely, whereas the 2nd order kernel in C cells can account for up to 60% of the C cells response power, it generally accounts for no more than

25% with the N cells. The N cell oscillations were about 30 Hz with a peak to peak time of approximately 30 msec.

3. SPIKE AND WAVE DISCHARGES FROM GANGLION CELLS THAT FIRE SPONTANEOUSLY

During many of the intracellular recordings made in cells of the inner retina, simultaneous extracellular recordings were made from ganglion cells. Occasionally, a spontaneous firing ganglion cell was detected. Extracellular recordings are much more reliable for recording meaningful spontaneous activity than intracellular recordings. Intracellular spontaneous activity would often result from cell injury during the impalement and, consequently, had limited physiological relevance for the study of normal retinal function. The catfish retina has notable spontaneous activity that has been observed intracellularly in amacrine cells and ganglion cells, primarily in the form of oscillations at 30 Hz. It was uncertain whether the oscillations were conveyed to the ganglion cells and communicated by them as spike discharges. Spike discharges may be an important force driving oscillations via the feedback from ganglion cell dendrites to C cells, and analysis of interspike intervals is a preliminary attempt to help clarify if the pattern of spontaneous spiking behavior is consistent with such a role.

When a spontaneous firing ganglion cell was encountered, the spike train was recorded for a few minutes both at a mean level of light and in darkness before preceding to time-variant light stimuli. The spontaneous firing cell was categorized as a GA, GB, or GC based on its response to steps inputs from darkness. Spontaneous firing GB cells (n=14) were encountered more often than GA cells (n=5); spontaneous GC cells were infrequently encountered (n=1). It is uncertain

why GB cells (regardless of whether they fired spontaneously) were encountered more frequently than GA cells. Perhaps, they are more numerous; the catfish retina has been characterized as an OFF-dominant retina (Sakai & Naka, 1987a).

Fig. 52 and 53 show interspike interval histograms from two of the GA cells both at mean levels and in darkness. One of the cells (fig. 52) demonstrates robust spiking at mean levels and in darkness. The histogram for this cell shows a narrow distribution of interspike intervals with a peak at 26 msec for both mean and dark levels. This interval corresponds to a frequency of approximately 38 Hz. The histogram for the other GA cell (fig. 53) has a much broader distribution both at a mean and in dark, but especially at a mean luminance. The peak of the histogram in darkness was at 34 msec (29 Hz) and at a mean background was 50 msec (20 Hz). Interestingly, a smaller peak was observed for this cell in darkness at around 13 msec. This smaller early peak was often observed in other cells as well.

Fig. 54 shows one of the more defined histograms obtained from the spontaneous activity of a GB cell. In darkness, a dominant interspike interval of 25 msec corresponding to 40 Hz is observed as well as shorter interspike interval peak at 8 msec. The histogram for this cell becomes ill-defined at mean light levels. Fig. 55 shows a more typical histogram for GB cell spontaneous activity. No clear interval peak is apparent in the histogram of this cell under either mean or dark levels. In general, the GB cell histograms showed fewer and much more random spontaneous spiking events than the GA histograms. On the contrary, the GA cells showed more organized and robust spiking near a firing frequency of 30 Hz, especially in darkness.

Spontaneous activity was also recorded intracellularly. In one notable case involving a very steady recording from a C cell, spontaneous depolarizations occurred at a rate of 2-3 per second and with fixed amplitude at both mean and dark levels (fig. 37d). The very stable baseline of the recording suggests that the spontaneous depolarizations cannot be attributed to noise. Furthermore, the discrete nature of the magnitude of these depolarizations is consistent with an excitatory input from a spontaneously spiking ganglion cell. The duration of approximately 300 ms for these wave potentials makes it unlikely that the spontaneous depolarizations represent action potentials in a damaged GC cell.

B. THEORETICAL

Although the incorporation of two bipolar pathways in the model does increase the number of parameters, the inclusion of ON- and OFF-bipolar inputs to C cells is well supported by numerous sources. For example, injection of depolarizing current pulses into ON- or OFF-bipolars of the carp retina is excitatory to transient cells at the onset of the pulse, but no response is observed at the offset (Kujiraoka *et al.*, 1988). Similar results are reported by Sakai for catfish (personal communication). In experiments which reduce the contribution from ON-bipolars to third order neurons, the ON-response of transient ON/OFF cells to light steps was also greatly reduced or absent. For instance, the use of APB or chloride free medium, both of which inactivate the ON-pathway, abolished the ON-response in transient cells in the rabbit and mudpuppy retinas, respectively (Bloomfield & Dowling, 1985; Masland *et al.*, 1984; Miller & Dacheux, 1976). And, light step inputs that were below the threshold of the ON-pathway but did activate the OFF-pathway only activated the OFF-component of transient cell step responses in mudpuppy (Frumkes & Miller, 1979). Furthermore, in the present study, while the 2^{nd} order kernel has been successfully fit assuming one type of bipolar input, bicuspid 1^{st} order kernels were not able to be fit without parallel inputs from both ON- and OFF-bipolar inputs. These findings are all consistent with the anatomy of the transient cells which have processes that extend to sublamina a and sublamina b (Kujiraoka *et al.*, 1988).

With respect to the filter components, only B_1^{on} was justified by a direct comparison with actual data from cell responses (fig. 22a). The other circuit

components such as B_2 and L_2 cannot be measured directly and have to be justified by other means.[5] Good evidence exists to support the presence of L_2 in the model. First, there is a negativity at 80 msec following the two peaks of the 2nd order diagonal (fig. 24b). Other transient cells often demonstrate this as well. As the bipolar cell contribution to the equation for the diagonal is squared (appendix C-ii), it cannot account for this negativity. In addition, the L_2 obtained from curve fits shows strong DC pass features (fig. 24h) and matches the experimental observation that sustained responses occur in C cells after current injection into the amacrine C cell syncitial layer (Naka & Christensen, 1981).

B_2, the bipolar presynaptic filter, is justified primarily by the observation that little if any DC from a voltage displacement induced in an ON-bipolar cell is preserved in the amacrine response. This is in agreement with the 1st order kernel of the amacrine cell which has little power at 0 Hz (fig. 24e). B_2, then, is deemed necessary to allow the bipolar filters, L_1^{on} and L_1^{off}, to be no-pass at 0 Hz, despite the fact that B_1^{on} and B_1^{off} have been observed to pass DC (fig. 22b). L_2 cannot be responsible for the lack of DC passage observed in amacrine cells by our model; the diagonal of the 2nd order kernel, which involves a convolution with L_2, does not have a time integral equal to 0 (fig. 24b).[6] The findings of Kujiraoka *et al.* (1988) that -

---

[5]Refer to fig. 21 for the circuit representation and to Appendix C-iii for the analytic forms of B_1^{on}, B_1^{off}, B_2, L_1^{on}, L_1^{off}, L_2.

[6]If L_2 equalled 0 at $\omega=0$, then the Fourier transform of $d(t_1)$ (call it $D(\omega)$) involves a convolution with L_2 (see Appendix C-ii) and also equals 0. Using the transform theorem (see Methods - Fourier analysis) gives:

$D(\omega) = \int_{-\infty}^{\infty} d(t_1)\exp(i\omega t_1)dt_1$ which for $\omega=0$ would give

$0 = \int_{-\infty}^{\infty} d(t_1)dt_1$.

This is not observed, so L_2 cannot equal 0 at $\omega=0$.

after blocking synaptic transmission - transretinal current pulses could elicit sustained responses in the transient cells of the carp, and the results from Naka & Christensen (1981) that the amacrine syncitium exhibits low pass behavior, further support the contention that the transient behavior of C cells does not emerge from the membrane properties of the transient cells themselves. These observations and the analytic form obtained for L_2 place the existence of a high-pass filter after B_1^{on} but before the convergence of the parallel paths at the C cell membrane. In fact, it is not unreasonable that some filtering should occur in the bipolar cell presynaptic terminals. Physiological correlates of B_2 might include the GABAergic effects at the bipolar presynaptic terminals on Ca^{++} influx that result in the transient release of transmitter despite persistent depolarization (Maguire *et al.*, 1989b). Thus, B_2 can represent high-pass signal processing in the bipolar cell that is not detectable by microelectrode recording. In this way, B_2 can account for effects of N amacrine cells on bipolar terminals while still preserving the simple parallel structure of the model. Filtering due to cable conduction as the signal spreads to the pre-synaptic dendrites could be accounted for by B_2 as well.

The 1st and 2nd order Wiener kernels and time-series responses of twenty-two of the twenty-six cells were analyzed with the L_1-N-L_2 model. The model achieved variable degrees of success depending on the particular cell and the modulation level of the light input. In general, the model worked well at high modulations, but performed progressively more poorly as the modulation level was decreased. The filter parameters determined from model fits of the twenty-two cells at light modulation level 1 (highest) are tabulated in Table 2a and 2b. Table 3a and 3b show

the parameter values from three cells for which the model performed well at lower modulations as well.

Fig. 29d-i shows the fits to the 1st order kernel and 2nd order kernel diagonal at the highest modulation level (1) and, for comparison, at the lowest modulation level (4) (fig. 29d-ii). In addition, the predicted slices, which were generated from the parameter values that optimized the fits to the 1st order kernel and diagonal, are shown. At the highest modulation level, the fits are quite good to the 1st order kernels and diagonals, and the predicted slices match quite well with the actual slices of the 2nd order kernel. However, at low modulation, while the fit to the 1st order kernel is passable, the fit to the diagonal is extremely poor, especially after 60 msec. The predicted slices are also very poor. In general, the model was inadequate at fitting many features of the kernels, such as oscillations, that had a relatively late appearance and long duration.

The fits of the model to responses of C cells to white noise inputs provide a more quantative and complete means of assessing the utility of the model based on its Mean Square Error (MSE) performance. At high modulation levels, the model surpassed the fits to white noise responses by the 1st and 2nd order Wiener kernels (with the exception of one cell). Whereas the average MSE for twenty-one C cells was 42.2% for the 1st and 2nd order Wiener kernel contributions, the model of the form of fig. 21b had an average MSE of 34.5% for those same twenty-one cells. This yielded an average improvement of 7.7%. As the modulation level was decreased, however, the model provided smaller and smaller improvements over the kernel contributions; dropping from the 7.7% average improvement at the highest

modulation level to a 4.0% improvement at the next level, then to an average improvement of 2.9% at the third highest level. Finally, in those cells that had recordings that were long enough to include a fourth decrease in modulation, the model dropped to a performance that was worse by 5.2% than the kernel contributions to the cell response.

Since the model provided variable results depending on the cell and white noise modulation level, it was important to establish criteria by which to assess the success of the model. Otherwise, the outcome of the model for a cell that was chosen inadvertently and inappropriately could lead to misleading conclusions from the model results. One important standard for screening involved the exclusion of cells that demonstrate prominent late occurring features in their kernels such as oscillations. Several criteria were used to assess the success of the model in individual cells which lacked significant late features in their kernels. First, the model achieved small MSEs for acceptable cells, signifying that the model could successfully emulate the response of the C cell. Also, the identical filter and static-nonlinearity parameters that were obtained from optimization fits on one four second segment of time series data yielded good fits when applied, without the flexibility for further parameter adjustment, to other white noise segments and step inputs. Thus, the model could successfully predict responses in new time series segments for these cells. Finally, the same filter parameters optimized from time series fits subsequently were able to fit the 1^{st} order kernel and 2^{nd} order kernel diagonals and slices with good success. Previously, the fits of the model to the kernels were used to obtain the

initial value settings of the filter parameters for the time domain fits. The reverse procedure provided an additional check on the model.

Although the average improvement of the model over the kernel contributions was 7.7% at high modulation levels, for some cells, using the criteria above, the model demonstrated substantially greater success. For example, in the cell whose kernels are shown in fig. 46a,b, the MSE of the model was 17.7% as compared to 35.3% based on kernel contributions. Thus, the model provides nearly a 20% improvement over the MSE that was derived from the empirically determined 1st and 2nd order kernels. The 1st and 2nd order kernel diagonals and slices are shown with the matching model fits in fig. 46c for this cell. The same parameters that were optimized to give the MSE of 17.7% over one time-series data segment gave a MSE of 22.5% over another adjacent time segment. The fit of the model to the time series response of the C cell to white noise light input is shown in fig. 46g. The fit is quite good. Especially notable is the accomplishment of the model with respect to the excellent phase alignment that occurs between the model peaks and those of the actual response. The shortcoming of the model appears to reside with the mismatches of the model and response peak heights, and this was usually evident as an undershooting by the model. The implication, then, is that the model does well at replicating the kinetics of the C cell response but is deficient somehow in generating the correct magnitude of the peak responses.

The 1st order kernel of the C cell of fig. 46a has a striking resemblance to an OFF-bipolar cell impulse response (fig. 46d). In fact, the 1st order kernel of the C cell was accounted for in the model primarily by the OFF-bipolar pathway (fig. 46d

shows ON and OFF contributions). A small amount of cancellation between pathways occurs with the 1st order kernel in this instance. The 2nd order kernel diagonal, however, consists of contributions from both ON- and OFF-pathways, based on the 2nd order contributions from their respective static-nonlinearities (fig. 46d).

Results of the model fits suggest differences between the ON- and OFF-bipolar inputs to C cells. First, the ON-bipolar impulse response of the model has a peak response time that is significantly later, by about 6 msec, than that of the OFF-bipolar pathway (fig. 46e). Also, the ON-bipolar impulse response is more biphasic than the OFF-bipolar impulse response. The more biphasic nature of the ON-pathway is also evident by the model's attempt to allocate a greater portion of the fit of the second peak along the diagonal to the ON- inputs (fig. 46d). This tendency for the ON-bipolar path to be more latent and more biphasic than the OFF-bipolar path is seen in other cells as well (fig. 39e, 38c). For example, even though the cell of fig. 32 has a 1st order kernel that shows strong ON-dominance, the model indicates that the peak response of the ON-bipolar input lags that of the OFF-pathway by about 7 msec (fig. 32e). The greater latency for ON-bipolars is consistent with the findings of Frumkes and Miller (1979) previously discussed.

As a further challenge, the model was tested with step inputs at the same mean as the white noise input of fig. 46g. The same filter and static-nonlinearity parameter settings that were optimized by fits to the white noise signal were held fixed and applied to various step heights. Fig. 46h shows the predicted response of the model to various step heights as compared to the actual responses of the cell. With fairly good success, the model was able to predict the response of the cell to

both step increments and step decrements. The ability of the model to effectively predict the response of the cell often depended greatly on the height of the step input. For example, fig. 32g shows the predicted responses when the same parameter settings of a model were applied to different step heights. Very different degrees of success were seen in the outcomes for each step height. The dependence of the fit on the step height tends to underscore the highly nonlinear nature of these cells and the importance of the relation between the light input (with respect to features such as modulation depth) and the functional adjustment of the model settings.

The static-nonlinearity generated by the model for the cell of fig. 46f had many distinct features. Along the ON-pathway, a polyphasic polynomial displays strong even-order components to its shape. On the contrary, the OFF-pathway for this particular cell is much more odd-order in appearance, which may explain the strong OFF-bipolar nature of the 1st order kernel for this C cell.[7] By comparison, fig. 34d shows the static-nonlinearities from a cell in which both the ON- and the OFF-pathways were polyphasic and very similar to each other in basic structure. Such complex polyphasic shapes to the polynomials were common among the model results for many cells (fig. 32f, fig. 39g), reflecting the nonlinear nature of the bipolar inputs to C cells. Interestingly, the polynomials show a region of diminished slope near the origin of the static-nonlinearity that represents a global minimum (fig. 46f(OFF), fig. 40g(OFF)), local minimum (fig. 46f(ON)), or point of inflection (fig. 40g(ON)).

---

[7]It should be noted that the endpoints of the abscissa correspond precisely with the span of input values into the static nonlinearity and do not exceed these values.

The kernels of the two C cells shown in fig. 39 and 40 (C Cells #2 and #3 of tables, respectively) were among the few that demonstrated good fits to the model at several modulation levels (fig. 39d-i,ii,iii; fig. 40d-i,ii,iii,iv).[8] Both these cells incidentally had bicuspid shaped 1st order kernels. As a result, these cells were used to assess changes in model parameters that occurred with decreases in modulation depth. In both these cells, the OFF-bipolar input had a peak response time that was approximately 4 msec in advance of the ON-bipolar peak response time. In one C cell, this 4 msec lead was observed at three successive modulation level decreases (fig. 39e). In addition, each of these cells exhibited a slight slowing of both bipolar paths with decreasing modulation levels. For example, the model of the C cell of fig. 39f gave an ON-bipolar input whose peak response slowed down from 24 msec to about 28 msec, while the OFF-bipolar input showed a similar slowing in the peak response time from 21 msec to 26 msec. The model of the cell of fig. 40f also demonstrated a slowing in peak response time of both the ON- and OFF-bipolar inputs for identical decreases in modulation level; the ON-path slowing from 27 to 30 msec, and the OFF- from 24 to 27 msec.

A comparison in these cells of the static-nonlinearities of the ON- and OFF-pathways across different modulation levels revealed some important features of the model. Fig. 39g and fig. 40g show the static-nonlinearities for the ON- and OFF-pathways of the model of two C cells. The fits for the ON- and OFF-nonlinearities are shown at three different modulation levels for each cell. The shapes of the

---

[8]Table 3a and 3b show the filter parameters from model fits at three modulation levels for each of three C cells.

static-nonlinearities are very similar between the two different cells, consistent with the fact that these cells both had bicuspid shaped 1st order kernels.[9] The ON- and OFF-pathway nonlinearities both exhibit strong odd-order shapes, a common feature of C cells with bicuspid 1st order kernels. Also, both the ON- and OFF-nonlinearities show the plateaus near the origin at all modulation levels. However, whereas for the OFF-nonlinearity this plateau ressembles a saturation or rectification process for negative input values, the plateau appears more as an inflection point in the ON-nonlinearity. In fact, the ON-nonlinearity has a steep positive slope at both the positive and negative extemes of input, and, while a slight tendency towards saturation may occur at large positive inputs, no such tendency is observed for large negative inputs. Remarkably, with only slight modifications, the same basic form of the nonlinearities in both the ON- and the OFF-pathways is preserved at the three different modulation depths.

In some other cells (fig. 34d, fig. 32f), in which the static-nonlinearities were not as monotonic as these two cells, an interesting pattern occurs. At a lower modulation level, the static-nonlinearity of each pathway can be viewed as a smaller portion of the previous static-nonlinearity corresponding to a higher modulation level for the cell. In other words, a narrower and narrower segment centered around the origin is taken from an original curve corresponding to the static-nonlinearity at the

---

[9]These cells were also from the same retina and demonstrated somewhat slower kinetics than was seen in most of the other cell recordings. The possibility does exist that the preparation was aging and that the lack of notable feedback inputs from ganglion cells can be attributed to this. However, despite the slower kinetics, which was not that unusual, these cells exhibited strong physiology. In addition, after these two recordings, other healthy cell recordings were obtained from the preparation.

highest modulation level. The implication is that the actual apparatus responsible for the nonlinearity remains rather fixed and independent of the modulation level, but the inputs to that nonlinearity may decrease with lower modulation levels. Consequently, the input may sample less of the domain of the static-nonlinearity at low modulations. This does not signify that the gain of the inputs to the nonlinearity is decreasing at low modulations. It simply indicates that the gain is not increasing as much as the depth of the light input has decreased with the drop in modulation.

Some attempts were made to fit C cell responses with a refined version of the model that treated the amacrine cell more realistically as a membrane capacitive structure in parallel with variable conductances (fig. 21b). This model did not offer any significant improvement with respect to MSEs over the fits obtained by the linear-nonlinear-linear sandwich model. Other modifications, then, are required to account for the shortcomings of the sandwich model. One adaptation involved the inclusion of an additional static-nonlinearity to the parallel sandwich model to create a L_1-N_1-L_2-N_2 structure. It was speculated that perhaps such a structure would be better able to compensate for voltage gated properties and match the heights of the response peaks better. In fact, the L_1-N_1-L_2-N_2 model did improve the fit to C cell responses to white noise inputs, reducing the MSE from 33% to 26% in one cell (whose kernels are shown in fig. 38). This result suggests that some benefit may result from incorporating voltage gated properties into the model.

VI. DISCUSSION

A. EXPERIMENTAL

The variety of kernel shapes including oscillations, "humps", and other changes observed at different modulations makes the prospect of correlating a mechanism to the contrast gain phenomenon a formidable task. However, after careful analysis of these results and application of the circuit scheme of fig. 5e, a mechanism is proposed for the contrast effects recorded from the inner retina cells of the catfish retina.

A key feature of the circuit model of fig. 5e involves the convergence of two basic types of inputs onto C cells. The first type consists of direct centripetal input from bipolars: information in the outer retina is processed and conveyed to the inner retina. The second type of input on to C cells involves a feedback from other cells in the inner retina (presumed to be ganglion cells in the circuit schematic). Several results from the present study suggest the existence of such dual types of inputs. First, some of the C cell kernels clearly demonstrate additive properties. For example, some C cell kernels have features that indicate that they actually represent the summation of two quite distinct kernels. This is consistent with the premise that the C cell is a point of convergence for two different types of inputs. As the modulation level is decreased, the 1st order C kernels (*e.g.* fig. 33a, fig. 34a, fig. 35a) demonstrate the gradual emergence of a depolarizing peak at 60 to 65 msec followed by an oscillation. This newly emerging peak appears to be part of a waveform that

is added to a pre-existing kernel; its nature is not expected from a model of the C cell involving a single type of input (e.g. bipolar cells) whose kinetics merely have been adjusted with decreasing modulation depth.

The gradual emergence of this peak implies that there is an input to the C cell that becomes more pronounced at lower modulation levels. In all the cells in this study, the kernels adopted new forms such as oscillations and broad depolarizing humps, and these new features became more prominent as modulation level was decreased. The gradual emergence of entirely new and different features under different stimulus conditions also suggests that there are two different types of inputs to C cells that behave very differently. Many of the features that begin to appear at lower modulations appear late in the kernel. Oscillations and "humps" are not seen before 60 msec and may continue up to the 150 msec mark. Thus, it is inconsistent that such late features are due to direct bipolar inputs; bipolar cells are generally biphasic and have peak reponses between 30 and 40 msec with a subsequent reversal peak at around 55 msec. The late features, then, are probably attributable to feedback inputs which would involve more intervening synapses and a longer transit time.

The implications, therefore, are that direct bipolar inputs are the primary inputs at high modulation levels, but that at lower modulation levels, feedback inputs become important as well. This premise is in agreement with the result that a model of C cell responses involving only ON- and OFF-bipolar inputs was able to fit the early peaks (35 and 55 msec) of 1st and 2nd order kernels, but unable to contend with late features such as oscillations (fig. 29d-ii). This indicates that such a model is

inadequate at low modulation, and the primary deficiency probably resides in the need to incorporate a feedback input into the C cell.

The C cell response to direct input will have a time course similar to that of bipolar cells, with peaks at about 35 and 55 msec that reflect the roughly 20 Hz band-pass nature of bipolar cells. The three- or four-eyed structure of the C cell 2nd order kernels (fig. 23) is consistent with a model that includes some squaring of biphasic bipolar inputs. This is seen along the diagonal of the 2nd order kernel as a frequency doubling of the bipolar input with peaks at about 35 and 55 msec that are both positive (as opposed to the polarity reversal of the second peak one observes in bipolar cells themselves). This frequency doubling along the diagonal, with a peak to peak time of about 20 msec, can be seen in the frequency domain as a strong band at 40 Hz.[10] Thus, contributions from direct bipolar contacts can account for the four-eyed structure of C cells and can account for events that generally occur within the first 55 to 60 msec of C cell kernels. Hence, at high modulation depths, when most C cell kernels have none of late features beyond 55 msec, the C cell can roughly be viewed as solely receiving bipolar inputs and was modelled as such (fig. 21a,b).

---

[10]The 20 msec peak to peak interval that characterizes the early part of C cell 2nd order kernels is fundamentally different from the 30 to 35 msec peak to peak interval that characterizes the oscillations which can follow at the lower modulation depths, even though a casual observation without careful attention to the peak to peak interval might relate these two separate phenomenon as part of a single process. This distinction is further underscored by the fact that the oscillations, when in both 1st and 2nd order kernels, usually have dominant frequencies at 30 hz; frequency doubling of the late oscillations is not prominent along the diagonal (fig. 36a,b, fig. 44) in contrast to the case for the direct bipolar inputs (fig. 33c).

A prediction can be made for the arrival of feedback inputs to C cells based on the fact that these inputs are presumed to course two more synapses (via ganglion cells) once a signal arrives at the sustained amacrine N cells. With an estimate of approximately 6 msec per synapse (Sakai & Naka, 1988a), once bipolar input arrives at the NA and NB cells (about the same time it arrives at the C cell) another 12 msec passes before feedback reaches the C cell. Hence, the C cell should receive some feedback at about 50 or 55 msec. Perhaps a 5-10 msec delay can be added to account for slower bipolar cells, since variation does exist in bipolar cell kinetics (Sakuranaga & Naka, 1985a). This delay should show up in the direct inputs to C cells as well. Consequently, feedback via ganglion cells can overlap the latter part of direct inputs. So, the time interval from 40 to 60 msec could involve both direct and feedback input, whereas before 40 msec only direct inputs will arrive at C cells, and after 60 msec only the feedback inputs will arrive. Of course these time windows depend on the bipolar kinetics. If feedback does contribute to the kernels during the 40 to 60 msec period, it is reasonable to expect that the effects of feedback also will be evident during the period after 60 msec. Again, the lack of any late features will support the assumption that the C cell receives primarily bipolar inputs.

The direct bipolar inputs to C cells involve a parallel convergence of ON- and OFF-pathways in the current circuit scheme (fig. 5e).[11] There is much support for this proposal in the literature (Kujiraoka *et al.*, 1988; Frumkes & Miller, 1979). Indeed, the current experiments revealed that the responses of all C cells to

---

[11]The feedback from ganglion pathways also involves a convergence of ON- and OFF-paths.

decreasing heights of light steps are characterized by a gradual decline in the transient response at step increment relative to the transient depolarization at step decrement (fig. 40c). This is consistent the view that two different inputs (one that contributes to the C cell's response at light onset; the other, at light offset) are responsible for the transient ON/OFF behavior of C cells. Hence, while both the ON- and OFF-response transients decreased at lower step levels, they do not decrease in a proportional manner. In fact, a cell that may have been ON-dominant at high modulation levels actually may become OFF-dominant at lower modulation levels. In many cases, at the lowest step levels the cell only will show a transient response during light offset, and no response to step increments. Thus, although there presumably is a variation between the strength of ON- or OFF-bipolar inputs to a given C cell which may determine the ON- or OFF-character of that cell, the relative contribution of the OFF-response as compared to the ON-response increases at lower modulation levels, regardless of the relative strengths at higher modulation levels. Thus, with respect to the direct bipolar inputs, much more variability is observed between C cells under high modulation conditions in which there is greater interplay between ON- and OFF-pathways than under low modulation conditions in which the OFF-inputs dominate. However, in a few cells that were very ON-dominant at high modulation levels, the ON- and OFF-responses may have become more equal in magnitude at lower modulation levels.

The dominance of OFF-responses at low modulations in this study are consistent with findings by Frumkes and Miller (1979) that depolarizing bipolars have a one-half to one log unit higher threshold to light inputs as well as a longer latency

of response as compared to hyperpolarizing bipolars.[12] A possible explanation for the threshold difference is that the post-synaptic receptors differ greatly between ON- and OFF-bipolars. The ON-bipolars have receptors that are APB sensitive, whereas the OFF-bipolar receptor is believed to be kainate sensitive.

As a result of the difference in sensitivity between ON- and OFF-bipolars, the change in shape of the early peaks (before 60 msec) in C cell 1st order kernels (*e.g.* fig. 39a, fig. 34a, fig. 41a) can be attributed to a shift in balance between the contributions of ON- and OFF-bipolar inputs that depends on the modulation level of the light stimulus. Despite the presence of much variation in the shape of 1st order kernels between C cells at high modulation levels, these kernels, with few exceptions, became more OFF-like and much more simlar across cells at lower modulations. Fig. 34a shows the 1st order kernels from a C cell that had a strong OFF-bipolar character at the highest modulation which became even more OFF-like at lower modulation levels. Fig. 41a demonstrates the 1st order kernels from a cell that had a strong ON-type behavior in the form of a depolarization peak at high modulation levels which gradually dissipated with decrease in modulation. Finally, fig. 39a demonstrates 1st order kernels from a cell with a bicuspid appearance at high modulation levels that become decreasingly bicuspid and more OFF-like at lower modulation levels. The bicuspid shape is postulated to represent a composite structure that is a synthesis of significant inputs from both ON- and OFF-bipolars.

---

[12]It should be distinguished, though, that the Frumkes and Miller finding refers to the sensitivity to flashes in darkness, or absolute sensitivity, whereas responses to steps around a mean luminance indicates the contrast sensitivity.

The 1st order kernel represents an odd-power contribution to the C cell response. Therefore, differences in polarity, such as those that exist between ON- and OFF-bipolar contacts to C cells, are preserved and allow for 1st order kernels that reflect significant cancellation between the ON- and OFF-inputs. This yields a hybrid structure such as the bicuspid form of fig. 39a. Modelling attempts indicate that it derives from the summation of two biphasic 1st order kernels of opposite polarity (from ON- and OFF-bipolar contacts) that have different kinetics and scaling properties. The first negativity is considered to represent the influence of the OFF-bipolar input (which has a shorter latency than the ON-bipolar input), and this negativity increases as modulation level decreases. The second negativity is presumed to represent a contribution from the late, negative portion (around 60 to 70 msec) of the ON-bipolar biphasic impulse response, and it diminishes at lower modulations, consistent with the decreasing significance of ON-bipolar inputs under such conditions.

The three cells presented in fig. 39a (bicuspid), fig. 41a (ON-), and fig. 34a (OFF-) are representative examples for the types of 1st order kernels obtained in the twenty-six C cells used for this study. Basically, the nature of the direct bipolar components can be categorized into three types based on the shape of the 1st order kernel at high modulation levels (when feedback inputs are a minimum and provide no interference); ON-dominant, OFF-dominant, or shared. The ON-dominant form was much less common than the others, whereas the other two forms occurred with equal frequency. This may reflect the fact that the catfish retina has been characterized as OFF-dominant because of the greater prevalence of OFF-type cells.

Using the classification scheme above, based on the 1st order kernel, the balance between the ON- and OFF-transients of step responses of C cells could be predicted from the shapes of the 1st order kernels.

Unlike the 1st order kernels, the 2nd order kernels show much less variability in shape with respect to the early input contributions from bipolar cells (measured at high modulation levels). The 2nd order kernels are usually of a four-eyed structure (sometimes three-eyed) and have a diagonal that is usually bimodal (fig. 39b). Since the 2nd order kernel involves an even-ordered nonlinearity, the polarity difference between ON- and OFF-paths is not relevant and, consequently, cannot cause the significant cancellation that was observed with the 1st order kernels. In fact, current modelling efforts suggest that the much smaller power contribution to the response of C cells from 1st order kernels as compared to 2nd order kernels is due primarily to the cancellation effects that occur with the former. Consequently, the even order terms, which do not cancel, predominate (mainly 2nd order component), accounting for the nonlinear squaring behavior of the C cell.

In general, even at the lower modulation levels, the late features attributable to feedback inputs (oscillations and the broad depolarization humps), though often evident, were not as conspicuous as they were in the 1st order kernels. Thus, the relative lack of both cancellation effects and contributions from feedback inputs makes the 2nd order kernels best suited to assess the changes in kernel structure that are due mainly to bipolar inputs. First, all the C cells demonstrated a clear scaling of early peaks (35 and 55 msec) with decreasing modulation depth (fig. 39b). The appearance of such scaling in 1st order kernels was sometimes seen (fig. 39a) but was

often obscured by the cancellation phenomenon and the interference of feedback inputs.

Often, an increase delay of 5 to 10 msec in response time of the two peaks on the diagonal of the 2nd order kernel was observed along with the increase in scaling at decreasing modulation depths (fig. 39b, 40b). This occurred gradually along with the scaling property and is consistent with the findings of Shapley and Victor (1978, 1979a) that kinetics slow down with decreasing contrast. This peak response time delay was also apparent in some of the 1st order kernels (fig. 39a).

Similar to the direct bipolar inputs, the feedback inputs are proposed to be from both ON- and OFF-pathways (fig. 5d,e); the GA and GB ganglion cells, respectively. However, the inputs from the ganglion cells exert quite different effects on C cells than bipolar cells. The more pronounced appearance of feedback effects at lower modulation levels and the occurrence of these effects later along the time axis of the kernels are some of the attributes that are believed to distinguish the feedback inputs of ganglion cells from the direct inputs of bipolar cells. Two prominent feedback effects observed in C cells are the oscillations and the broad depolarization humps. These feedback effects were observed to varying degrees in all twenty-six C cells of this study. The oscillations (n=12) and the hyperpolarizations followed by depolarization humps (n=14) (Table 1) were approximately equally as likely to occur in C cells. Interestingly, these two phenomenon were usually mutually exclusive, implying that the occurrence of one somehow precludes the occurrence of the other. Perhaps it should be expected that

a broad continuous depolarizing influence, up to 60 msec in length, would upset the dynamics necessary to support oscillations.

Oscillatory behavior is especially suggestive of feedback. In particular, oscillations are very often observed with a negative feedback loop. In fact, such a loop is found in the proposed circuit schematic for the catfish inner retina (fig. 5d). The negative feedback is provided via the C to NA inhibitory synapse. The closed trisynaptic loop constituted by the C to NA to GA to C connections would be expected to have a complete transit time of approximately 18 msec based on the estimate of 6 msec per synapse. One course through this loop would result in a phase reversal, and hence, two transits through the loop, having a duration of 36 msec, are necessary for one complete peak to peak cycle of oscillation in a C cell. The frequency based on the 36 msec travel time is about 30 Hz. The other cells involved in this loop show similar oscillatory behavior as would be expected. For example, a 30 Hz oscillation is evident along the diagonal of a 2^{nd} order kernel from a NA cell shown in fig. 47b. This 30 Hz oscillation is the same frequency that has been observed with the spontaneous oscillations of NA and NB cells (Hosokawa & Naka, 1985) as well as with the reponses of NB cells to current injection into NA cells (Sakai & Naka, 1990b). The background section provides an explanation for the design of the circuit diagram of fig. 5d,e and its relation to 30 Hz oscillations in the inner retina.

But, according to this circuit, the loop involving the C to NB to GB to C connections might be expected to antagonize the other negative feedback loop involving the ON-pathway NA and GA cells. The OFF-pathway loop consists

entirely of positive synapses and is, therefore, a positive feedback loop. However, just as variations in the strength were observed for the ON- and OFF-bipolar connections to C cells, a variation can be expected for the GA and GB contacts. It is proposed that C cells that demonstrate oscillations in their kernels have weaker GB contacts as compared to GA contacts. This is consistent with the finding in current injections between NA and NB cells that while injection in a NA cell could evoke strong 30 Hz oscillations in an NB cell, reverse injection into the NB cell of that same NA/NB couple provided only very weak excitation in the NA cell (Sakai & Naka, 1990b). Perhaps, oscillations can be observed only between couples for which the GB feedback to C cells is weaker than the GA feedback.

Alternatively, C cells in which the GB contacts were stronger than the GA contacts would also be expected to occur. This may be the situation that occurs with the broad depolarization humps. These humps, usually seen in the 1st order kernels, are always preceded by a strong, wide hyperpolarization around 50 to 55 msec (*e.g.* fig. 38a, fig. 37a) that may overlap some of the residual responses attributed to the early direct bipolar inputs. Often, this feedback hyperpolarization can appear to be a scaling of one of the bipolar inputs, especially for bicuspid type structures (*e.g.* fig. 38a, fig. 27a). However, the scaling would occur over the second negativity which is presumed to originate from ON-bipolar contacts and, consequently, should shrink with decreasing modulation levels, not increase. The other alternative is that the strong hyperpolarization develops from the first negativity which probably represents the OFF-bipolar inputs. This would require that the kinetics of the OFF-bipolar cell slow down from a peak response time of 35 msec at high modulation levels to a

response time of 55 msec at low modulation levels. However, C cells that do not have the broad depolarization humps and are OFF-bipolar dominant (hence lacking cancellation from the ON-bipolar path or interference from the 55 msec hyperpolarization) show a slowing of only 5 to 8 msec (fig. 34a) with decreasing modulation levels. That such drastic kinetic changes occur in one cell but not the other for identical stimulus adjustments seems unlikely. In addition, a few C cell 1st order kernels, that had a bicuspid form whose second negativity was late along the time axis (indicative of slower bipolar kinetics to begin with), reveal that the strong hyperpolarization that develops at low modulation levels probably does not develop from a scaling of bipolar inputs (fig. 36a). Also, the peaks along the diagonal of the 2nd order kernel (which are thought to represent a squaring of the biphasic bipolar kernels) most often do not coincide with the hyperpolarization. In fact, in fig. 38a,b the occurrence of the hyperpolarization peak in the 1st order kernel at 55 msec places it directly between the two peaks that occur along the diagonal at 40 msec and 65 msec. Thus, the timing of the hyperpolarization does not occur in a manner that is consistent with its being a consequence of the scaling of bipolar inputs. Finally, it is interesting that the 55 msec hyperpolarizations, with only two notable exceptions (discussed below), were always followed by a broad depolarization hump. Thus, the hyperpolarization and the broad depolarization appear to be kinetically related and part of a single biphasic structure. This collection of observations strongly indicates that the hyperpolarization at 55 msec is not related to the direct bipolar inputs.

Instead, this hyperpolarization may be interpreted as representing the feedback input from GB cells, whose biphasic kernels have an initial negativity

followed by a positivity. This negativity would be expected to arrive at the C cell at near 55 msec. The subsequent broad depolarization hump would be initiated by the late positive portion of the biphasic GB 1st order kernel. The depolarization would persist due to the recurrent excitement from the positive feedback loop. Interestingly, occasionally a multiple dimpling would be observed on the crest of the broad depolarizations (fig. 37a, fig. 38a). The time increment between the dimples was 15 to 20 msec. This is consistent with the time necessary for one transit around the positive feedback loop. The second dimple, then, may represent a resurgence of excitement due to additional positive feedback via this loop.

While the relative contribution of GA or GB contacts can influence the behavior of the C cells in very different, mutually inconsistent ways (the former involving negative feedback and the latter, positive feedback), a few C cells showed some interesting and delicate balances between the two types of feedback inputs. For example, one cell that demonstrated 30 Hz oscillations at low modulation levels in both the 1st order kernel and the diagonal of the 2nd order kernel (fig. 36a,b), provides an exception to the general observation that 1st order kernels with a strong 55 msec hyperpolarization subsequently are followed by a broad depolarization. The other exception comes from the C cell (fig. 29a,b) that had much stronger oscillations along the 2nd order kernel diagonal than in the 1st order kernel. The 1st order kernel from this cell seemed to show a cancellation phenomenon at around 110 msec that is probably due to polarity differences between the GA and GB feedbacks. Thus, the reason the oscillations are more prominent in the 2nd order kernel is probably because the even order nonlinearities do not exhibit cancellation effects that can

occur from polarity differences in the inputs. So, in these two cells that show a strong hyperpolarization at 55 msec as well as subsequent oscillatory behavior, the GA and GB cells are likely to be roughly comparable in strength. Much more common, though, is the situation that one of the feedback inputs dominates the other.

Interestingly, the cell of fig. 36 also showed a small 60 Hz component along the diagonal of the 2nd order kernel. This was apparent as a strong band in the frequency domain (fig. 36c) and, in the time domain, appeared to be aligned in phase with the peaks of the 30 Hz oscillation. While it is difficult to interpret oscillations along the diagonal of the 2nd order kernel, some speculation is possible. One interpretation for this is that a strong GA feedback exists that is responsible for the 30 Hz oscillation, but, also, some mild but significant GB feedback is present that is essentially driven by the negative feedback loop. According to this scheme, a feedback to the C cell that is excitatory will result, after one transit through the positive feedback loop, in a mild excitation from GB cells, but, after one transit through the negative feedback loop, in a stonger inhibition from GA cells. These two effects then add at the C cell. Subsequently, during the portion of the cycle when the C cell receives strong inhibition from GA cells, one transit time later the C cell will receive a mild inhibition from GB cells of the positive feedback loop, but strong excitation from the GA cells of the negative feedback loop. Thus, the appearance along the diagonal of a dominant 30 Hz sinusoid over-riding a weaker 60 Hz one can be viewed as the consequence of a superposition of the nonlinear components of a strong 30 Hz oscillation with a mild feedback from GB cells (that

is precisely out of its phase). Linear superposition of two 30 Hz sinusoids will give a 30 Hz sinusoid and can explain why no strong 60 Hz component is seen in the 1st order kernel (fig. 36a,c).

Another interpretation is that the 60 Hz component may correspond to a frequency doubling of a 30 Hz input by the 2nd order nonlinearity. However, this view cannot account for the strong 30 Hz component along the diagonal. The existence of a 30 Hz component in both the 1st and the 2nd order kernels may be suggestive of a mild compressive nonlinearity along the predominantly linear feedback loops. The frequency doubling that occurs with the highly nonlinear bipolar inputs to C cells would be much less likely with such a compression (or enhancer) nonlinearity.

An interesting relation occurs between the nature of the 1st order kernel at high modulation (*i.e.*, OFF-, bicuspid, or ON-like; F,B, or N of Table 1) and the 1st order behavior at low modulation (*i.e.*, oscillatory or with a hyperpolarization followed by a depolarization hump; O or H of Table 1). In general, H was associated with F or B classifications, while O^+ (strong oscillations) occurred with N or B categories in three of four cells. In fact, all cells that were classified with N showed strong oscillatory behavior at low modulations. In addition, when oscillations and late hyperpolarizations were observed together (O/H), the associated waveform at high modulation was B in both cases. This is quite reasonable considering that ON-bipolar and GA contacts both occur in sublamina b while OFF-bipolar and GB contacts occur in sublamina a. Thus, it is likely that a C cell that receives strong inputs from ON-bipolars might also receive strong contacts from GA cells. The

converse situation holds for OFF-bipolars and GB cells. This pattern offers additional evidence that oscillatory behavior is related to strong ON-inputs while the hyperpolarizations are attributed to strong OFF-inputs. The association of the two O/H behaving cells with a bicuspid 1st order kernel at high modulations is consistent with the dual innervation of these cells.[13]

The tendency for the putative feedback inputs of GA and GB cells to become more prominent in Wiener kernels at lower modulations makes them very distinct from the bipolar inputs (which are most conspicuous at high modulation levels). The reason for this difference can most likely be associated with the nature of the bipolar inputs which results in a highly nonlinear, mainly 2nd order, power contribution to the C cell response. The feedback inputs from the very linear ganglion cells (Sakai & Naka, 1987a, 1988a), on the contrary, have much smaller nonlinear components. In fact, current injection studies (Sakai & Naka, 1988b, 1990a, 1990b) have revealed the connections between amacrine cell couples, ganglion cell couples, and amacrine/ganglion cell couples to be very linear (even when the opposing cell of the couple was from a different ON-OFF categorization).

Nonlinear terms are expected to become much more predominant at high modulation levels because, by definition, they involve higher order powers of the input. Conversely, they are expected to become less significant at lower modulation

---

[13]It might be argued that the classifications of F, B, N, O, or H depend more on the location of the intracellular electrode impalement (either closer to sublamina a or sublamina b) than on the strength of ON- or OFF-inputs. However, it is unlikely that the impalement would be stable enough for the multi-modulation level experimental paradigm had not the impalement been near the C cell soma. Regardless, the arguments regarding the nature and association of the input-types still hold.

levels, whereas linear terms become increasingly important under such conditions. Therefore, that the linear feedback inputs should become more remarkable at lower modulation levels is quite consistent. In fact, an increase in the contribution of 1st order kernels to the response power of C cells is a common occurrence in nearly all the cells studied. In a few cells, for example, the power contribution of the 1st order kernel rose from around 10% at high modulation (level 1) to near 50% at low modulation levels (*e.g.* cell #24 and #17 - Table 1). This transition may reflect the greater contribution of feedback inputs at lower modulation levels, and the tendency for feedback inputs such as oscillations and humps to become more pronounced under the low modulation conditions tends to underscore further their linear attributes.

In addition, the tendency of oscillations to be much more prominent in the C cell 1st order kernels than the 2nd order kernels further stresses the linear nature of the feedback inputs. In fact, for many of the kernels that displayed depolarization humps at lower modulation levels, the 1st order kernel appeared to reflect the late GB feedback inputs entirely, whereas the 2nd order kernel appeared to represent the bipolar inputs (fig. 30a,b; fig. 37a,b; fig. 38a,b). Also, if oscillations were present in both kernels, they were generally much more mild in the 2nd order kernel. Oscillations were more pronounced in the 2nd order kernel in only one cell of the twelve that demonstrated oscillatory behavior. When oscillations were present in the 2nd order kernels to a significant degree (five cells), all of the 2nd order kernels contributed 30% or less to the response power of the cell. Three of these cells had

2nd order kernels that contributed less than 15%, including the one cell with more pronounced oscillations in the 2nd order kernel (fi2g. 29a,b).

On the contrary, oscillations were more common in 2nd order kernels than 1st order kernels in the N cells studied. But, in these cells the 2nd order kernel generally accounts for 25% or less of the response power whereas the 1st order kernel can account for upwards of 50%. The impression is that the oscillations occur in the kernels that tend to have lower power contributions, such as the 1st order kernel of C cells and the 2nd order kernel of the N cells. Likewise, they are less common in kernels that usually have high power contributions, such as the 2nd order kernel of C cells and the 1st order kernel of N cells. A possible explanation for this is that the feedback input is not as strong as the feedforward ribbon synapse input from the bipolar cells (Fain, 1977). Consequently, the oscillations are only apparent when direct bipolar inputs do not mask or interfer with them. It is likely that the direct and feedback inputs have different power contributions from each order of Wiener kernel in order to characterize their respective signals. Hence, the feedback inputs should be most prominent in those kernels that have minimal contributions from direct bipolar inputs but measurable feedback contributions. As the feedback inputs are characterized as linear, it is not surprising that they are most prominent in the C cell 1st order kernels; especially since the bipolar inputs are strongly nonlinear. Conditions which favor linear inputs (such as low modulation levels) will help to accentuate the presence of oscillations. That the 1st order kernel was twice as strong as the 2nd order kernel (29% power contribution as opposed to 14.5%) in the one C cell that had more substantial oscillations in its 2nd as opposed to 1st order kernel

(fig. 29a,b) provides additional support for the premise that feedback inputs are evident in the kernels that have weak contributions from direct bipolar inputs.

Generally, the direct bipolar inputs to N cells are strongly linear. However, some oscillatory behavior is observed along the diagonal of the 2nd order kernel of N cells. This may be attributed to the weakly nonlinear contribution of bipolar inputs to N cells which allows even a mild nonlinearity related to the feedback inputs to be evident.

The fact that oscillations can be unveiled in kernels when the bipolar contributions to these kernels are weak further underscores the point that the oscillations behave very differently than the bipolar inputs. In fact, they seem to be quite robust in the absence of bipolar inputs. It might be argued that the oscillations occur at low modulations and in low power response kernels because of a greater possibility of contamination by noise, other autonomous phenomenon, or numerical errors at low modulation levels. Several observations argue against this: 1) oscillations did occasionally occur in kernels with higher power contributions in cells that were very prone to oscillate (fig. 49a - 1st order of NB; fig. 43b - 2nd order of C); 2) oscillations did not occur in horizontal cells at low modulation, even though the 2nd order kernel was quite low; 3) the oscillations are generally at 30 Hz, the same frequency which has been observed in spontaneous oscillations of N cells and in the response of NB cells to current injection of NA cells (Hosokawa & Naka, 1985; Sakai & Naka, 1990b); 4) the oscillations are found to have similar phase relation in the 1st order kernels across several cells, with a positivity at 60-70 msec and a completion of a cycle with another positivity at 100-110 msec (compare fig. 32, fig. 33a, fig. 35a,

fig. 43a); 5) repeat kernels taken from different times in the same cell yield the same oscillatory kernel; 6) the oscillations generally extinguish before 150 msec along the 1st order time axis indicating that they are deterministic and not the result of superposition with an autonomous behavior; 7) the relation described above between the presence of oscillatory behavior (O^+) at low modulations and the usual occurrence of ON- or bicuspid shaped (N or B) 1st order kernels at high modulations shows a strong correlation of the oscillations with other robust behavior of C cells (Table 1). Therefore, the oscillations seem to have a sound physiological basis. Finally, the occurrence of depolarization humps in the 2nd order kernel of C cells was also much rarer than in 1st order kernels, but when the broad depolarizations were apparent in 2nd order kernels (4 cells of 14), the power contributions of the 2nd order kernels were also very small (in the range of 26-17%) (fig. 45b).

An enormous range of behaviors is possible for C cells as a result of their central role in a complex circuitry. No doubt, the variety of responses and many shapes of the 1st and 2nd order kernels, makes the C cell one of the most remarkable cells in the catfish retina. This is a consequence of the many inputs they receive; from bipolar as well as ganglion cells, from ON- as well as OFF-pathways. These different types of inputs - combined with the great deal of variability that exists in the relative strengths between them - is the key to the diversity. Figs. (39a,b,c; 33a,b,e; 35a,b,c; 37a,b,c; 36a,b,d) show the 1st order kernels, diagonals of the 2nd order kernels, and step responses from five representative cells that were chosen to highlight and define some of the differences that were observed between C cells. The kernels in fig. 39a,b are from a cell that was slightly OFF-dominant at high

modulation levels and became progressively more OFF-dominant at lower modulation levels. This was observed in the step responses as well. Both negativities of the bicuspid structure are observed to slow by about 5 msec with lower modulation levels. This cell is unique in that only weak late features are observed at low modulation levels, suggesting that the feedback from ganglion cells is not substantial. Since it lacks interference from ganglion cell feedback, such a cell is suitable for analysis of bipolar inputs to C cells as they relate to adjustment of modulation levels.

The kernels and the step responses in fig. 33a,b,e characterize a cell that is strongly ON-dominant. Unlike, the previous cell, this cell demonstrates an increase in oscillatory behavior at low modulation levels, suggestive of strong GA feedback. The initial positive peak at 35 msec does not show much scaling or any slowing of kinetics at low modulation levels; an apparent lack of contrast gain effects on the early peaks, observed in another ON-dominant cell as well (fig. 32a). This is in sharp distinction to the smooth scaling observed in the 1st order kernel of the previous OFF-dominant cell. The difference between the two cells may relate to the fact that the enhancement from contrast gain in the ON-dominant cell is counterbalanced by the greater threshold and reduced sensitivity of ON- as compared to OFF-bipolar cells at lower modulation levels (Frumkes & Miller, 1979), which would also allow for a stronger cancellation effect from OFF-bipolar inputs at lower modulation levels. The OFF-dominant cell, on the contrary, had stronger OFF-bipolar inputs to begin with, which only got stronger at the lower modulation levels (*e.g.* fig. 39c).

The cell of fig. 35 provides an example showing an equal balance between ON- and OFF-bipolar contibutions that persists to low levels of modulation. This

balance was maintained in the step responses at low levels as well for this particular cell (fig. 35c). The late, robust oscillatory behavior in the 1st order kernel is suggestive of a strong GA feedback. Consequently, the 55 msec negativity is more consistent with a contribution from opposed bipolar inputs than from a GB input.

Other cells (fig. 37, 36) emphasize some of the features associated with putative GB cell feedback. The cell of fig. 37a shows the typical 55 msec hyperpolarization and subsequent broad depolarization hump. This evolved, as modulation levels decreased, from a kernel that initially had bicuspid negativities. The bicuspid form reflects the roughly equal contribution from ON- and OFF-bipolars, as is apparent from the step responses. A persistence of bipolar contributions at the lowest modulation level, perhaps mainly from OFF-bipolars, is seen as a positive peak at 45 msec along the 2nd order kernel diagonal. No contribution is made by the 1st order kernel at 45 msec along its time axis. This is consistent with the view that at low modulations the 1st and 2nd order kernels may represent distinct inputs; the 1st order kernel primarily represents linear GB feedback (21% power contribution) whereas the 2nd order kernel represents the bipolar input (53.5% power contribution). A double dimple is apparent on the depolarization hump of the 1st order kernel; the first dimple is attributed to the positive portion of the initial GB biphasic impulse, and the second to a subsequent GB excitation due to transit through the positive feedback loop. A very few cells (two in this study, *e.g.* fig. 36a, Table 1 - O/H) demonstrated a 55 msec hyperpolarization characteristic of putative GB inputs but also displayed oscillatory behavior indicative of strong GA

inputs. As discussed, an approximately equal contribution from both types of ganglion cells is presumed to be the basis for this behavior.

In short, almost any variation in the strength of contribution of bipolar and ganglion inputs has been observed - from ON-dominant, to OFF-dominant, to mixed - often with one type of pathway dominating at the level of the bipolar inputs and another dominating at the level of the ganglion cell inputs. In addition, none of the variations in the strengths of inputs appears to be significantly more frequent than any other variation; GA predominance is about as common as GB predominance, and, although fewer ON-dominant bipolar C cells were observed, a substantial number of cells with 1st order kernels having bicuspid structures did occur. The variations, therefore, appear to be random. Fortunately, I obtained enough C cell recordings to observe a vast diversity of C cell responses. The task of deciphering the functional correlates for each kernel would have been much more formidable had this not been the case.

Compared with the C cells, the N cells seem to behave in a much more homogeneous and predictable manner. In particular, the 1st order kernels of N cells showed much less variability between cells than did the 1st order kernels of C cells. This is probably attributable to the fact that N cells are believed to receive inputs from either ON- or OFF-bipolar types, but not both to any substantial degree. The reduced number of input types and the concomitant lack of cancellation effects results in much less diversity in the kernel structure. In addition, the absence of the

cancellation phenomenon which affected the odd-order terms in C cells explains the strongly linear, 1st order behavior of N cells.

The late features (such as oscillations) that were attributed to ganglion cell feedback become much more prominent at low modulations. This was also observed with C cells, but there are some important distinctions between the oscillations of N and C cell types. First, while the oscillations were more prominent in the 1st order kernels of C cells, they are more prevalent in the 2nd order kernels of N cells. As discussed above, this probably relates to the tendency of the weaker feedback inputs to be manifest in the kernel which makes the smallest power contribution to the cells response, since such kernels are less likely to involve masking by the direct bipolar inputs. In addition, while oscillations were detectable in approximately 50% of C cells, they were a prominent feature of the 2nd order kernels in all seven of the N cells analyzed. The oscillations tended to last longer in N cells as compared to C cells. Often the oscillations would persist for 200 msec or longer in N cells, but were much less robust in C cells after 150 msec.

Some important distinctions are found between the oscillations in the 2nd order kernels of NA cells as compared to NB cells. In NA cells, the oscillations appeared to be a more consistent component of the kernel, although too few N cells were analyzed to make any definitive judgments. One of the NB cells was actually extraordinarily oscillatory in nature (demonstrating oscillations in the 1st order kernel as well), but the other was much less so (fig. 49; 48, respectively). In addition, both of the NB cells exhibited a cancellation type effect at 90 to 100 msec that was not evident in NA cells. However, one of the NA cells did demonstrate a smaller 60 Hz

component superimposed on a stronger 30 Hz component along the diagonal (fig. 50b). This was similar to what was observed in certain C cells postulated to receive feedback inputs from both GA and GB cells. Most likely, a similar explanation applies here; the C cell that provides input to the NA cell receives feedback inputs from GA and GB cells. The observation that NA cells more consistently appear to show oscillatory behavior probably can be attributed to the proximity in the inner plexiform layer of the GA as opposed to GB feedbacks (sublamina b) and the consequent dominance of the former (via the GA to C to NA path). Similarly, the appearance of cancellation effects in the NB 2nd order kernels results from the nearness of GB feedbacks (sublamina a). As the GB feedback is generally more short-lived than the duration of oscillations, oscillations may resume after the cancellation from GB inputs has dissipated. The implication here is that C cells can act locally to a certain degree, endowing NA and NB cells with slightly different properties.

C cells also act globally. Otherwise, oscillations would not be conveyed to NB cells at all, as a result of the segregation of ON- and OFF-pathways into sublamina b and sublamina a, respectively. Cancellation effects of GA and GB feedback inputs would not be observed in NB cells either, without global interactions. Findings in the rabbit suggest that such local behavior is possible in starburst amacrine cells (Miller & Bloomfield, 1983)

The 1st order kernels of NA and NB cells are very similar kinetically, but are of opposite polarity (fig. 47, fig. 48). While the first peak at around 40 msec shows little sensitivity to modulation level, the following peaks are quite sensitive to

adjustments in modulation level. In fact, dramatic increases in 1st order kernel size are seen at low modulation. This is similar to the scaling that was observed with the kernels of C cells, most consistently in the 2nd order kernel, but also in the 1st order kernels that did not demonstrate strong cancellation effects (fig. 34a,b; fig. 31a,b). However, the C cells exhibited dramatic scaling even in the earliest 35 msec peak. In addition, while the peaks in the kernels of C cells that were postulated to represent direct bipolar inputs slowed down with decreasing modulation, speeding up (in peaks other than the first) was observed in the N cells with drops in modulation level. In the C cells, faster kinetics were attributed to the feedback inputs which have a 30 Hz component as opposed to the biphasic bipolar inputs which have a frequency domain band from 0 to 20 Hz (fig. 22b). A similar explanation probably applies here, with the faster kinetics of feedback inputs contributing to N cell behavior at low modulation levels.

A theory is presented as follows. The N cells receive direct inputs from the two population types of bipolar cells, both from the same polarity type - either ON or OFF. One provides sustained inputs to N cells, and the other consists of transient-type bipolars that have recurrent synapses with the type N cells (fig. 5c,d). The sustained bipolars are postulated not to receive pre-synaptic GABAergic inputs and, consequently, do not show sensitivity to modulation depth the way the terminals of the transient ones do. The sustained population, then, provides a mechanism for detecting the absolute variance of the light input. This measurement is conveyed to the N cells and, then, to the transient bipolar terminals via the recurrent synapses. The transient bipolar terminals are inhibited at high modulation levels; a decreased

scaling and speeding up of the bipolar kinetics is evident in the Wiener kernels of C cells. Conversely, at low modulation levels, the relative scaling and sensitivity of C cell kernels is increased. The C cells are, in general, depolarizing cells in response to the direct bipolar inputs. This attribute results from the strong 2^{nd} order contribution from bipolar inputs. Thus, the increased scaling and sensitivity of C cells at low modulations probably results in a relative inhibition delivered to NA cells and a relative excitation to NB cells (fig. 5d). This may explain the enhancement of the second negative peak in the 1^{st} order kernel of NA cells and the second positive peak in the 1^{st} order kernel of NB cells. The best explanation for the lack of a contrast effect in the first peak of the N cells is that this peak represents input from sustained bipolars and that the input from C cells would tend to antagonize this input (due to the sign inversion of C to NA inputs).

Alternatively, some of the enhancement of the second peak may stem from feedback inputs from the GA cell depolarization. This could explain the speeding up of kinetics at lower modulation levels as well as the development of a more oscillatory triphasic response as opposed to the biphasic response observed at high modulation levels. According to this, the initial depolarization of the NA cell due to bipolar inputs would course the negative feedback loop and result in the addition of a hyperpolarizing input via C cells. This hyperpolarizing input would be approximately 20 msec after the initial depolarization and, hence, would augment the hyperpolarization of NA cells attributed to the biphasic bipolar inputs. The triphasic 1^{st} order kernel response of NA cells at very low modulation would result from an additonal round through the negative feedback loop. A similar model is proposed

for NB cells, whereby the NB cells also receive negative feedback inputs via C to NB contacts. However, in the two NB cells analyzed (fig. 48, fig. 49), no interference from GB feedback was evident in the 1st order kernels, despite the fact that some cancellation interactions were observed in the 2nd order kernels. That cancellation involving feedback inputs was detected in NB 2nd order kernels, but not in the 1st order kernels is puzzling, especially since one of the NB cells clearly shows feedback in the form of oscillations. Therefore, although GB feedback was presumed to be primarily linear and exhibited a strong influence on the shape of C cell 1st order kernels, with respect to N cells, the negative feedback loop (fig. 5d,e) appears to be the dominant influence in the 1st order kernels of both NA and NB cells.

Oscillations also tend to last longer in N cells than C cells. One possible explanation for this stems from findings by Vaney *et al.* (1989) that in rabbit the transient cholinergic amacrines have a great deal of dendritic field overlap with as many as twenty-five to seventy other cells forming a very crowded plexus. Consequently, it seems likely that a single N cell could receive inputs from several C cells. Only a few C cells , then, would have to demonstrate strong oscillatory behavior in order for it to become a dominant feature of the N cells. Perhaps in an assembly of C cells linked to N cells, oscillatory behavior is able to exert more of an organizing influence than the positive feedback effects of GB inputs. So, while GB feedbacks were postulated to be significant in individual C cells approximately 50% of the time, with respect to the global affect of C cells on N cells, GB feedback may have a subordinate role. This may be related to the consideration that a biphasic impulse response is not propagated as effectively through a positive feedback path

as through a negative feedback loop. In the positive feedback case, the biphasic nature of a bipolar input can initiate antagonistic signals; a hyperpolarizing signal that is cancelled by a feedback of the depolarizing one. With the negative feedback, the initial depolarization of the biphasic bipolar input may actually enhance, due to negative feedback, the subsequent bipolar hyperpolarization.

The changes in kernel shapes that occur in C and N amacrine cells with adjustment of the modulation level of light inputs have been interpreted with respect to the network of fig. 5d. This circuit schematic initially was devised in this thesis for its ability to explain numerous amacrine-amacrine, amacrine-ganglion, and ganglion-ganglion current injection cell couples (see Background). This same, relatively simple, circuit diagram now has been applied to address the very complex transitions in cell behavior in the inner retina that occur with changes in modulation depth. The success with which it has achieved this aim certainly underscores its merits, and the cumulative evidence for support of the circuit is now quite substantial.

Other findings in this study are also consistent with the circuit of fig. 5d. First, the spontaneous spiking, particularly in GA cells, has an interspike interval that correlates well with the 30 Hz spontaneous activity that has been recorded intracellularly in cells of the inner retina. The occasional short interspike interval peak near 10 msec on the histogram probably corresponds, then, to instances of multiple spiking at a single crest of an oscillation. It was proposed that spontaneous spiking may provide the necessary nonlinear force to drive oscillations in the inner retina (see Background section).

The present finding certainly supports this possibility, but it is unclear whether the organized spiking is a cause or effect of the 30 Hz oscillations; only a correlation between spike behavior and membrane oscillations is suggested. Since the phenomena of spontaneous membrane oscillations and spontaneous spiking are proposed to be intimately related via a feedback loop, the distinction as to which supports the other may be immaterial. In fact, they may sustain each other. The incidental finding in one C cell of spontaneous depolarizations (fig. 37d) supports the notion that spiking cells can influence amacrine cell behavior in an excitatory manner and further substantiates the significance of feedback inputs from ganglion cells.

The negative feedback loop has been characterized as much more capable of organizing concerted activity than the positive feedback loop of GB cells. The NA or NB cells, which have a strong disposition towards oscillatory behavior of long duration, are good examples. For instance, the 2^{nd} order kernels at low modulation levels (fig. 47b, fig. 48b) and the responses of sustained amacrines to step inputs of light have strong oscillatory features (fig. 51, fig. 4). The notion that the negative feedback loop provides a strong organizing circuitry is supported by the present finding that GA cells, which are a component of the negative feedback, have much more defined spontaneous spiking behavior than the GB cells.

That ganglion cell spikes can fire spontaneously in a coherent manner also implies that the oscillations are conveyed beyond the retina and may subserve a function in more central visual processing. Several possible speculative roles for oscillations are available, and some were discussed in the Introduction section.

B. THEORETICAL

Based on the analysis of inputs to C cells presented above, a model of C cell function that is based on bipolar inputs alone must be considered incomplete. This would be true especially in C cells that demonstrated marked feedback inputs. C cells that display oscillations or depolarization humps would be particularly poor candidates for such a model. However, most manifestations of the feedback inputs are only apparent at the lower modulation levels. In fact, a few cells did not show sizeable feedback inputs even at low modulations. Therefore, a model based on bipolar inputs might be acceptable for most cells at high modulation levels and, for a few cells, at low modulation level. This is consistent with the result that, at the highest modulation level, the model provided significant improvements over the power contributions from the 1^{st} and 2^{nd} order Wiener kernels, whereas it performed with less effectiveness at the lower modulation levels.

The deficiency of the model at low modulation levels is related to an inability to account for phenomenon such as oscillations that become increasingly more prominent at low modulations. The example of fig. 29d-ii (level 4) clearly shows that, while the model can account for some features of the Wiener kernels at low modulations, it is quite inadequate at fitting the oscillatory features that occur along the diagonal of the 2^{nd} order kernel. Since these oscillatory features are presumed to result from multiple passes through a negative feedback loop, the deficiency of the present model, which does not include such a feedback loop, is not surprising. Additional features will have to be added to the model in order to address more

effectively the existence of feedback inputs if the model is to be applied more universally to all C cells at all modulation depths.

While a parallel path L_1-N-L_2 model that only includes bipolar inputs may be too simplistic to be useful for a thorough and complete analysis of C cell function, such a model is reasonable if parsimony of parameters is an important preliminary consideration. This approach allows for a better assessment of which elements of the model are essential and what contributions they make to the response of the cell. A minimal model is also more likely to be more constrained and less likely to show undesirable and physiologically unnatural compensation that could otherwise occur from accessory elements in a model. Thus, the deficits of a minimal model are more clearly delineated, which allows for a better appraisal of the embellishments necessary for an improved model. The present L_1-N-L_2 model is considered a minimal one, based on previously published data and salient features of the kernels measured in this study.

Presently, the model is considered only for cells at a given modulation level that show little or no evidence in their 1st and 2nd order kernels of traits that have been attributed to feedback inputs. In addition to oscillations, such traits include the late appearing broad depolarization humps that are preceded by a strong hyperpolarization. Although the model could not be applied to all cells at all modulation levels with equal success, for many cells it proved quite effective and offered useful results and insights into retinal function. In fact, the present model (fig. 21b) was capable of reproducing the 1st and 2nd order kernels of many of the transient C amacrine cells (especially at high modulation levels) and able to provide

good fits to actual C cell responses to white noise and step inputs as well. While the model does have notable shortcomings such as the lack of feedback inputs, the model also has genuine merits under circumstances that minimize these shortcomings. Thus, although the model is overly simplisitic, through choice of the proper stimulus conditions such as high modulation or by careful screening for cells that do not show strong ganglion feedback effects, study of some key features of C cell physiology are possible.

For instance, the parallel pathway structure of the model allows for a clarification of the kinetic differences between ON- and OFF-bipolar inputs to C cells. As an example, the ON-bipolar input consistently was found in the model to have a greater latency than the OFF-bipolar input by approximately 4 msec. The greater latency for ON-bipolars is consistent with the findings of Frumkes & Miller (1979) who, as was previously discussed, also noted an increased threshold for ON-bipolar responses. A possible explanation for the latency was attributed to the difference in the APB receptor of ON-bipolar cells as compared to the kainate receptor of OFF-bipolar cells. The APB receptor is believed to operate via intracellular second messengers such as cGMP that link the binding of ligand to the receptor indirectly with channel closing events (Gottesman & Miller, 1992). The kainate receptor, on the contrary, contains the ion channel as part of a single subunit complex, and ligand binding leads directly to channel activation. Greater diffusional delay may contribute to the latency of ON-bipolar cells also (Dacheux *et al.*, 1979). The more direct route for receptor binding and channel activation explains the decreased latency of the OFF-pathway. Perhaps the observation that the ON-bipolar

inputs tended to be more biphasic than the OFF-bipolar inputs also can be attributed to receptor differences between the two pathways.

In addition, both the ON- and OFF-pathway peak response times increase by equal amounts with decreasing modulation depths so that the latency between ON- and OFF-pathways is preserved across modulation levels. This speeding-up of bipolar kinetics with a faster peak response time at higher modulations is consistent with the observations of Shapley and Victor that the mechanism of contrast gain becomes more high-pass at higher contrasts (Shapley & Victor, 1978, 1979a). A possible mechanism for the change in bipolar kinetics that occurs with adjustment of the modulation level may depend on inputs from sustained amacrine cells onto the pre-synaptic bipolar terminals.

While GABAergic inputs from sustained amacrines to ON-bipolar terminals have been characterized in many species such as mudpuppy (Miller *et al.*, 1981a, 1981b), goldfish (Tachibana & Kaneko, 1988; Kaneko & Tachibana, 1987), carp (Kondo & Toyoda, 1983), and mouse (Suzuki *et al.*, 1990), the existence of sustained amacrine inputs to OFF-bipolar cells and the exact pharmacological nature of that input is more controversial. Studies in mudpuppy indicate that sustained ON-amacrine inputs are GABAergic, but sustained OFF-amacrine inputs are glycinergic (Miller *et al.*, 1981b), whereas in the carp and goldfish, no glycine sensitive bipolar axon terminals are observed (Kondo & Toyoda, 1983; Tachibana & Kaneko, 1988). As an additional variant, ON- and OFF-bipolars of mice each show sensitivity to both GABA and glycine (Suziki *et al.*, 1990). The results of the model which indicate a slowing of similar degrees in both the ON- and OFF-bipolar pathways suggests that

inputs from sustained OFF-amacrine cells to OFF-bipolar presynaptic terminals do exist. As GABA and glycine are both inhibitory neurotransmitters that can affect chloride conductances, definitive assessment cannot be made as to which transmitter is used for the OFF-pathway. However, if the bipolar cell is assumed to be isopotential, a $GABA_B$ mechanism that does not involve a membrane polarization might be the favored choice for both pathways, since contrast gain effects are not observed in ON- or OFF-bipolar recordings of catfish (Sakai & Naka, 1987b).

The present L_1-N-L_2 model also allowed the exploration of some of the highly nonlinear features of the bipolar synapses with C cells. The static-nonlinearities for both ON- and OFF-pathways of the model demonstrated very complicated polyphasic properties. In many ways, the functions that represented the static-nonlinearities were very surprising and demonstrated unusual physiological properties. For instance, many studies in the retina and other parts of the central nervous system have characterized the nonlinearities at synapses as monotonic functions, often of an exponential form.

Numerous examples from the literature are available. Exponential functions have been used to model the interaction between presynaptic and postsynaptic voltages of rod-bipolar synapses in the toad (Belgum & Copenhagen, 1988). A model by Falk and Fatt for vertebrate rods assumes that transmitter release is an exponential function of presynaptic potential and that post-synaptic voltages are proportional to transmitter release (Falk & Fatt, 1972). In addition, Liley (1956) observed that depolarizations or hyperpolarizations of presynaptic nerve terminals of the rat diaphragm effected the frequency of miniature end-plate potentials

(MEPPs) in an exponential manner. Controlling the presynaptic membrane polarization through external K^+ concentrations had similar effects on the MEPP frequency (Katz, 1962). Also, Katz and Miledi (1967) found that the application of tetrodotoxin to the squid giant synapse resulted in a gradual decline in the presynaptic spike potential that was mimicked by a logarithmic drop in postsynaptic potential, with no postsynaptic potential detectable for presynaptic spikes less than 40 mv in amplitude.

These exponential features allow the synapse to behave effectively as a rectifier. Such rectification has been observed in a signal clipping feature of rod outputs to horizontal cells in the salamander retina (Atwell *et al.*, 1987). Furthermore, Victor and Shapley (1979b) have defined the nonlinearity associated with the contrast gain control mechanism as behaving much like a full-wave rectifier. The assumption would be that each ON- and OFF-pathway acts as a saturating, monotonic half-wave rectifier and that the convergence at the C cell of the two pathways of opposite polarity results in a full-wave rectifying nonlinearity. The static-nonlinearities of the present modelling results do not support this inference. First, the static-nonlinearities tend to become very flat near the origin, not sharp as would be the case for a rectifier.

In addition, the static-nonlinearities are not monotonic in shape for each pathway but, instead, are often polyphasic in structure. In fact, the model performed more poorly in the few instances when adaptations were implemented that constrained each static-nonlinearity to a monotonic exponential form, or to a half-wave rectification type form which clipped for input values less than zero. For

example, a MSE of 23% for a polynomial version was increased by 5-15% when a saturating exponential form was used. An approximate increase of 30% in MSE was observed with use of a rectified version. Since little improvement in MSE was provided by extending the order of the polynomial to eight, the polyphasic shape of the fourth order polynomials are unlikely to be related to a truncation of terms. However, some of the dips observed at the positive extremes of the static-nonlinearities may relate to the fact a Gaussian distributed input makes fewer excursions to the extremes; the model would be most successful by fitting excursions near the mean of the input.

The lack of concordance of the present results with those of Victor and Shapley may relate to the inability of their sum of sinusoids method to fully appreciate odd-order powers in the static-nonlinearity; the grating stimulus allows for cancellation between effects from deviations above and below background. In addition, the method used by Victor and Shapley to approximate the shape of the nonlinearity measured the dependence of the even-ordered terms on contrast by taking a root mean squared average of the even-ordered harmonic components (1979b). This is a more indirect approach than the method used in this manuscript of directly fitting the time series. Hence, while the sum of sinusoids method allows for minimal interference by noise and may be less computationally intensive (especially for higher order kernels), the white-noise method may be more advantageous in the present context. Several possible features of signal conduction through a synapse can be responsible for the unusual shapes generated by the model for the static-nonlinearities.

First, studies in squid axons have implicated calcium currents as a source of synaptic nonlinearity. Although Ca^{++} causes the release of transmitter in direct proportion to its concentration (Llinas *et al.*, 1981b), Ca^{++} influx increased in an e-fold manner in response to pre-synaptic voltage changes that were within a depolarization range of less than 40 to 50 mv (Llinas *et al.*, 1981a). Thus, the dependence of Ca^{++} influx on pre-synaptic voltage can provide the source of the exponential nonlinearity described in the studies mentioned above. However, Ca^{++} influx decreased at depolarizations greater than 60 mv from the holding potential of -70 mv. In fact, at depolarizations greater than 100 mv, the Ca^{++} flux dropped to nearly zero. While this depolarization is much greater than the maximum deviation of 10-15 mv generated in nonspiking retinal cells, the retinal cells have a resting potential that, at approximately -40 mv (Tachibana & Kaneko, 1988; Kaneko & Tachibana, 1987), is much more depolarized than the holding potential of the squid axons. Damage of the cells from intracellular electrode impalement could be responsible for further depolarization of the resting membrane potential. Consequently, the saturation or dips that are observed in the static-nonlinearities at large positive inputs (fig. 46f; fig. 32f) may be a result of the decline in Ca^{++} influx and concomitant decrease of transmitter release at large pre-synaptic depolarizations.

Another possible explanation for the dips in the static-nonlinearity for large excursions of input is receptor desensitization. Both ON- and OFF-bipolar cells are believed to communicate to third order neurons such as transient amacrines by excitatory amino acids (EAA), most notably glutamate (Massey & Miller, 1990; Linn *et al.*, 1991). Occasionally, other transmitters have been suggested for bipolars (Neal

et al., 1989; Jager & Wassle, 1987; Pourcho & Goebel, 1987). The EAA receptors, including both non-NMDA and NMDA types, are well described in the retina (O'Dell & Christensen, 1989a,b; Gottesman & Miller, 1992; Huba & Hoffmann, 1991; Massey & Miller, 1990). Both non-NMDA and NMDA receptors have been characterized in transient cells in the mudpuppy (Dixon & Copenhagen, 1992). Non-NMDA receptors can show a rapid desensitization of up to 75%, and NMDA receptors show some desensitization in the absence of the coagonist, glycine.[14] The desensitization effect is more prominent at larger agonist concentrations. One explanation for the desensitization is that high and low affinity sites for the non-NMDA agonists exist (consistent with the Hill coefficient of approximately two) and that at high concentrations, the low affinity site becomes active and results in a decreased conductance of the receptor channel (O'Dell & Christensen, 1989a). Thus, the dips in the static-nonlinearity at large input values may represent the attempt of the model to compensate for the rapid desensitization and cooperativity associated with non-NMDA receptors.

Other factors attributable to receptor pharmacology also probably contribute to the polyphasic complexities of the static-nonlinearity. Whereas conductances mediated by non-NMDA receptors demonstrated a linear I-V relation, NMDA generated conductance changes showed an I-V relation that had a positive slope above -40 mv but reversed and had a negative slope thereafter until, at -90 mv, no

---

[14]Glycine can act as an inhibitory neurotransmitter at supramicromolar levels (Huba & Hoffman, 1991). The coagonist effect is at a submicromolar level which, since glycine is one of the most prevalent amino acids, is probably always present under normal physiologic circumstances (Dingledine *et al.*, 1990).

conductivity was apparent (Dixon & Copenhagen, 1992). Thus, unlike the non-NMDA conductance, the I-V curve for the NMDA mediated current is very nonlinear, with an even ordered symmetry around -40 mv. The nonlinear behavior is attributed to the effects of Mg^{++} which blocks the Ca^{++} current flow of the channel at hyperpolarized potentials, conferring a voltage dependence to the channel (Mayer *et al.*, 1984; Nowak *et al.*, 1984; Mittman *et al.*, 1990; Sommer & Seeburg, 1992). Apparently, a single amino acid change in the protein structure of the EAA receptor/channel complexes can cause dramatic effects in conductance properties, changing a linear voltage independent channel into a voltage gated one (Sommer & Seeburg, 1992).

The NMDA receptor-channel complex, then, has significant voltage-gated properties. The light evoked conductance change in the transient amacrines includes effects from both non-NMDA and NMDA channels. It has the general form of a cubic polynomial and resembles the static-nonlinearities from model fits (fig. 39g; fig. 40g). Therefore, though the L_1-N-L_2 sandwich (fig. 21b) does not account for voltage-gated properties, the polyphasic shape of the static-nonlinearity may represent an effort to compensate for voltage-gated properties of the physiology. The more realistic membrane model (fig. 21c) yielded similar cubic forms for the synaptic ligand-gated conductances, g^{on} and g^{off} (fig. 38d - static-nonlinear model; fig. 38e - gated conductance model). In fact, a remarkable resemblance is found between fig. 38d and fig. 38e which indicates that the full membrane model is not hampered by taking its linearized current injection version - the L_1-N-L_2 model.

The dose-response curve for NMDA effects on the firing rate of ganglion cells (Massey & Miller, 1990) or on conductance changes in horizontal cells (O'Dell & Christensen, 1989b) is a standard monotonic sigmoid function with a Hill coefficent of one. So, the polyphasic results of the ligand-gated conductance model do not correlate with the physiology of NMDA receptors, and the membrane model also must be too simplistic. Thus, the unusual ligand-gated conductances generated by the membrane model (similar to the static-nonlinearities of the sandwich model) also probably represent the attempt of the model to compensate for voltage-gated or other nonlinear properties of the system, such as receptor desensitization.

Since NMDA receptors have nonlinear voltage-gated conductances while the non-NMDA receptors behave in a linear voltage independent manner, a differential expression of these receptor types may account for functional differences between cells. In fact, while NMDA receptors are very rare in outer retinal cells such as horizontals and bipolars (Slaughter & Miller, 1983, 1985; Massey & Miller, 1987)[15] which demonstrate very linear physiology, they are much more common in cells of the inner retina which display more nonlinear behavior (Huba & Hoffmann, 1991; Massey & Miller, 1990; Gottesman & Miller, 1992; Coleman & Miller, 1988; Linn *et al.*, 1991; Lin & Massey, 1991). Even within the inner retina, distinctions in expressivity are observed. In the Tiger salamander, for example, the highly nonlinear transient amacrines were sensitive to NMDA while the more linear sustained

[15]Although, NMDA receptors have been reported in the horizontal cells of the catfish (O'Dell & Christensen, 1989b).

amacrines were not (Dixon & Copenhagen, 1992). Therefore, the NMDA receptor may provide an important means for generating nonlinearities in neural systems.

The colocalization of NMDA with non-NMDA receptors may be necessary for NMDA receptor function. Since NMDA receptors become dominant at more depolarized states and non-NMDA receptors dominate at hyperpolarized states, non-NMDA receptors may be necessary to generate membrane depolarization (Mittman *et al.*, 1990). However, as discussed above, retinal cells generally are more depolarized at rest than other neurons of the central nervous system. For example, the measured resting membrane potential of ON- and OFF-ganglion cells of the mudpuppy (Arkin & Miller, 1988a,1988b), or solitary bipolars of the goldfish (Tachibana & Kaneko, 1988; Kaneko & Tachibana, 1987), was approximately -40 mv. In fact, noise in the baseline of ganglion cells of the Tiger salamander was abolished by addition of AP-7 (a NMDA antagonist), indicating that NMDA receptors produce a physiological effect at resting potentials.

The bipolar to transient amacrine synapse appears to be exceptional and unique in the retina with respect to its highly nonlinear, polyphasic, and often even-ordered behavior. Cells in the outer retina such as bipolars and horizontal cells are dynamically very linear in behavior, and cell interactions of the inner retina also have been characterized as very linear based on the results from current injection couples. Such cell couples include the amacrine/amacrine, ganglion/ganglion, and amacrine/ganglion pairings (Sakai and Naka, 1988b, 1990a, 1990b). C cells receive inputs via both the ON- and OFF-bipolar synapses, and the confluence of two very nonlinear paths confers a great deal of complexity and variability to their response

properties. The multitude of shapes of 1st order C cell kernels makes this quite apparent.

The convergence of pathways of opposite polarity permits cancellation, which most certainly contributes to the variability in C cell 1st order kernels. Victor and Shapley (1979) concluded that subunit pooling of inputs, which is responsible for the broad spatial extent and lack of center/surround effects in the contrast gain control mechanism, occurs after the nonlinearity. The results of the present experiments and modelling efforts provide strong support that cancellation does indeed occur, at least between ON- and OFF-pathways and especially between odd-ordered components. As the ON- and OFF-inputs contact the C cell at different sublaminae of the inner plexiform layer, the cancellation can extend over large distances. The even-ordered contributions which tend not to cancel would allow for effective subunit pooling as described by Victor and Shapley.

The model reveals cancellation particularly in cells which have bicuspid shaped 1st order kernels. Fig. 40e reveals the bicuspid shaped 1st order kernel of this C cell to be the result of significant cancellation between the ON- and OFF-bipolar kernels. Both ON- and OFF-paths make approximately equal contributions to the 2nd order kernel diagonal. The very strong contribution of the 2nd order kernel to the response power (54.3%), as compared to the 1st order kernel (11.6%), can probably be attributed to strong cancellation in the latter and summation in the former. The static-nonlinearities of both pathways demonstrate strong odd-order powers to their shapes (fig. 40g), consistent with such cancellation. In general, when models posited significant odd-order components in the static-nonlinearities of both the ON- and

OFF-pathways, the C cells could be expected to have bicuspid 1st order kernels. Likewise, when the shape of the static-nonlinearity of one pathway could be characterized as more odd-order than the opposing pathway, the nature of the 1st order kernel (ON or OFF) would gravitate towards the path that behaved more odd-order. Therefore, although the 1st order kernel accounts for a small percentage of the response power, it remains a valuable indicator of the shape of nonlinearities - even or odd - that can be expected to occur along the ON- and OFF-pathways.

Whether a consistent difference between the static-nonlinearities of the ON- and OFF-paths exists is difficult to assess. The variability in shape of the nonlinearity along a single pathway, as evidenced for example by the disparate shapes of the 1st order kernels, makes distinctions between the two pathways difficult to make. However, quite frequently the OFF-pathway would appear to be more monotonic and less polyphasic than the ON-pathway (fig. 46f, fig. 39g). But, in the cell of fig. 32, both the ON- and OFF-paths have strong even order nonlinearities to their shape (fig. 32f). Interestingly, for this particular C cell, the 1st order kernel was ON-dominant and modelled almost entirely by the ON-bipolar pathway (fig. 32d). The 2nd order kernel involved contributions from both ON- and OFF-paths, but more so from the OFF-pathway. Thus, ON-dominant C cell 1st order kernels seem likely to occur when the OFF-path involves strong 2nd or higher order nonlinearities. Since ON-dominant 1st order kernels are much less common than the bicuspid or OFF-dominant types, the OFF-pathway as compared to the ON-pathway may contain more significant 1st order components.

Thus, some differences between ON- and OFF-bipolar inputs may exist. Possibly, the source of these differences may relate to distinctions between the relative numbers of receptor types that are excited on the post-synaptic C cell by each pathway. For example, both linear behaving non-NMDA receptors and nonlinear behaving NMDA receptors have been described on transient amacrine cells (Dixon & Copenhagen, 1992). Perhaps the ON- and OFF-bipolars excite these receptors to different degrees; the ON- favoring the NMDA receptor, the OFF favoring the non-NMDA receptor. However, the variability in shape of the nonlinearity for a particular type of bipolar input makes any statements regarding differences between ON- and OFF-bipolar inputs rather tenuous. Indeed, the differential excitablility of receptors may vary significantly along a single path. In addition, some shape differences between the static-nonlinearities of ON- and OFF-pathways may relate to a different range of inputs from bipolars for the different pathways. For example, the ON-pathway input was predicted by the model to be more biphasic than the OFF-, and this may result in a relative DC shift of inputs into the OFF-nonlinearity. In fact, Table 2b shows that the mean of the high- and low-pass filter parameters at high modulation is different for the ON- and OFF-pathways, with the OFF- being more narrowly band tuned.[16]

The scaling observed with 1st and 2nd order kernels reflects a contrast gain adjustment that is presumed to reside near the level of the bipolar and C cell interaction. One possible explanation is that the C cell is potentiated to be more

[16]The OFF-pathway becomes less band tuned at low modulation levels (Table 3b)

sensitive to bipolar inputs. The mechanism of contrast gain control, then, would reside within the C cell itself and not the bipolars. Accordingly, the bipolar cell kernels would not be expected to show any changes, such as scaling, with variation in the depth of modulation. Another alternative is that the bipolar cells indeed do increase their gain at low modulation levels and the scaling observed in C cell kernels may reflect the increased gain of bipolar inputs. In addition, a change of scaling can reside in the static-nonlinearity itself without any change of gain in the bipolar inputs, merely by shifting the output of the bipolar cells to a different functional range of the static-nonlinearity or changing the behavior of the nonlinearity. For example, this could occur if the bipolar cell became more or less biphasic in nature, resulting in a DC shift of the input delivered to the static-nonlinearity.

Any combination of these alternatives is also possible. The observation that kinetics changes, with a slowing of the peak response time, occurred at lower modulation depths (*e.g.*, fig. 39) indicates that some change does occur in the bipolar and/or amacrine filter. One way to address the issue as to which filter is adjusted is to compare the relative scaling that occurs in 1^{st} order as compared to 2^{nd} order kernels with a decrease in modulation depth. If the scaling is much greater in the 2^{nd} order kernel relative to the 1^{st} order kernel (on the order of being squared), the pre-filter, which provides input to the nonlinearity, would be expected to be the source of increased sensitivity that occurs at low modulation levels. If the scaling of 1^{st} and 2^{nd} order kernels is approximately the same, this would imply that contrast adjustments occur after the nonlinearity. However, as a significant amount of

cancellation in the 1st order kernel can occur between ON- and OFF-paths, it is important to compare the scaling of the 1st order and 2nd order kernels in cells that do not have indications of significant cancellation. Six cells that appeared to meet this condition (fig. 31, 35, 39, 42, 44, 46) were primarily OFF-like at high modulations. In these cells, an approximate doubling of the scaling of the 1st order kernel at lower modulations corresponded to a scaling of 4-7 times for the 2nd order diagonal. Consequently, the mechanism of contrast gain adjustment at different modulation levels appears to involve sensitivity changes in the bipolar inputs to C cells.

Results from the model offer additional support that adjustments in the pre-filter are important in the mechanism of sensitivity adjustment that occurs with changes in modulation levels. First, the basic shape of the static-nonlinearity does not change much with decreasing modulation.[17] Thus, the factors which generate the nonlinearities of the system are relatively fixed under the present stimulus conditions of variable modulation depth. This should not be interpreted as implying that the mechanism of contrast gain does not depend on the nonlinearity. In fact, the nonlineartiy may be a crucial component of the mechanism. Instead, it implies simply that the overall shape of the nonlinearity does not change much with contrast. Hence, a model, such as the L_1-N-L_2 sandwich that employs nonlinearities that are static, is quite reasonable and justified. Further indication that the scaling of inputs

[17]The preservation of shape of the nonlinearities across modulation levels indicates that the mumerical method is not degenerate and converges consistently to a nonlinearity of similar structure. So, although the static-nonlinearities can have very complex features, the algorithm converges repeatedly to these same features at each modulation level and thereby lends a greater credence to the numerical outcome.

into the nonlinearity is the variable that seems most dependent on the modulation level - not a change in the shape of the nonlinearity - is provided by the observation that the static-nonlinearity at low modulations often appears to contain a shorter segment of the domain for the static-nonlinearity that occurred at high modulations.[18] This is consistent with the conclusion of Shapley and Victor (1980) that changes related to contrast gain occur prior to the generation of the nonlinearity, probably via a feedback from cells after the nonlinearity. The findings by Sakai and Naka that kernels measured from bipolar cells do not change with modulation level (Sakai & Naka, 1987b) would imply that the adjustment of bipolar inputs occurs presynaptically and is not reflected by recordings from the soma. This lends further support to the suggestion that the recurrent synapse between sustained amacrine cells and the pre-synaptic terminals of bipolar cells may function to adjust the gain of the bipolar cell inputs to C cells.

[18]Recall that a decrease in the overall magnitude of the bipolar inputs into the nonlinearity occurs at low modulatons despite the fact that bipolar sensitivity may be increased.

VII. LEGENDS

A. TABLES

TABLE 1 - Mean Square Errors (MSEs; see Appendix B) for the 1st order Wiener kernel contribution (1st) and both the 1st and 2nd order kernel contribution (2nd) at different modulation levels. Level 1 was for the highest variance, with each succeeding level being 1/2 the variance of the previous modulation level (see Methods - Experimental). Symbols are included to describe the quality of the kernels. Early features of 1st order kernel at high modulation (level 1): N - ON-type, B - bicuspid shape, F - OFF-type. Late features observed at low modulation levels (3 or 4): O - oscillations with superscript '+' for strong and 'm' for mild; H - broad hyperpolarization followed by depolarization plateau at low modulation. The appropriate figure reference (in parenthesis) is aligned with the matching cell #. Twenty-six transient C cells are listed.

TABLE 2 A) - Parameters determined by model fits at modulation level 1 for cells 1-22. Analytic forms for the parameters are provided by Appendix C-iii: ON-bipolar filter (B_1^{on}), OFF-bipolar filter (B_1^{off}), pre-syn filter (B_2), and amacrine filter (L_2). **B)** - Summation of high-pass taus denoted H (numerator of filter; *e.g.* $\tau_1 + \tau_1''$ for τ^H_{ON}; $\tau_1' + \tau_1''$ for τ^H_{OFF}) and low-pass taus denoted L (denominator of filter; *e.g.* $\tau_2 + n\tau_3 + \tau_2''$ for τ^L_{ON}; $\tau_2' + n\tau_3' + \tau_2''$ for τ^L_{OFF}): ON-path (L_1^{on}), OFF-path (L_1^{off}), amacrine filter (L_2). The means and standard deviations for each of the high- or

low-pass parameters is provided and shows good consistency among the population of 22 cells. The OFF-Path filter is more narrowly tuned than the ON-path filter.

TABLE 3 A) - Parameters determined by model fits at modulation level 1 through level 3 (value in parentheses) for cells 1-3. Analytic forms for the parameters are provided by Appendix C-iii: ON-bipolar filter (B_1^{on}), OFF-bipolar filter (B_1^{off}), pre-syn filter (B_2), and amacrine filter (L_2). **B)** - Summation of high-pass taus denoted H (numerator of filter) and low-pass taus denoted L (denominator of filter): ON-path (L_1^{on}), OFF-path (L_1^{off}), amacrine filter (L_2). The only consistent pattern to emerge was that the ratio of τ^H_{OFF} to τ^L_{OFF} increased at lower modulation levels implying that the OFF-path filter was less band tuned at lower modulation levels.

TABLE 4 - lists polarity and peak response times for various combinations of cell couples used for current injection recordings. The 1st cell of the pairing was injected with white noise current, and responses were recorded from the 2nd cell. (modified from Sakai & Naka - 1988a,b)

B. FIGURES

FIG. 1 Schematic of retina showing the basic organization into layers with 5 principal cell types including photoreceptors (rods and cones), horizontal cells, bipolar cells, amacrine cells, and ganglion cells. Flat and invaginated cone bipolar synapses are demonstrated; the former being sign-preserving, the latter, sign-inverting. (modified from Kandel & Schwartz, 1985)

FIG. 2 Responses were recorded from two electrodes placed in a horizontal cell soma and in a bipolar cell. The dashed lines are 1st order kernels for the light-evoked response of horizontal cells. In **A)**, the solid lines are the 1st order Wiener kernels generated from the response of an ON-bipolar cell to light or to current injection in the horizontal cell. The solid lines of **B)** show the 1st order kernels of an OFF-bipolar cell to light and current injection. Light evoked kernels from bipolar cells and horizontal cells were recorded simultaneously. Note the greater biphasic nature of the light as opposed to current evoked response in both ON- and OFF-bipolar cells. Also, note the greater biphasic nature of the light-evoked kernels of bipolar cells as compared to horizontal cells. (modified from Sakai & Naka, 1988c)

FIG. 3 A) Receptive field profiles of a cone at four mean luminance levels and four horizontal cell somas and axons. The method employed involved cross-correlating a travelling random grating input with the response of the cell. **B)** Receptive field

profiles for bipolar and ganglion cells generated by a single moving bar and by random travelling gratings. (modified from Sakai & Naka, 1988c)

FIG. 4 Step response (100 msec flash in darkness), 1st order kernel, and 2nd order kernel, respectively, from **A)** an NA cell, **B)** an NB cell, and **C)** a C cell. (modified from Sakai & Naka - 1987a, 1990a and Sakuranaga & Naka, 1985c)

FIG. 5 Circuit schematic outlying some of the connections considered important in explaining the observed physiology of the retina. **E)** represents a composite circuitry which was developed in this study to characterize transient C amacrine connections. This circuitry does not demonstrate spatial interactions of cells or interactions between like cells. R -photoreceptors; B - bipolar cells (superscript s for sustained and t for transient types); H - horizontal cells; N - sustained amacrines; C - transient ON/OFF amacrines; G - ganglion cells. The qualification A or B represents ON- of OFF-, respectively. The t type bipolar cells are those that are proposed to have GABA or glycine receptors at their presynaptic terminals.

FIG. 6 A1) shows 1st order kernels; solid line is for an NA cell, dashed is for GA cell. **A2)** and **A3)** are contour plots for 2nd order kernels for an NA and a GA cell, respectively. **B1), B2),** and **B3)** show similar kernels for NB and GB cells. In the contour plots, solid lines indicate depolarizing peaks and dashed lines indicate hyperpolarizing troughs. Note the similarity in structure between the kernels of the

sustained amacrines and those of their ganglion cell counterparts. (modified from Sakai & Naka, 1990a)

FIG. 7 shows the fast depolarizing 1st order kernels for current injection responses between pairs of similar ON- (A) or OFF- (B) cells. The kernels from three different pairs are superimposed with normalized peak amplitudes. The peak response time is approximately 6 msec for each pairing. (modified from Sakai & Naka, 1990a)

FIG. 8 shows triphasic 1st order kernels from ganglion cells after white-noise current injection into C, NA, and NB amacrines. The kernels were generated by cross-correlating the current input with the ganglion cell spike discharges. The kernels of four cells are superimposed for each pairing. Note that the kernels from GB cells (B) have a strong depolarizing peak irrespective of the type of amacrine cell in the pairing. The converse situation is observed with the kernels from GA cells (A), with a strong hyperpolarization, or spike suppression, occurring in the 1st order kernel regardless of amacrine cell type. The peak response time is approximately 20 msec for the pairings shown. (modified from Saka & Naka, 1988a)

FIG. 9 shows the 1st order kernels from pairings of ganglion cells obtained by cross-correlating the current input into a ganglion cell with the spike discharges recorded from another ganglion cell. Some fast responses for pairings of ganglion cells of the same type are shown (top row). Slow triphasic kernels for pairings of the same type are also observed, but not shown here. Kernels from ganglion pairings of opposite

type are shown and were always of the slow form (bottom row). As in FIG. 8, the slow kernels recorded from GA cells (**A**) were hyperpolarizing while the slow kernels recorded from GB cells (**B**) were depolarizing. Four kernels are shown superimposed for each type of pairing. (modified from Sakai & Naka, 1988b)

FIG. 10 shows 1st order kernels from **A**) GA and **B**) GB ganglion cells with injection of white-noise current into C cells. Three kernels are shown for each pairing. Note the increased biphasic shape of the GA as opposed to GB kernel waveform. (modified from Sakai & Naka, 1988a)

FIG. 11 Histograms for peak response times of 1st order kernels for **A**) ganglion to ganglion transmission and **B**) amacrine to ganglion transmission. Two clusters are revealed for fast and slow conduction, with few pairings showing a peak response time intermediate to the two clusters. (modified from Sakai & Naka, 1988b)

FIG. 12 A) Simultaneous recordings from a NA and a GA cell are shown in response to a flash of light in darkness. **B**) shows the response of a GA cell to current injection in a NA cell with a depolarizing pulse (2nd trace) and hyperpolarizing pulse (3rd trace). **C**) shows the response of a NA cell after current injection in a GA cell. Note the oscillatory nature of this response. (modified from Sakai & Naka, 1990a)

FIG. 13 A) shows simultaneous recordings of a NB and a GB cell in response to a light flash. **B**) shows the response in a GB cell to depolarizing and hyperpolarizing

current pulses injected into a NB cell. **C)** shows the response of a NB cell to current pulses injected in a GB cell. **D)** shows 1st order kernels for NB → GB transmission (solid) and GB → NB transmission (dashed). (modified from Sakai & Naka, 1990a)

FIG. 14 A), B), and **C)** contain intracellular recordings from GB, GA, and a NA cell, respectively, with responses triggered by optic nerve stimulation as indicated by the arrows in each trace. Note the mild oscillation in the NA cell. (modified from Sakai & Naka, 1988b)

FIG. 15 A) Light-evoked responses of a NA and a NB cell recorded simultaneously. Note the 30 Hz oscillations. **B)** shows the response of the NB cell after delivery of a current pulse to the NA cell. The second trace is the response to a depolarizing pulse, and the fourth trace is the response to a hyperpolarizing pulse. The response is initially sign-preserving with a damped oscillation at 30 Hz. **C)** The response of the NA cell is shown following current injection in the NB cell. The response is much smaller than was observed in **B)**. The current pulses were 10 msec in duration. (modified from Sakai & Naka, 1990b)

FIG. 16 A) compares the 1st order kernel for NA → NB transmission (solid) and for NB → NA transmission (dashed). The gain and the phase of the Fourier transform of the kernels is contrasted in **B)** and **C)**, respectively. Note the sign-inversion for NB → NA transmission and the strong 30 Hz component for transmission in either direction. (modified from Sakai & Naka, 1990b)

FIG. 17) Top traces show the sinusoidal current injected into a NA cell, marked I. The responses from a NB cell are in the bottom traces, marked R. Note the frequency doubling that occurred with 20 Hz injections (B), and the strong response with 35 Hz injections (C). (modified from Sakai & Naka, 1990b)

FIG. 18) The peak frequency of noise from a NA cell is plotted against the peak frequency of noise recorded simultaneously from a NB cell. The ranges were from 20 to 50 Hz for each pairing, with an average of 35 Hz. Note the strong concordance for each pairing. (modified from Sakai & Naka, 1990b)

FIG. 19) The cross-correlation of membrane dark noise between **A)** a NA/NB and **B)** a NA/NA pairings of amacrines is shown for simultaneous recordings for each pairing. Note the phase inversion between the two types of pairings. (modified from Sakai & Naka, 1990b)

FIG. 20 A) An RC circuit with a voltage generator, $V_S(t)$. The voltage measured across the resistor ($V_R = V_1 - V_2$) behaves as a single-stage high-pass filter, whereas the voltage measured across the capacitor ($V_C = V_2 - V_3$) behaves as a single-stage low-pass filter. The Bode plots showing the gain and phase of the low-pass filter and high-pass filter are shown in **B)** and **C)**, respectively. $\tau = RC$ is the time constant that determines the cut-off frequency of the filters.

FIG. 21 **A)** Representation of amacrine C cell anatomy showing parallel ON- and OFF-bipolar inputs. **B)** Schematicized circuit representation for transient cells. The spatially uniform light activates each parallel pathway. L_1^{on} and L_1^{off} are linear filters representing the processing done by ON- and OFF-bipolar cells, respectively. N_1 and N_2 represent static-nonlinearities at synapses for ON- and OFF-paths, respectively. L_2 is a filter in the amacrine cell membrane. See Appendix C-iii for analytic forms of the filters. C) Electrical circuit representation of transient cell membrane physiology. The impedance, Z, that would be responsible for filtering in the membrane is in parallel with the variable conductances, g_{on} and g_{off}.

FIG. 22 **A)** On-bipolar 1st order kernel. Data is solid, model is dashed. $\tau 1 = .0379, \tau 2 = .0084, \tau 3 = .00497, n = 10$. **B)** The Fourier transform of the 1st order kernel is shown (solid) with the model transfer function, B_1^{on} (dashed). Notice the strong DC component. See Appendix C-iii for the analytic form for B_1^{on}. Arbitrary units on ordinate.

FIG. 23 Contour plot of a 2nd order Wiener kernel of a C cell demonstrating the typical four-eyed structure. Kernel values for given τ's project out of the plane. The orientation of the diagonal and two slices used in model fits are shown for reference. Solid lines of the contour represent positivities whereas the dashed lines indicate negativities.

FIG. 24 A) 1st order amacrine kernel. Data is solid, model is dashed. see Appendix C-ii,iii for the analytic form. For B_1^{on}, $\tau 1 = .745$, $\tau 2 = .0328$, $\tau 3 = .00486$, $n = 10$; for B_1^{off}, $\tau 1 = .150$, $\tau 2 = .122$, $\tau 3 = .00418$, $n = 10$; for B_2, $\tau 1 = .142$, $\tau 2 = .0208$; for L_2, $\tau 1 = .0455$, $\tau 2 = .0157$, $\tau 3 = .01432$, $n = 1$ for this one example ($n = 10$ for L_2 in other cells modelled). **B)** Diagonal of 2nd order kernel. Notice negativity at 120 msec. **C)** reconstructed slice at 40msec. **D)** reconstructed slice at 80 msec. See Fig. 23 for orientation of diagonal and slices. **E)** Frequency representations of 1st order kernel of transient amacrine. Notice sharp cut-off at 0 Hz. **F)** Diagonal of transient amacrine 2nd order kernel. Notice strong DC component. **G)** Predicted impulse responses from model fits corresponding to L_2. **H)** L_2. Notice strong DC component. See Fig. 21b for schematicized circuit location of L_2 and Appendix C-iii for analytic form. Data is solid, model is dashed for graphs A) - F). Arbitrary units on ordinates.

FIG. 25 A) Response (top trace) and white noise stimulus (bottom trace) from a horizontal cell shown at three different modulation levels. Each succeeding modulation level has a variance one-half of the preceding level, with the variance of the highest modulation level as one-quarter of the mean luminance. Note the great reduction in response amplitude at the lower modulation levels. Arbitrary units on the ordinate. **B)** Distribution of response amplitudes from the horizontal cell in A). The drop in variance of the response matches the drop for the stimulus, with the innermost distribution corresponding to the lowest stimulus modulation level. **C)** 1st order Wiener kernels from a horizontal cell at four different modulation levels.

Level 1 corresponds to the highest modulation level; level 4, the lowest. Minimal change is observed in the shape or amplitude of the kernels, which explains the proportional drop in response amplitude with decreasing stimulus amplitudes seen in A) (*i.e.* no compensation is evident from the kernels to indicate an attempt to increase the response relative to the stimulus at low modulation levels).

FIG. 26 A) Response (top trace) and white noise stimulus (bottom trace) from a transient C amacrine cell shown at three different modulation levels. Each succeeding modulation level has a variance one-half of the preceding level, with the variance of the highest modulation level as one-quarter of the mean luminance. Note the response amplitude of the cell exhibits only a mild reduction in response amplitude despite the large reduction in stimulus modulation depth. Arbitrary units on the ordinate. B) Distribution of response amplitudes from the transient amacrine cell in A). The drop in variance of the response is much less prominent than was observed in 25 B). The innermost distribution corresponds to the lowest stimulus modulation level. The asymmetric shape of the distribution conveys the nonlinear behavior of the transient amacrine cells as opposed to the horizontal cells. The attempt to maintain the response amplitude of the amacrine despite decreasing stimulus modulation levels implies some mechanism of gain adjustment that makes these cells more sensitive at low modulation levels and distinguishes these cells from cells such as the horizontals of the outer retina. This will be evident from the changes in the shape and amplitude of the kernels of the amacrine cells (*e.g.*, Fig. 29)

FIG. 27 A) Response (top trace) and white noise stimulus (bottom trace) from a NA amacrine cell shown at three different modulation levels. Each succeeding modulation level has a variance one-half of the preceding level, with the variance of the highest modulation level as one-quarter of the mean luminance. Similar to the type C amacrine cell, the response amplitude of the NA cell exhibits only a mild reduction in response amplitude despite the large reduction in stimulus modulation depth. Arbitrary units on the ordinate. **B)** Distribution of response amplitudes from the NA amacrine cell in A). The drop in variance of the response is much less prominent than was observed in 25B). The innermost distribution corresponds to the lowest stimulus modulation level. The attempt to maintain the response amplitude of the amacrine despite a decreased stimulus modulation indicates an increased sensitivity in NA cells at low modulation levels. This is similar to what was observed for the type C cells (Fig. 26).

FIG. 28 A) Response (top trace) and white noise stimulus (bottom trace) from a NB amacrine cell shown at three different modulation levels. Each succeeding modulation level has a variance one-half of the preceding level, with the variance of the highest modulation level as one-quarter of the mean luminance. Similar to the type C and NA amacrine cells, the response amplitude of the NB cell exhibits only a mild reduction in response amplitude despite the large reduction in stimulus modulation depth. Arbitrary units on the ordinate. **B)** Distribution of response amplitudes from the NB amacrine cell in A). The innermost distribution corresponds to the lowest stimulus modulation level. As in Fig. 26 and Fig. 27, the

response amplitude of NB cells shows a minimal reduction compared to the reduction in stimulus modulation.

FIG. 29 A) 1st order Wiener kernel from type C transient amacrine cell. Level 1 corresponds to the highest modulation level of the white noise input, with level 4 corresponding to the lowest modulation variance (see Methods - Experimental). Note the increase in amplitude of the kernels at low modulation levels. The greatest increase in scaling appears between level 2 and level 3. A change in shape of the 1st order kernel from a bicuspid structure at high modulation to a strong 55 msec hyperpolarization at low modulation is apparent. B) Along the diagonal of the 2nd order kernel, the emergence of 30 Hz oscillations which fade by 130 msec are apparent at low modulations. A progressive increase in amplitude is also observed along the diagonal. C) Fourier transform of 2nd order kernel diagonal showing a 2nd peak at near 35 Hz. D) Fits of model to 1st order kernel, diagonal of 2nd order kernel, and two slices at 34 msec and 66 msec. Model fit is dashed. **i)** corresponds to modulation level 1 (highest) and **ii)** to level 4 (lowest). Note the poor fit along the diagonal at modulation level 4. Arbitrary units on ordinate.
(Cell #5)

FIG. 30 A) 1st order kernel of a C cell at four different modulation levels. The kernel shape is more bicuspid at the high modulation levels. A change of shape is more prominent than any change in amplitude as modulation depths are decreased. Note the appearance of a late depolarization after 100 msec which is not apparent

in the diagonal of the 2nd order kernel (**B**)). Unlike the 1st order kernel, the diagonal shows a progressive increase in amplitude at low modulation levels. Arbitrary units on ordinate.
(Cell #8)

FIG. 31 A) An increase in amplitude but little change in shape of this OFF-like 1st order C cell kernel is observed with a decrease in modulation level. An increase latency of the peak response time is observed at low modulations, with a value of approximately 33 msec as compared to a 27 msec value at high modulations. **B)** The 2nd order kernel diagonal shows a typical increase in amplitude at low modulations. Some mild oscillations are also apparent at the lowest modulation level. Note the greater scaling that occurs along the 2nd order kernel diagonal relative to the 1st order kernel at low modulation levels. Arbitrary units on ordinate.
(Cell #23)

FIG. 32 A) 1st order kernel from a C cell with an initial depolarization. A gradual and progressive emergence of oscillations is apparent by the peaks at 70 and 110 msec and appears to be superimposed on the earlier signal. No increase in the initial peak amplitude at 40 msec is observed. **B)** Diagonal of the 2nd order kernel. The strong negativity at 70 msec arises from the 2nd peak moving off-diagonal and leaving a trough in between along the diagonal. **C)** Fits of 1st order kernel, diagonal of 2nd order kernel, and two slices of the 2nd order kernel at 34 and 66 msec by the model (dotted) at modulation level 1 (highest). **D)** Contribution of the ON- (left column)

and OFF- (right column) pathways to the 1st order kernel (top row) and diagonal of the 2nd order kernel (bottom row) at modulation level 1. The 1st order kernel consists entirely of ON- contributions, whereas the diagonal receives contributions from both ON- and OFF-pathways. Model contribution is dashed. **E)** Model predictions for ON- (solid) and OFF- (dashed) inputs to the amacrine C cell with normalized ordinate showing a greater latency by approximately 5 msec for the ON-input (modulation level 1). **F)** Polynomial shapes predicted for ON- (top) and OFF- (bottom) static-nonlinearities. The OFF- polynomial incorporates the reverse polarity of the OFF-bipolar input into the polynomial itself. The shapes of the nonlinearities are polyphasic, especially for the ON-pathway (**F-i** - modulation level 1; **F-ii** - modulation level 2). The abscissa spans only the output L_1^{on} or L_1^{off} (whichever the case may be). **G)** Top traces for each graph show the actual (solid) and predicted model (dotted) responses of a C cell to various step heights, shown by the bottom trace. The best fits by the model occur with the largest step increments and decrements which occur at time 2.3 to 3.3 sec. The DC shift of the model is an arbitrary parameter for the model and should not be used to assess the quality of the fit. Units for axes other than time are arbitrary in all graphs.
(Cell #14)

FIG. 33 A) 1st order kernel from a C cell, initially with a depolarizing peak characteristic of ON-type behavior. The emergence of oscillations at low modulation levels is apparent by the gradual development of a peak at 60 msec. Minimal scaling is observed in the 1st peak at 30 msec as the modulation level changes. **B)** The

diagonal of the 2nd order kernel shows an increase in scaling with each drop in modulation depth. Very few if any of the features observed in the 1st order kernel after 55 msec are apparent in the diagonal. C) Alignment of ON-bipolar like 1st order kernel (solid) and the diagonal of 2nd order kernel (dashed) for modulation level 2. This demonstrates the frequency doubling property that can characterize the 2nd order kernel. D) Fourier transforms of the 1st order kernel (top) and of the 2nd order kernel diagonal (bottom) for modulation level 4 showing the strong 30 Hz component of the 1st order kernel at low modulation. E) Response of the C cell to three different step heights. Steps are shown by the lower trace of each graph, and the responses by the upper trace. At lower step heights, the response to an increase in luminance that occurs for step increment onsets or decrement offsets decreases relative to the response to luminance decreases (*e.g.* small response at 8.8 and 9.5 sec along the time axis as compared to 9.0 and 9.3 sec). Notice the doublet structure of the response to the largest steps. This may be suggestive of nonlinearities such as voltage-gated properties. Arbitrary units on ordinate.
(Cell # 26)

FIG. 34 A) OFF-type 1st order kernel from C cell showing progressive scaling and an increased latency of the peak response time with decrease in modulation. Mild 30 Hz oscillations appear at the low modulation levels. The quality of the recording may have deteriorated at the level 4 modulation level, accounting for the decrease in amplitude of this kernel. **B)** 2nd order kernel diagonal. Note the greater scaling that occurs along the 2nd order kernel diagonal relative to the 1st order kernel at low

modulation levels. **C)** Response of the C cell to large (top) and small (bottom) step increments. A decrease is noted in the response at onset relative to offset at the low step height. **D)** Static-nonlinearities for the ON- (top) and OFF- (bottom) pathways of the model for modulation levels 1 through 4 (**D-i** through **D-iv**, respectively). Arbitrary units on ordinate.

(Cell #1)

FIG. 35 A) 1st order kernel of bicuspid shape recorded from C amacrine. The bicuspid structure is preserved with decreasing modulation level, and an increase in scaling is observed at the low modulation levels. Oscillations appear with decreasing modulation, with the gradual emergence of the peak at 70 msec. **B)** 2nd order kernel diagonal which does not demonstrate the strong late oscillatory features of the 1st order kernel. **C)** Response of C cell to step inputs. The response of the cell to step onset relative to offset is preserved with decreasing step height. Arbitrary units on ordinate.

(Cell #11)

FIG. 36 A) 1st order kernel from C cell with a bicuspid shape at high modulation level, but the development at low modulations of a strong initial hyperpolarization at 55 msec as well as some mild oscillations. A deterioration in the quality of the recording can explain the drop in amplitude of the kernel at modulation level 4. This decrease in amplitude is also observed along the diagonal. **B)** The diagonal of the 2nd order kernel shows some oscillatory behavior as well, with a dominant

component near 30 Hz and a smaller component at twice this frequency. **C)** The Fourier transforms of the 1st order kernel (top) and the 2nd order kernel diagonal (bottom) show the 30 Hz component that is common to each as well as a 60 Hz component that is most evident on the diagonal. **D)** Responses to step inputs. The response at step onset was greater than that at step offset for high step heights but the response at step onset and offset became nearly equal at the lower step height. Arbitrary units on ordinate.

(Cell # 10)

FIG. 37 A) 1st order kernel from C cell that was bicuspid in shape at modulation level 1 but developed into a structure with an initial strong hyperpolarization (55 msec) followed by a broad depolarization. **B)** Diagonal of 2nd order kernel. Little temporal overlap of features is observed between the 1st order kernel and the diagonal of the 2nd order kernel. **C)** Response to step heights showing a decrease in response at step onset at low step heights. **D)** Spontaneous discharges of uniform height from the C cell in darkness (top trace). An enlarged segment of the time-series shows the discharges to be approximately 30 msec in duration. Arbitrary units on ordinate.

(Cell #18)

FIG. 38 A) 1st order kernel with bicuspid shape at high modulation levels and a strong hyperpolarization at 55 msec followed by a depolarization for low modulation levels. **B)** Diagonal of 2nd order kernel. **C)** Model prediction for inverse transform

of L_1^{on} (solid) and L_1^{off} (dashed) showing a greater latency in the ON-pathway input to C cells as opposed to the OFF-pathway. Ordinate is normalized for comparison. **D)** Static-nonlinearities corresponding to model structure of fig. 21B for the ON- (top) and OFF- (bottom) pathways. The ON-polynomial is polyphasic and relatively flat near the origin. The OFF-polynomial is more monotonic and asymptotic near the origin. **E)** Model predictions for ligand-gated conductances based on structure of fig. 21C. The shape of the polynomials for the conductances is almost identical in shape to the static-nonlinear polynomials of D). Arbitrary units on ordinate. (Cell #13)

FIG. 39 A) 1st order kernel with bicuspid structure at high modulations that, at lower modulations, became progressively more OFF-like with a greater latency in the peak response time. **B)** Diagonal of 2nd order kernel, also with a greater latency in the peak response time at low modulations. Note the greater scaling that occurs along the 2nd order kernel diagonal relative to the 1st order kernel at low modulation levels. **C)** Response to steps showing a greater response with decreases in luminance than with increases which became even more accentuated at lower step heights. **D)** Model fits (dotted) of 1st order kernel, diagonal of 2nd order kernel, and two slices of the 2nd order kernel at 34 and 66 msec at modulation level 1 (**D-i**), level 2 (**D-ii**), and level 3 (**D-iii**). The fits are adequate for each of the modulation levels. **E)** Model predictions for the inverse transforms of L_1^{on} (solid) and L_1^{off} (dashed) at three modulation levels showing the persistence of the greater latency of the ON-pathway at all levels. The ON-pathway is also more biphasic at each level. Ordinates are

normalized for effective comparison. **F)** Comparison of inverse transform of L_1^{on} (top) and L_1^{off} (bottom) at three modulation levels. A greater latency of 4 msec is observed for both L_1^{on} and L_1^{off} with decreasing modulation level. **G)** Static-nonlinearities of L_1-N-L_2 model for ON- (top) and OFF- (bottom) pathways at modulation level 1 (**G-i**), level 2 (**G-ii**), and level 3 (**G-iii**). The ON- path is polyphasic while the OFF- is monotonic with a saturating quality. The basic structure of the nonlinearities is preserved across all modulation levels. Units for axes other than time are arbitrary for all graphs.

(Cell #2)

FIG. 40 A) 1st order kernel of a C cell with a bicuspid structure at high modulation level which became more OFF-like at low modulation levels. **B)** Diagonal of 2nd order kernel showing a progressive increase in amplitude at low modulation. The later occurrence of the peaks along the time axis of this C cell as compared to others indicates a slower kinetics. **C)** Response to steps showing that a strong response to increments in luminance became more weak at low step heights. **D)** Model fits (dotted) of 1st order kernel, diagonal of 2nd order kernel, and two slices of the 2nd order kernel at 34 and 66 msec at modulation level 1 (**D-i**), level 2 (**D-ii**), level 3 (**D-iii**), and level 4 (**D-iv**). The fits are adequate for each of the modulation levels. **E)** Contribution of the ON- (left column) and OFF- (right column) pathways to the 1st order kernel (top row) and diagonal of the 2nd order kernel (bottom row) at modulation level 1. The predicted contribution from each pathway according to the model (dashed) shows that the small bicuspid structure of the 1st order kernel results

primarily from the cancellation between the ON- and OFF-pathways of different kinetics. The diagonal, however, results from the summation of contributions from both ON- and OFF-pathways. **F)** Comparison of inverse transform of L_1^{on} (top) and L_1^{off} (bottom) at four modulation levels. A greater latency of approximately 4 msec is observed for both ON- and OFF-pathways with decreasing modulation level. Note the greater biphasic nature of the ON-pathway. **G)** Static-nonlinearities of L_1-N-L_2 model for ON- (top) and OFF- (bottom) pathways at modulation level 1 (**G-i**), level 2 (**G-ii**), level 3 (**G-iii**), and level 4 (**G-iv**). The OFF-path shows more saturation at the endpoint than the ON-path. The basic structure of the nonlinearities is preserved across modulation levels. Arbitrary units for axes other than time.
(Cell #3)

FIG. 41 A) 1st order kernel from C cell showing some ON-bipolar features at modulation level 1, progressing to a more bicuspid shape at level 2, and then finally appearing more OFF-like at the lowest modulation depth (level 4). **B)** Diagonal of 2nd order kernel. Arbitrary units on ordinate.
(Cell #9)

FIG. 42 A) 1st order kernel of C cell that was initially bicuspid at high modulation, becoming more OFF-like at low modulation levels. **B)** Diagonal of 2nd order kernel. The lack of scaling observed between modulation level 3 and level 4 may be explained by a deterioration in the quality of the cell recording. Note the greater

scaling that occurs along the 2nd order kernel diagonal relative to the 1st order kernel at low modulation levels. Arbitrary units on ordinate.
(Cell #21)

FIG. 43 A) 1st order kernel from C cell showing a strong tendency towards oscillation as the modulation depth was decreased. **B)** Oscillations are also apparent along the diagonal of the 2nd order kernel at low modulations. Arbitrary units on ordinate.
(Cell #19)

FIG. 44 A) 1st order kernel and **B)** diagonal of 2nd order kernel from C cell. The 30 msec peak to peak oscillation that begins to appear at low modulation levels in the 1st order kernel has the same frequency along the diagonal: no frequency doubling is observed (unlike the case for the direct bipolar inputs - Fig. 23C. Note the greater scaling that occurs along the 2nd order kernel diagonal relative to the 1st order kernel at low modulation levels. Arbitrary units on ordinate.
(Cell #6)

FIG. 45 A) 1st order kernel from C cell with late depolarization near 100 msec. **B)** 2nd order kernel diagonal showing a late appearing feature near 100 msec as well. Arbitrary units on ordinate.
(Cell #15)

FIG. 46 A) 1st order kernel from C cell with OFF-type appearance. **B)** Diagonal of 2nd order kernel. Note the greater scaling that occurs along the 2nd order kernel diagonal relative to the 1st order kernel at low modulation levels. **C)** Fits of 1st order kernel, diagonal of 2nd order kernel, and two slices of the 2nd order kernel at 34 and 66 msec by the model (dotted) at modulation level 1 (highest). **D)** Contribution of the ON- (left column) and OFF- (right column) pathways to the 1st order kernel (top row) and diagonal of the 2nd order kernel (bottom row) at modulation level 1. The 1st order kernel and 2nd order kernel diagonal consist primarily of OFF- contributions but receive significant input from the ON-pathway as well. Model contribution is dashed. **E)** Model predictions for the inverse transform of L_1^{on} (solid) and L_1^{off} (dashed) inputs to the amacrine C cell with normalized ordinate showing a greater latency by approximately 5 msec for the ON-path (modulation level 1). The ON-pathway is more biphasic than the OFF. **F)** Polynomial shapes predicted for ON- (top) and OFF- (bottom) static-nonlinearities at modulation level 1. For display purposes, the OFF- polynomial incorporates the reverse polarity of the OFF-bipolar input into the polynomial itself. The shapes of the nonlinearities are polyphasic, especially for the ON-pathway. The OFF-pathway static-nonlinearity is more monotonic in appearance, with a saturation near the positive endpoint. The abscissa spans only the output from L_1^{on} or L_1^{off} (whichever the case may be). **G)** Time series of white noise response with model fit (dotted) showing good phase alignment of peaks with some discrepancy with peak heights. **H)** Top traces for each graph show the actual (solid) and predicted model (dotted) responses of a C cell to various step heights, shown by the bottom trace. The best fits by the model occur with the largest

step increments and decrements which occur at time 2.3 to 3.3 sec. Units for axes other than time are arbitrary in all graphs.
(Cell #16)

FIG. 47 A) 1st order kernel from a NA cell showing little scaling of the 1st peak at 40 msec as the modulation depth is decreased. The 2nd peak, however, does show significant scaling at low modulation level. **B)** Diagonal of 2nd order kernel showing the emergence of oscillatory behavior at low modulations that persists up to 170 msec on the time axis. The mild decrease in scaling at modulation level 4 seen with the 1st order kernel is not observed along the diagonal, implying that a deterioration in the quality of the recording is not a cause of the mild decrease. Arbitrary units on ordinates.

FIG. 48 A) 1st order kernel from a NB cell showing an increased scaling as the modulation depth is decreased. The scaling of the 1st negativity at 40 msec is not as pronounced as that at 60 msec. **B)** Diagonal of 2nd order kernel. An unusual waveform developed at 100 msec at low modulation levels. Arbitrary units on ordinates.

FIG. 49 A) 1st order kernel from a NB cell showing an increased scaling and the emergence of 30 Hz oscillations as the modulation depth is decreased that are still

detectable at 250 msec. **B)** Diagonal of 2nd order kernel showing robust oscillations as late as 150 msec. Arbitrary units on ordinates.

FIG. 50 A) 1st order kernel from a NA cell showing an increased scaling as the modulation depth is decreased. The scaling of the 1st negativity at 40 msec is not as pronounced as that at 60 msec. **B)** Diagonal of 2nd order kernel. Arbitrary units on ordinates.

FIG. 51 A) Response of a NB cell to a step of light from darkness showing that after the initial hyperpolarization, a depolarization followed by 30 Hz oscillations is observed. The response suggests that, after the initial hyperpolarization attributed to OFF-bipolar inputs, other inputs of a depolarizing nature are affecting the behavior of the NB cell. **B)** Response of the NB cell to a step from a mean level of luminance to darkness. Arbitrary units on the ordinate.

FIG. 52 Interspike interval histogram from a GA cell in darkness **(A)** and at the mean level of luminance **(B)**. Bins are 2 msec in width and the histograms show a peak near the interspike interval of 26 to 28 msec corresponding to a frequency of approximately 35 to 40 Hz.

FIG. 53 Interspike interval histogram from a GA cell in darkness **(A)** and at the mean level of luminance **(B)**. Bins are 2 msec in width. Two peaks in the histogram of A) are observed at 10 msec and 34 msec. Since the peak at 34 msec is larger, if

the spikes are related to 30 Hz membrane oscillations, roughly one spike occurs per oscillation. This is in agreement with observation of fig. 12A which shows a GA cell having one spike per oscillation. The peak of the histogram at a mean level of luminance in B) is near 50 msec and has a broader distribution than occurs in A) suggesting that the GA cell exhibits different spontaneous behavior depending on the background level of luminance.

FIG. 54 Interspike interval histogram from a GB cell in darkness (**A**) and at the mean level of luminance (**B**). Bins are 2 msec in width. Two peaks in the histogram of A) are observed at 6 msec and 26 msec. The distribution in B) is much broader than occurs in A) suggesting that the GB cell exhibits a different spontaneous spiking behavior depending on the background level of luminance.

FIG. 55 Interspike interval histogram from a GB cell in darkness (**A**) and at the mean level of luminance (**B**). Bins are 2 msec in width. The behavior observed with this cell is more typical of GB spontaneous spiking behavior than is seen with fig. 54. A broad distribution of interspike intervals occurs in both darkness and at the mean level of luminance.

TABLE 1 - Mean Square Errors Using Computed Wiener Kernels

CELL #	MSE (%)								COMMENTS
	LEVEL 1		LEVEL 2		LEVEL 3		LEVEL 4		
	1st	2nd	1st	2nd	1st	2nd	1st	2nd	
1 (f34)	77.0	33.6	61.4	22.3	46.6	21.7	38.8	28.6	F,O
2 (f39)	81.8	46.0	78.5	37.2	72.4	35.1			B,O^m
3 (f40)	88.4	34.2	79.4	23.2	67.9	20.1	59.5	25.0	B,H
4	67.9	37.8	65.0	36.9	60.8	43.6			F,H
5 (f29)	94.0	54.2	92.1	37.6	78.8	52.7	71.0	56.4	B,O/H
6 (f44)	93.2	50.5	92.9	45.7	91.7	45.2	87.7	60.8	F,O^m
7	84.4	44.1	75.6	37.0	67.9	47.4			F,O^m
8 (f30)	90.3	47.9	94.6	43.9	94.5	47.8	94.5	74.7	B,H
9 (f41)	86.6	40.3	95.4	34.7	77.6	45.7	75.0	55.0	B,H
10 (f36)	92.8	39.0	97.0	36.6	76.7	31.9	76.1	62.3	B,O/H
11 (f35)	95.4	55.2	95.2	44.9	92.8	37.0	83.4	41.3	B,O^+
12	79.0	47.6	87.1	46.6	95.8	44.4	95.2	43.9	F,O^m
13 (f38)	88.0	44.3	84.1	33.1	72.0	34.1	67.4	54.8	B,H
14 (f32)	79.0	25.5	85.7	34.9	88.6	55.9	90.3	62.9	N,O^+
15 (f45)	90.8	43.2	71.1	32.8	56.5	30.4			F,H
16 (f46)	83.3	35.3	71.8	26.7	50.7	21.9			F,H
17	80.1	39.4	76.9	33.7	66.1	25.6	52.5	21.7	B,H
18 (f37)	96.2	50.3	95.6	42.0	92.3	31.2	79.0	25.4	B,H
19 (f43)	84.7	43.6	86.3	33.9	79.1	37.7	69.0	38.5	F,O^+
20	92.5	39.2	88.1	29.7	77.4	30.1	64.4	41.8	F,H
21 (f42)	93.1	42.1	94.9	29.3	83.4	27.2	72.5	35.4	B,H
22									F,H
23 (f31)	68.0	37.5	68.2	39.8	75.8	62.7			F,O^m
24	90.9	34.3	75.4	28.7	60.3	27.2	53.02	34.3	F,H
25	96.7	49.7	97.0	37.8	85.8	36.5	69.9	45.2	B,H
26 (f33)	82.7	37.0	86.4	30.7	85.6	39.6	81.5	54.3	N,O^+

TABLE 2 A) - Filter Parameters for Model Fits

CELL #	ON-BIPOLAR FILTER			OFF-BIPOLAR FILTER			PRE-SYN FILTER		AMACRINE FILTER		
	τ_1	τ_2 x10^{-3}	τ_3 x10^{-3}	τ_1'	τ_2' x10^{-2}	τ_3' x10^{-3}	τ_1'' x10^{-2}	τ_2'' x10^{-3}	τ_1'''	τ_2''' x10^{-2}	τ_3''' x10^{-3}
1 (f34)	1.45	16.0	4.85	.081	6.52	3.67	4.65	.335	.293	9.79	.830
2 (f39)	.669	.063	4.87	.045	7.99	3.01	3.00	2.91	.292	5.41	1.41
3 (f40)	1.06	15.4	4.16	.297	8.88	3.47	3.29	3.60	.161	9.86	1.48
4	.688	4.92	6.40	.267	4.68	4.97	10.4	28.6	.354	41.5	1.24
5 (f29)	.842	9.61	4.78	.108	5.17	3.80	5.47	1.82	.351	14.0	.756
6 (f44)	.796	3.05	4.95	.233	11.2	3.50	1.87	.087	.416	6.79	1.04
7	.817	3.81	4.44	.124	7.88	3.45	2.67	.312	.203	29.1	1.01
8 (f30)	.954	1.03	3.90	.134	8.85	2.08	.624	.321	.129	3.69	1.70
9 (f41)	1.07	1.00	5.39	.201	7.75	3.08	.639	.390	.004	7.75	1.22
10 (f36)	.912	1.50	6.18	.077	6.33	3.91	3.60	.310	.089	5.73	1.33
11 (f35)	1.02	1.04	3.83	.044	4.96	2.35	.436	.284	.349	4.52	1.42
12	.444	16.0	3.67	.067	8.26	2.88	.964	1.53	.520	4.23	.499
13 (f38)	.727	4.04	4.68	.144	7.94	3.35	2.72	4.50	.344	10.1	1.04
14 (f32)	1.26	24.1	4.05	.443	.378	3.68	17.6	73.9	.370	23.4	1.12
15 (f45)	1.57	23.8	5.16	.417	2.82	3.89	.443	.147	.212	24.9	.994
16 (f46)	.370	8.12	6.52	.293	4.30	4.93	2.58	.257	.376	28.9	.666
17	.417	8.67	3.76	.118	4.73	3.21	4.66	19.0	.289	7.96	1.16
18 (f37)	.403	.063	5.80	.118	12.0	3.21	1.84	.032	.127	3.54	1.41
19 (f43)	1.69	14.3	3.72	.204	20.2	3.15	.647	.344	.491	5.13	1.17
20	.675	8.16	5.67	.188	8.45	4.02	3.16	.125	.107	5.75	.967
21 (f42)	.957	2.50	4.39	.034	5.71	2.61	1.10	2.13	.270	5.02	.717
22	1.05	3.24	5.25	.167	6.53	4.08	2.33	.325	.239	4.59	.910

TABLE 2 B) - High- and Low-Pass Filter Parameters for Model Fits

CELL #	ON-PATH FILTER		OFF-PATH FILTER		AMACRINE FILTER	
	τ^{H}_{ON} x10^{-2}	τ^{L}_{ON} x10^{-2}	τ^{H}_{OFF} x10^{-2}	τ^{L}_{OFF} x10^{-2}	τ^{H}_{AMA} x10^{-2}	τ^{L}_{AMA} x10^{-2}
1 (f34)	149.65	6.48	12.75	10.22	29.30	10.62
2 (f39)	69.90	5.17	7.50	11.29	29.20	6.82
3 (f40)	109.29	6.06	32.99	12.71	16.10	11.34
4	79.20	9.75	37.10	12.51	35.40	42.74
5 (f29)	89.67	5.92	16.27	9.15	35.10	14.76
6 (f44)	81.47	5.27	25.17	14.71	41.60	7.83
7	84.37	4.85	15.07	11.36	20.30	30.11
8 (f30)	96.02	4.03	14.02	10.96	12.90	5.39
9 (f41)	107.64	5.53	20.74	10.87	0.40	8.97
10 (f36)	94.80	6.36	11.30	10.27	8.90	7.06
11 (f35)	102.44	3.96	4.84	7.34	34.90	5.94
12	45.36	5.42	7.66	11.29	52.00	4.73
13 (f38)	75.42	5.53	17.12	11.74	34.40	11.14
14 (f32)	143.60	13.85	61.90	11.45	37.00	24.52
15 (f45)	157.44	7.55	42.14	6.72	21.20	25.89
16 (f46)	39.58	7.36	31.88	9.26	37.60	29.57
17	46.36	6.53	16.46	9.84	28.90	9.12
18 (f37)	42.14	5.81	13.64	15.21	12.70	4.95
19 (f43)	169.65	5.18	21.05	23.38	49.10	6.30
20	70.66	6.50	21.96	12.48	10.70	6.72
21 (f42)	96.80	4.85	4.50	8.53	27.00	5.74
22	107.33	5.60	19.03	10.64	23.90	5.50
MEAN	93.58	6.253	20.69	11.45	27.21	12.99
S.D.	35.82	2.056	13.34	3.273	13.00	10.29

TABLE 3 A) - Filter Parameter Changes to Modulation Depth

CELL #	ON-BIPOLAR FILTER			OFF-BIPOLAR FILTER			PRE-SYN FILTER		AMACRINE FILTER		
	τ_1	τ_2 x10^{-3}	τ_3 x10^{-3}	τ_1'	τ_2' x10^{-2}	τ_3' x10^{-3}	τ_1'' x10^{-2}	τ_2'' x10^{-3}	τ_1'''	τ_2''' x10^{-2}	τ_3''' x10^{-3}
1(1)	1.45	16.0	4.85	.081	6.52	3.67	4.65	.335	.293	9.79	.830
1(2)	.953	2.42	7.24	.208	3.67	4.14	4.62	.159	.157	12.9	.810
1(3)	1.81	3.56	6.51	.333	2.27	3.78	1.16	5.76	.280	26.5	.472
2(1)	.669	.063	4.87	.045	7.99	3.01	3.00	2.91	.292	5.41	1.41
2(2)	.403	1.79	5.20	.461	5.81	3.70	2.03	.032	.116	11.7	1.50
2(3)	.314	3.58	4.57	.390	4.86	3.39	1.81	3.46	.094	6.84	1.60
3(1)	1.06	15.4	4.16	.297	8.88	3.47	3.29	3.60	.161	9.86	1.48
3(2)	.922	2.25	5.12	.240	4.74	3.79	1.58	2.59	.486	13.8	1.39
3(3)	1.09	4.65	4.66	.591	3.93	3.77	1.19	3.09	.525	26.0	1.52

TABLE 3 B) - High- and Low-Pass Filter Changes to Modulation Depth

CELL #	ON-PATH FILTER		OFF-PATH FILTER		AMACRINE FILTER	
	τ^H_{ON} x10^{-2}	τ^L_{ON} x10^{-2}	τ^H_{OFF} x10^{-2}	τ^L_{OFF} x10^{-2}	τ^H_{AMA} x10^{-2}	τ^L_{AMA} x10^{-2}
1(1)	149.65	6.48	12.75	10.22	29.30	10.62
1(2)	99.92	7.50	25.42	7.83	15.70	13.71
1(3)	182.16	7.45	34.46	6.63	28.00	26.97
2(1)	69.90	5.17	7.50	11.29	29.20	6.82
2(2)	42.33	5.38	48.13	9.51	11.60	13.20
2(3)	33.21	5.28	40.81	8.60	9.40	8.44
3(1)	109.29	6.06	32.99	12.71	16.10	11.34
3(2)	93.78	5.61	25.58	8.79	48.60	15.19
3(3)	110.19	5.44	60.29	8.01	52.50	27.52

TABLE 4 - Current Injection Couples (Polarity, PRT, Amplitude)

PAIR	*n*	POLARITY	PEAK RESPONSE TIME (msec)	AMPLITUDE (spikes· $nA^{-1}s^{-1}$)
I. Amacrine to Ganglion Cells (biphasic kernel waveforms)				
NA-GA	20	+	4.0±1.8	1.4±0.22
NB-GB	25	+	5.7±0.6	1.5±0.65
C-GA	4	+	4.0±0.0	1.2±0.02
C-GB	6	+	4.5±0.9	1.5±0.41
II. Amacrine to Ganglion Cells (triphasic kernel waveforms)				
NA-GA	64	-	20.8±3.1	0.9±0.59
NB-GA	19	-	22.3±3.1	0.9±0.47
C-GA	22	-	21.9±3.2	0.9±0.38
NB-GB	57	+	20.7±3.2	1.2±0.68
NA-GB	109	+	22.1±3.4	1.0±0.52
C-GB	16	+	21.4±1.6	1.5±0.74
NA-GC	12	+	21.7±2.4	0.7±0.43
NB-GC	3	+	19.7±0.5	0.8±0.13
C-GC	9	+	21.5±1.7	0.9±0.26
III. Ganglion to Ganglion Cells (biphasic kernel waveform)				
GA-GA	44	+	7.8±2.7	1.4±0.45
GB-GB	68	+	7.5±2.9	1.8±0.66
GA-GC	1	+	4.0	1.2
GB-GC	2	+	4.0±0.0	1.1±0.5
GC-GA	8	+	4.25±1.6	1.2±0.3
GC-GB	2	+	7.0±1.0	1.3±0.6
IV. Ganglion to Ganglion Cells (triphasic kernel waveform)				
GA-GA	3	-	19.2±1.0	0.9±0.3
GB-GA	68	-	23.6±3.4	0.9±0.6
GB-GB	46	+	20.2±6.4	1.4±0.5
GA-GB	25	+	22.2±2.8	1.1±0.6
GC-GB	1	+	22.0	1.1
V. Ganglion (self)				
GA	12	+		3.2±0.22
GB	37	+		3.9±0.49
GC	6	+		2.0±0.32
VI. Bipolar to Ganglion Cells				
BA-GA	5	+	6.6±0.9	1.0±0.35
BB-GB	8	+	6.4±1.7	1.2±0.23
BA-GB	1	+	22.0	1.2
VII. Horizontal to Ganglion Cells				
H-GA	34	+	16.4±2.8	1.5±0.32
H-GB	26	+	14.4±2.4	1.5±0.28

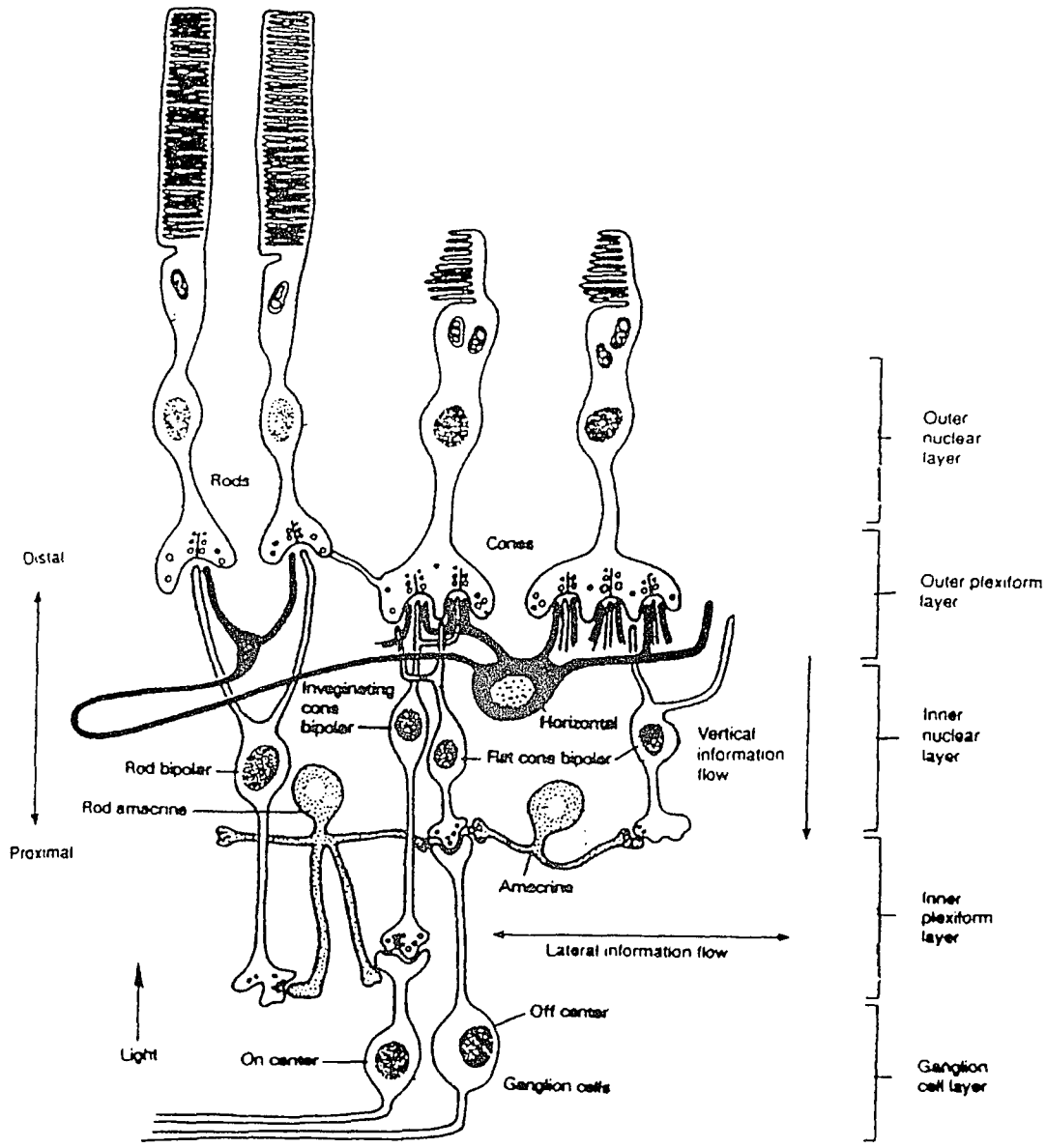
Rods
Cones
Distal
Proximal
Invaginating cone bipolar
Horizontal
Vertical information flow
Rod bipolar
Flat cone bipolar
Rod amacrine
Amacrine
Lateral information flow
Light
On center
Off center
Ganglion cells
Outer nuclear layer
Outer plexiform layer
Inner nuclear layer
Inner plexiform layer
Ganglion cell layer

FIG. 1

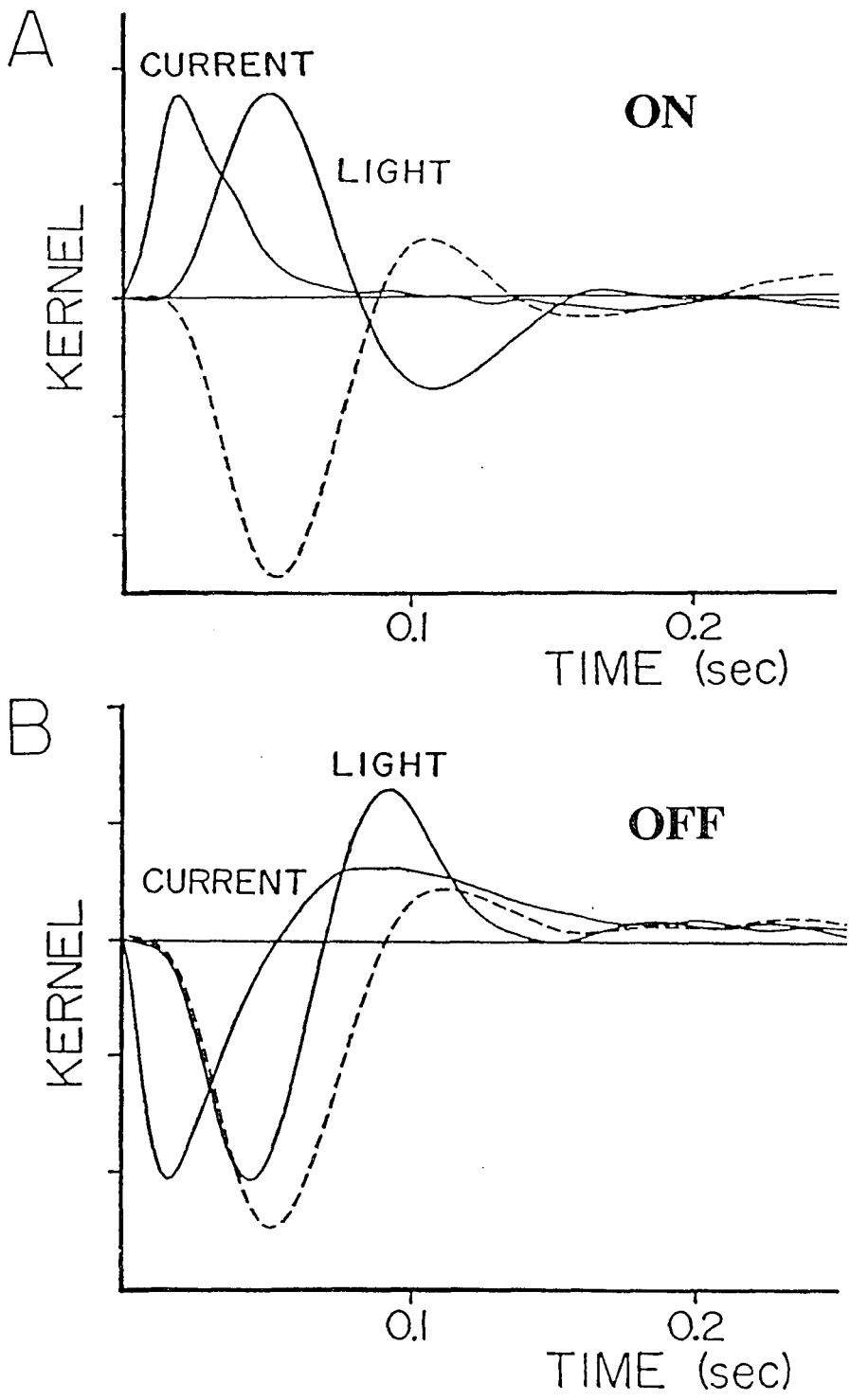
A
CURRENT
ON
LIGHT
KERNEL
0.1
0.2
TIME (sec)
B
LIGHT
OFF
CURRENT
KERNEL
0.1
0.2
TIME (sec)

FIG. 2

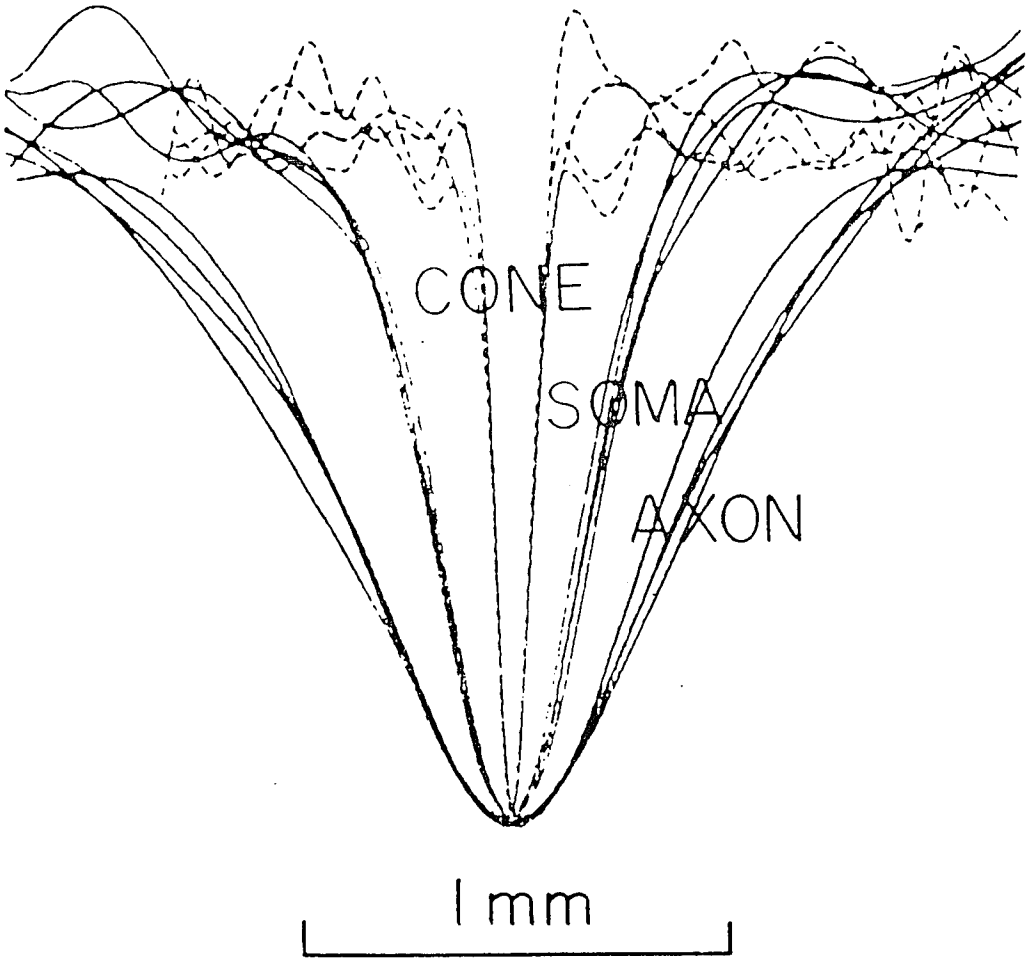

FIG. 3 A)

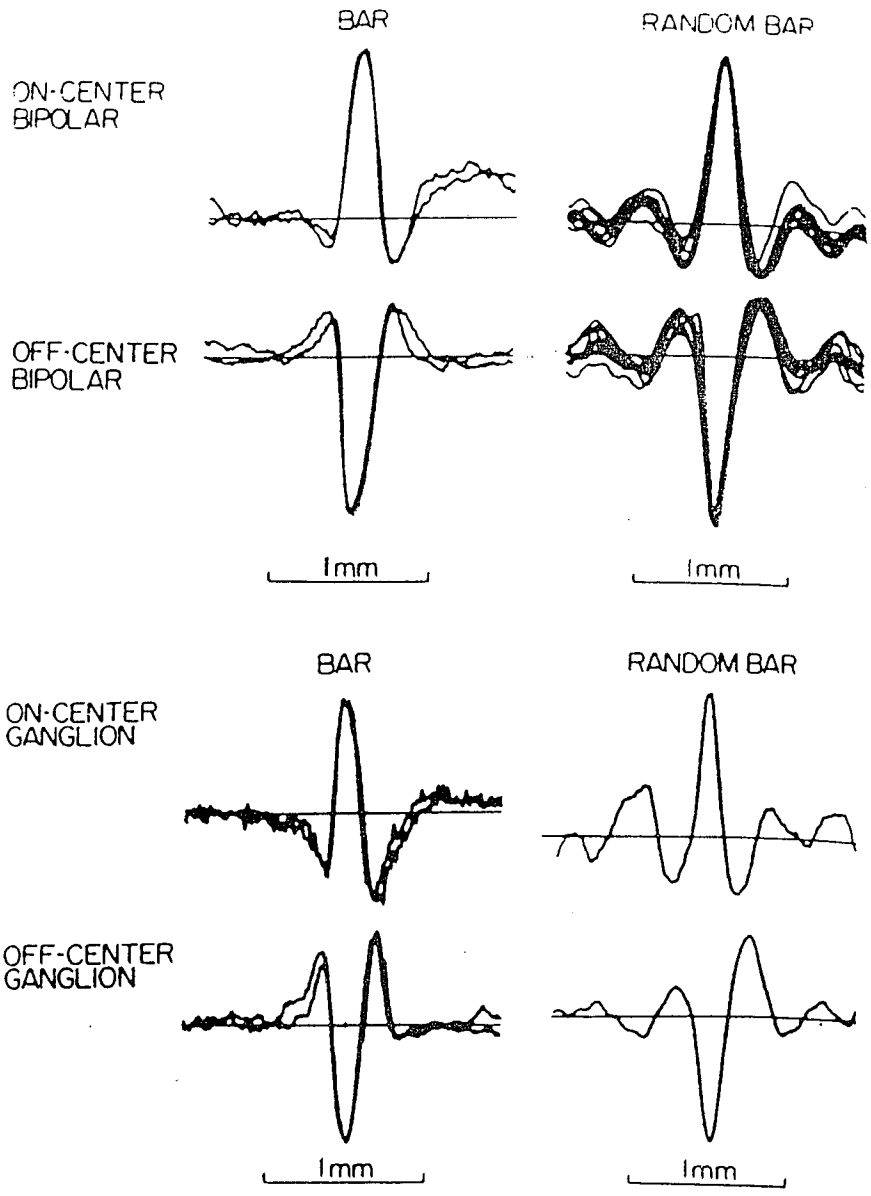
BAR
RANDOM BAR
ON-CENTER BIPOLAR
OFF-CENTER BIPOLAR
1mm
1mm
BAR
RANDOM BAR
ON-CENTER GANGLION
OFF-CENTER GANGLION
1mm
1mm

FIG. 3 B)

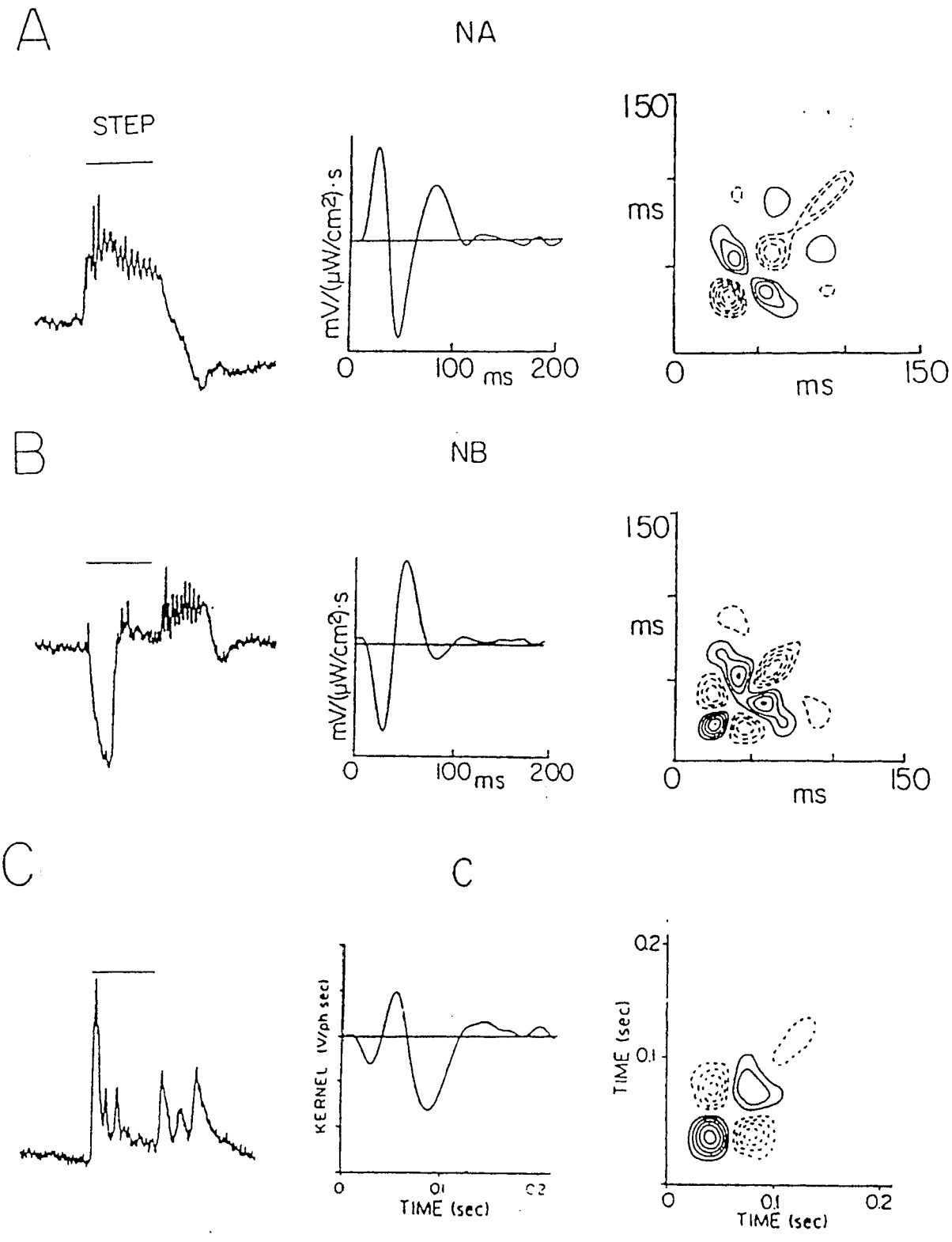
A
NA
STEP
mV/(μW/cm²)·s
0
100 ms
200
150
ms
0
ms
150
B
NB
mV/(μW/cm²)·s
0
100 ms
200
150
ms
0
ms
150
C
C
KERNEL (V/ph sec)
0
0.1
0.2
TIME (sec)
0.2
0.1
TIME (sec)
0
0.1
0.2
TIME (sec)

FIG. 4

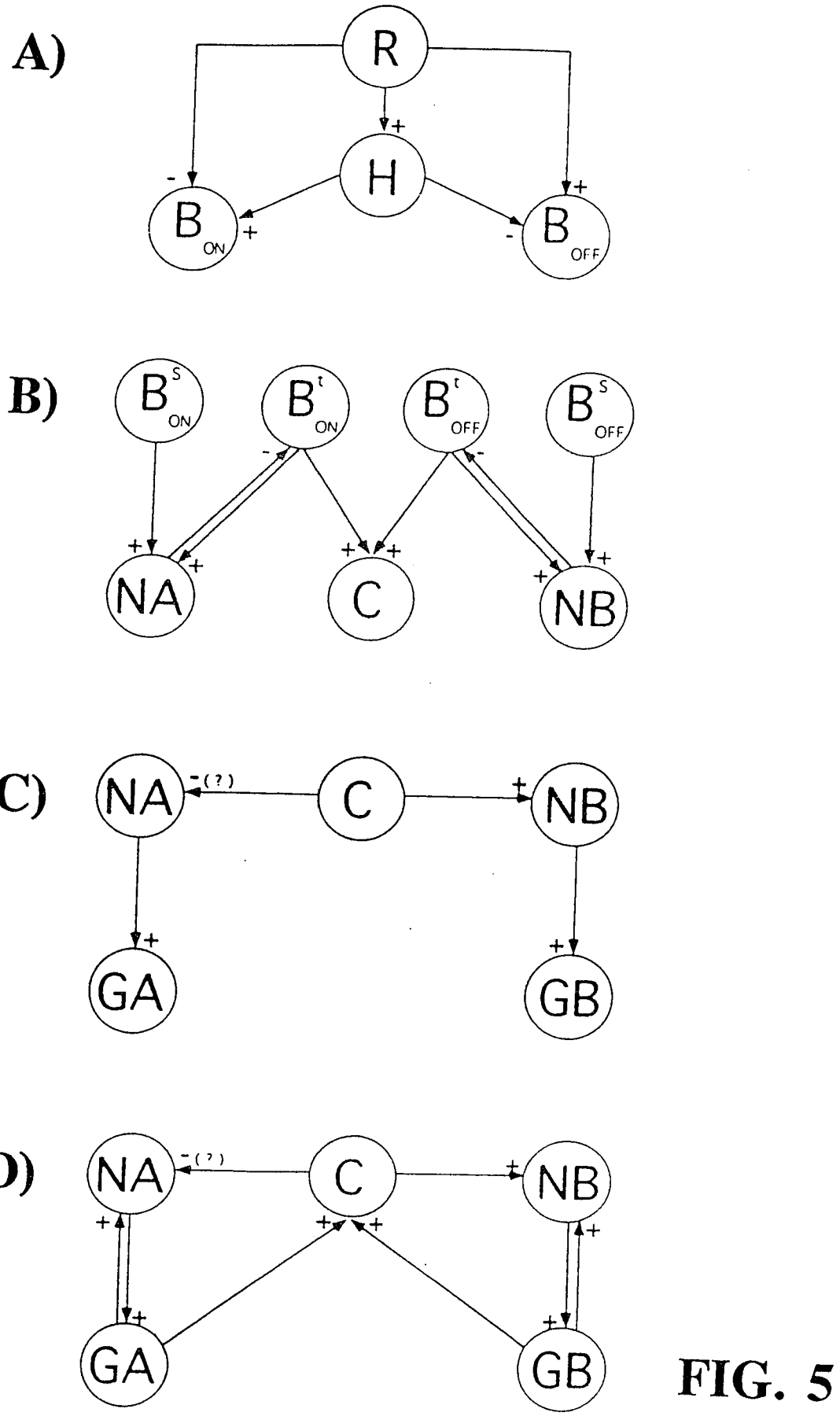
A)
R
H
B ON
B OFF
B)
B S ON
B t ON
B t OFF
B S OFF
NA
C
NB
C)
NA
C
NB
GA
GB
D)
NA
C
NB
GA
GB

FIG. 5

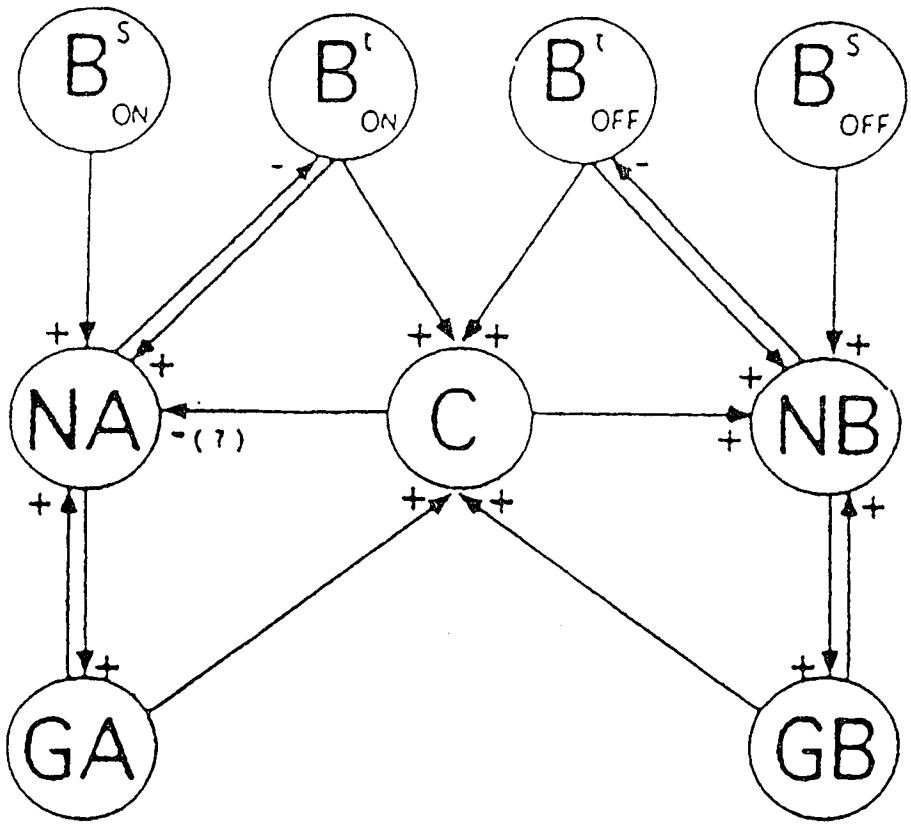

FIG. 5 E)

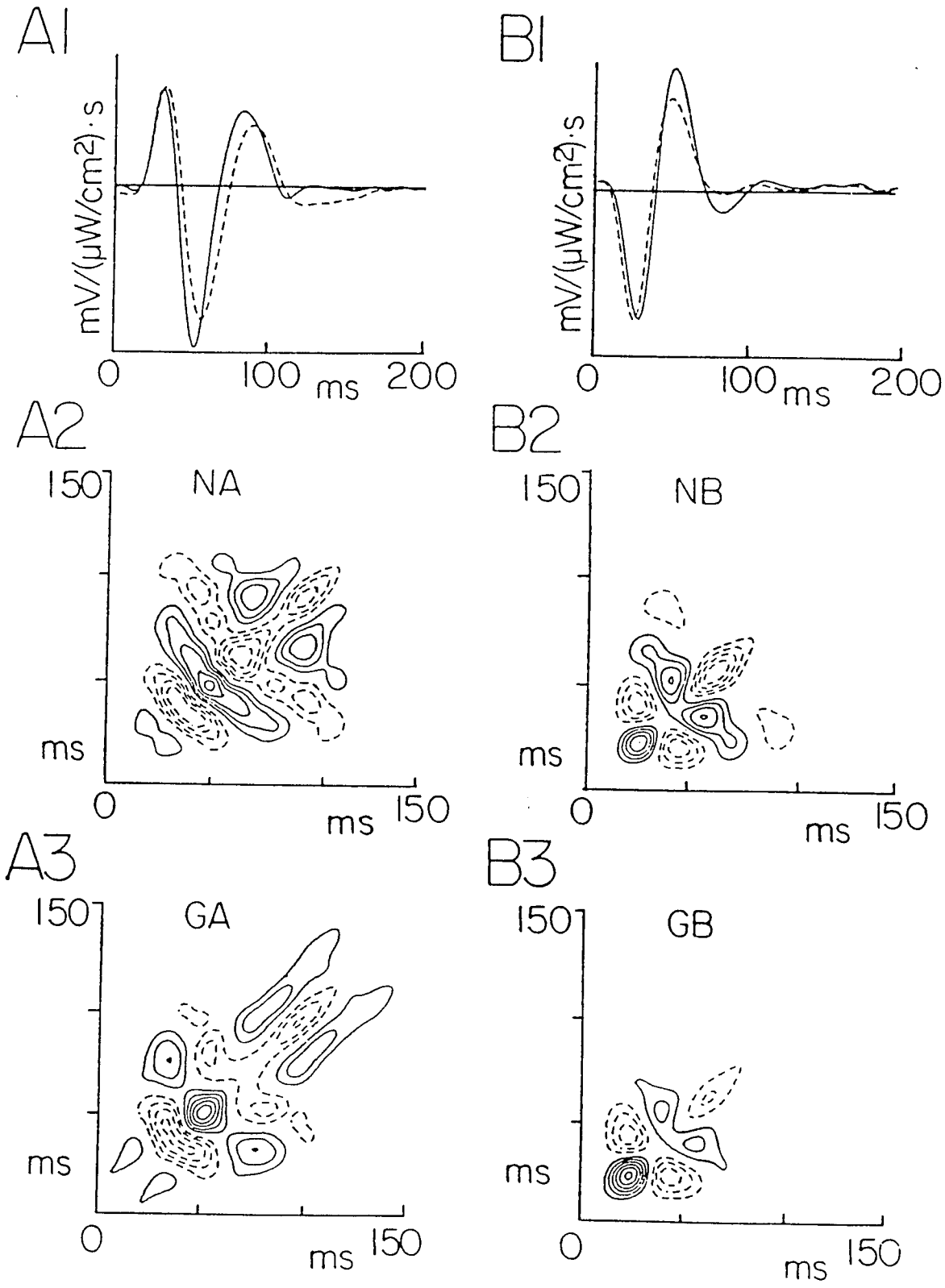
A1
mV/(μW/cm²)·s
0
100
ms
200
B1
mV/(μW/cm²)·s
0
100
ms
200
A2
150
NA
ms
0
ms
150
B2
150
NB
ms
0
ms
150
A3
150
GA
ms
0
ms
150
B3
150
GB
ms
0
ms
150

FIG. 6

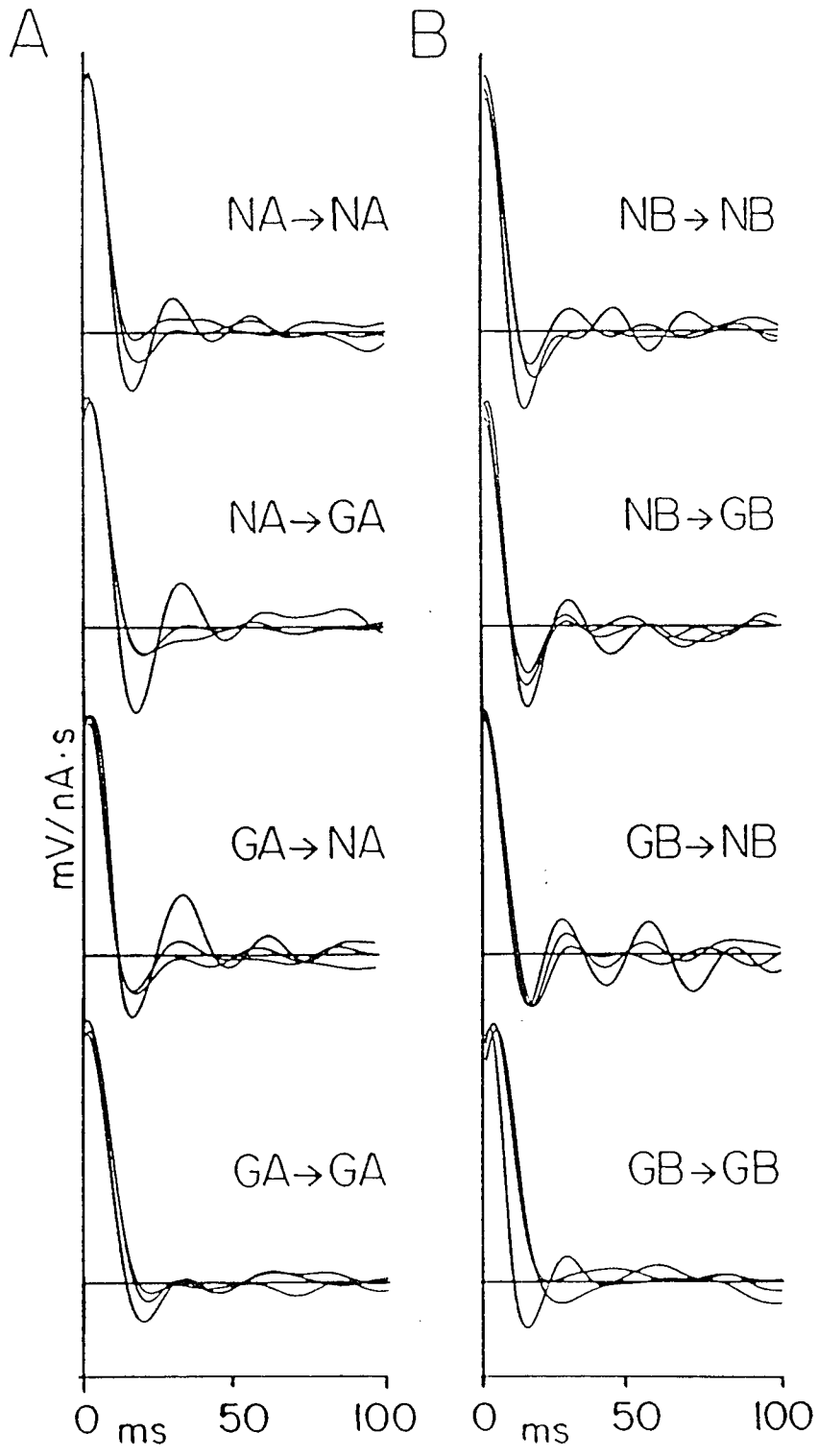
A
B
NA→NA
NB→NB
NA→GA
NB→GB
GA→NA
GB→NB
GA→GA
GB→GB
mV/nA·s
0 ms 50 100
0 ms 50 100

FIG. 7

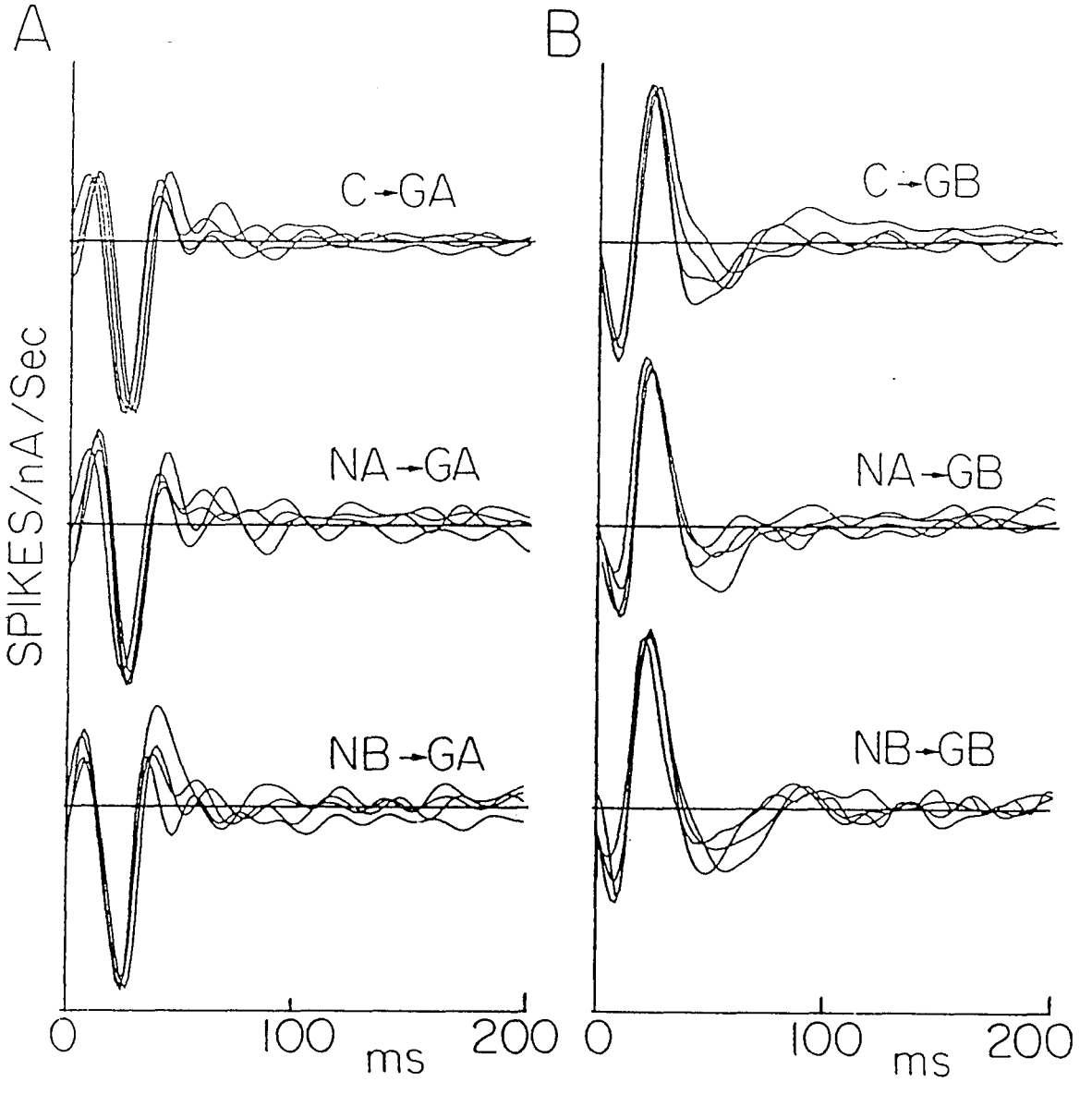
A
B
C→GA
NA→GA
NB→GA
C→GB
NA→GB
NB→GB
SPIKES/nA/Sec
0
100
ms
200
0
100
ms
200

FIG. 8

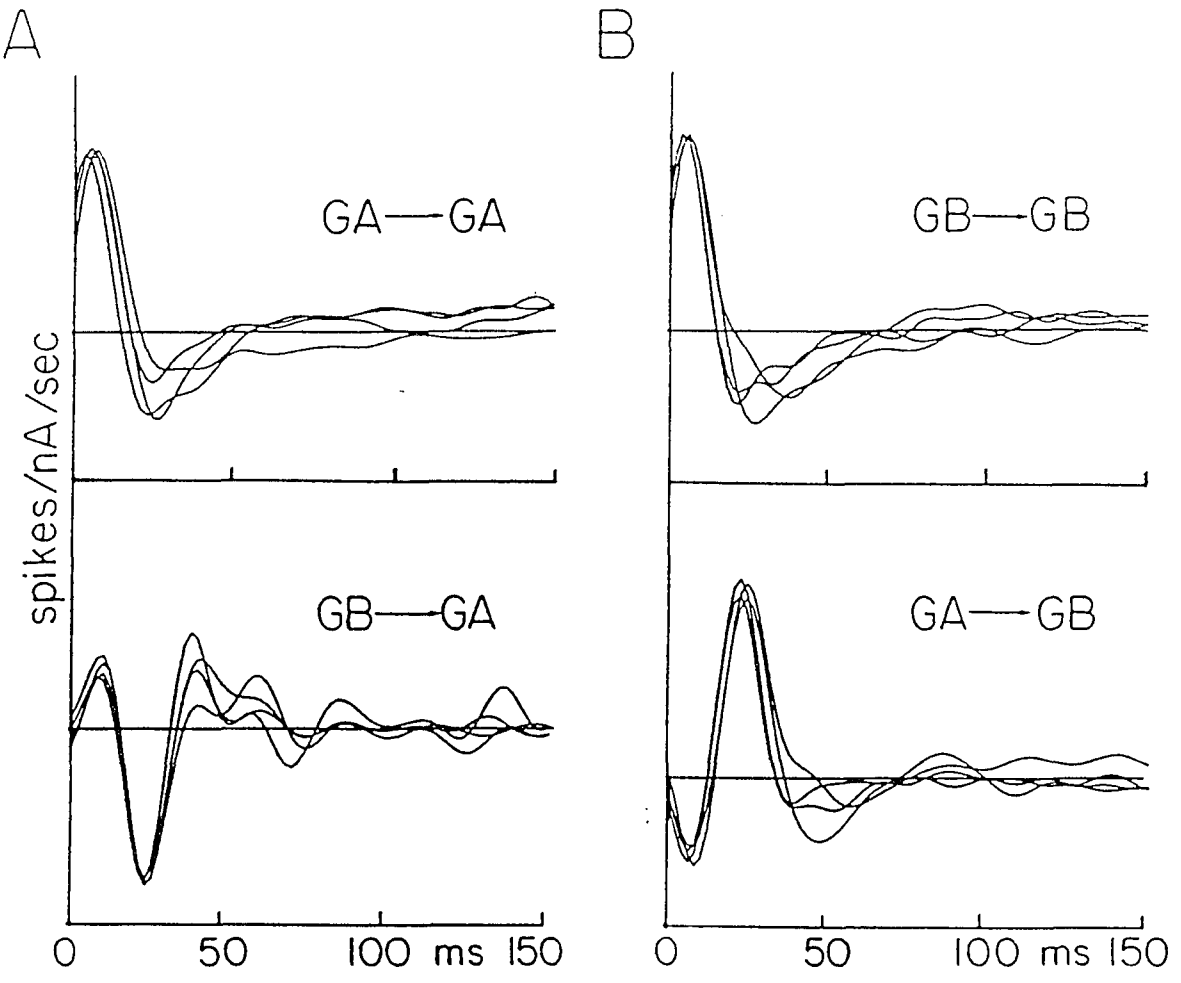
A
B
GA—GA
GB—GB
GB—GA
GA—GB
spikes/nA/sec
0
50
100 ms 150
0
50
100 ms 150

FIG. 9

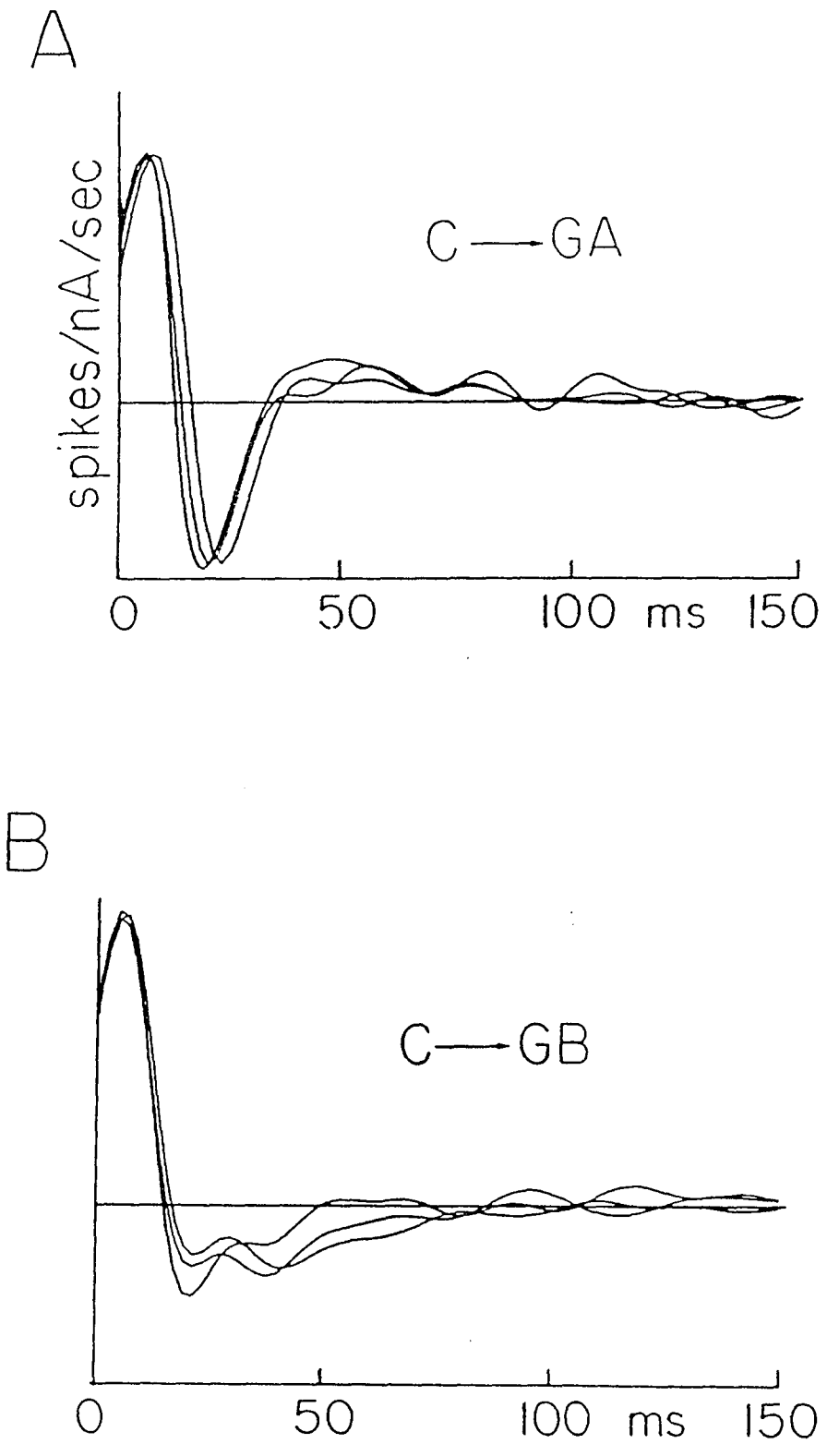

FIG. 10

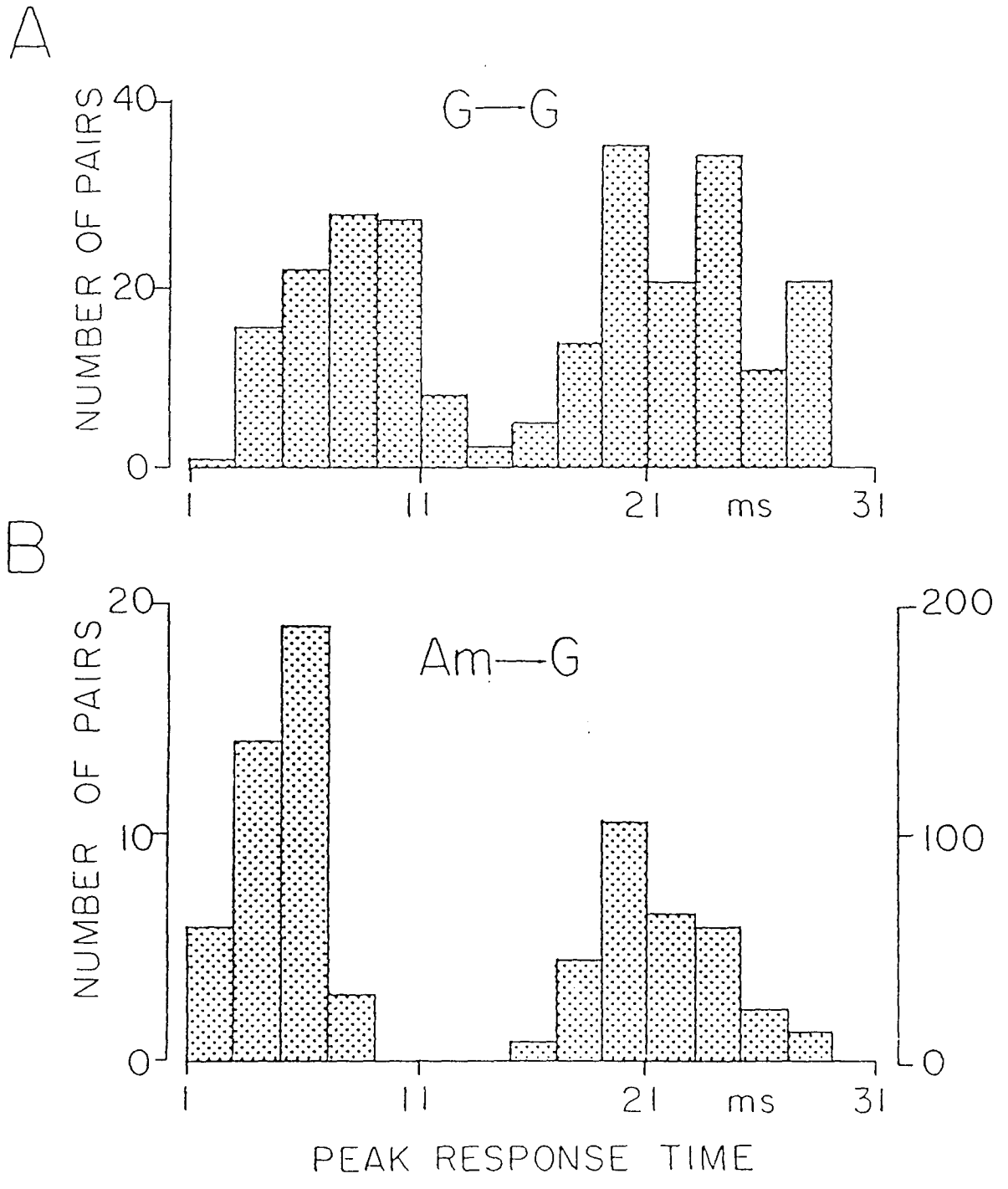
A
G—G
NUMBER OF PAIRS
40
20
0
1
11
21
ms
31
B
Am—G
NUMBER OF PAIRS
20
10
0
200
100
0
1
11
21
ms
31
PEAK RESPONSE TIME

FIG. 11

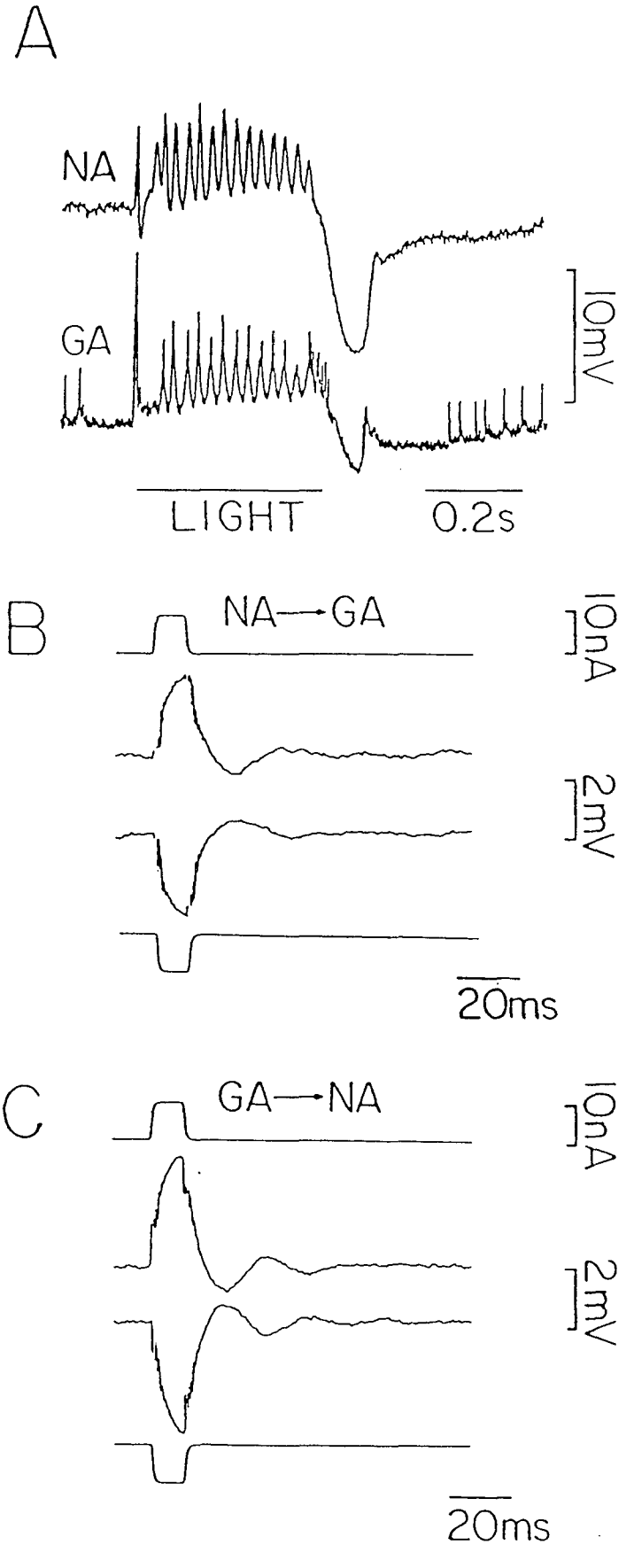

FIG. 12

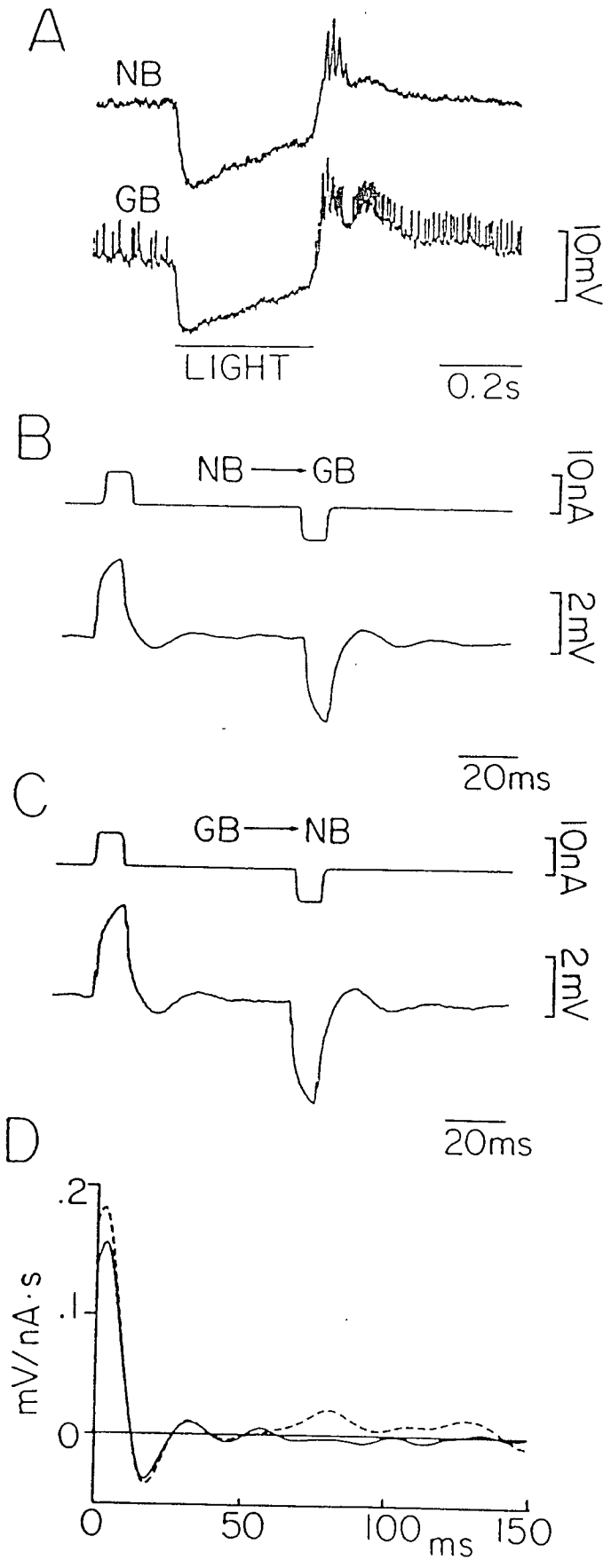
A
NB
GB
10mV
LIGHT
0.2s
B
NB → GB
10nA
2mV
20ms
C
GB → NB
10nA
2mV
20ms
D
.2
.1
0
mV/nA·s
0
50
100
ms
150

FIG. 13

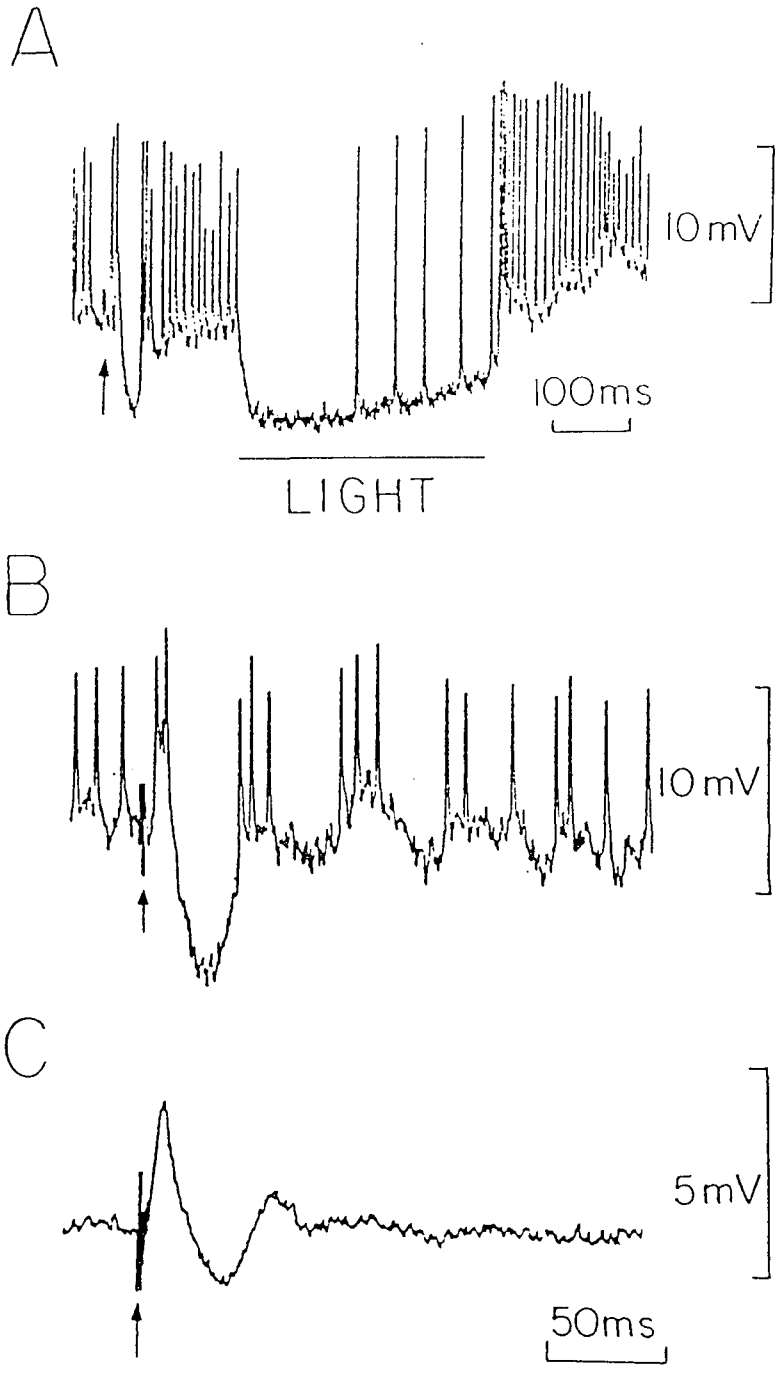

FIG. 14

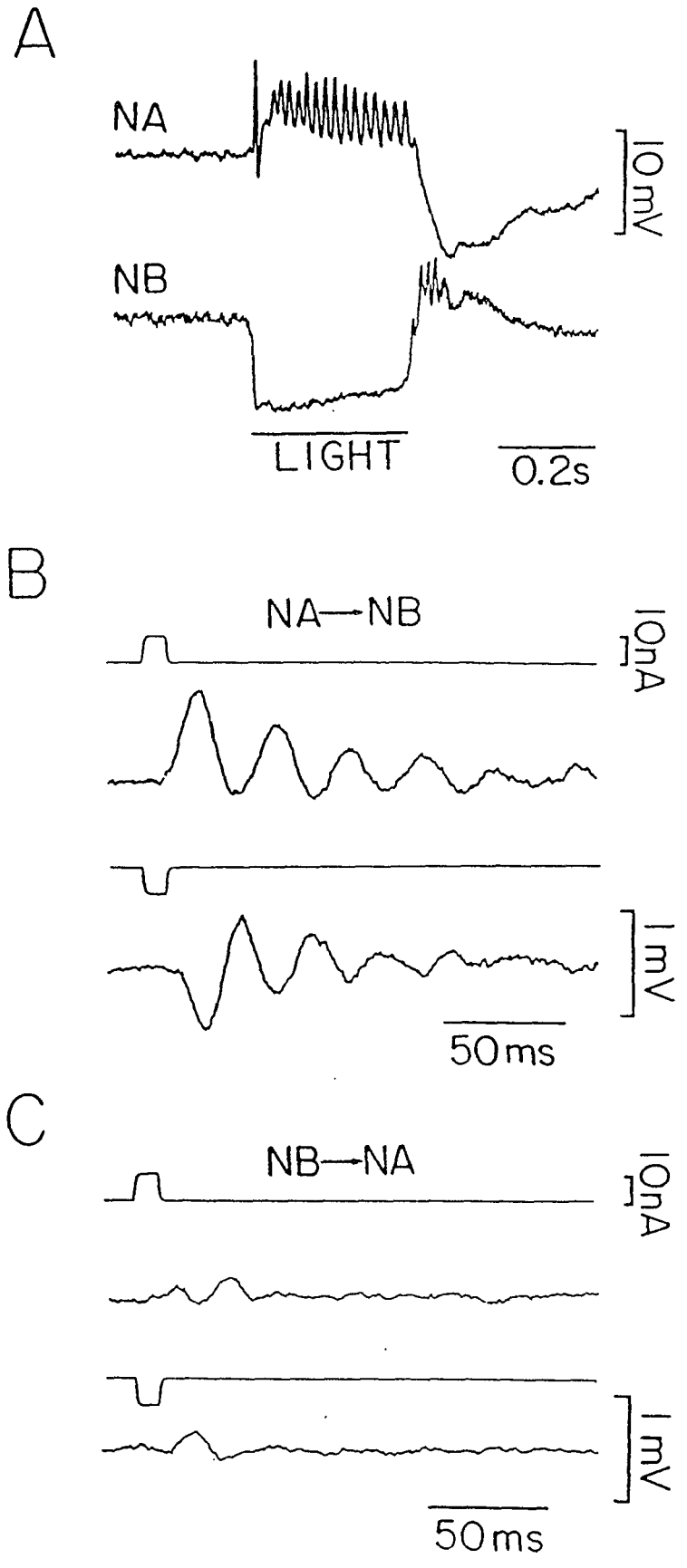

FIG. 15

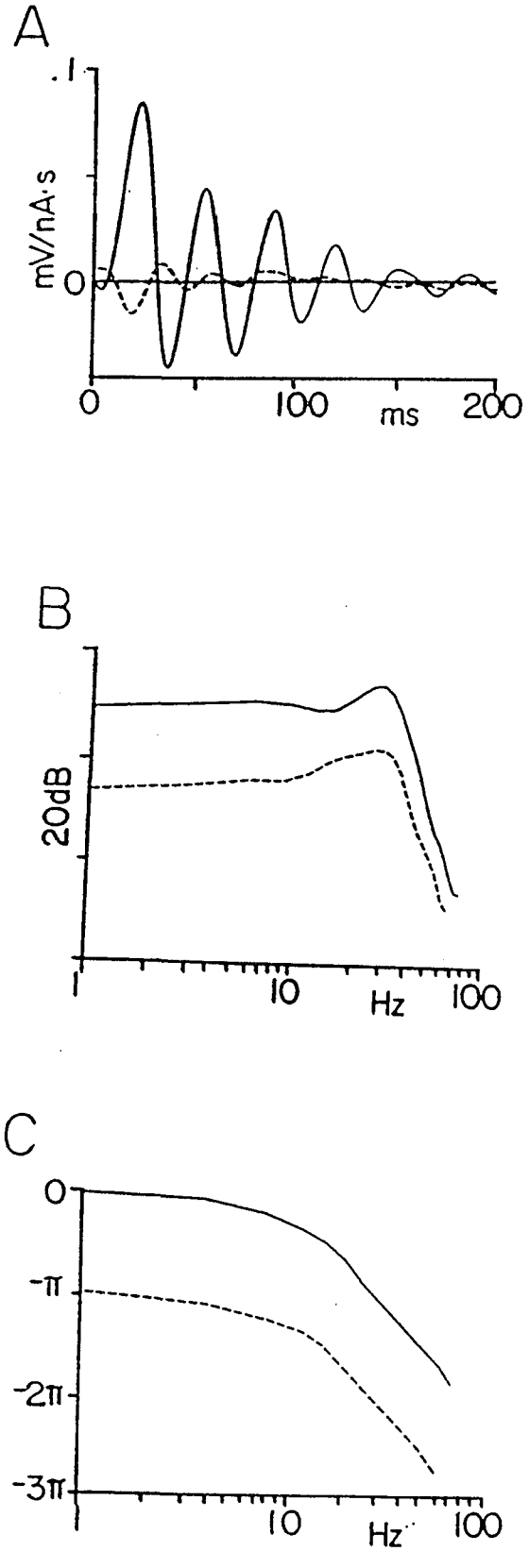

FIG. 16

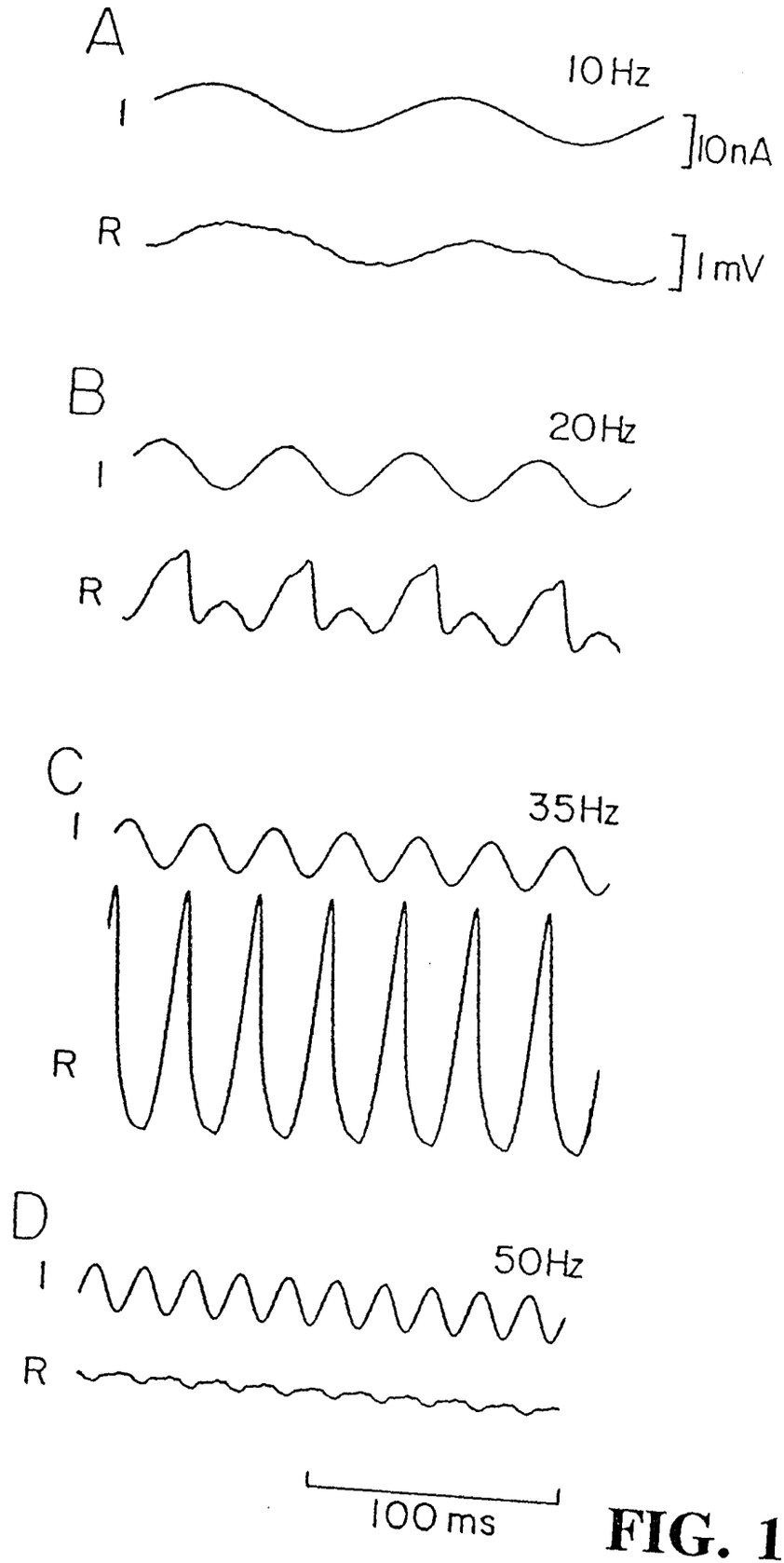

FIG. 17

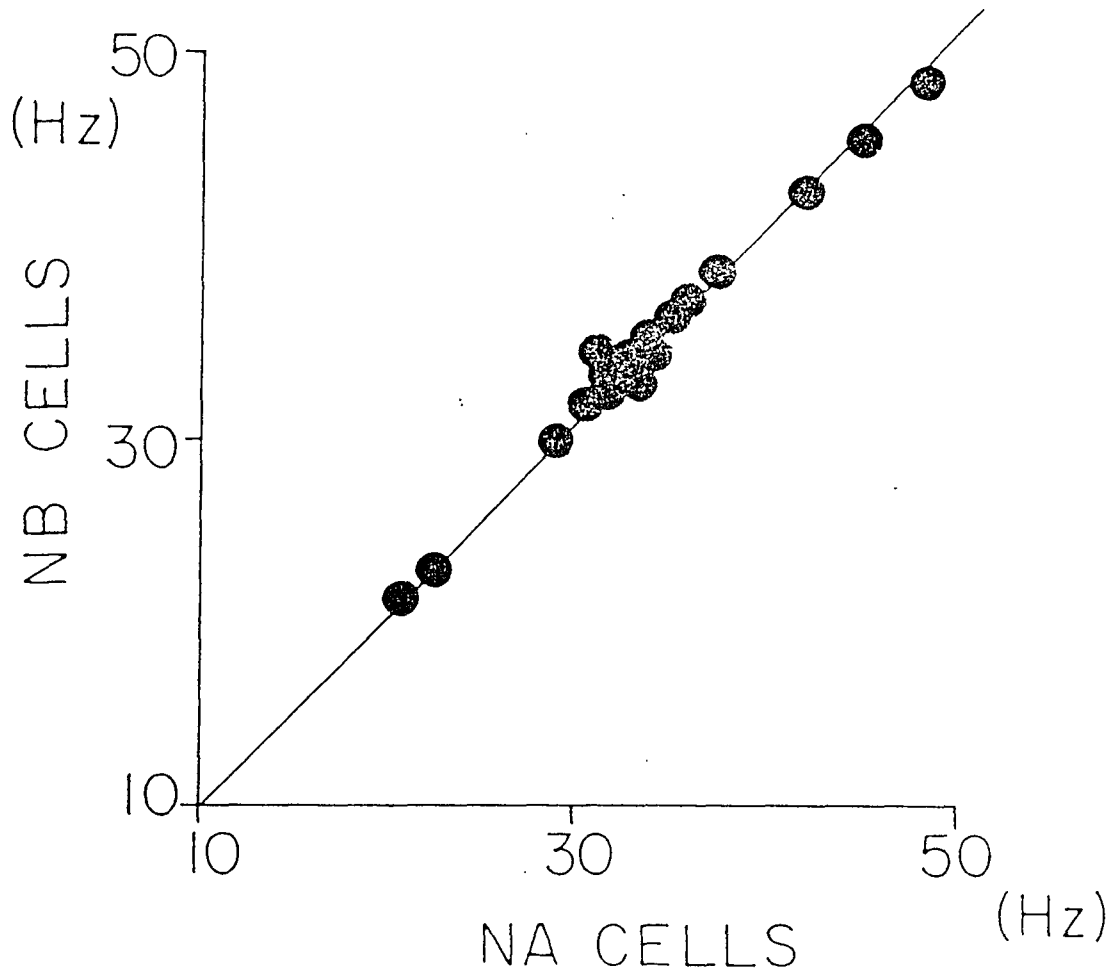

FIG. 18

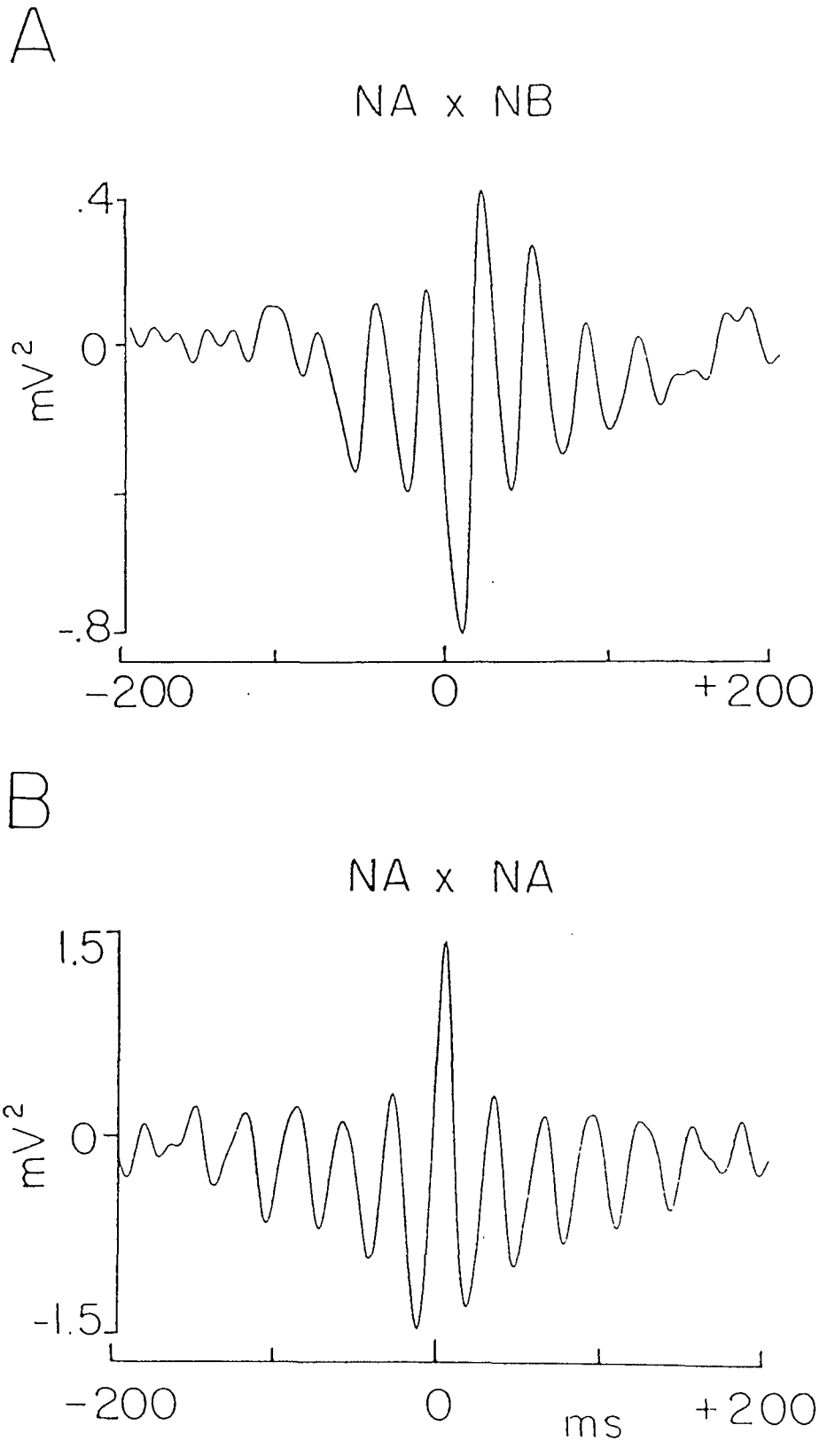

FIG. 19

A)

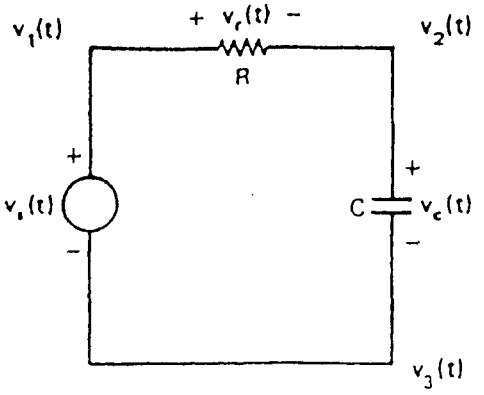
$v_1(t)$
+ $v_r(t)$ −
$v_2(t)$
R
+
$v_i(t)$
−
+
C
$v_c(t)$
−
$v_3(t)$

B)

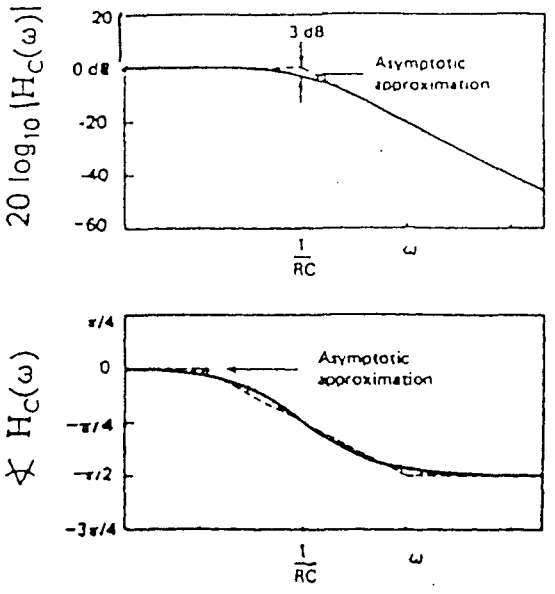
$20 \log_{10} |H_C(\omega)|$
20
0 dB
-20
-40
-60
3 dB
Asymptotic approximation
$\frac{1}{RC}$
ω
$\angle H_C(\omega)$
π/4
0
−π/4
−π/2
−3π/4
Asymptotic approximation
$\frac{1}{RC}$
ω

C)

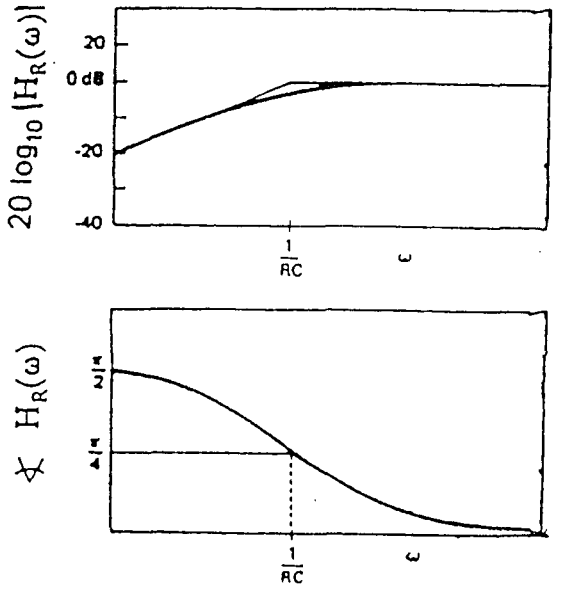
$20 \log_{10} |H_R(\omega)|$
20
0 dB
-20
-40
$\frac{1}{RC}$
ω
$\angle H_R(\omega)$
$\frac{\pi}{2}$
$\frac{\pi}{4}$
$\frac{1}{RC}$
ω

FIG. 20

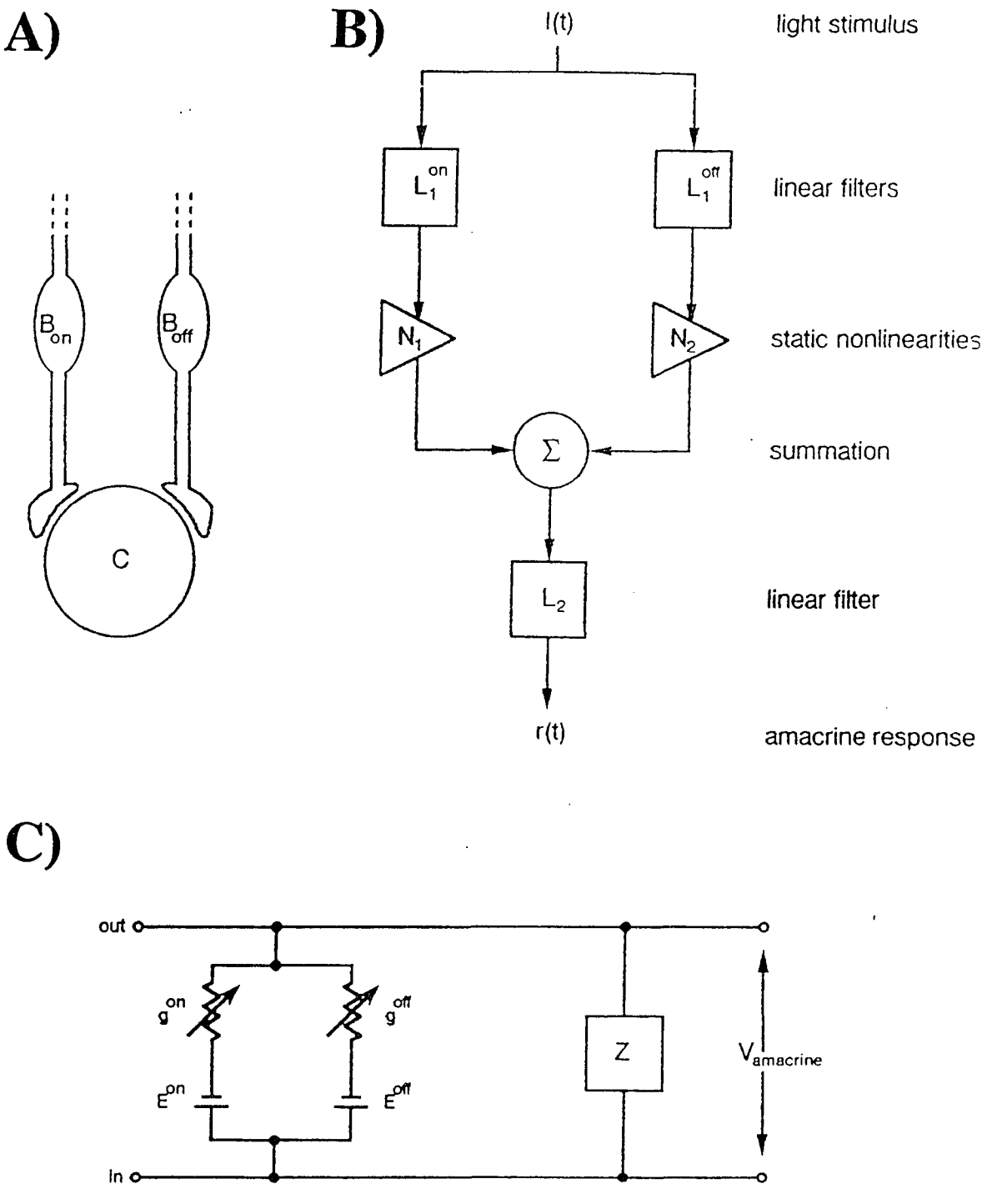
A)
B)
C)
B_{on}
B_{off}
C
I(t)
light stimulus
L_1^{on}
L_1^{off}
linear filters
N_1
N_2
static nonlinearities
Σ
summation
L_2
linear filter
r(t)
amacrine response
out
g^{on}
g^{off}
E^{on}
E^{off}
Z
$V_{amacrine}$
In

FIG. 21

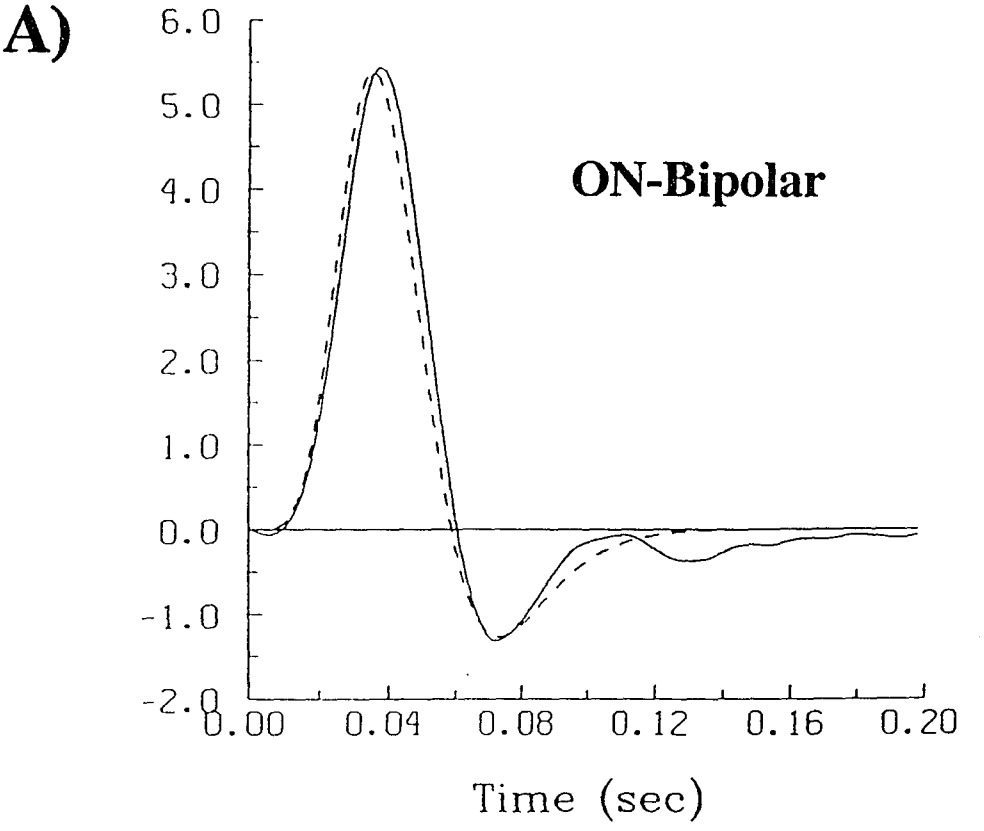
A)
6.0
5.0
4.0
3.0
2.0
1.0
0.0
-1.0
-2.0
ON-Bipolar
0.00
0.04
0.08
0.12
0.16
0.20
Time (sec)

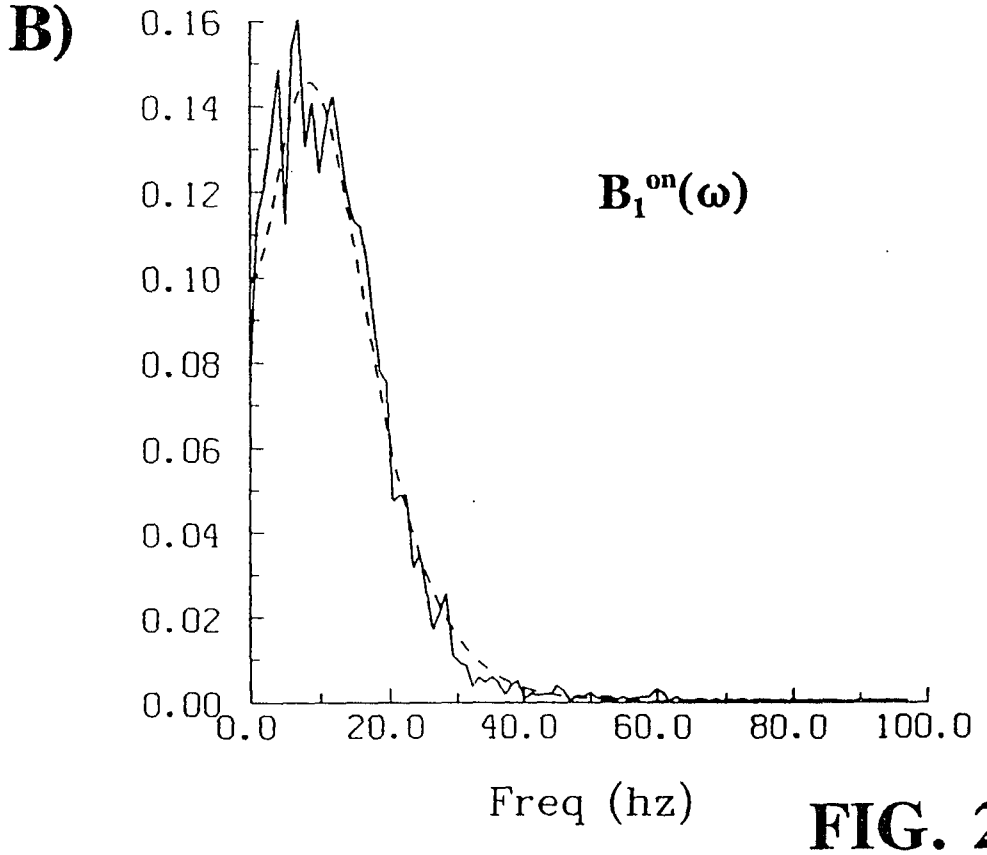
B)
0.16
0.14
0.12
0.10
0.08
0.06
0.04
0.02
0.00
$B_1^{on}(\omega)$
0.0
20.0
40.0
60.0
80.0
100.0
Freq (hz)

FIG. 22

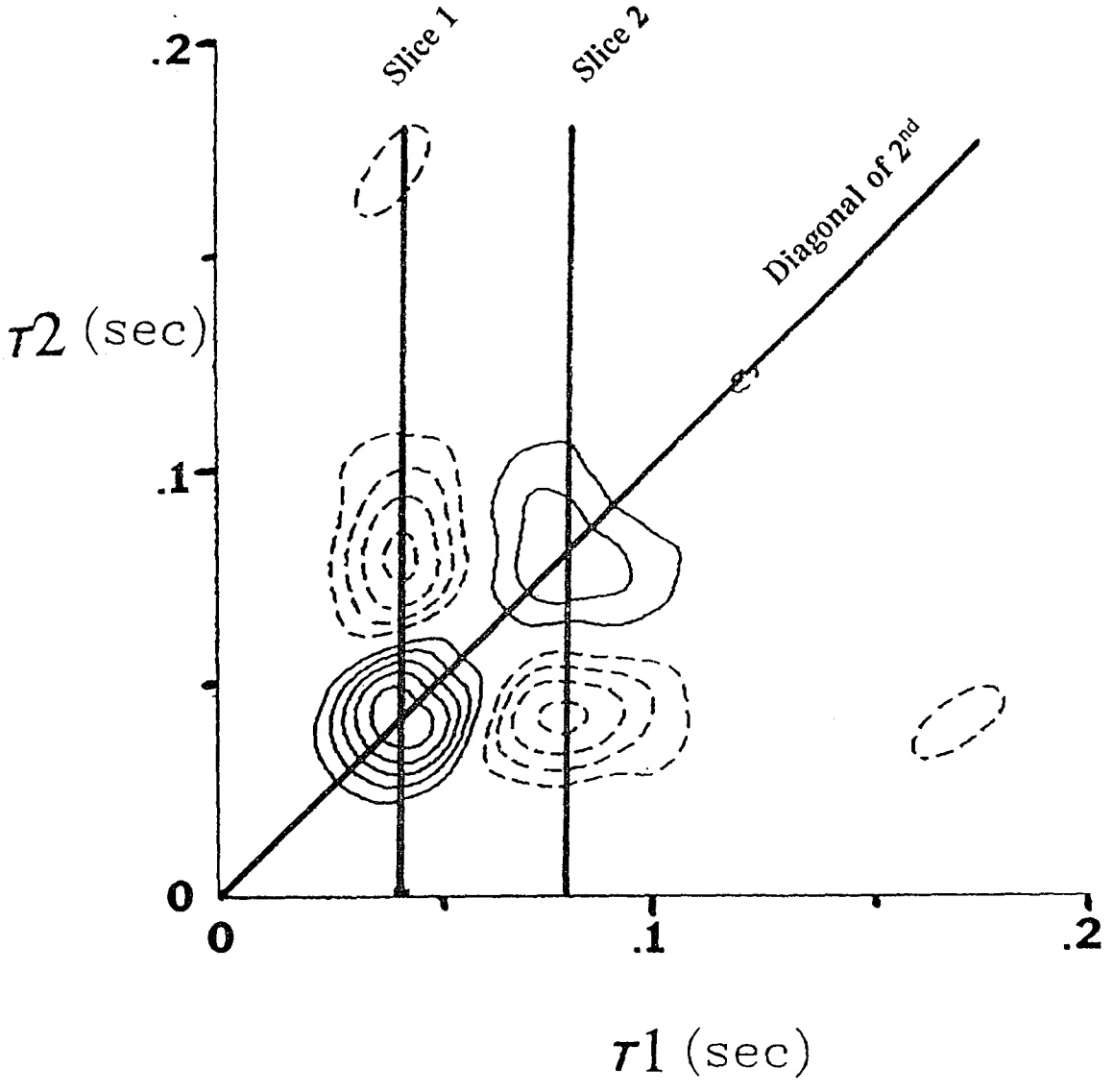

FIG. 23

A)

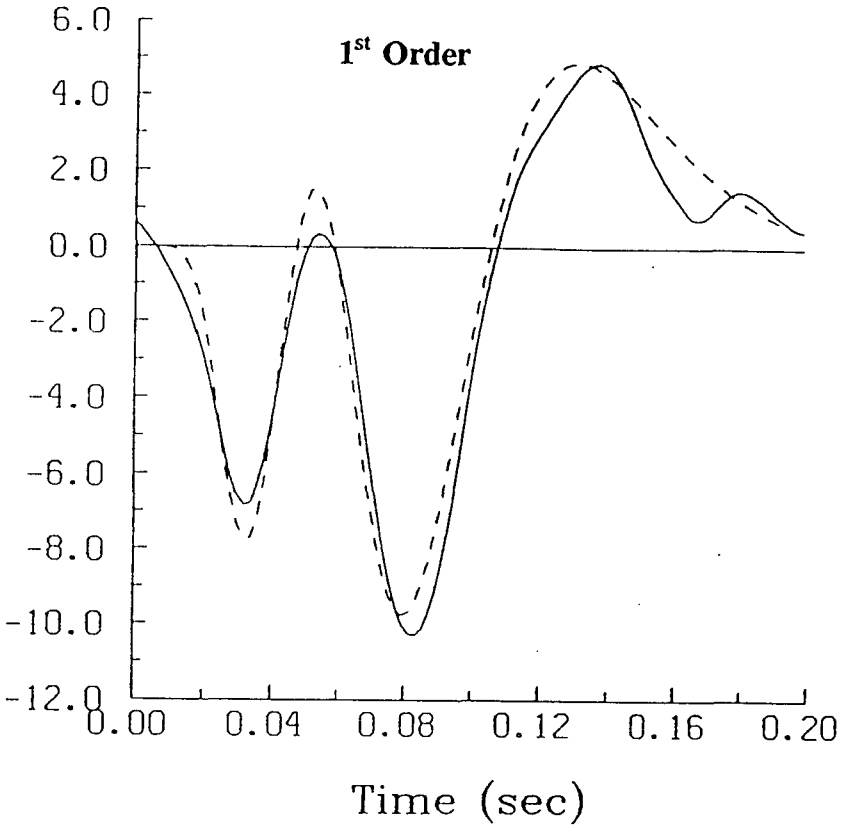
1st Order
6.0
4.0
2.0
0.0
-2.0
-4.0
-6.0
-8.0
-10.0
-12.0
0.00
0.04
0.08
0.12
0.16
0.20
Time (sec)

B)

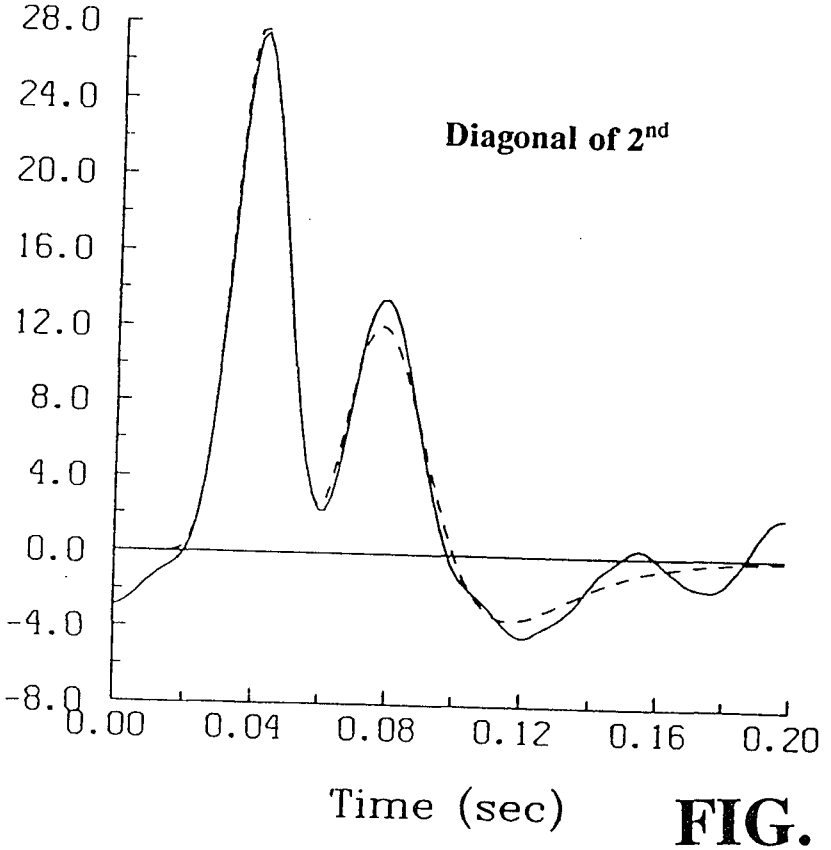
Diagonal of 2nd
28.0
24.0
20.0
16.0
12.0
8.0
4.0
0.0
-4.0
-8.0
0.00
0.04
0.08
0.12
0.16
0.20
Time (sec)

FIG. 24

C)

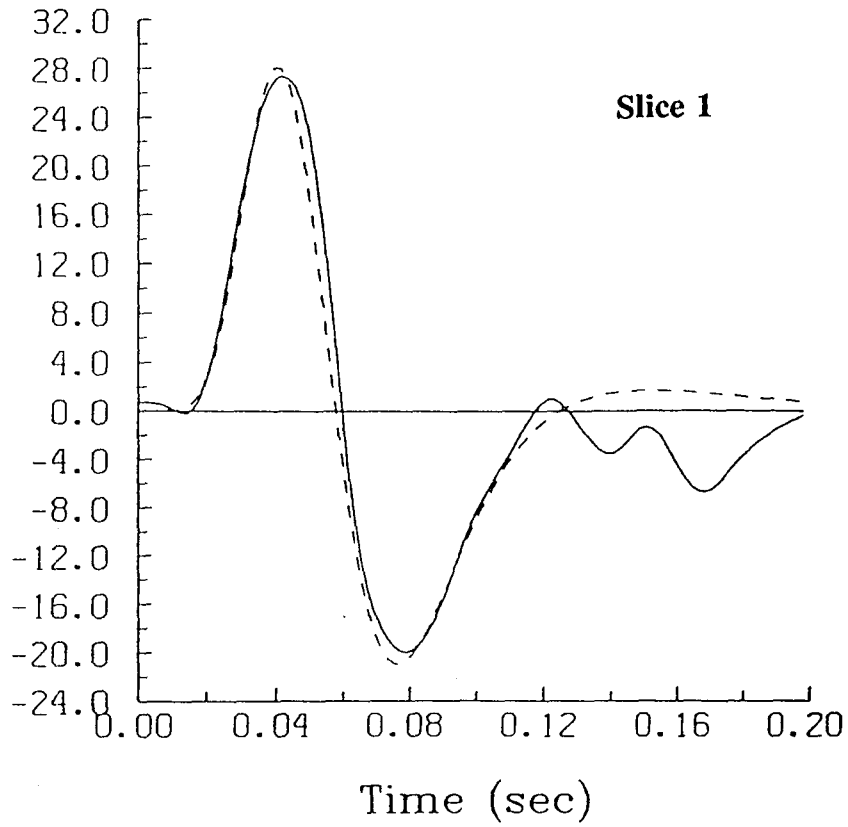
32.0
28.0
24.0
20.0
16.0
12.0
8.0
4.0
0.0
-4.0
-8.0
-12.0
-16.0
-20.0
-24.0
0.00
0.04
0.08
0.12
0.16
0.20
Time (sec)
Slice 1

D)

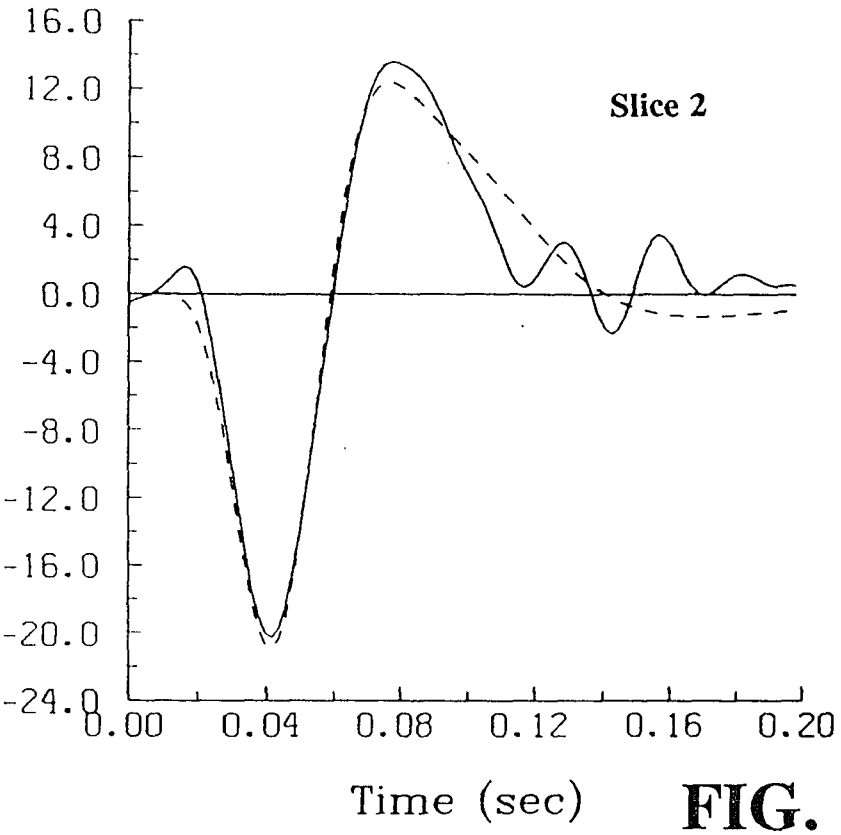
16.0
12.0
8.0
4.0
0.0
-4.0
-8.0
-12.0
-16.0
-20.0
-24.0
0.00
0.04
0.08
0.12
0.16
0.20
Time (sec)
Slice 2

FIG. 24

E)

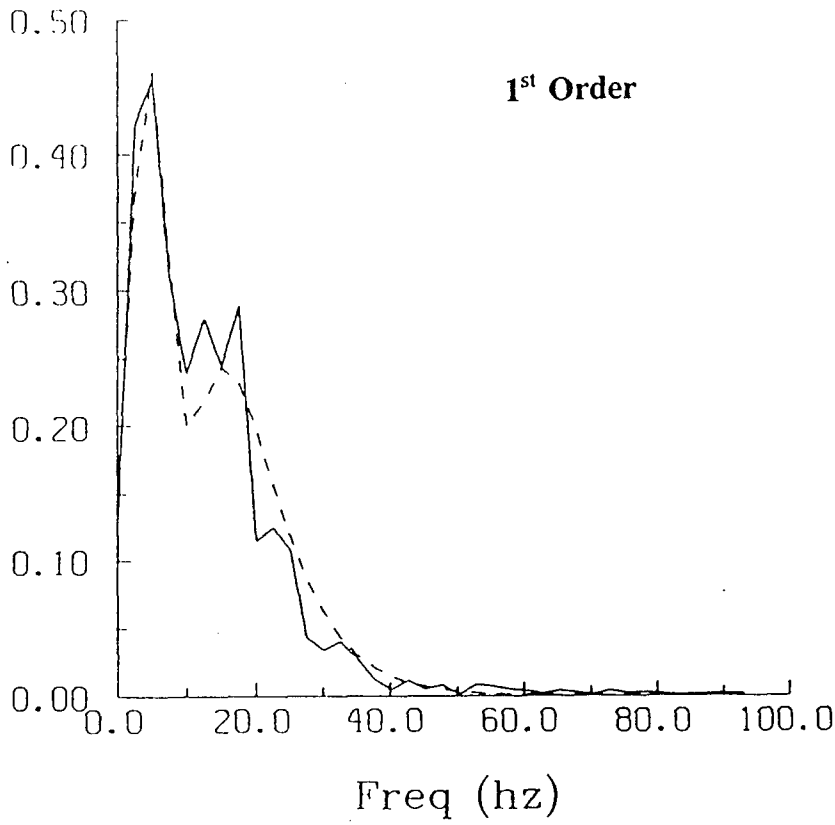
0.50
0.40
0.30
0.20
0.10
0.00
0.0
20.0
40.0
60.0
80.0
100.0
Freq (hz)
1st Order

F)

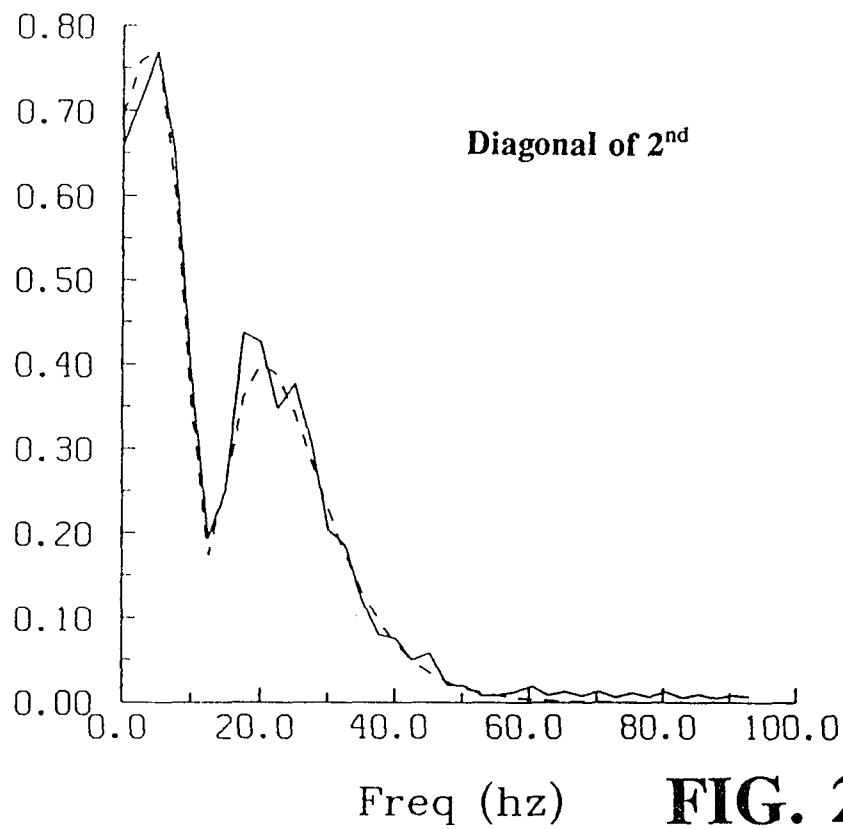
0.80
0.70
0.60
0.50
0.40
0.30
0.20
0.10
0.00
0.0
20.0
40.0
60.0
80.0
100.0
Freq (hz)
Diagonal of 2nd

FIG. 24

G)

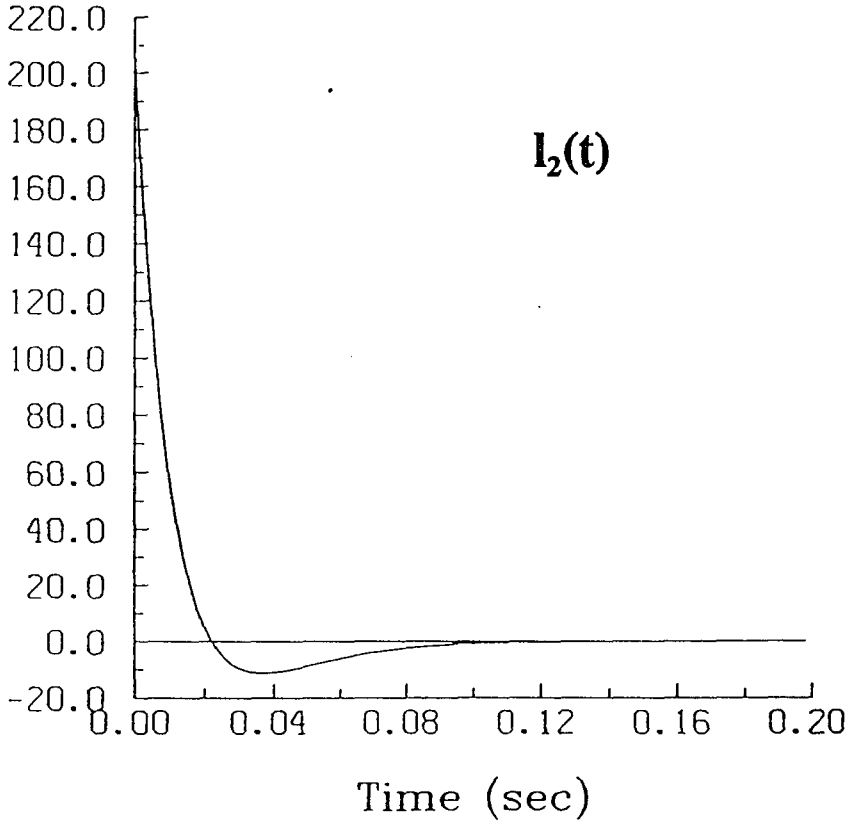
220.0
200.0
180.0
160.0
140.0
120.0
100.0
80.0
60.0
40.0
20.0
0.0
-20.0
0.00
0.04
0.08
0.12
0.16
0.20
$I_2(t)$
Time (sec)

H)

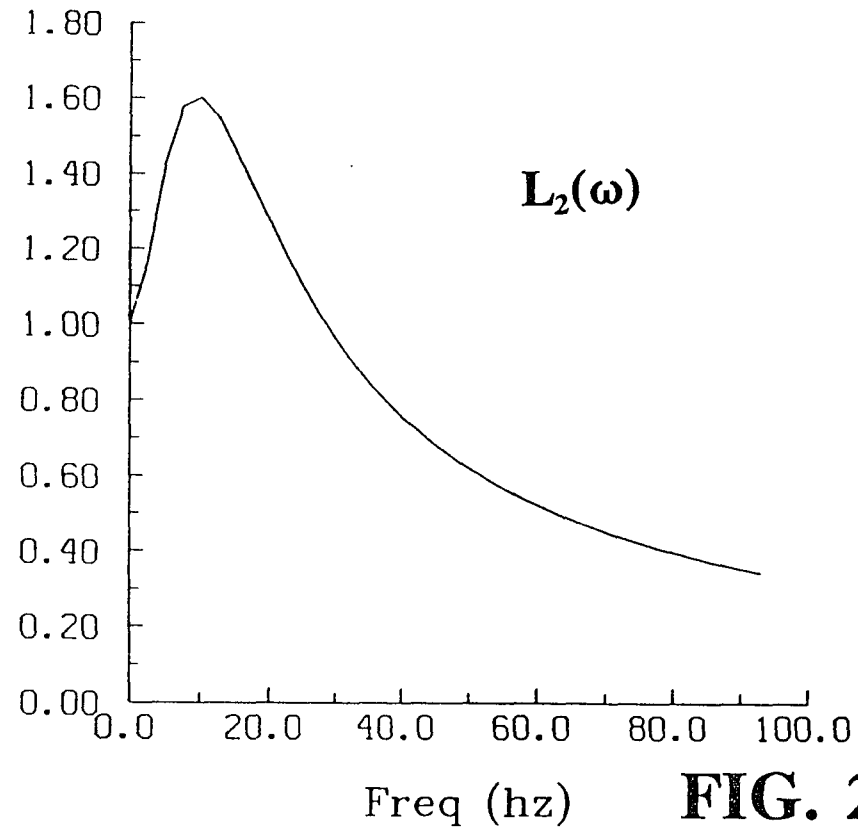
1.80
1.60
1.40
1.20
1.00
0.80
0.60
0.40
0.20
0.00
0.0
20.0
40.0
60.0
80.0
100.0
$L_2(\omega)$
Freq (hz)

FIG. 24

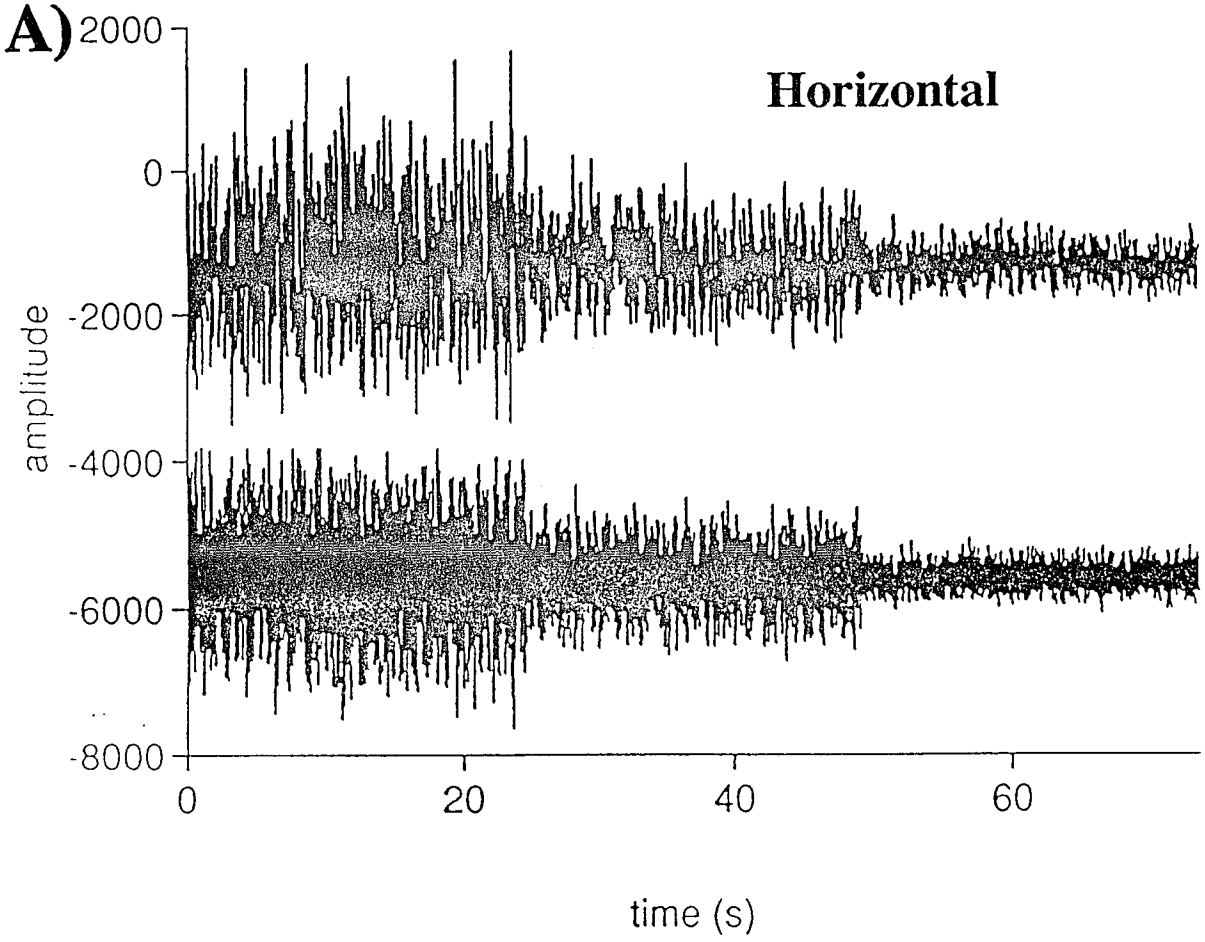
A)
Horizontal
2000
0
-2000
-4000
-6000
-8000
amplitude
0
20
40
60
time (s)

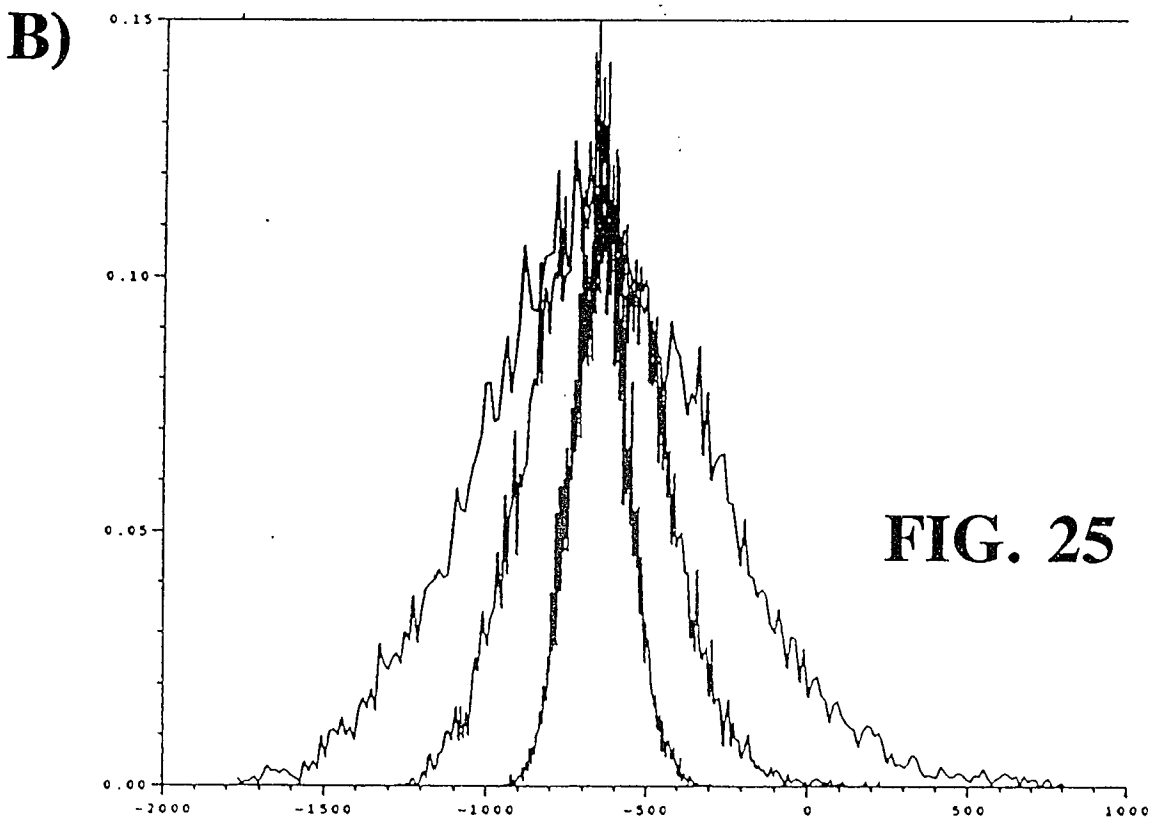
B)
0.15
0.10
0.05
0.00
-2000
-1500
-1000
-500
0
500
1000

FIG. 25

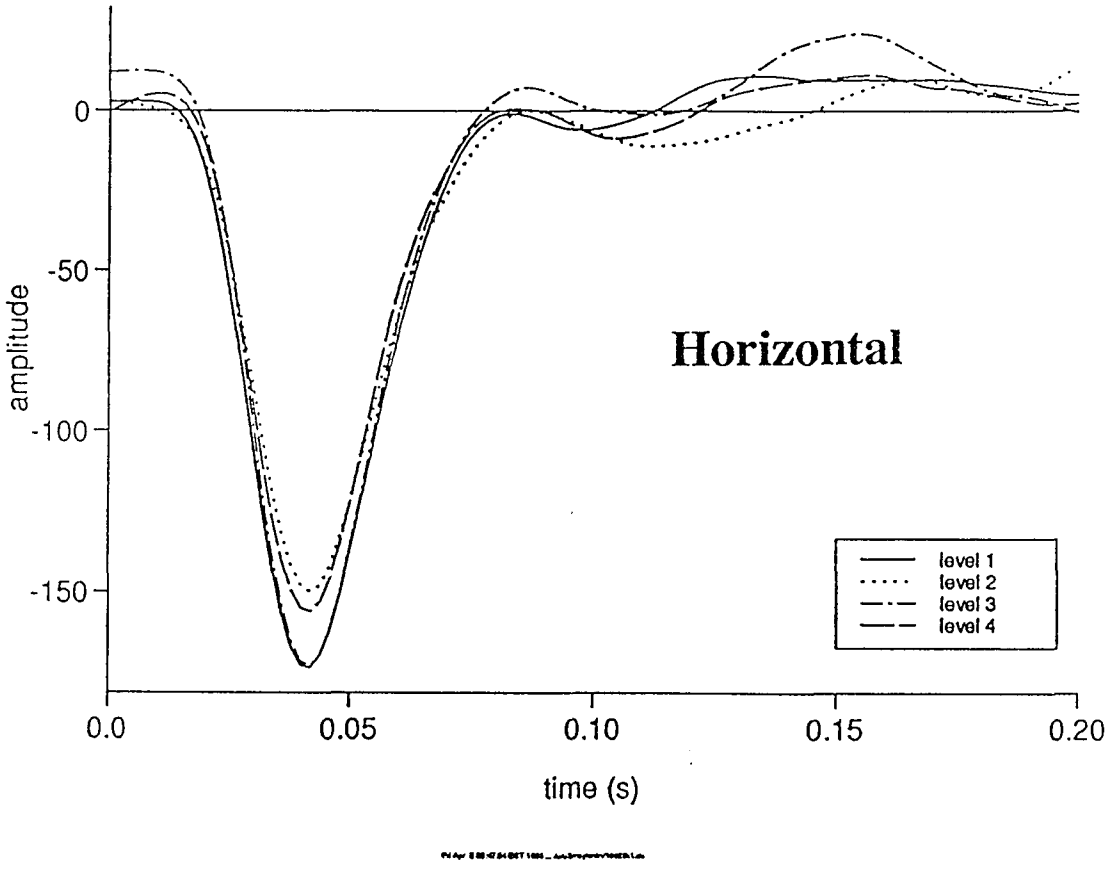
0
-50
-100
-150
amplitude
Horizontal
level 1
level 2
level 3
level 4
0.0
0.05
0.10
0.15
0.20
time (s)

FIG. 25 C)

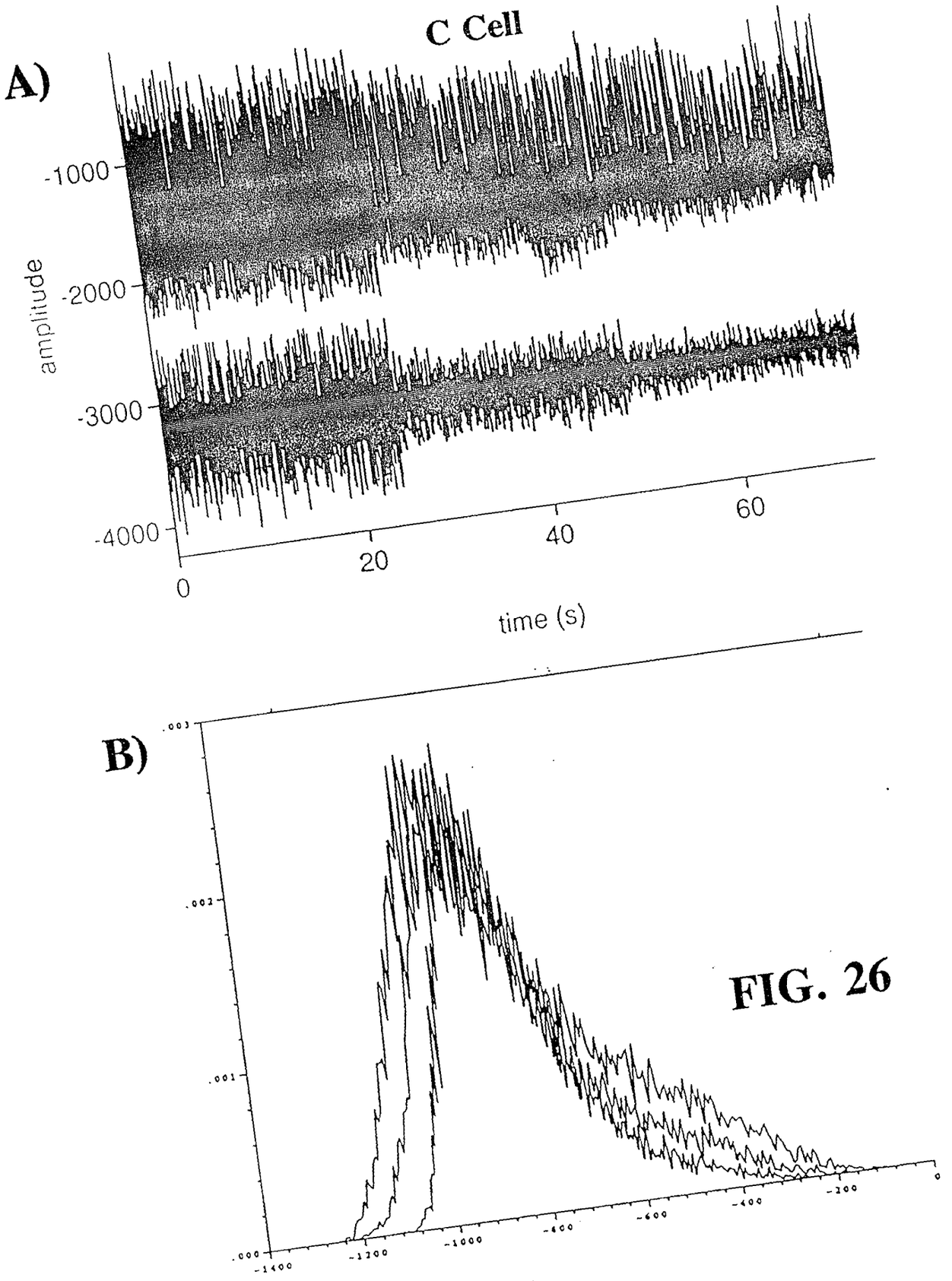
A)
C Cell
-1000
-2000
-3000
-4000
amplitude
0
20
40
60
time (s)
B)
.003
.002
.001
.000
-1400
-1200
-1000
-800
-600
-400
-200
0

FIG. 26

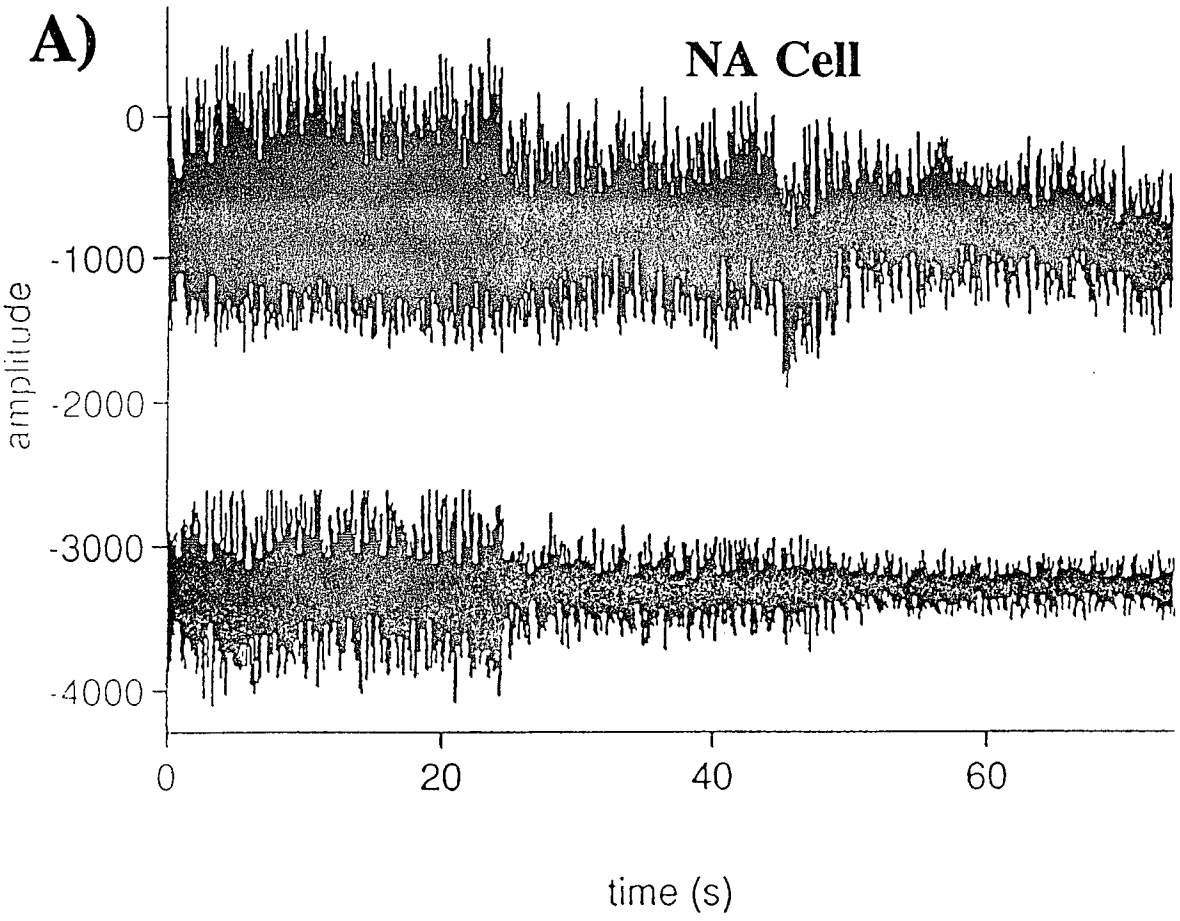
A)
NA Cell
0
-1000
-2000
-3000
-4000
amplitude
0
20
40
60
time (s)

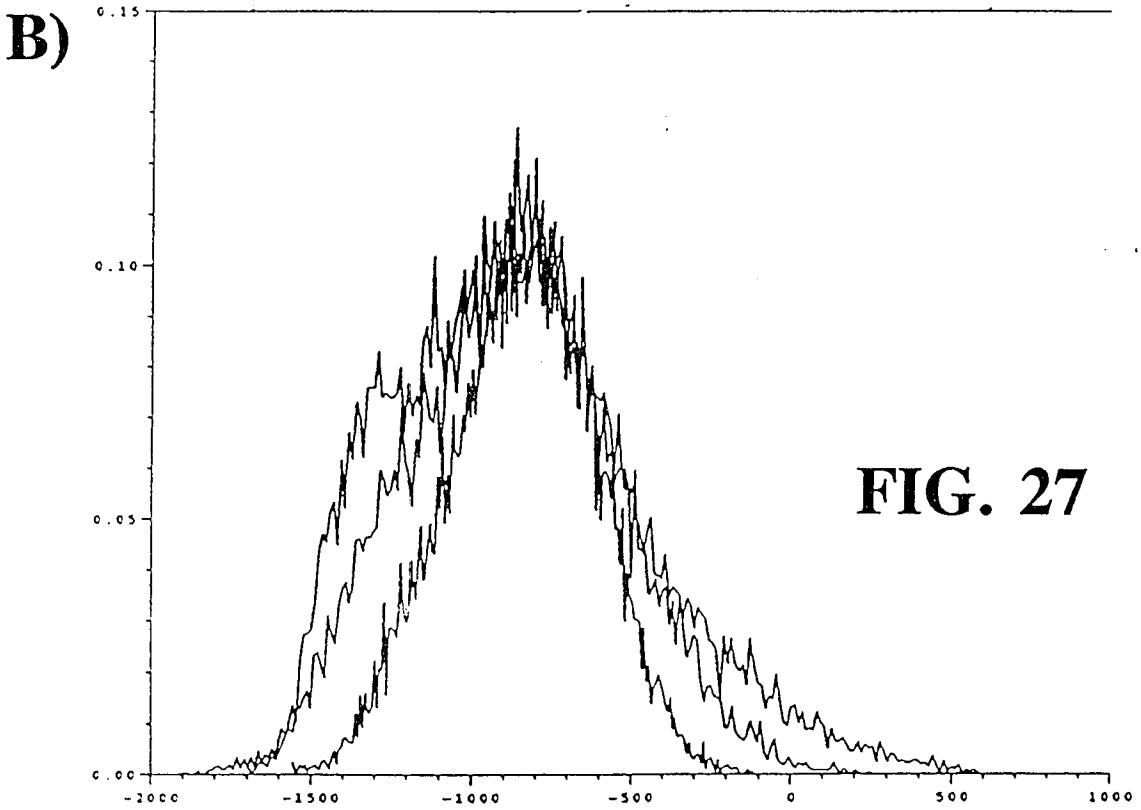
B)
0.15
0.10
0.05
0.00
-2000
-1500
-1000
-500
0
500
1000

FIG. 27

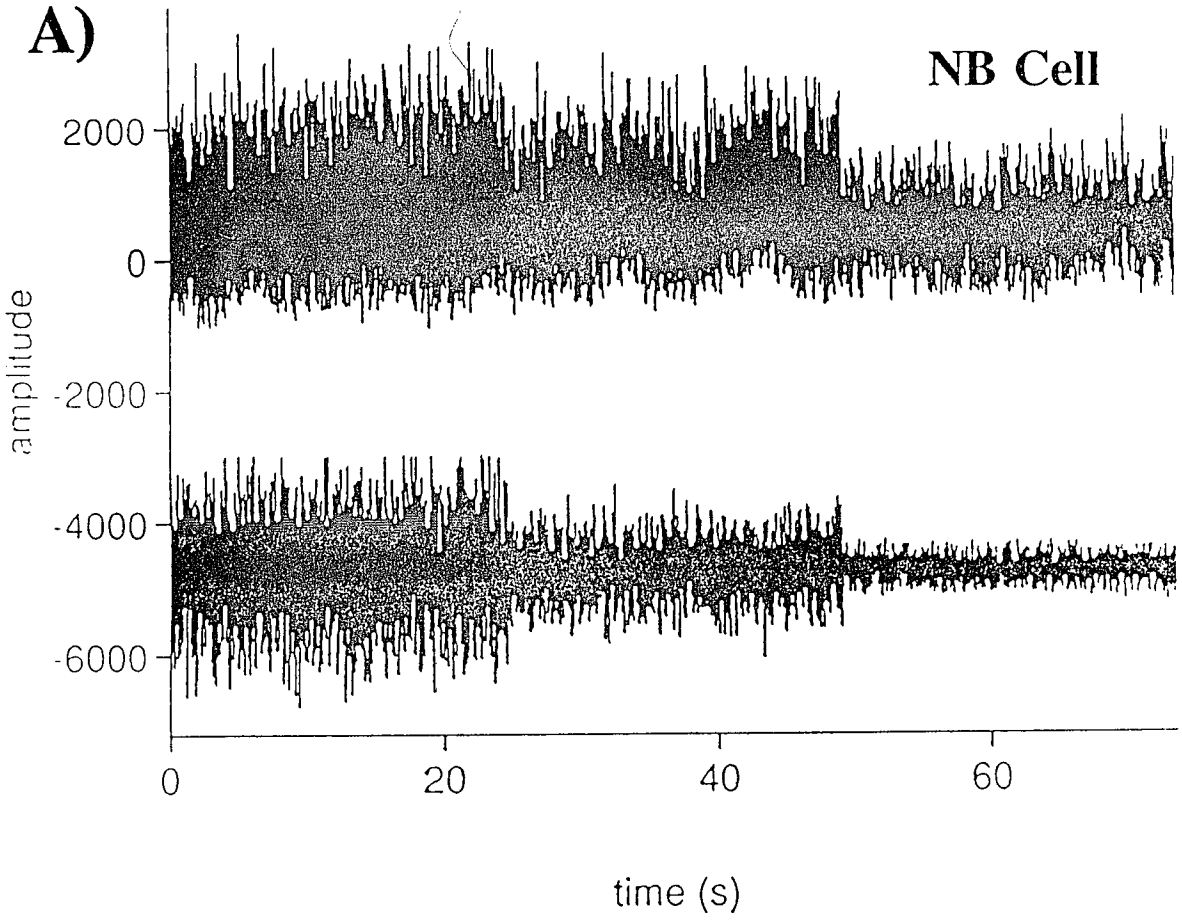
A)
NB Cell
2000
0
-2000
-4000
-6000
amplitude
0
20
40
60
time (s)

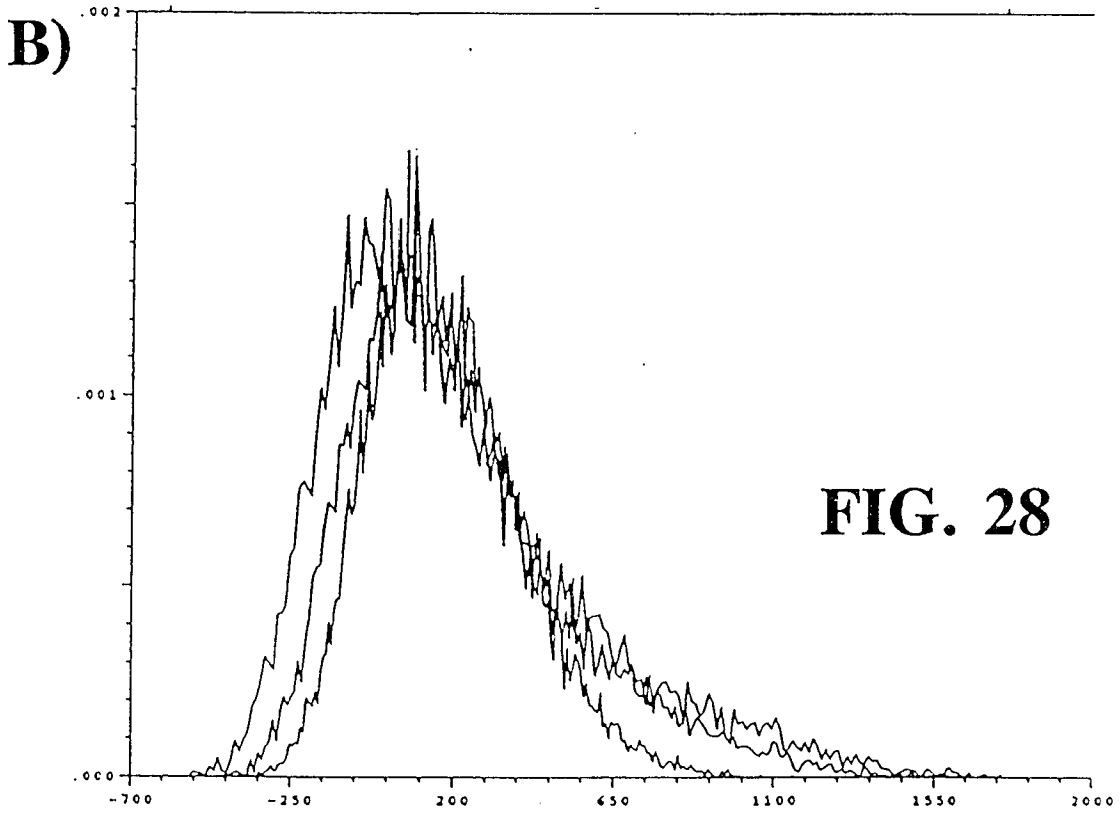
B)
.002
.001
.000
-700
-250
200
650
1100
1550
2000

FIG. 28

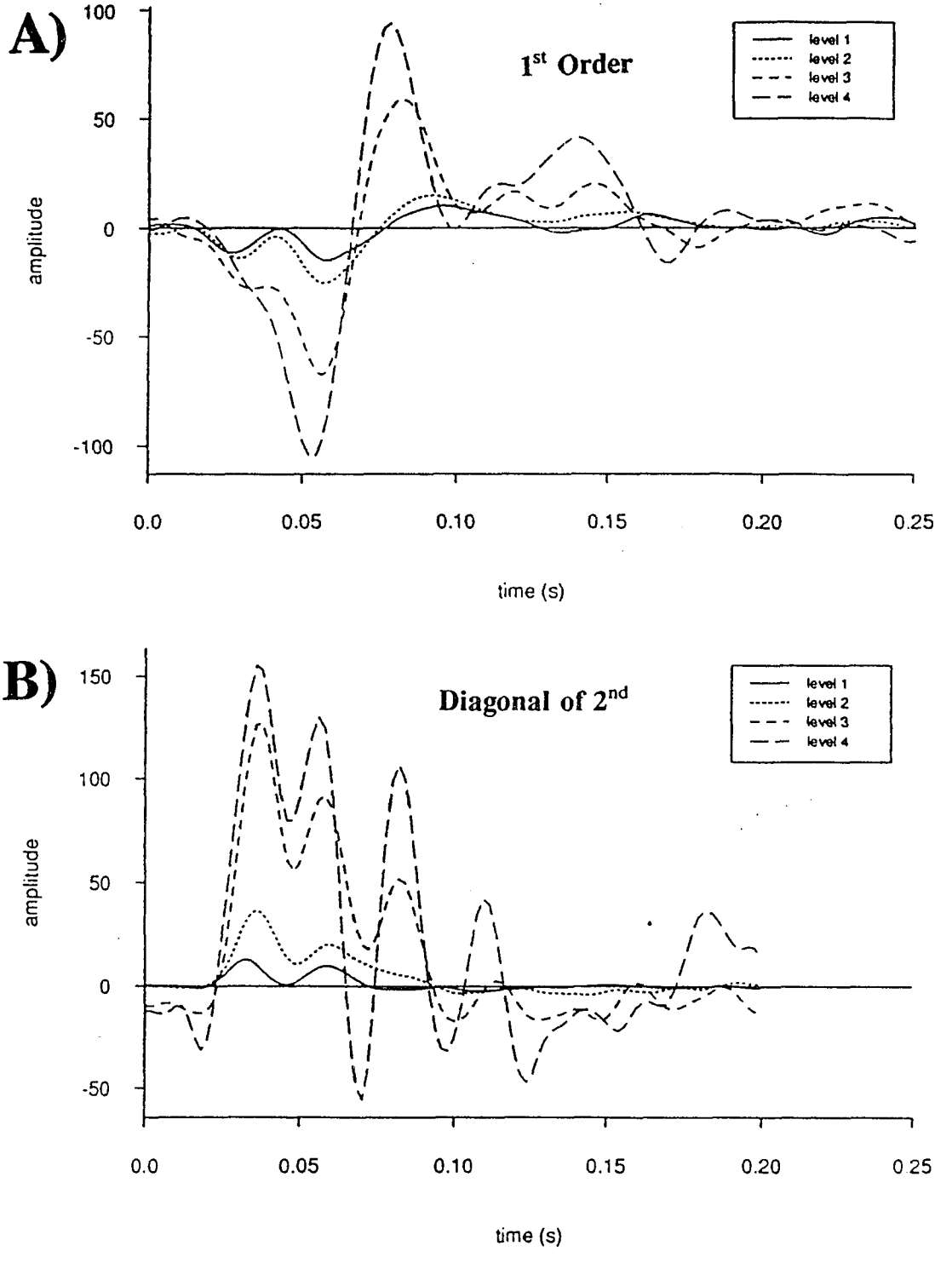
A)
1st Order
level 1
level 2
level 3
level 4
amplitude
100
50
0
-50
-100
0.0
0.05
0.10
0.15
0.20
0.25
time (s)
B)
Diagonal of 2nd
level 1
level 2
level 3
level 4
amplitude
150
100
50
0
-50
0.0
0.05
0.10
0.15
0.20
0.25
time (s)

FIG. 29

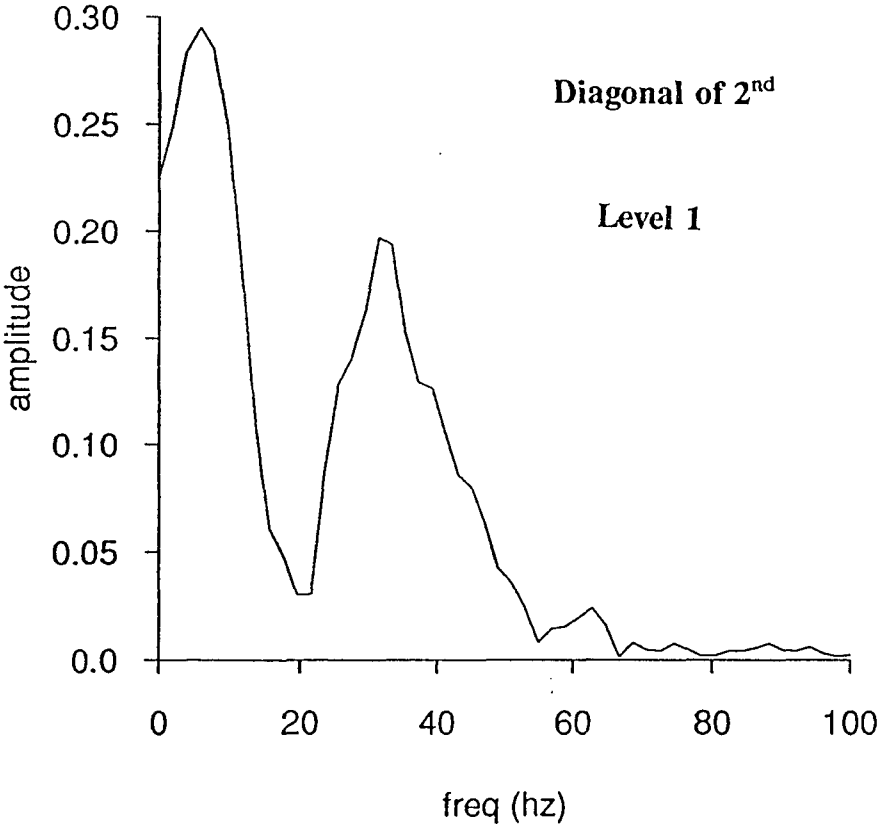
0.30
0.25
0.20
0.15
0.10
0.05
0.0
amplitude
Diagonal of 2nd
Level 1
0
20
40
60
80
100
freq (hz)

FIG. 29 C)

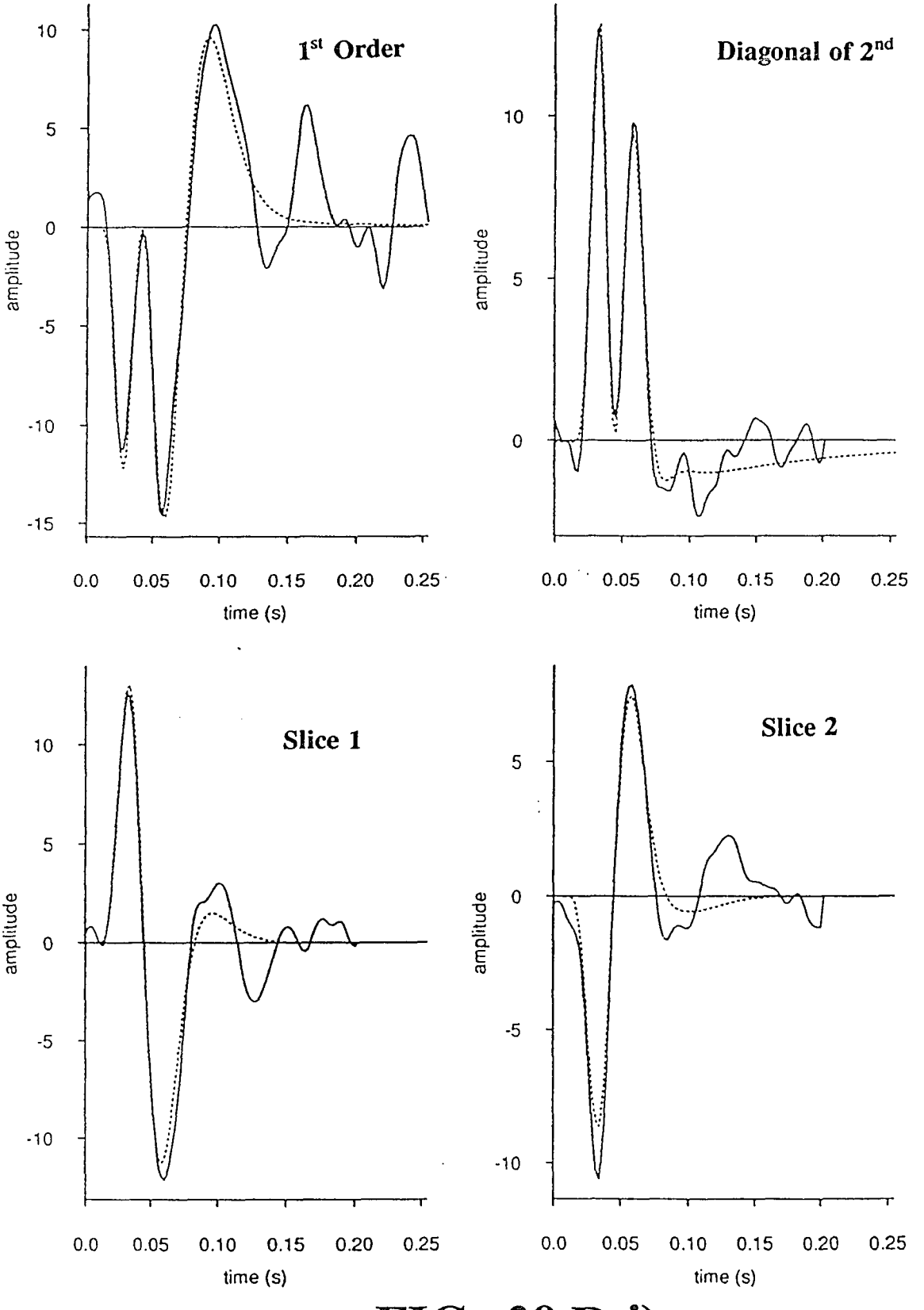
1st Order
Diagonal of 2nd
Slice 1
Slice 2
amplitude
time (s)
10
5
0
-5
-10
-15
0.0
0.05
0.10
0.15
0.20
0.25

FIG. 29 D-i)

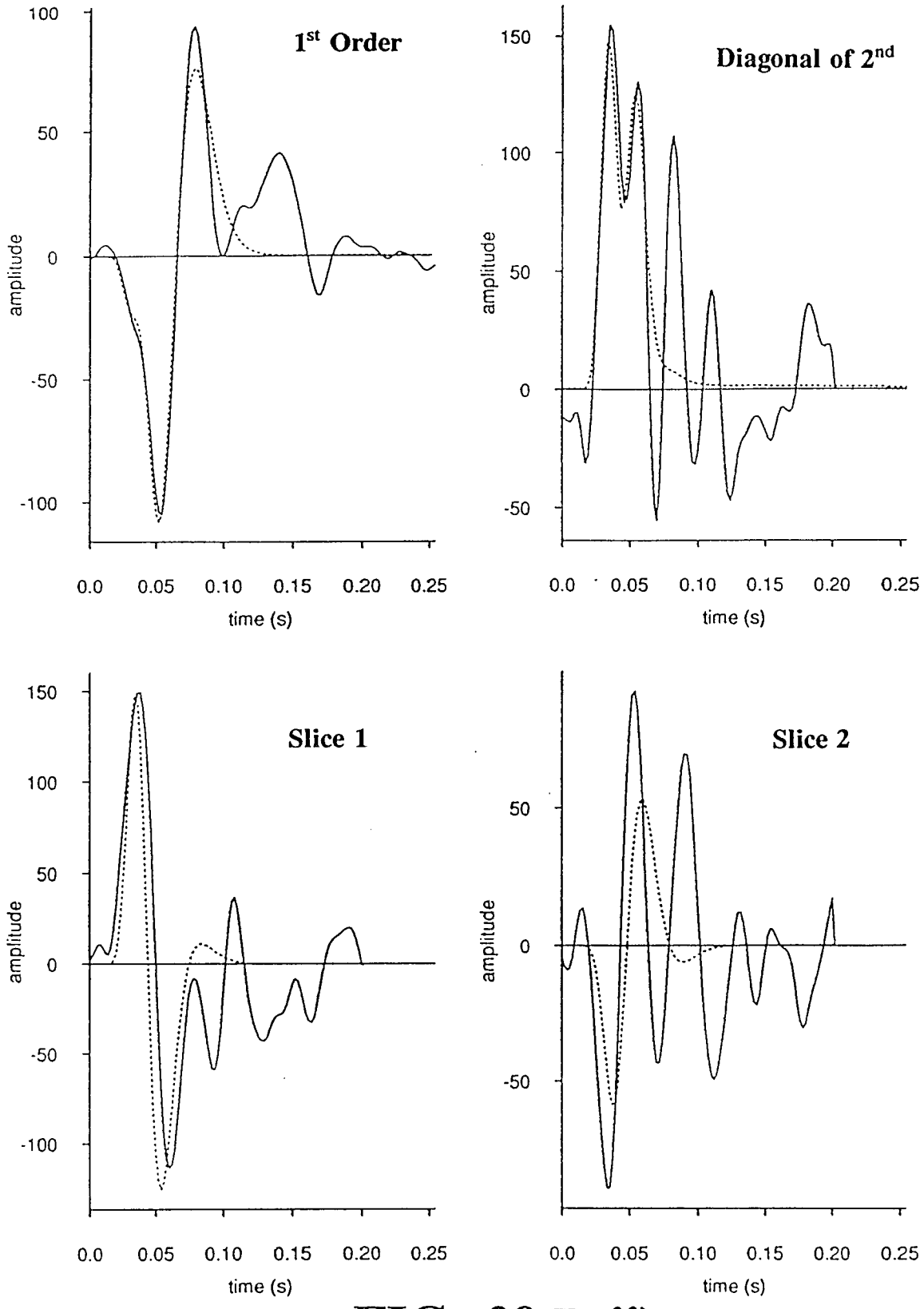
1st Order
Diagonal of 2nd
Slice 1
Slice 2
amplitude
time (s)
100
50
0
-50
-100
150
0.0
0.05
0.10
0.15
0.20
0.25

FIG. 29 D-ii)

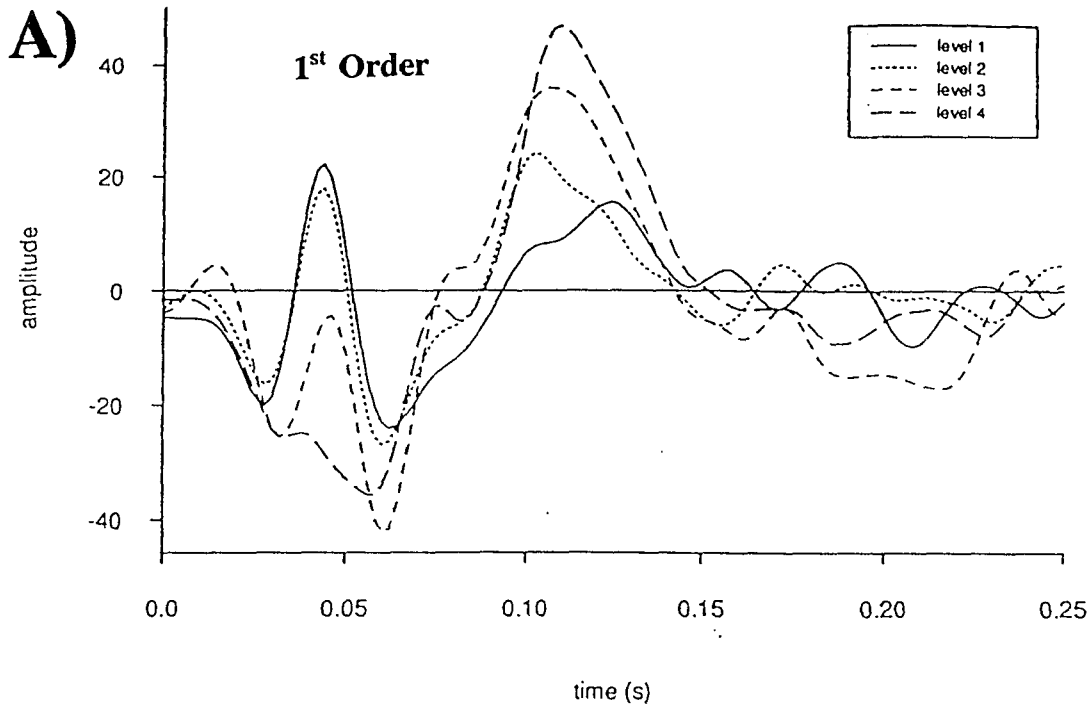

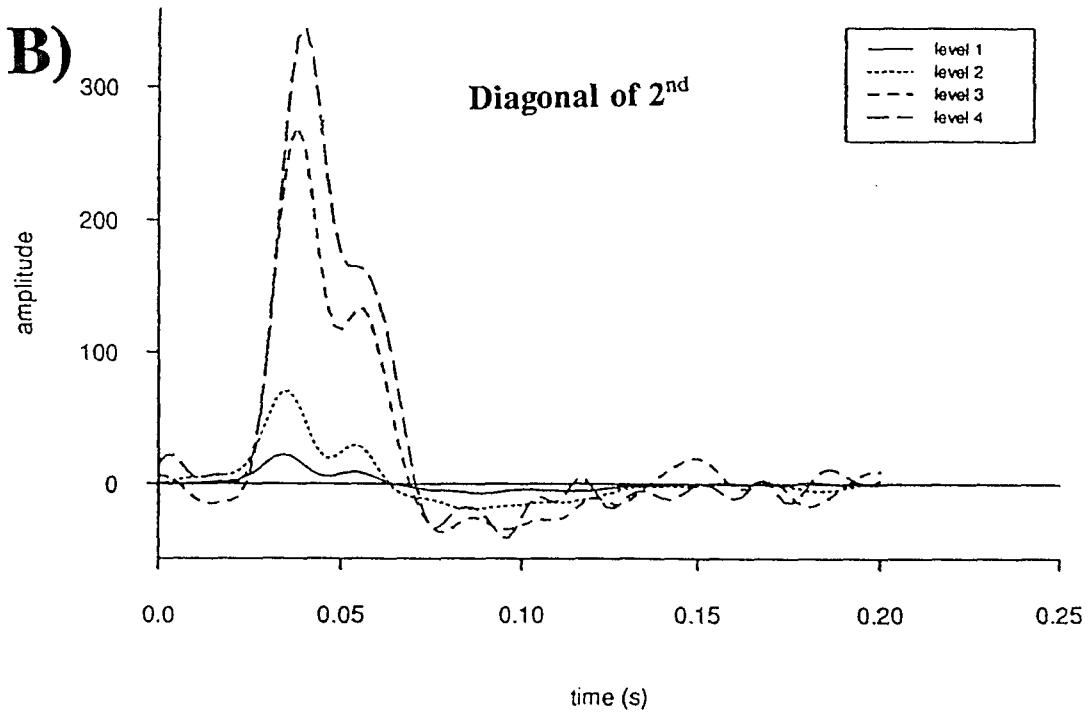

Mon Mar 29 18:05:48 EST 1993 ... /uu3/mayo/hv05009k2.de

FIG. 30

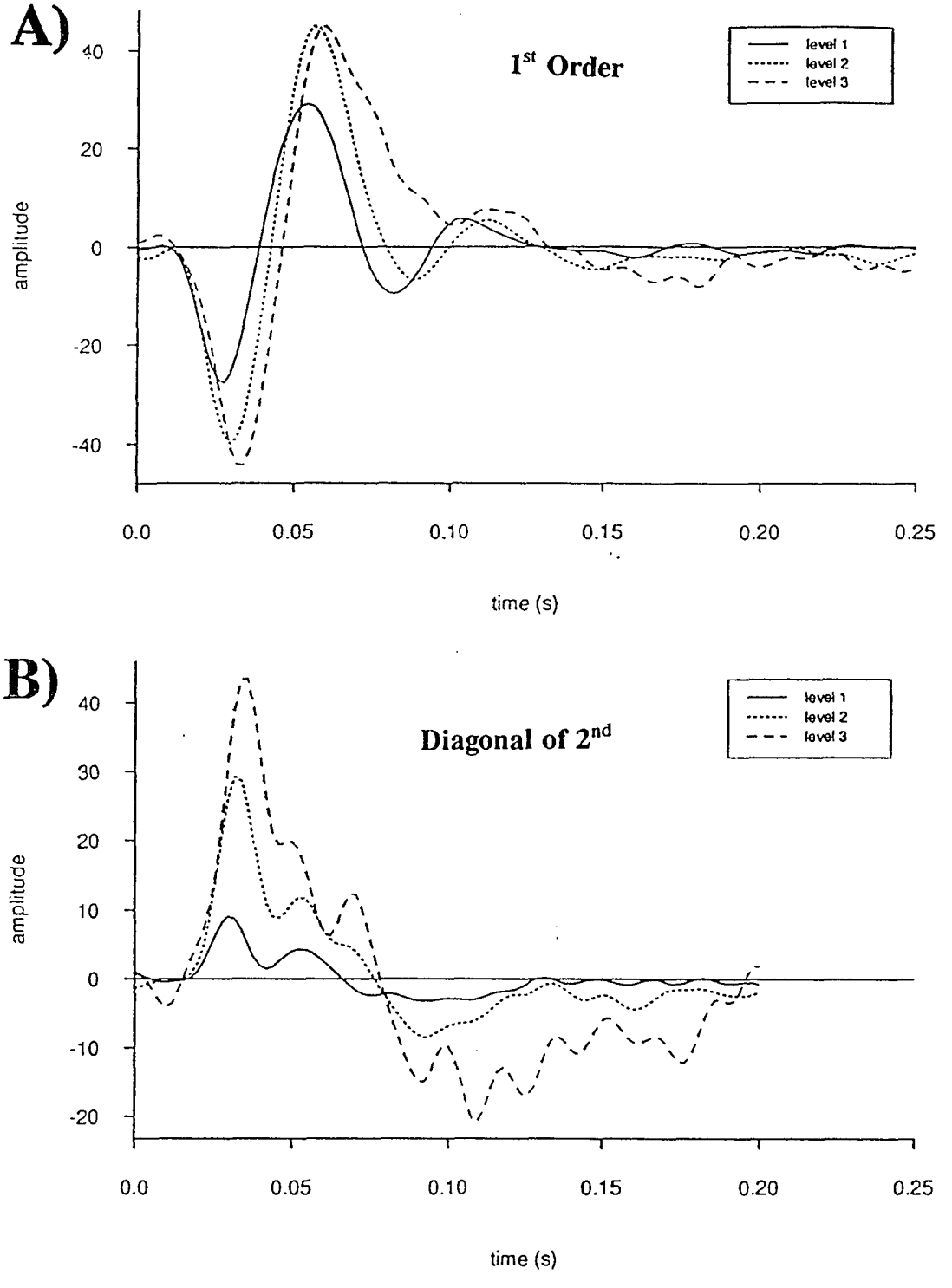

Mon Mar 29 18:05:32 EST 1993 ... AA/3/naykoo/n/06014k2.ds

FIG. 31

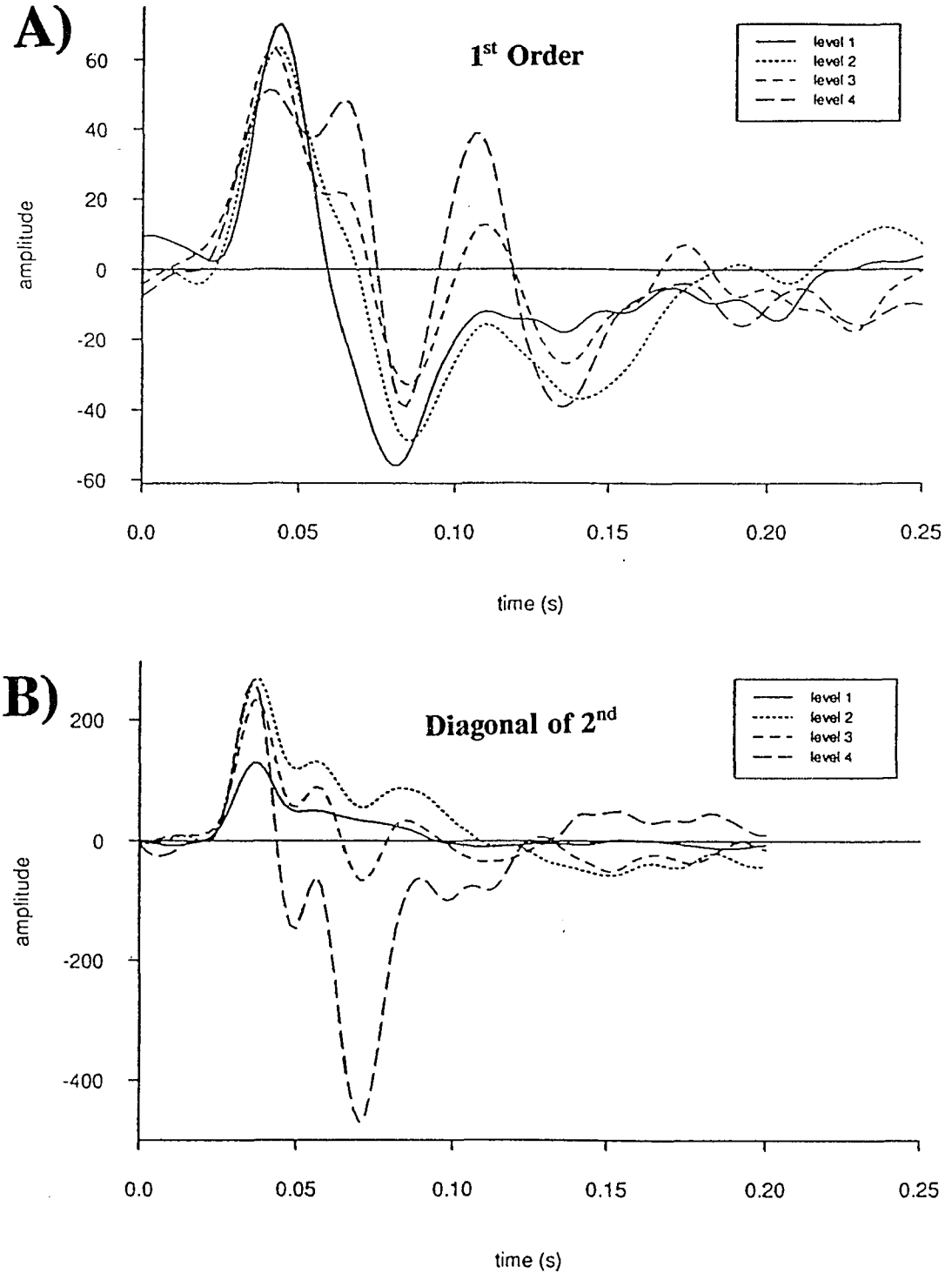

Mon Mar 29 18:44:32 EST 1993 ... /u/LG/naylor/n/16012k2.da

FIG. 32

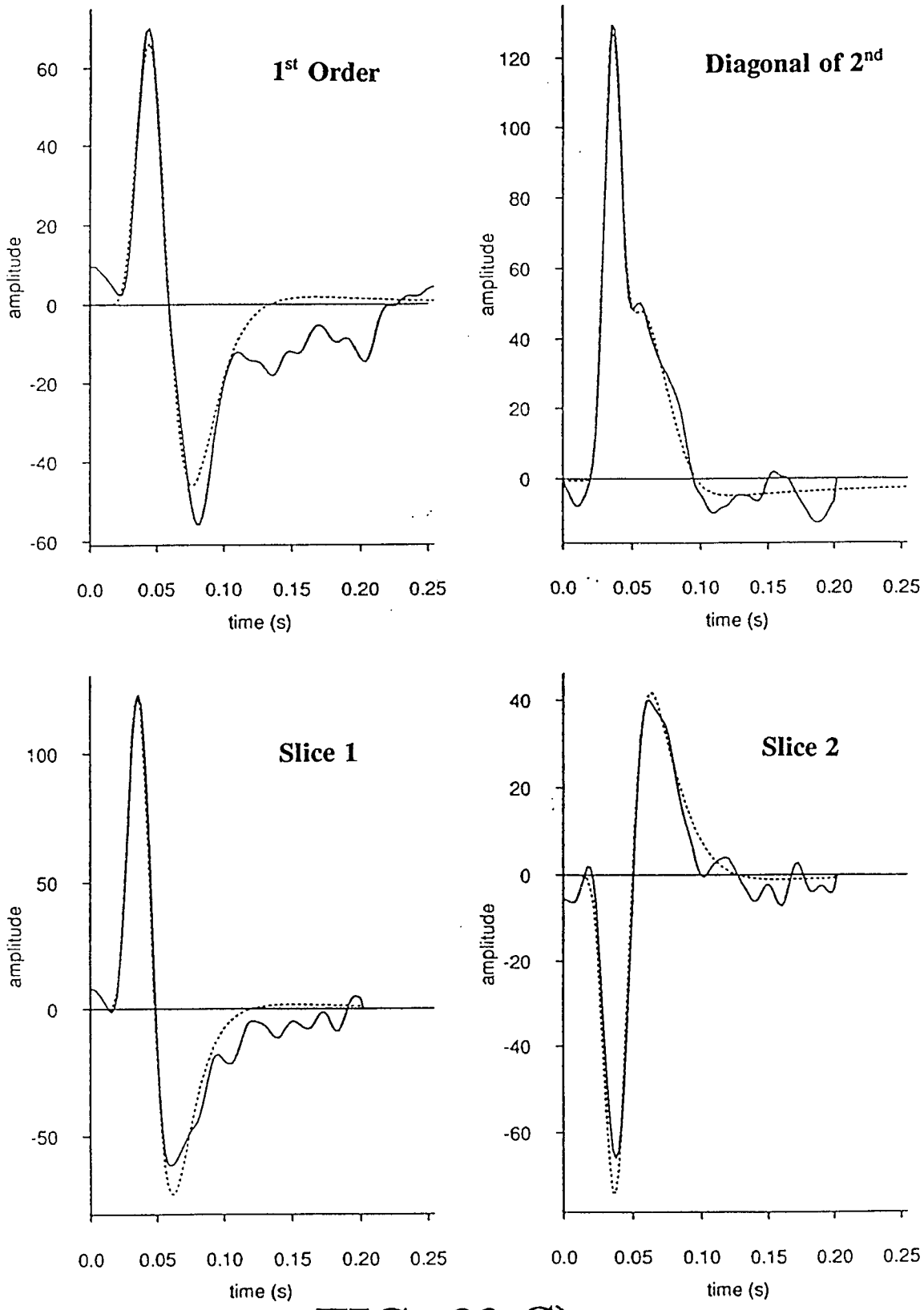
1st Order
Diagonal of 2nd
Slice 1
Slice 2
amplitude
time (s)
60
40
20
0
-20
-40
-60
120
100
80
60
40
20
0
50
-50
0.0
0.05
0.10
0.15
0.20
0.25

FIG. 32 C)

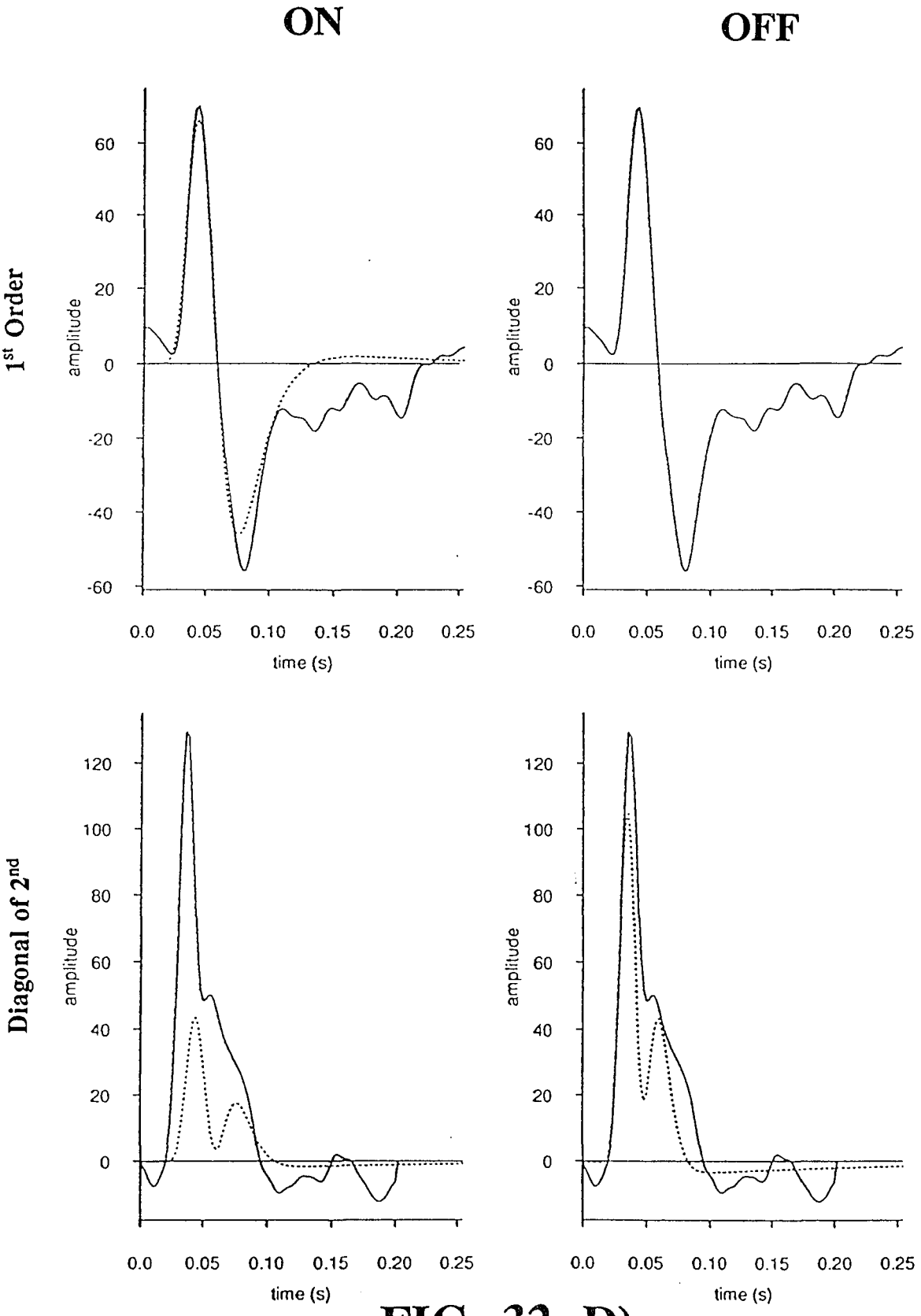
ON
OFF
1st Order
Diagonal of 2nd
amplitude
time (s)
60
40
20
0
-20
-40
-60
120
100
80
0.0
0.05
0.10
0.15
0.20
0.25

FIG. 32 D)

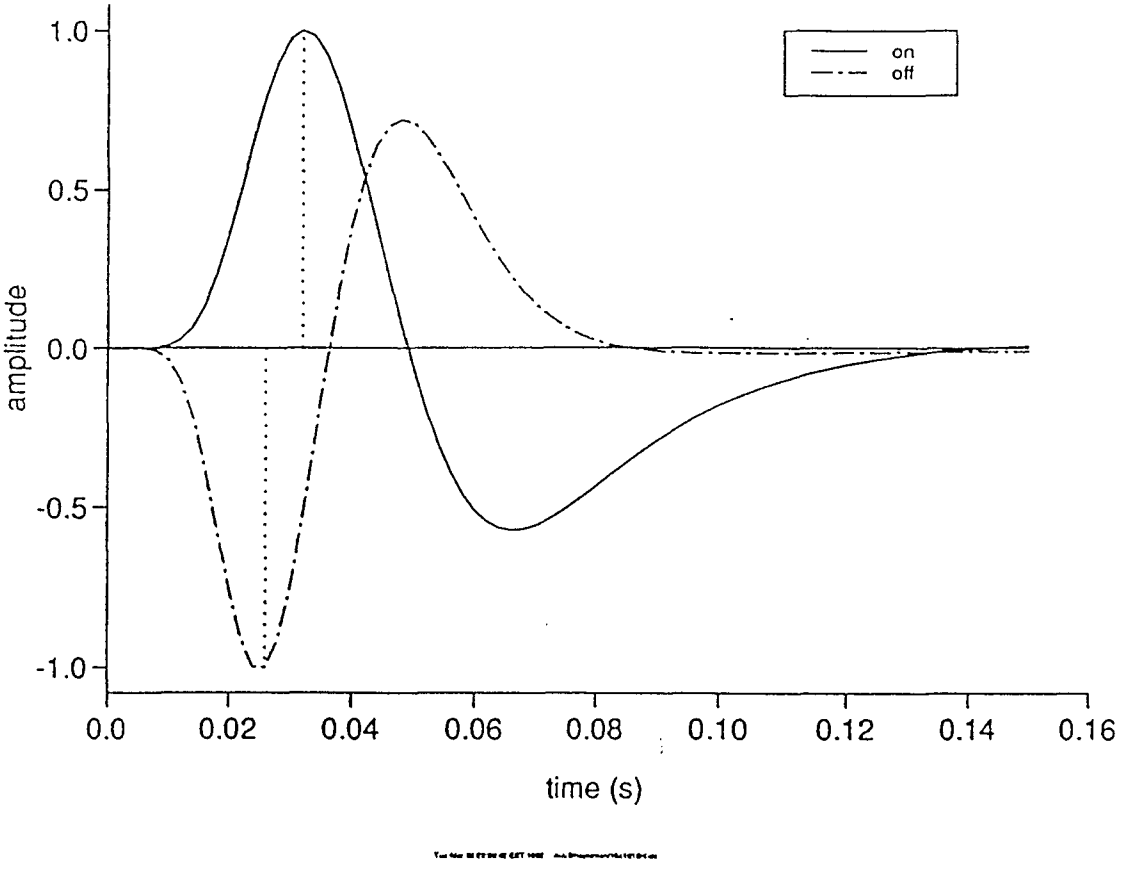
1.0
0.5
0.0
-0.5
-1.0
amplitude
on
off
0.0
0.02
0.04
0.06
0.08
0.10
0.12
0.14
0.16
time (s)

FIG. 32 E)

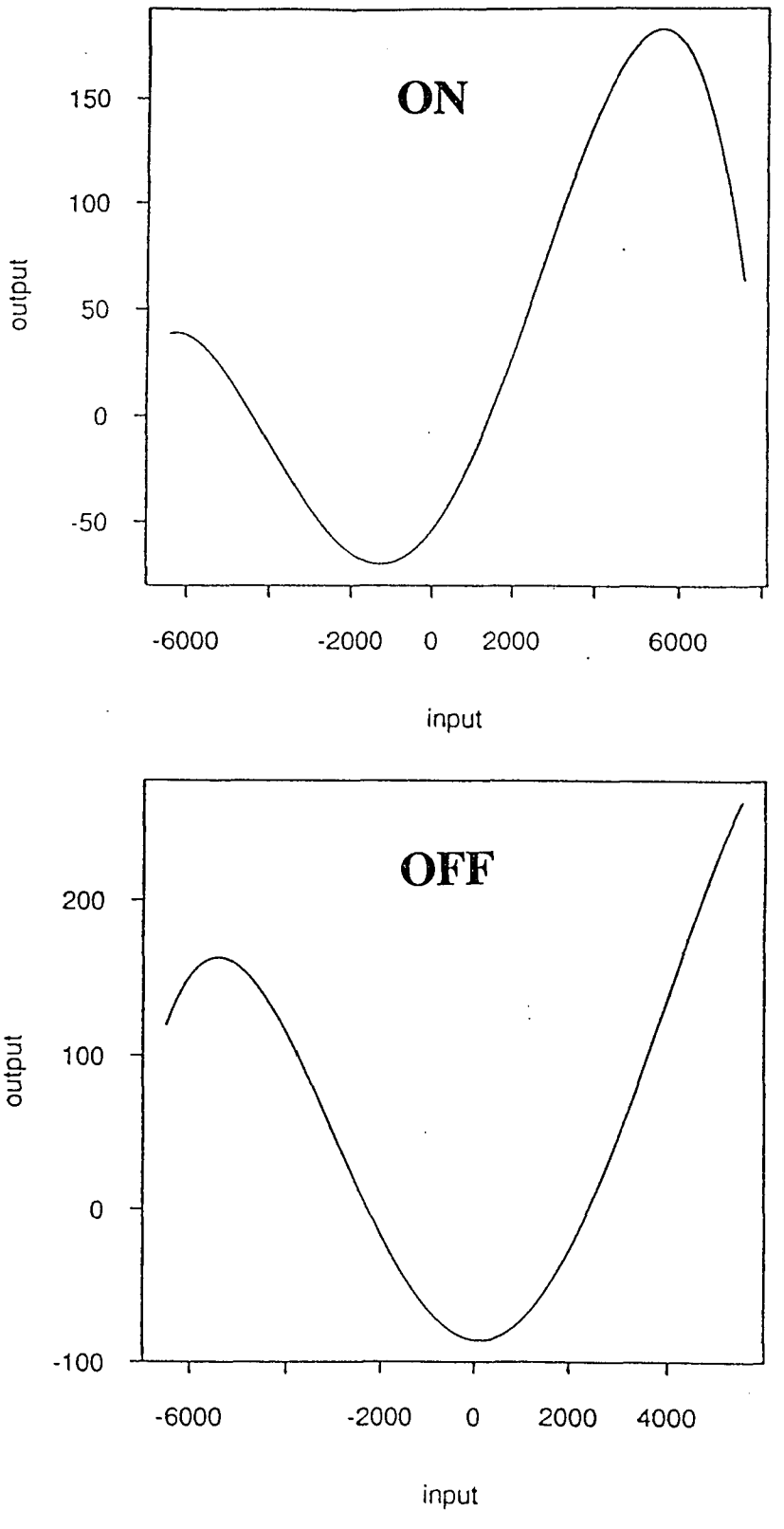
ON
150
100
50
0
-50
output
-6000
-2000
0
2000
6000
input
OFF
200
100
0
-100
output
-6000
-2000
0
2000
4000
input

FIG. 32 F-i)

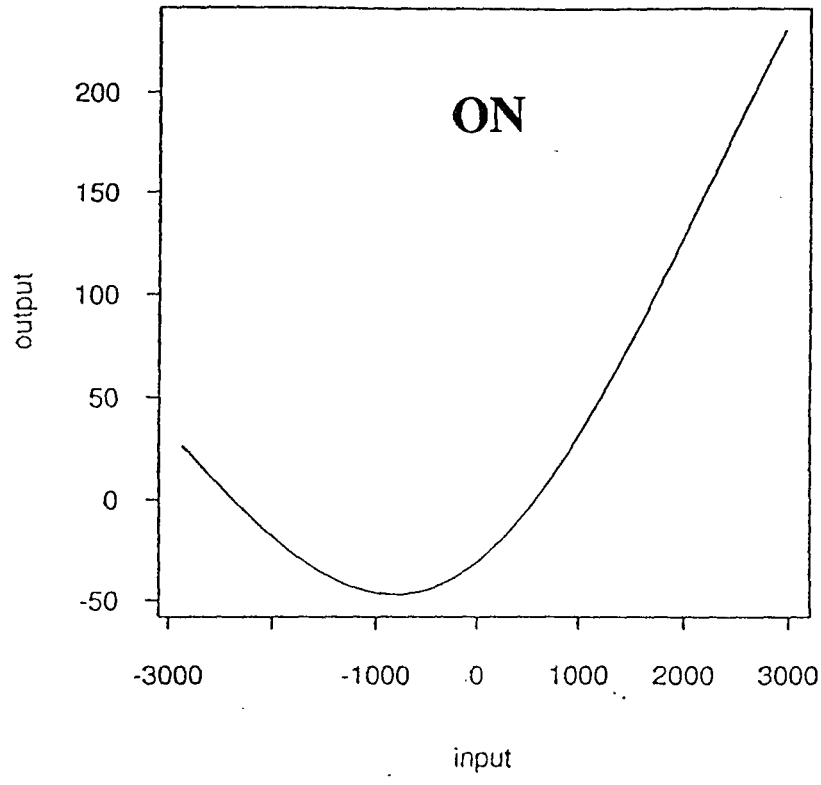
ON
200
150
100
50
0
-50
output
-3000
-1000
0
1000
2000
3000
input

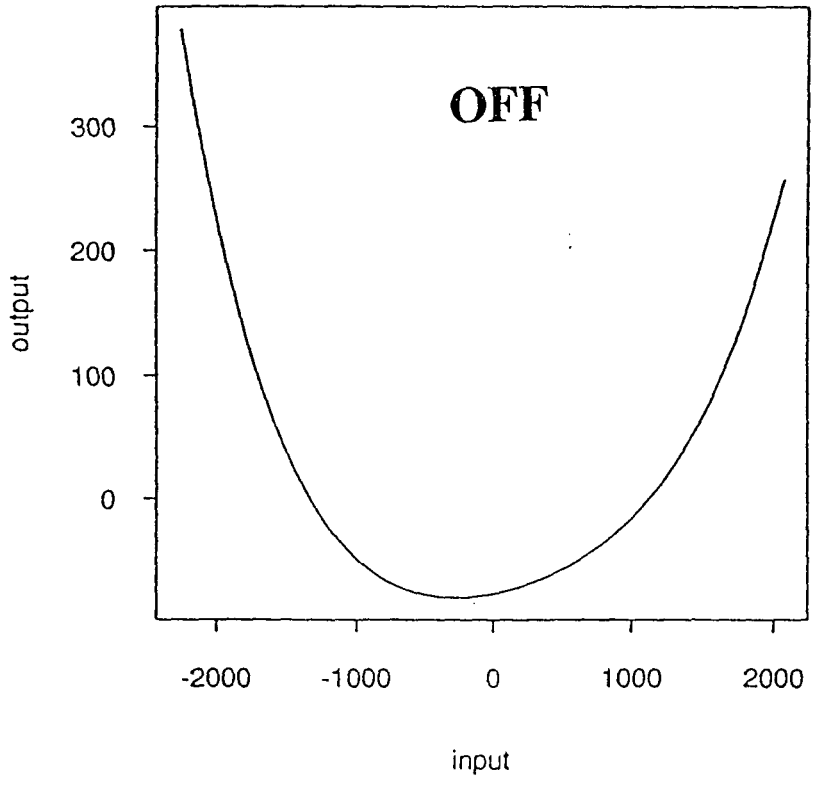
OFF
300
200
100
0
output
-2000
-1000
0
1000
2000
input

FIG. 32 F-ii)

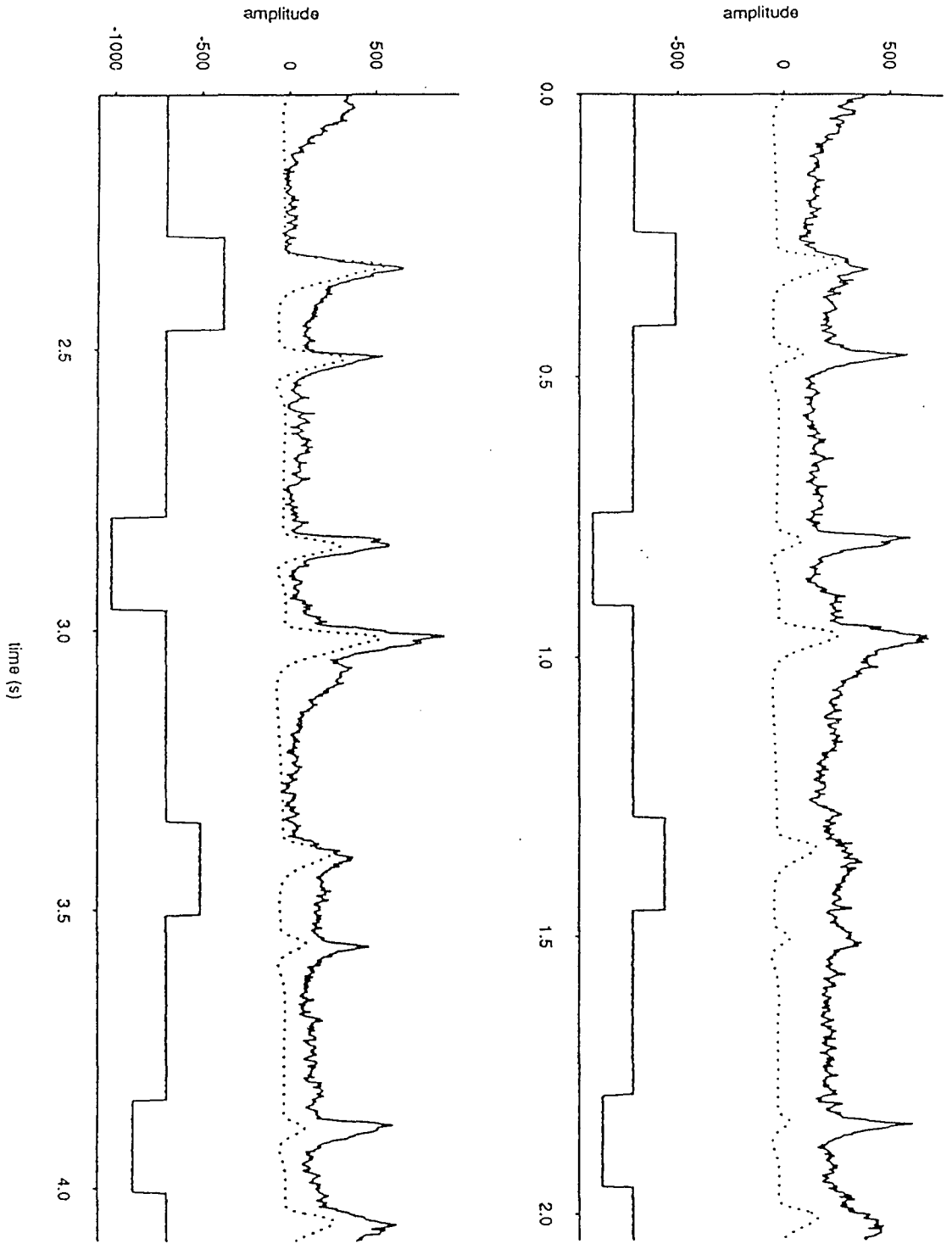
amplitude
500
0
-500
0.0
0.5
1.0
1.5
2.0
amplitude
500
0
-500
-1000
2.5
3.0
3.5
4.0
time (s)

FIG. 32 G)

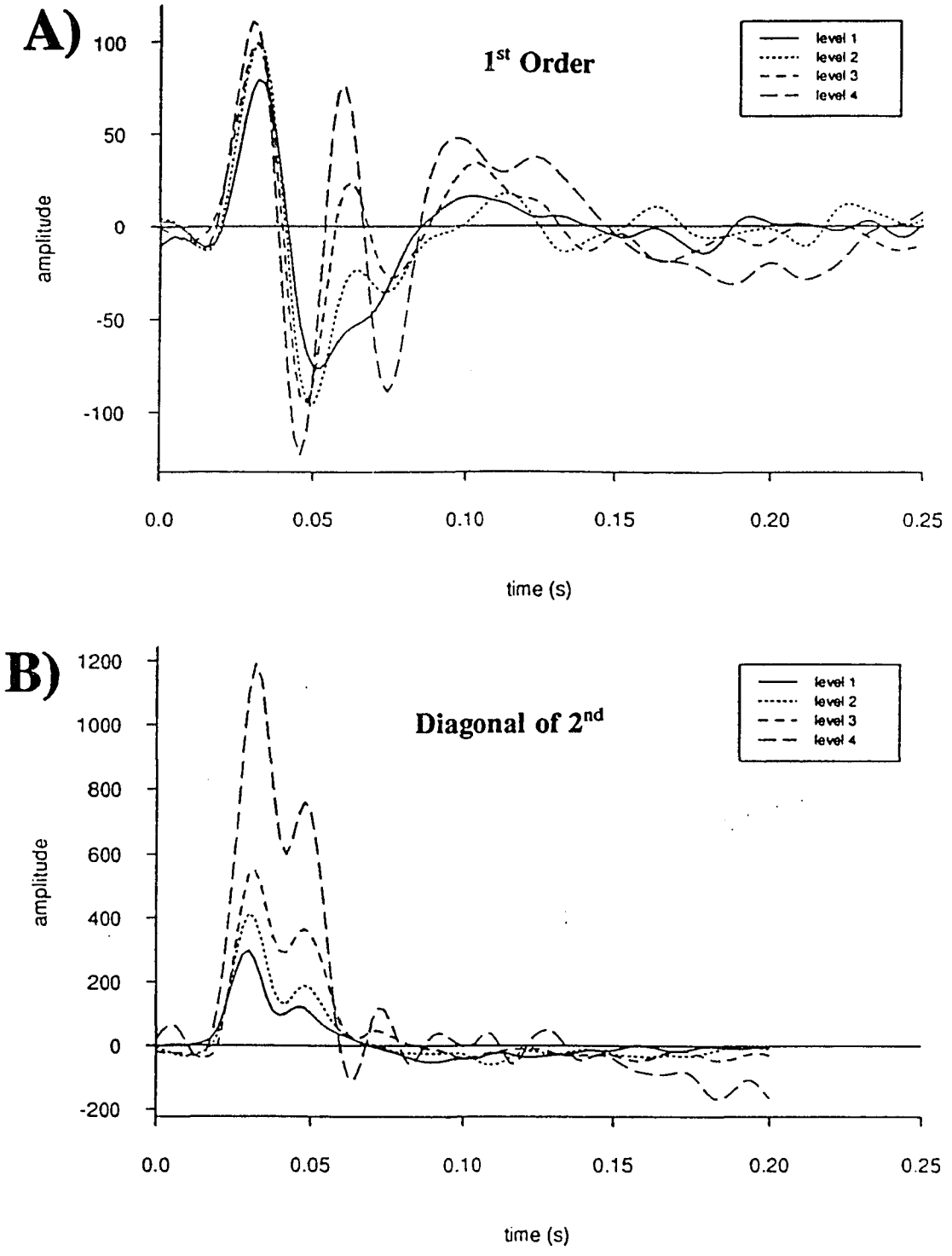
A)
1st Order
level 1
level 2
level 3
level 4
amplitude
100
50
0
-50
-100
0.0
0.05
0.10
0.15
0.20
0.25
time (s)
B)
Diagonal of 2nd
level 1
level 2
level 3
level 4
amplitude
1200
1000
800
600
400
200
0
-200
0.0
0.05
0.10
0.15
0.20
0.25
time (s)

FIG. 33

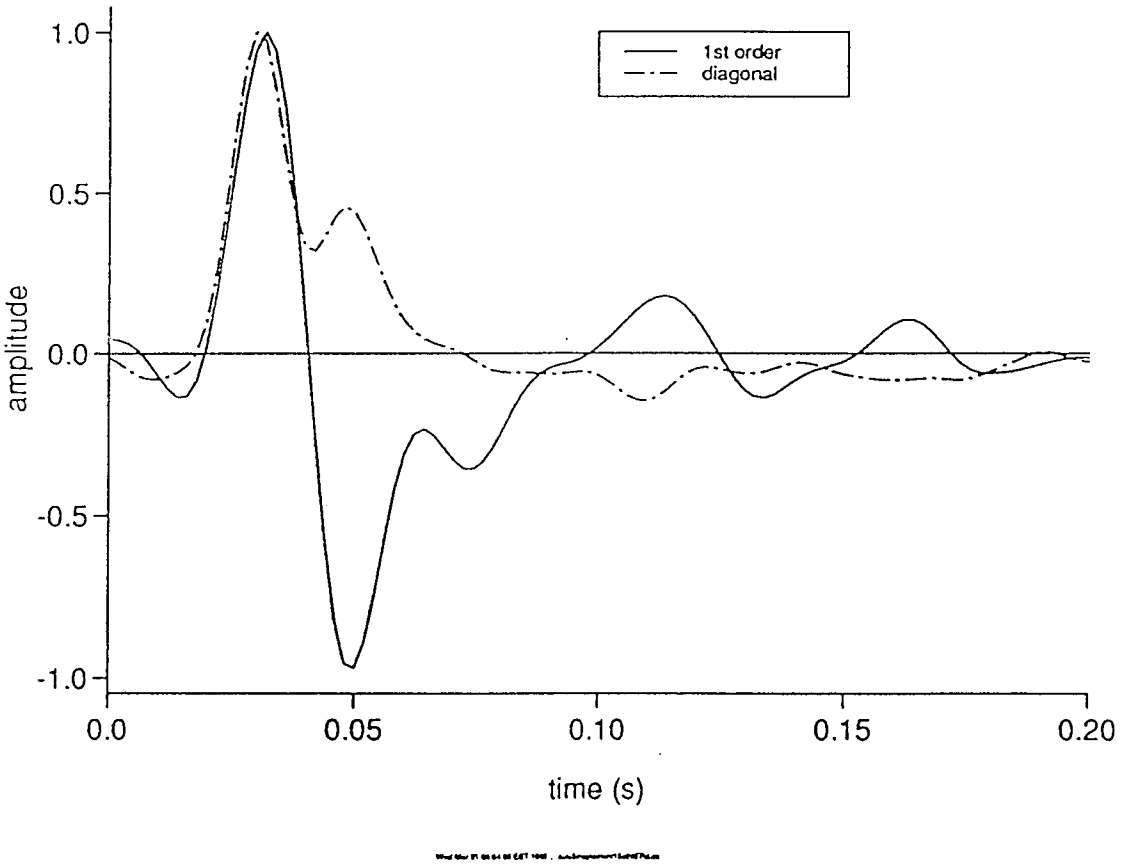
1st order
diagonal
1.0
0.5
0.0
-0.5
-1.0
amplitude
0.0
0.05
0.10
0.15
0.20
time (s)

FIG. 33 C)

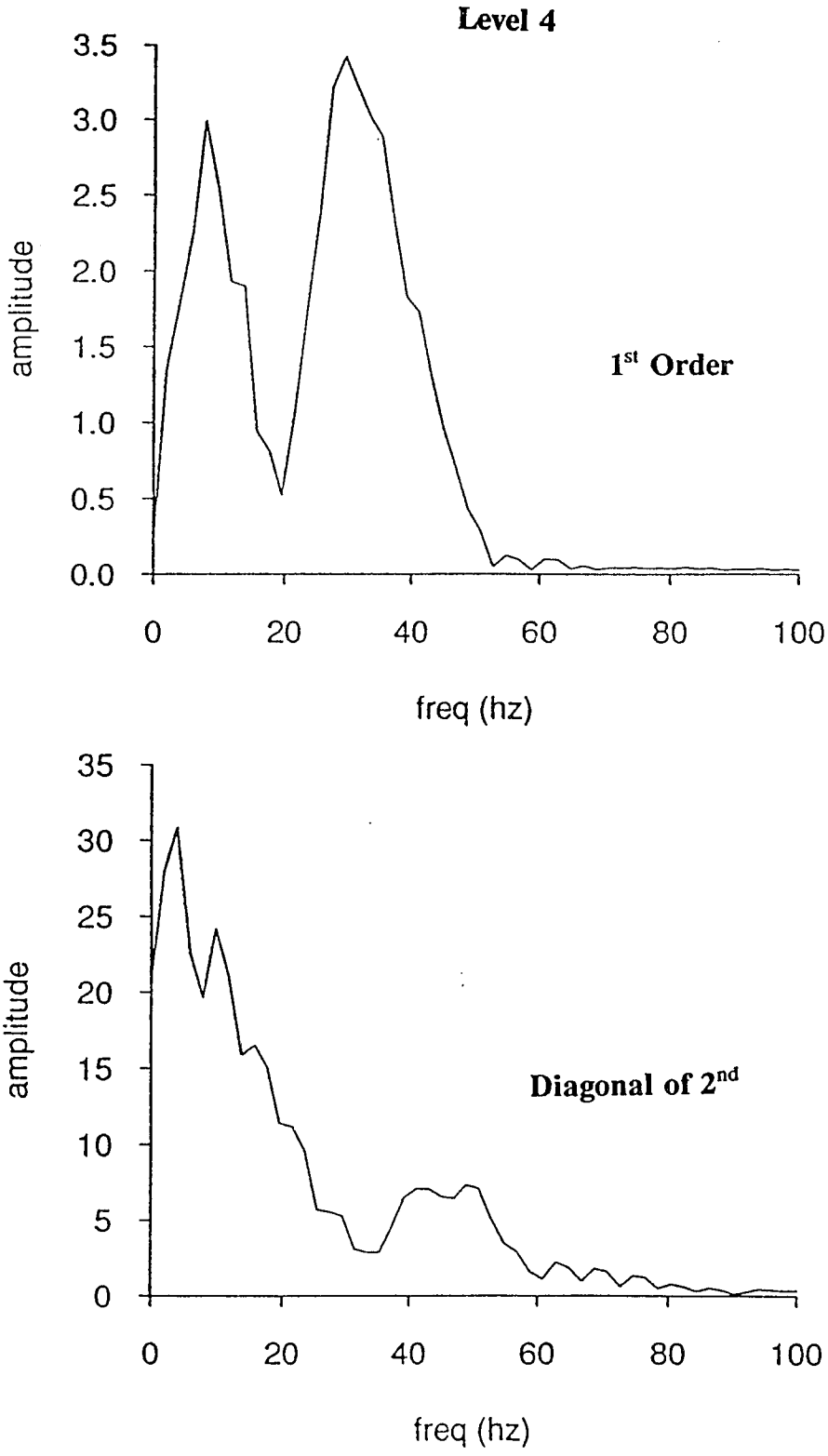
Level 4
3.5
3.0
2.5
2.0
1.5
1.0
0.5
0.0
amplitude
1st Order
0
20
40
60
80
100
freq (hz)
35
30
25
20
15
10
5
0
amplitude
Diagonal of 2nd
0
20
40
60
80
100
freq (hz)

FIG. 33 D)

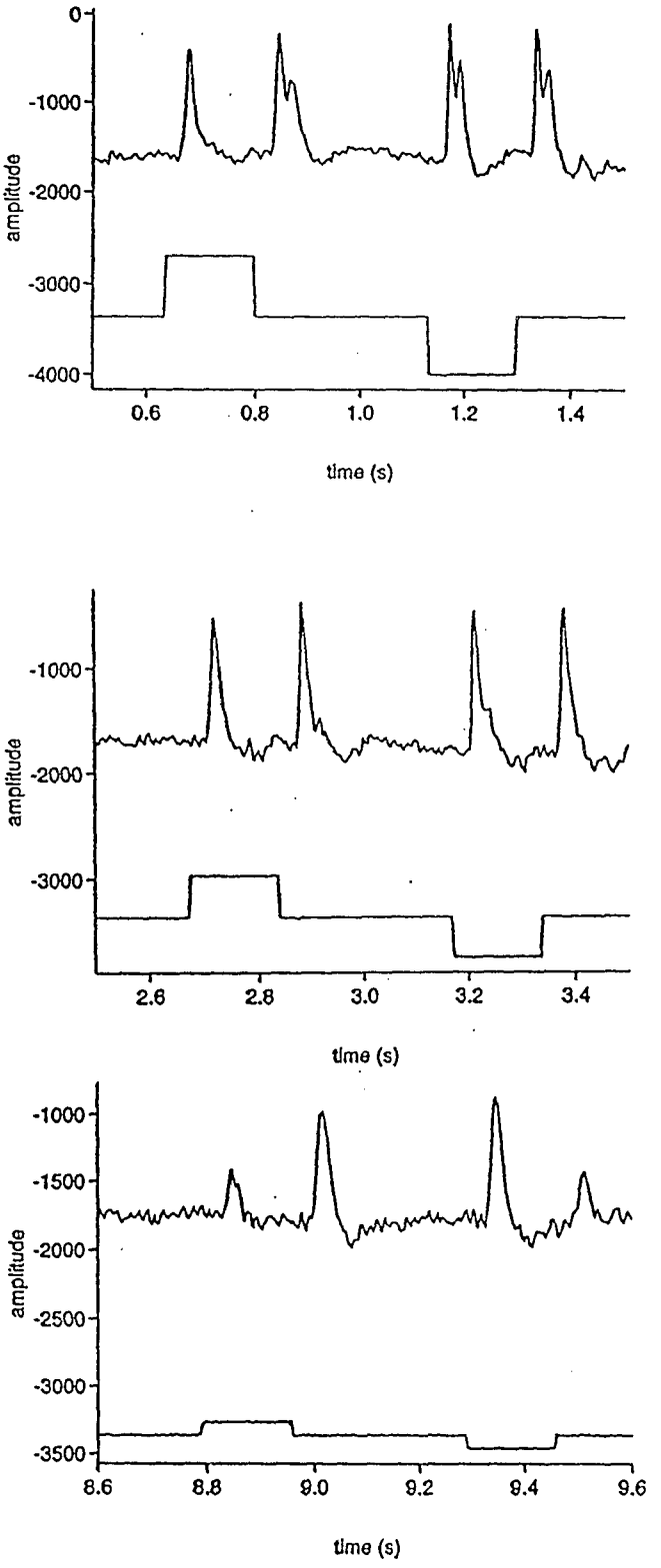
0
-1000
-2000
-3000
-4000
amplitude
0.6
0.8
1.0
1.2
1.4
time (s)
-1000
-2000
-3000
amplitude
2.6
2.8
3.0
3.2
3.4
time (s)
-1000
-1500
-2000
-2500
-3000
-3500
amplitude
8.6
8.8
9.0
9.2
9.4
9.6
time (s)

FIG. 33 E)

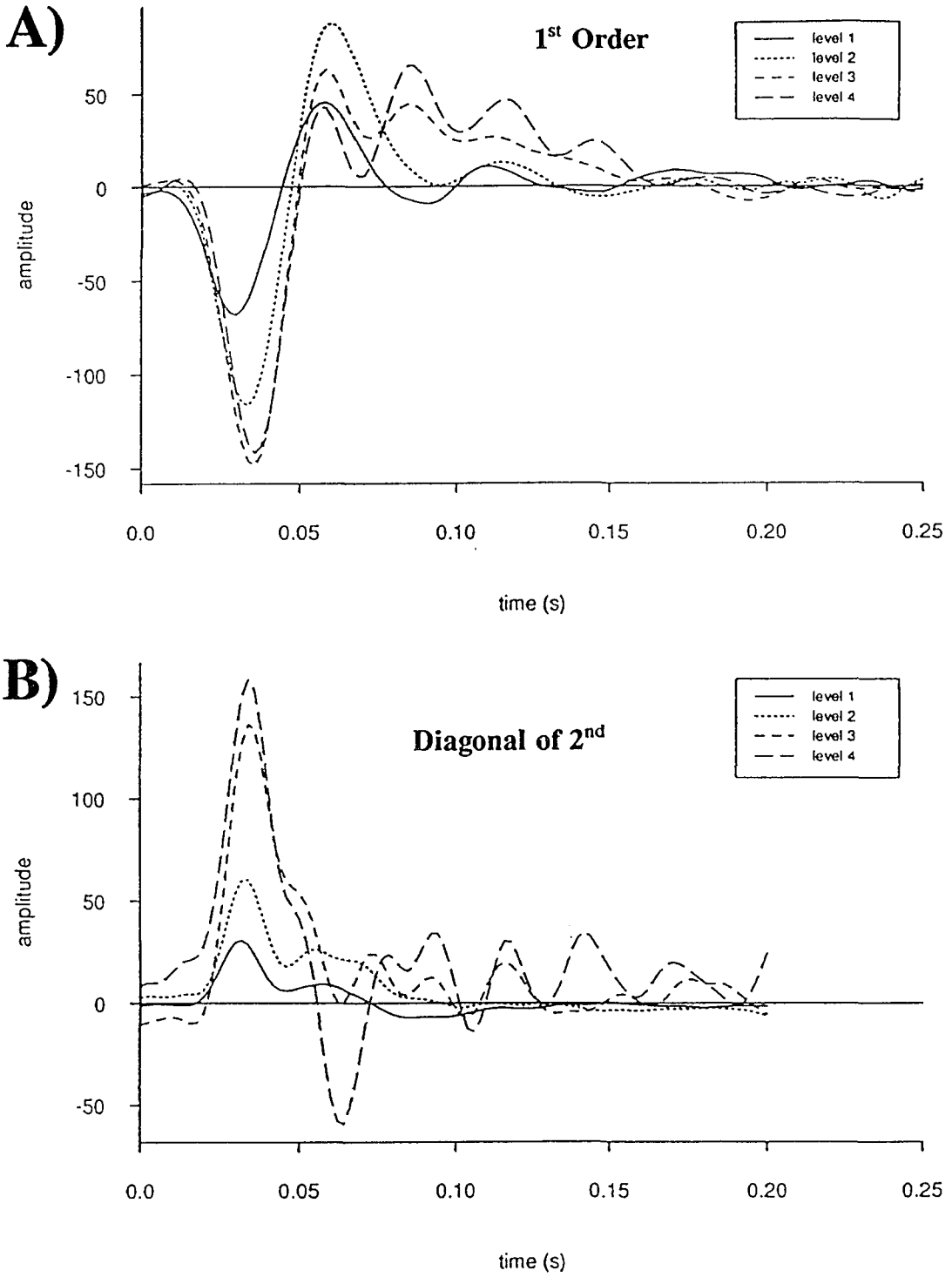
A)
1st Order
level 1
level 2
level 3
level 4
amplitude
50
0
-50
-100
-150
0.0
0.05
0.10
0.15
0.20
0.25
time (s)
B)
Diagonal of 2nd
level 1
level 2
level 3
level 4
amplitude
150
100
50
0
-50
0.0
0.05
0.10
0.15
0.20
0.25
time (s)

FIG. 34

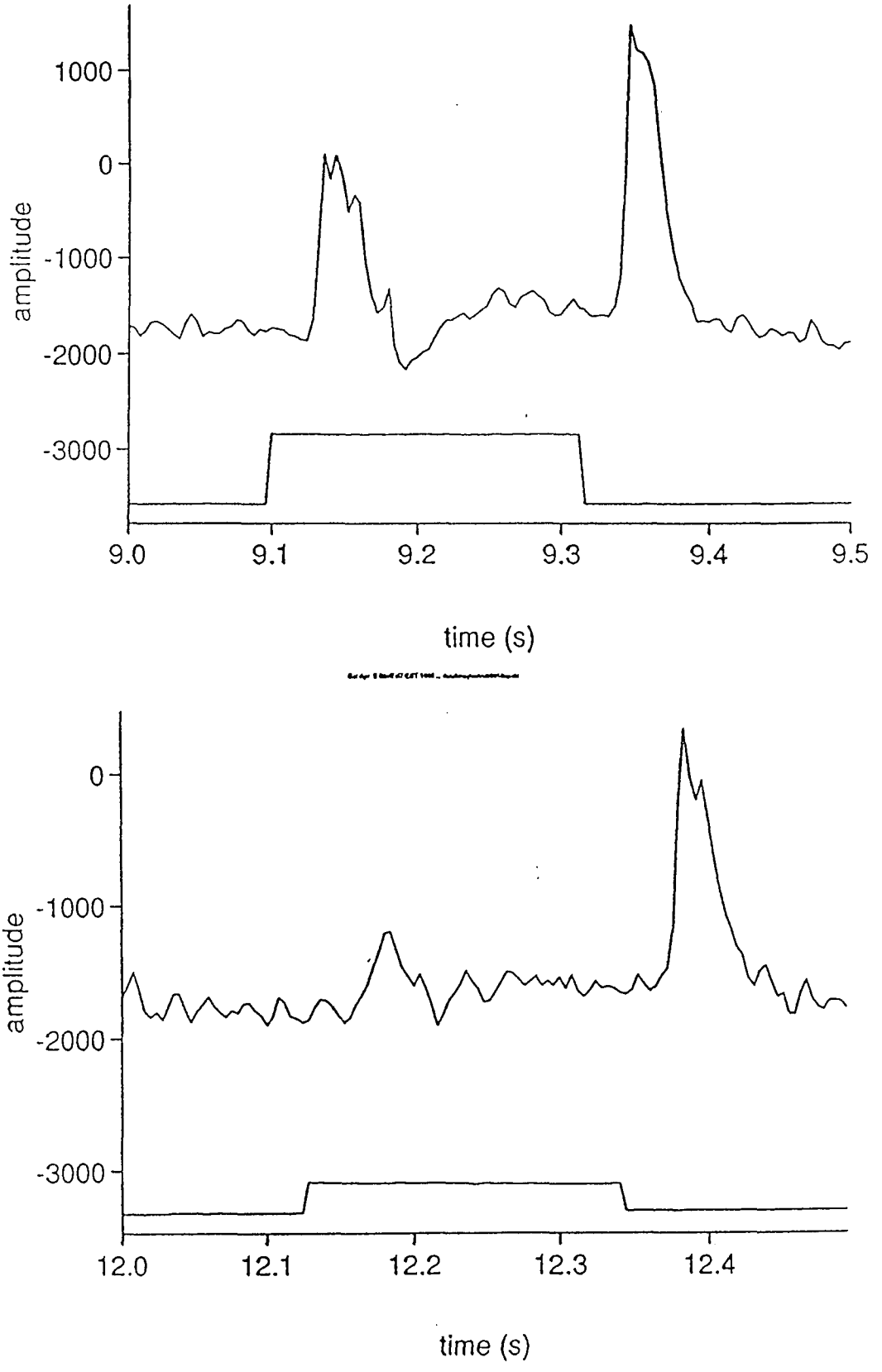
1000
0
-1000
-2000
-3000
amplitude
9.0
9.1
9.2
9.3
9.4
9.5
time (s)
0
-1000
-2000
-3000
amplitude
12.0
12.1
12.2
12.3
12.4
time (s)

FIG. 34 C)

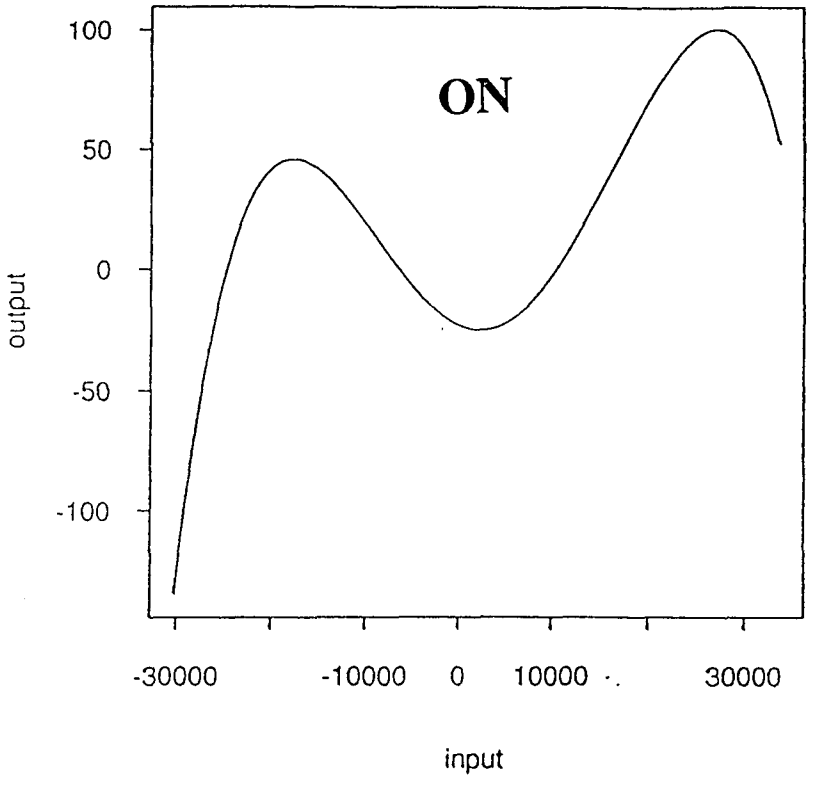
ON
100
50
0
-50
-100
output
-30000
-10000
0
10000
30000
input

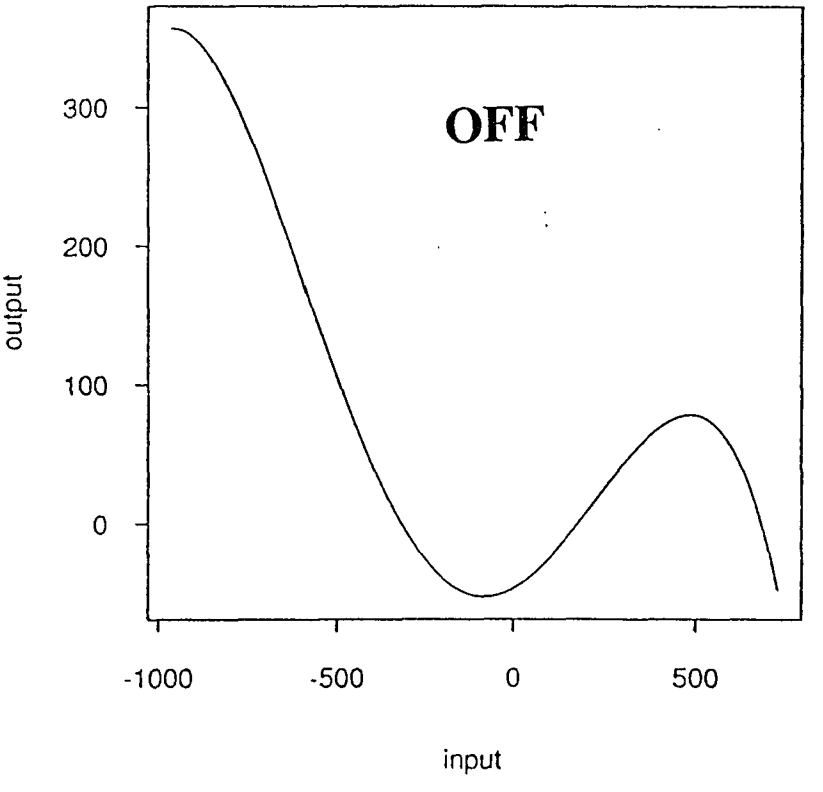
OFF
300
200
100
0
output
-1000
-500
0
500
input

FIG. 34 D-i)

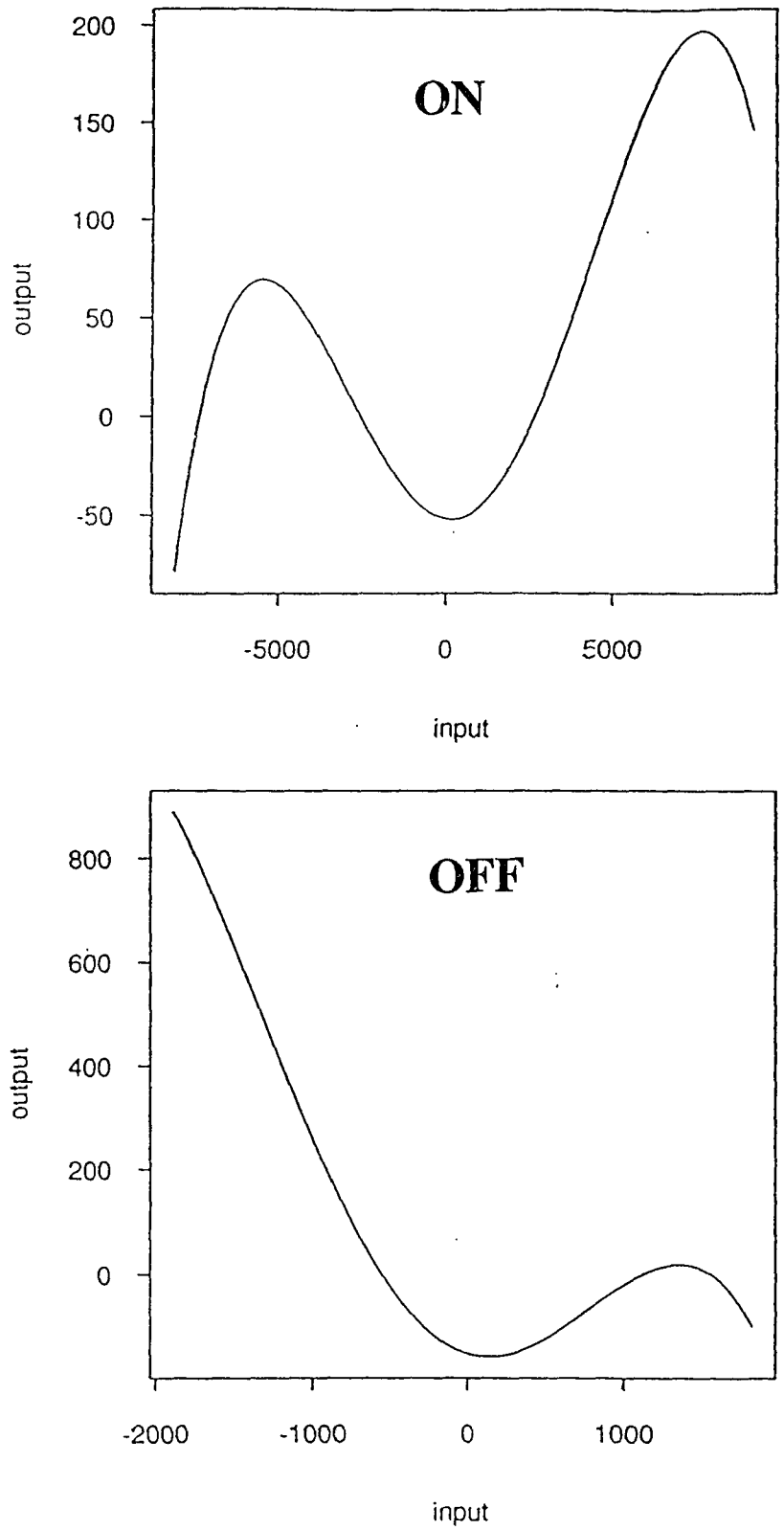
ON
200
150
100
50
0
-50
output
-5000
0
5000
input
OFF
800
600
400
200
0
output
-2000
-1000
0
1000
input

FIG. 34 D-ii)

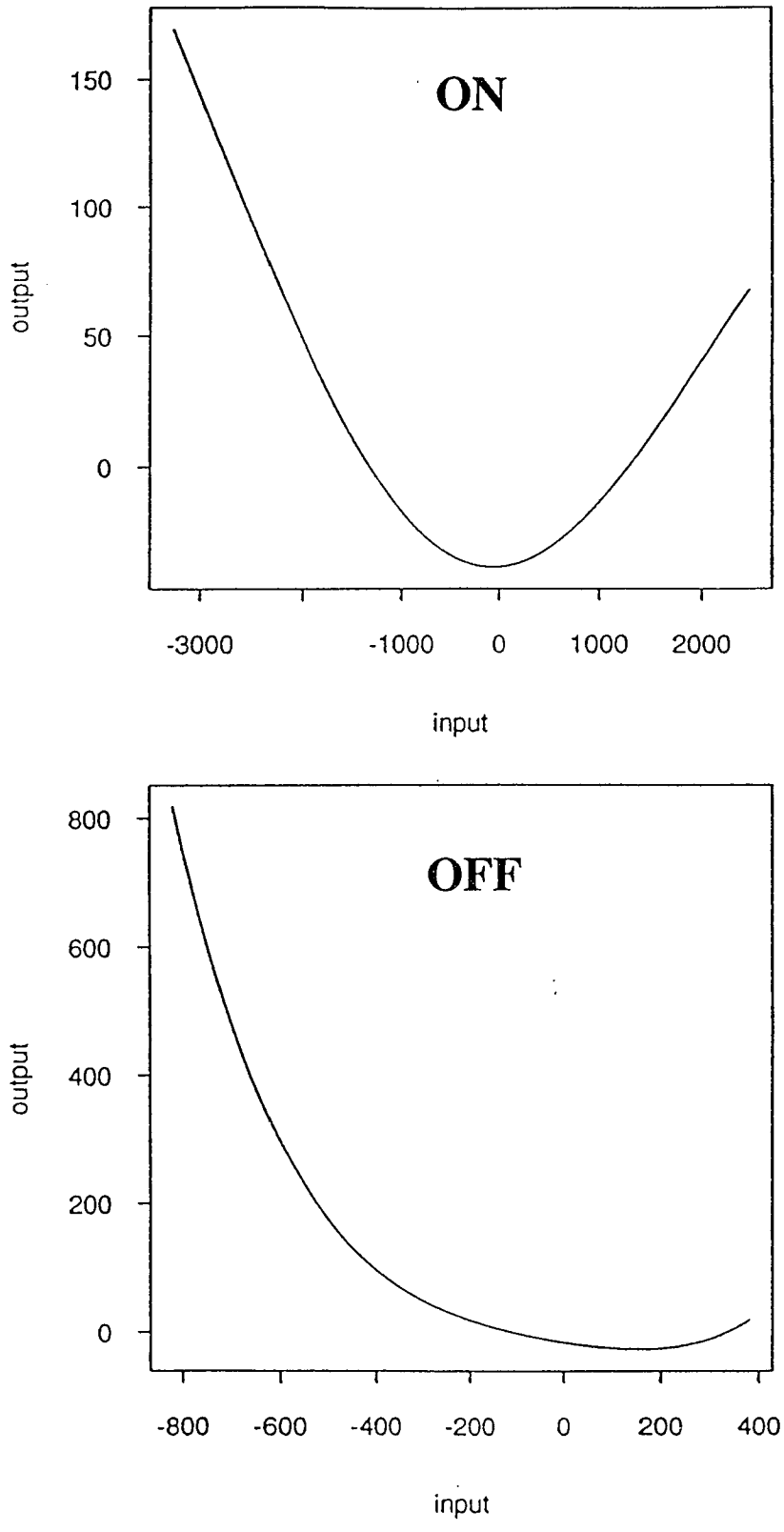
ON
150
100
50
0
output
-3000
-1000
0
1000
2000
input
OFF
800
600
400
200
0
output
-800
-600
-400
-200
0
200
400
input

FIG. 34 D-iii)

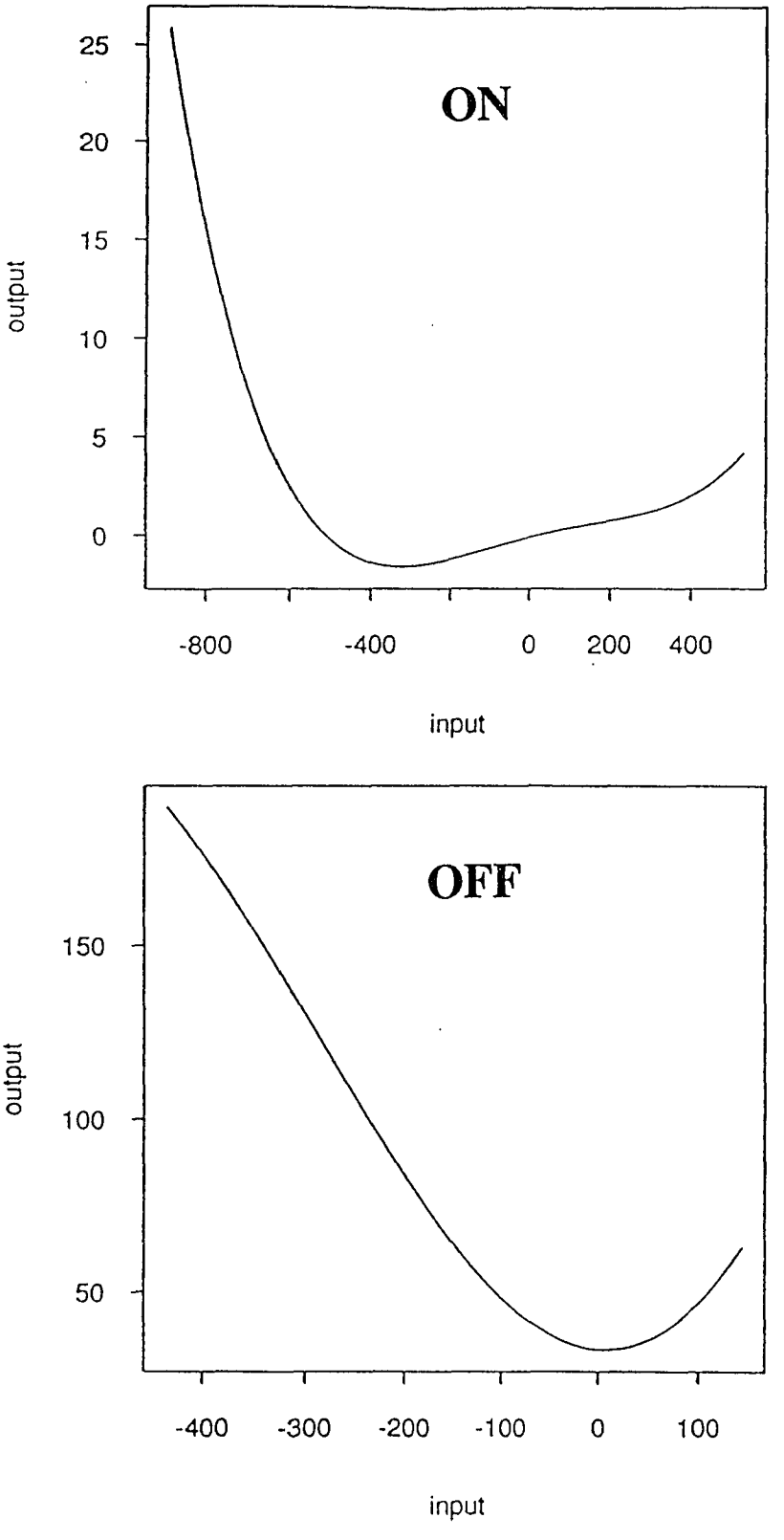
ON
output
25
20
15
10
5
0
-800
-400
0
200
400
input
OFF
output
150
100
50
-400
-300
-200
-100
0
100
input

FIG. 34 D-iv)

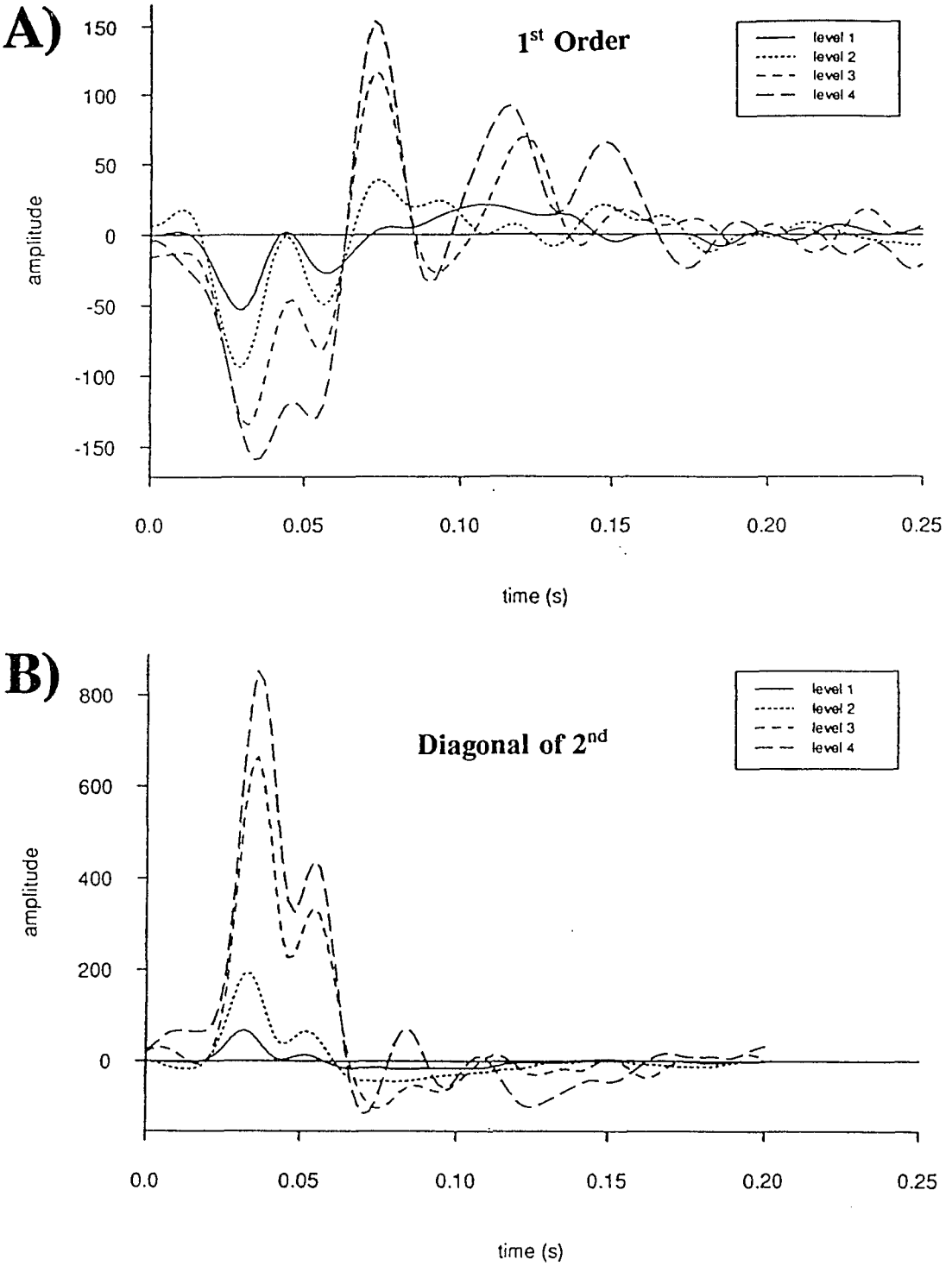

FIG. 35

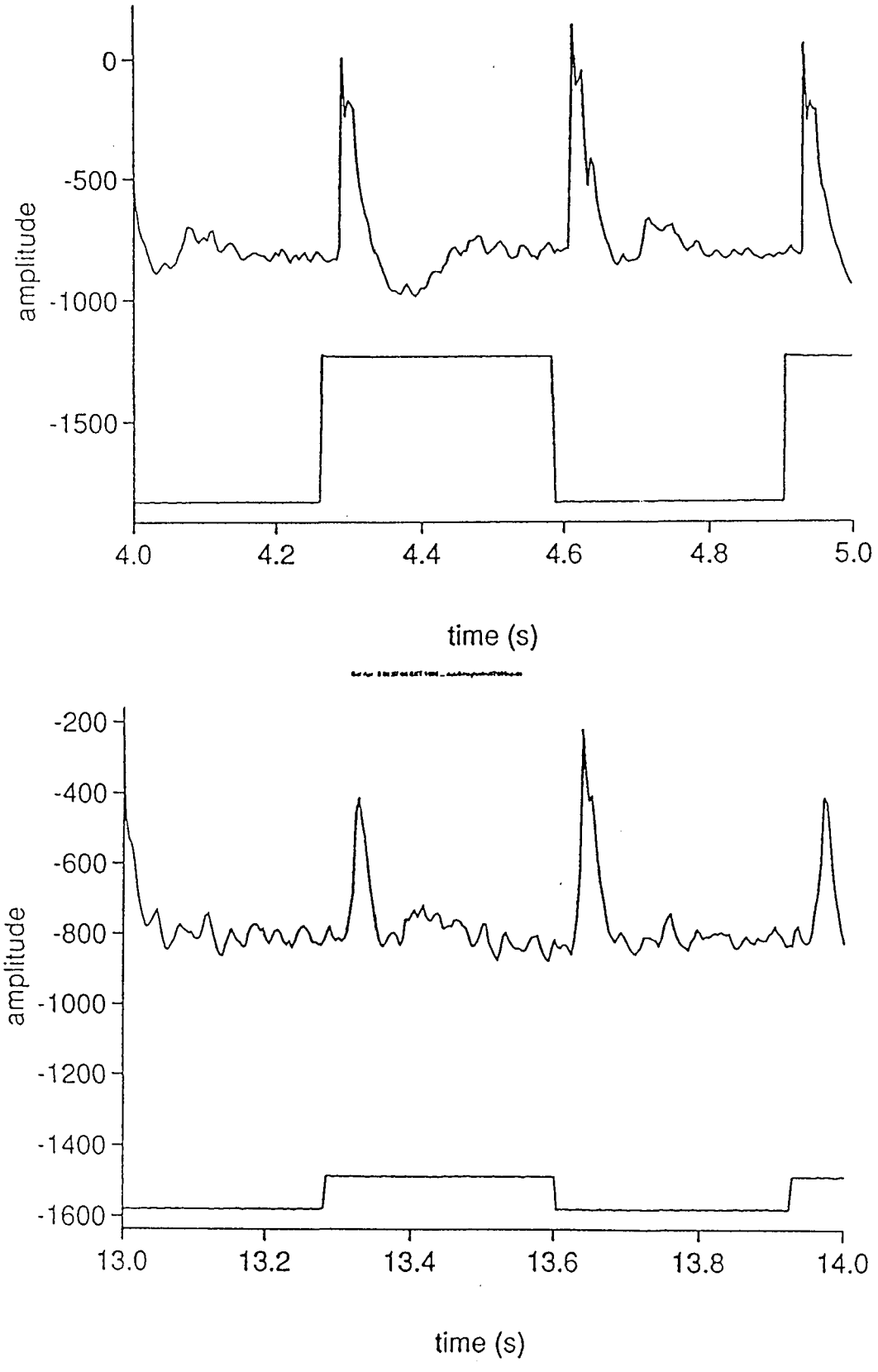
0
-500
-1000
-1500
amplitude
4.0
4.2
4.4
4.6
4.8
5.0
time (s)
-200
-400
-600
-800
-1000
-1200
-1400
-1600
amplitude
13.0
13.2
13.4
13.6
13.8
14.0
time (s)

FIG. 35 C)

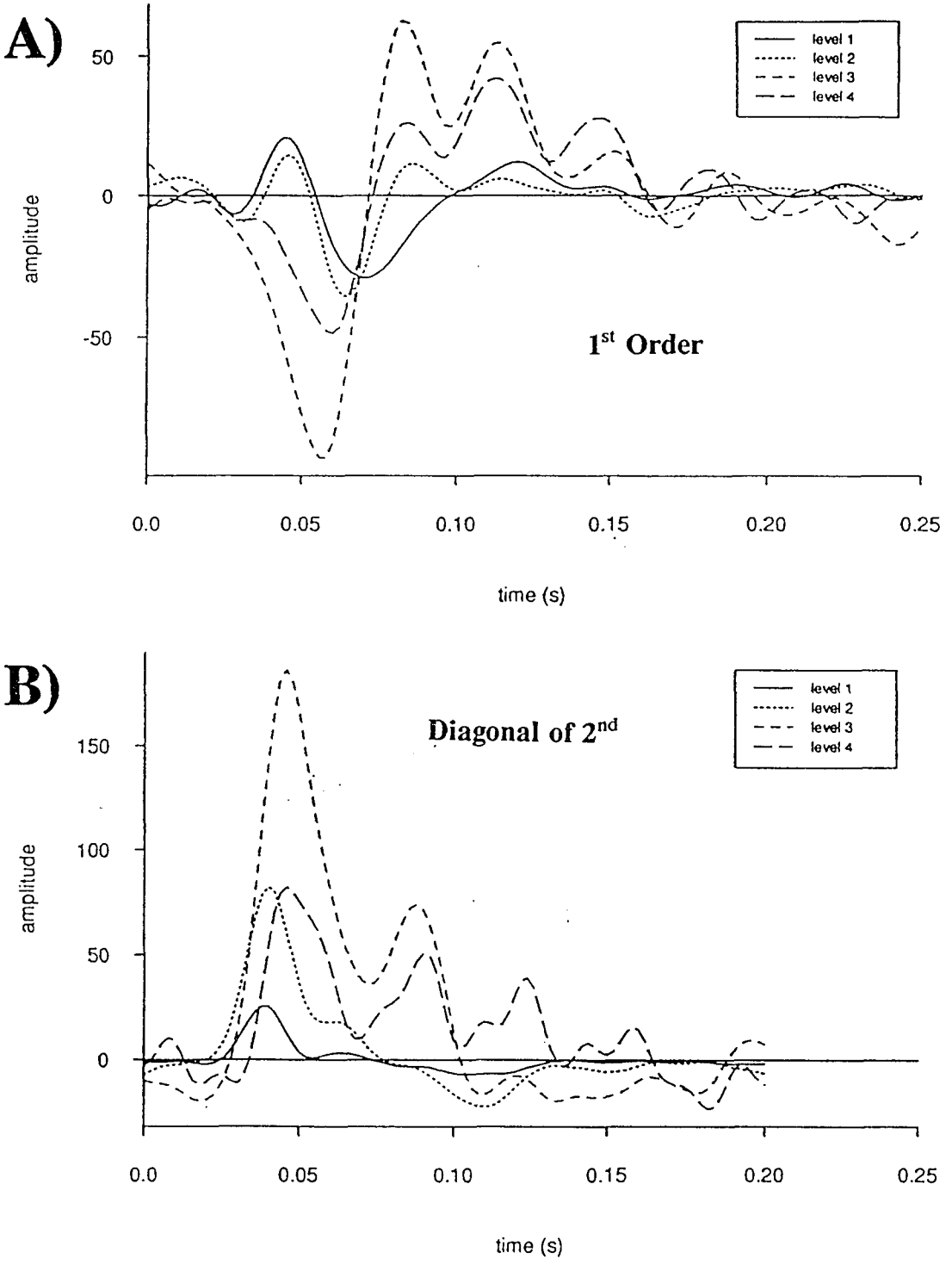

FIG. 36

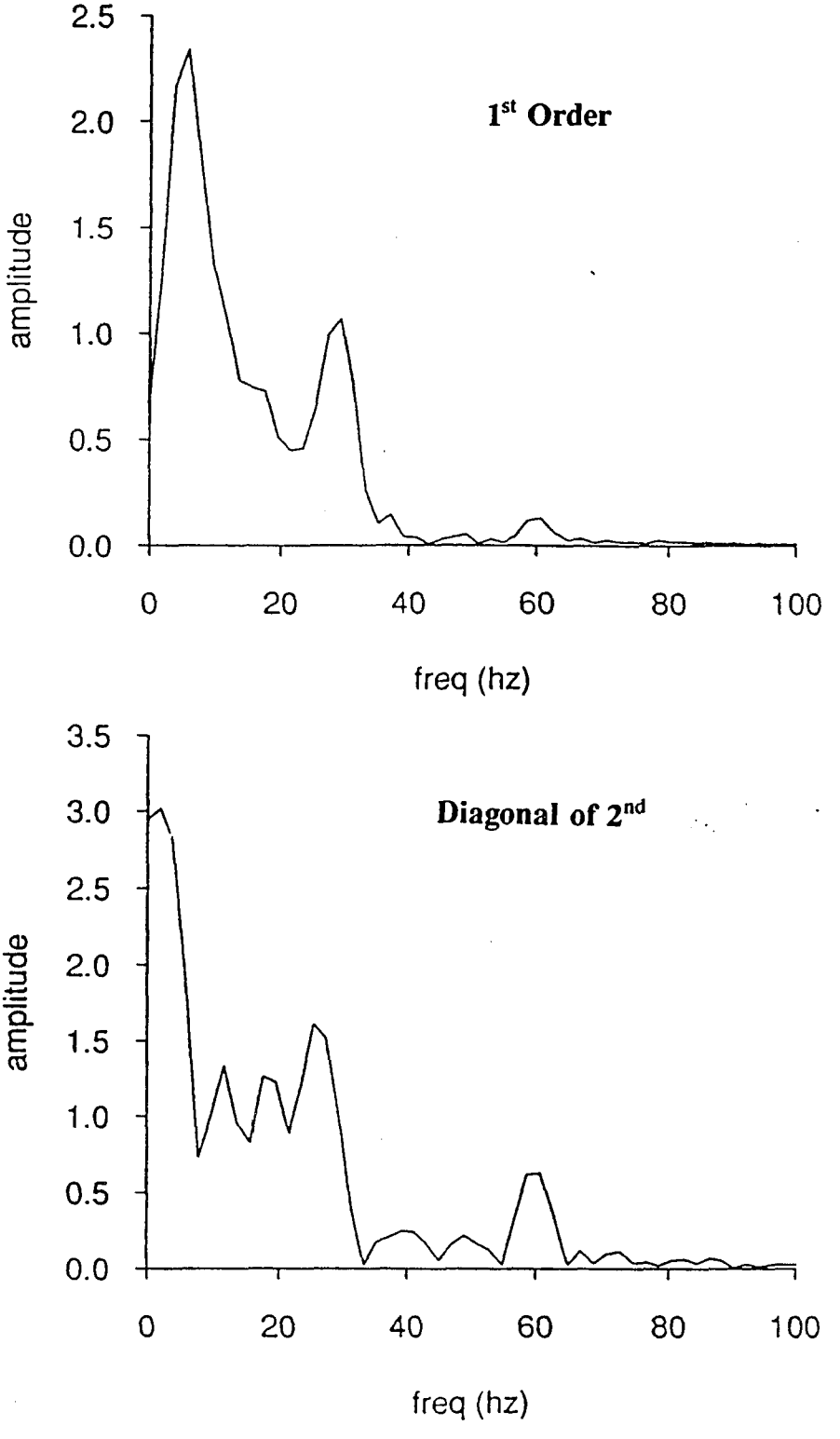
2.5
2.0
1.5
1.0
0.5
0.0
amplitude
1st Order
0
20
40
60
80
100
freq (hz)
3.5
3.0
2.5
2.0
1.5
1.0
0.5
0.0
amplitude
Diagonal of 2nd
0
20
40
60
80
100
freq (hz)

FIG. 36 C)

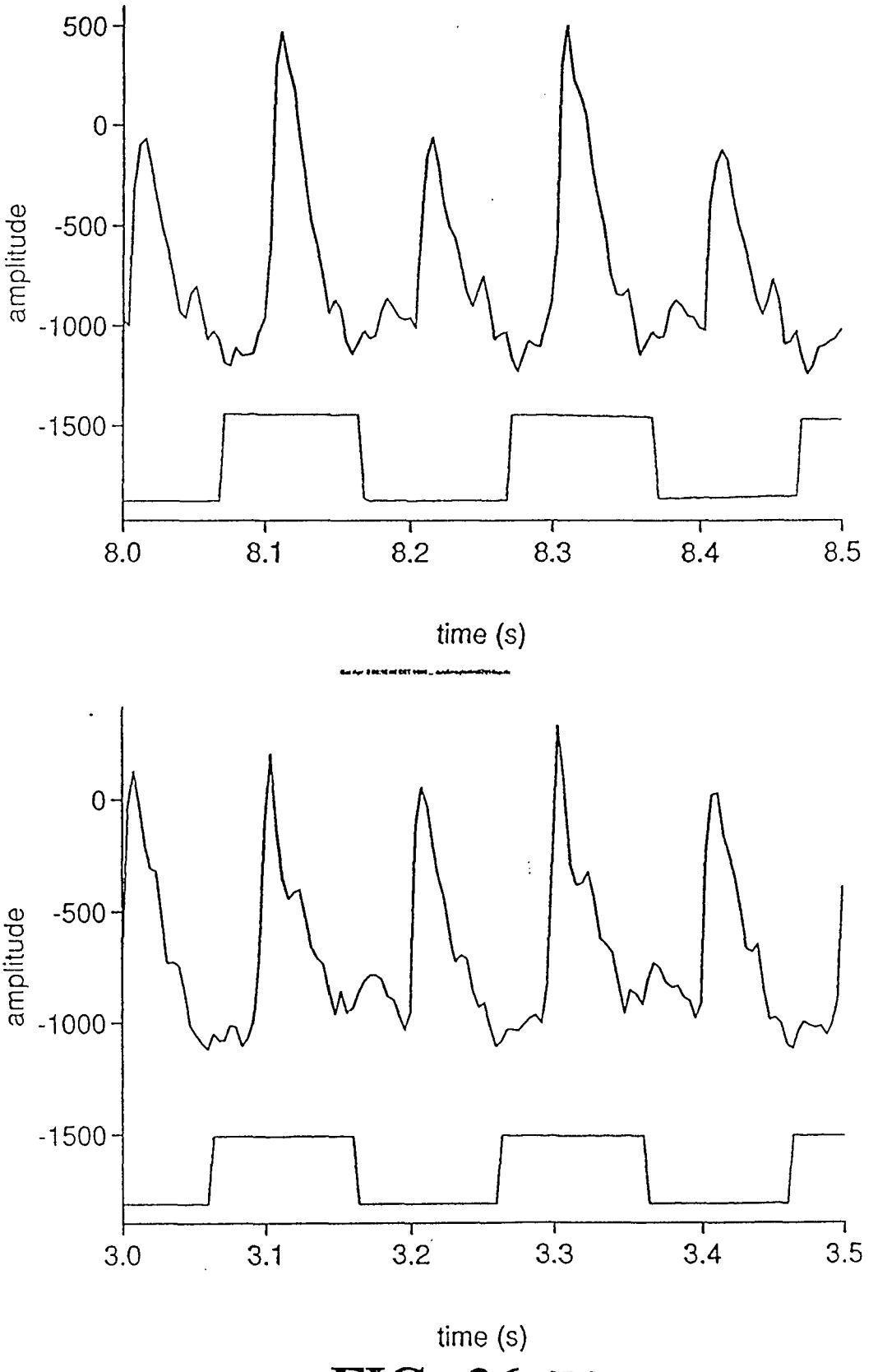
500
0
-500
-1000
-1500
amplitude
8.0
8.1
8.2
8.3
8.4
8.5
time (s)
0
-500
-1000
-1500
amplitude
3.0
3.1
3.2
3.3
3.4
3.5
time (s)

FIG. 36 D)

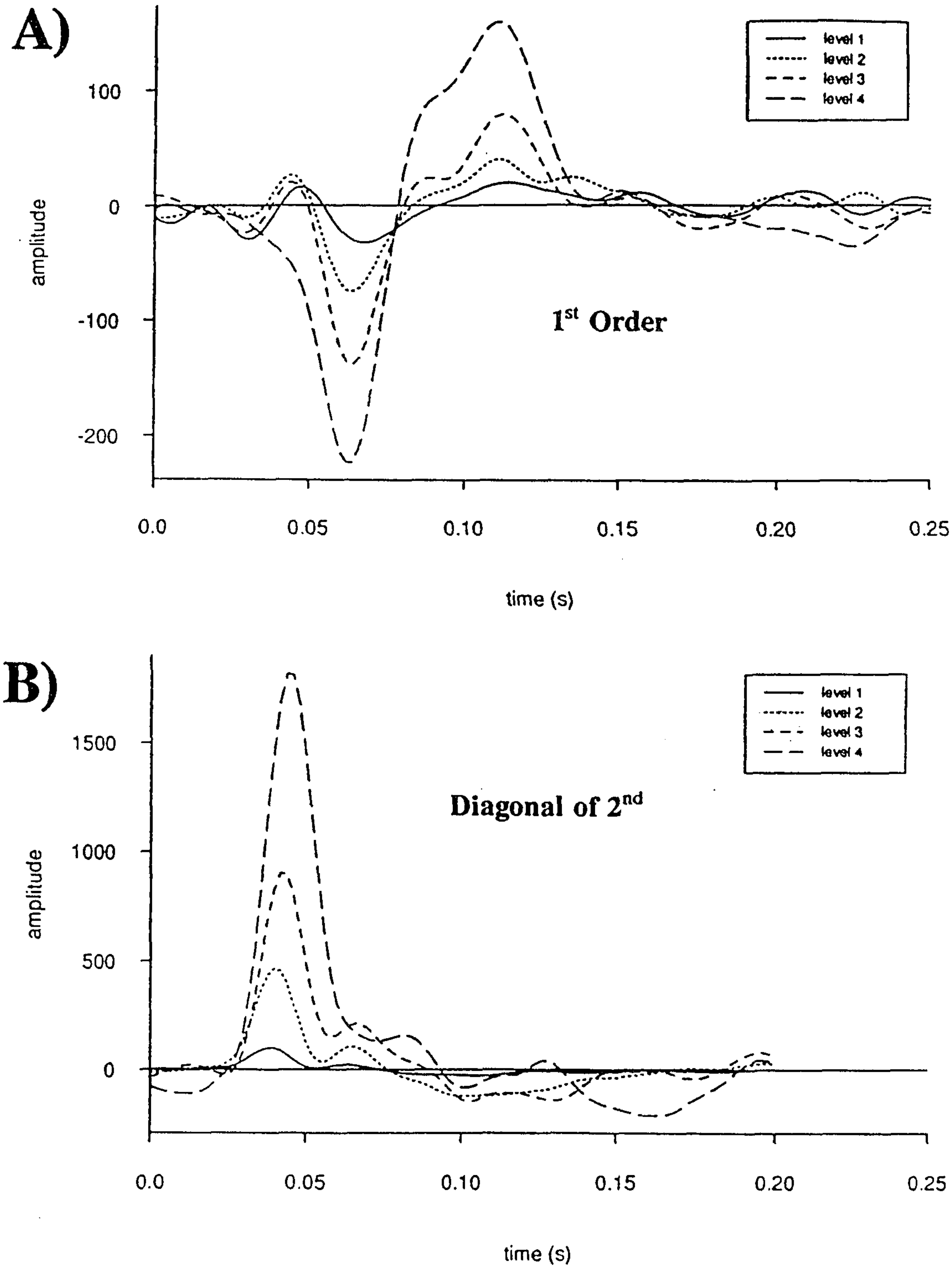
A)
level 1
level 2
level 3
level 4
100
0
-100
-200
amplitude
1st Order
0.0
0.05
0.10
0.15
0.20
0.25
time (s)
B)
level 1
level 2
level 3
level 4
1500
1000
500
0
amplitude
Diagonal of 2nd
0.0
0.05
0.10
0.15
0.20
0.25
time (s)

FIG. 37

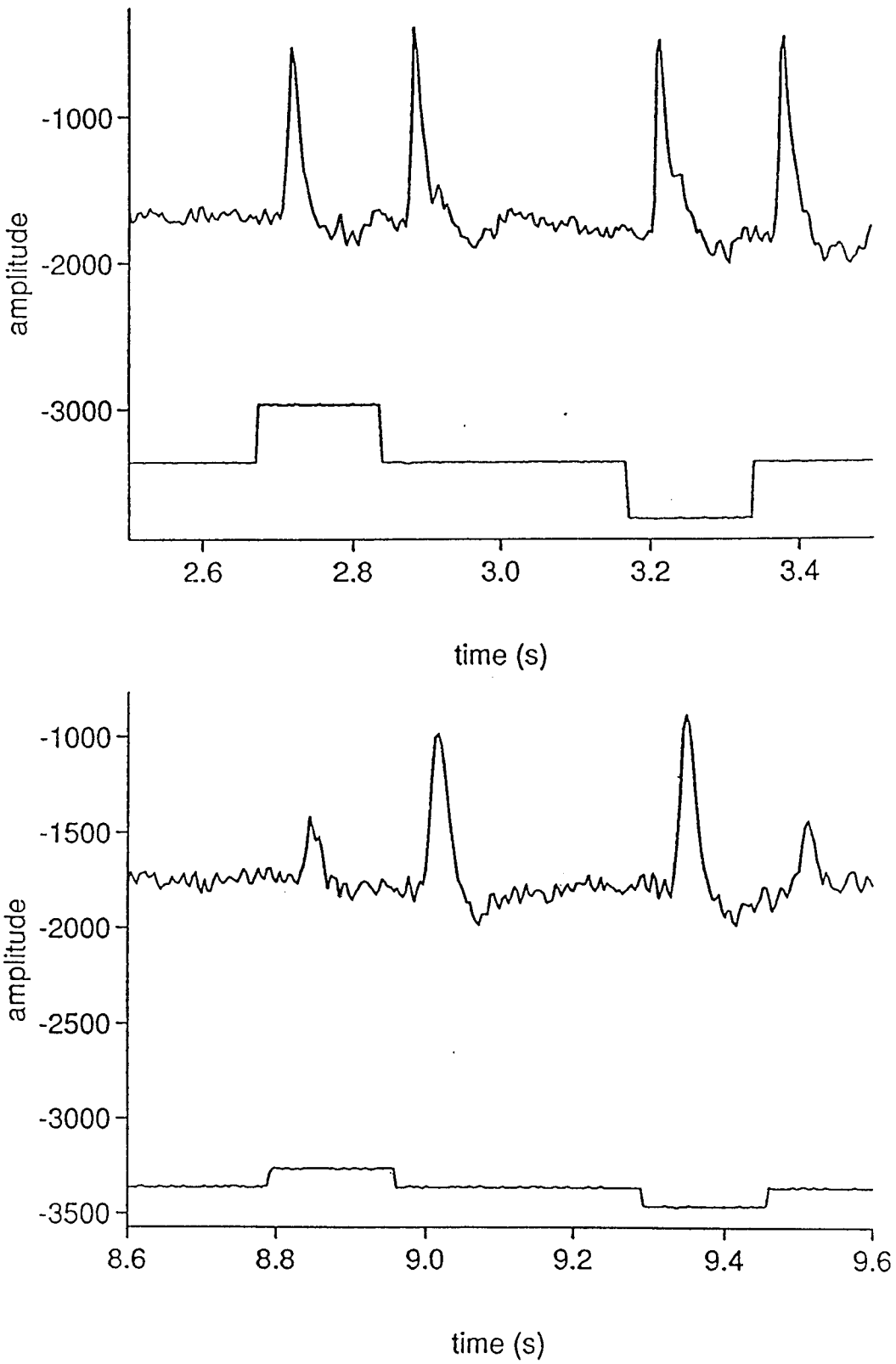
-1000
-2000
-3000
amplitude
2.6
2.8
3.0
3.2
3.4
time (s)
-1000
-1500
-2000
-2500
-3000
-3500
amplitude
8.6
8.8
9.0
9.2
9.4
9.6
time (s)

FIG. 37 C)

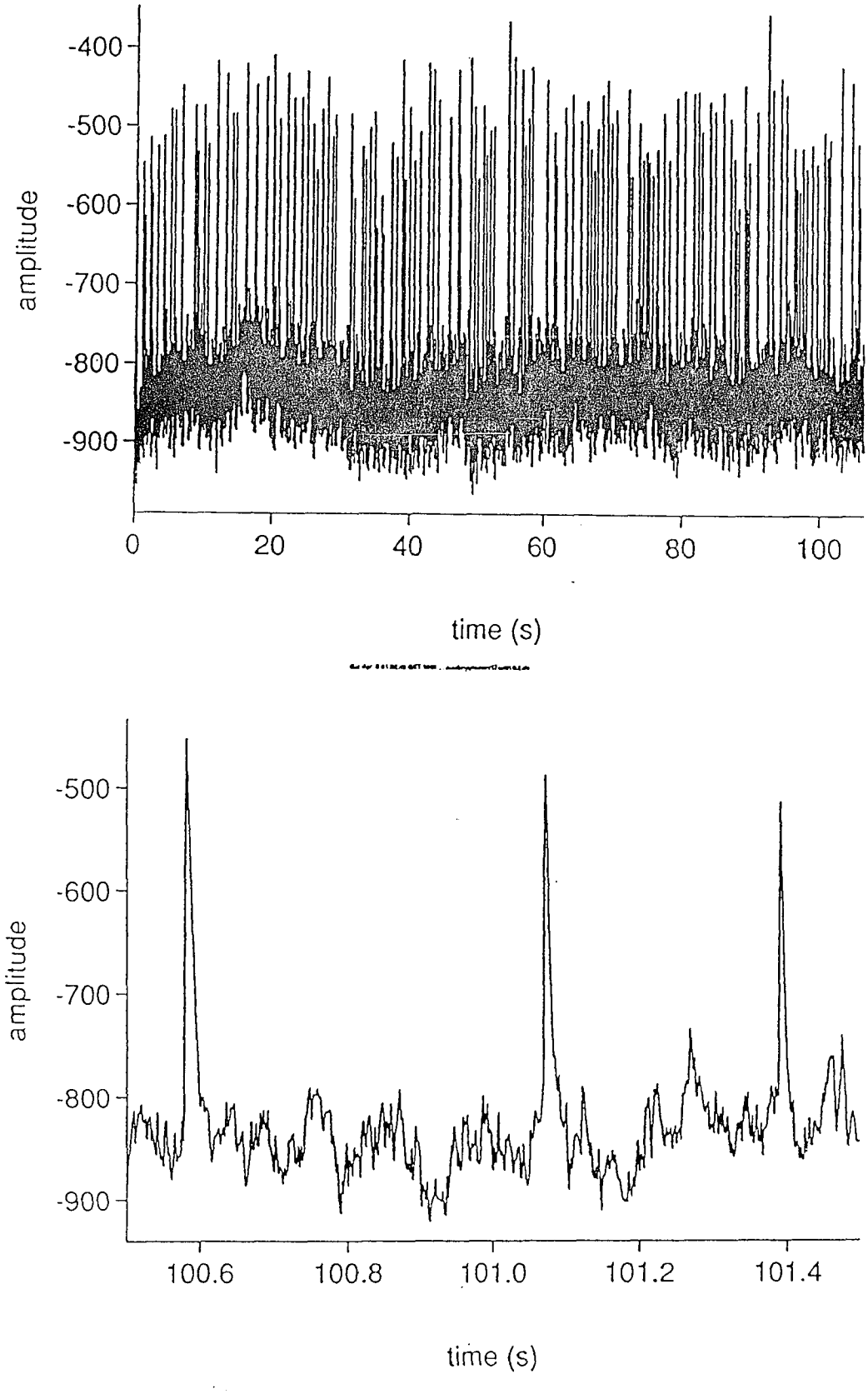
-400
-500
-600
-700
-800
-900
amplitude
0
20
40
60
80
100
time (s)
-500
-600
-700
-800
-900
amplitude
100.6
100.8
101.0
101.2
101.4
time (s)

FIG. 37 D)

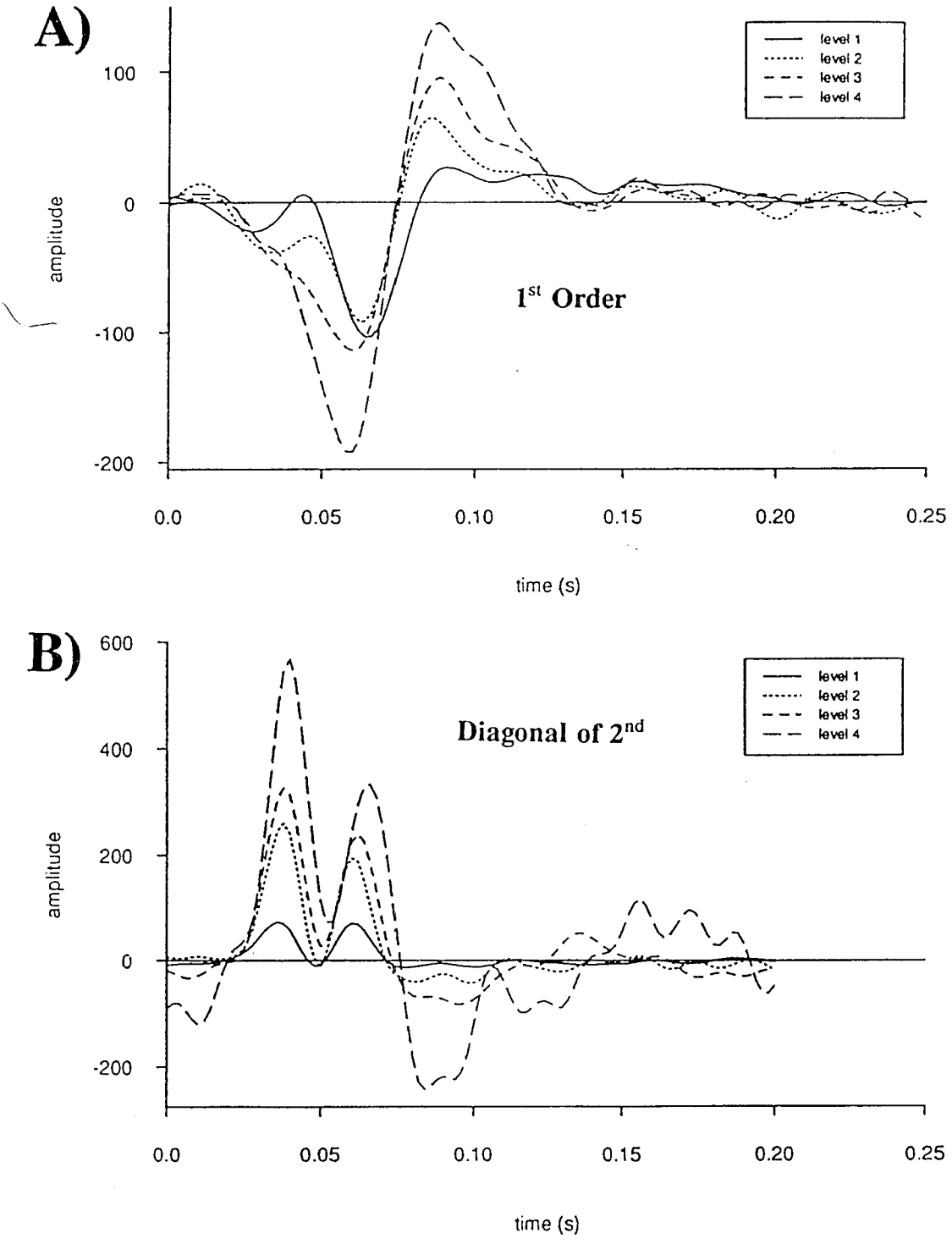
A)
level 1
level 2
level 3
level 4
100
0
-100
-200
amplitude
1st Order
0.0
0.05
0.10
0.15
0.20
0.25
time (s)
B)
600
400
200
0
-200
amplitude
Diagonal of 2nd
level 1
level 2
level 3
level 4
0.0
0.05
0.10
0.15
0.20
0.25
time (s)

FIG. 38

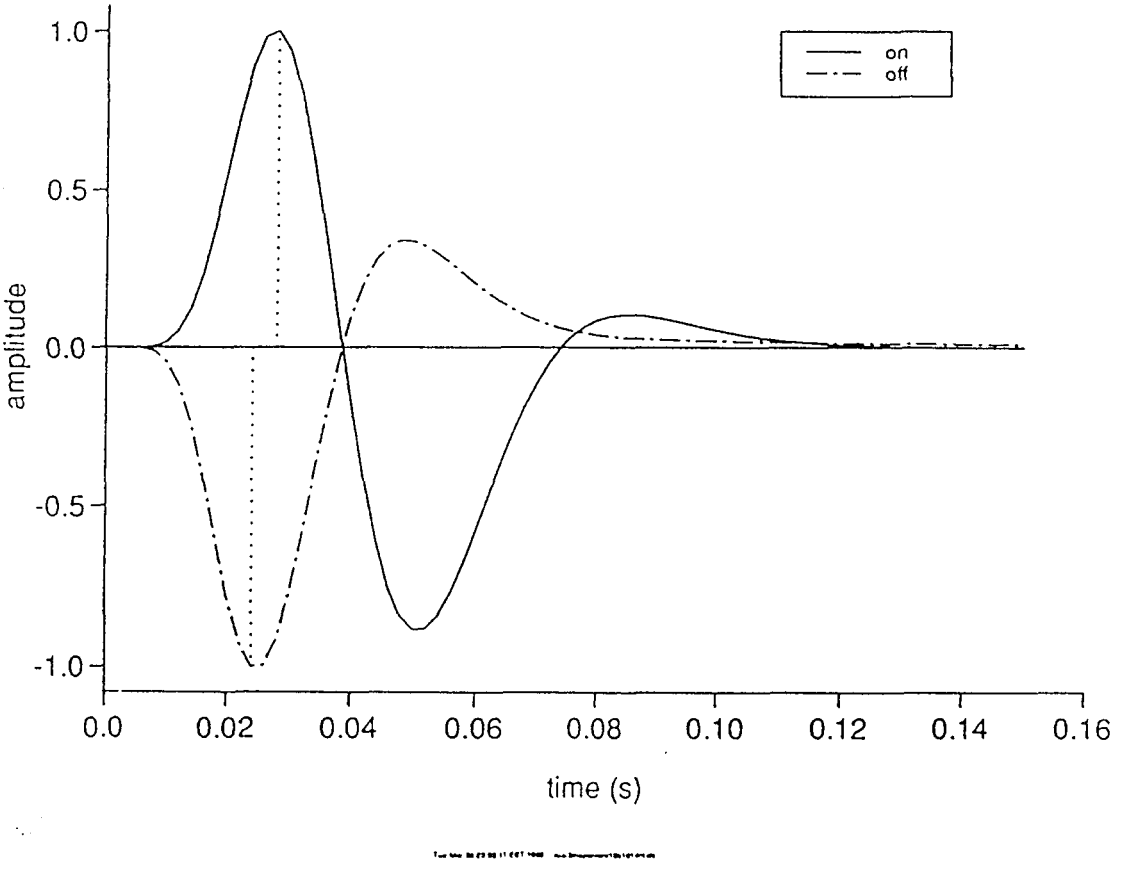
1.0
0.5
0.0
-0.5
-1.0
amplitude
on
off
0.0
0.02
0.04
0.06
0.08
0.10
0.12
0.14
0.16
time (s)

FIG. 38 C)

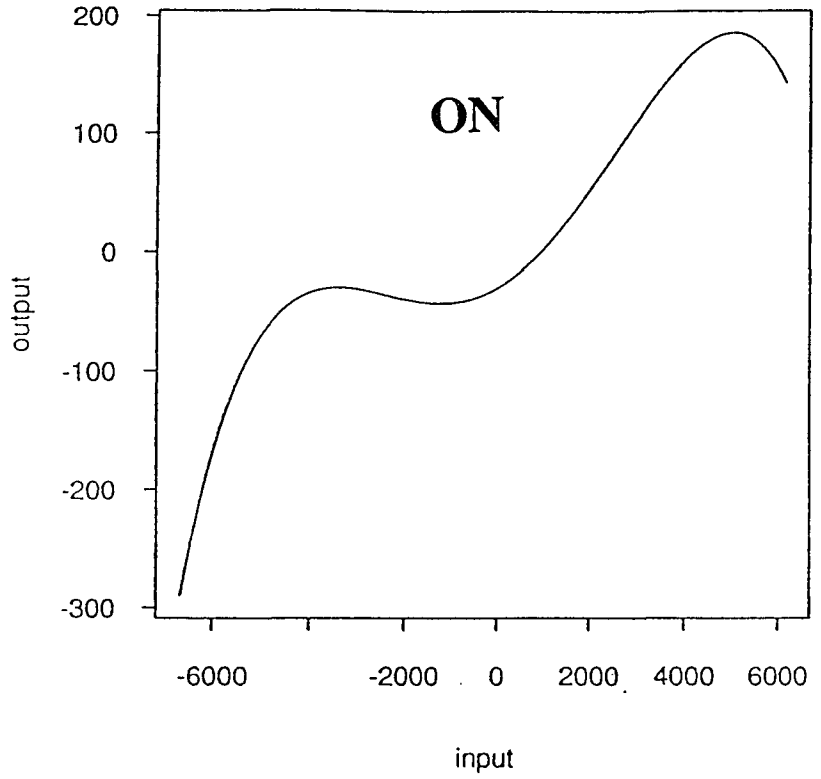
ON
200
100
0
-100
-200
-300
output
-6000
-2000
0
2000
4000
6000
input

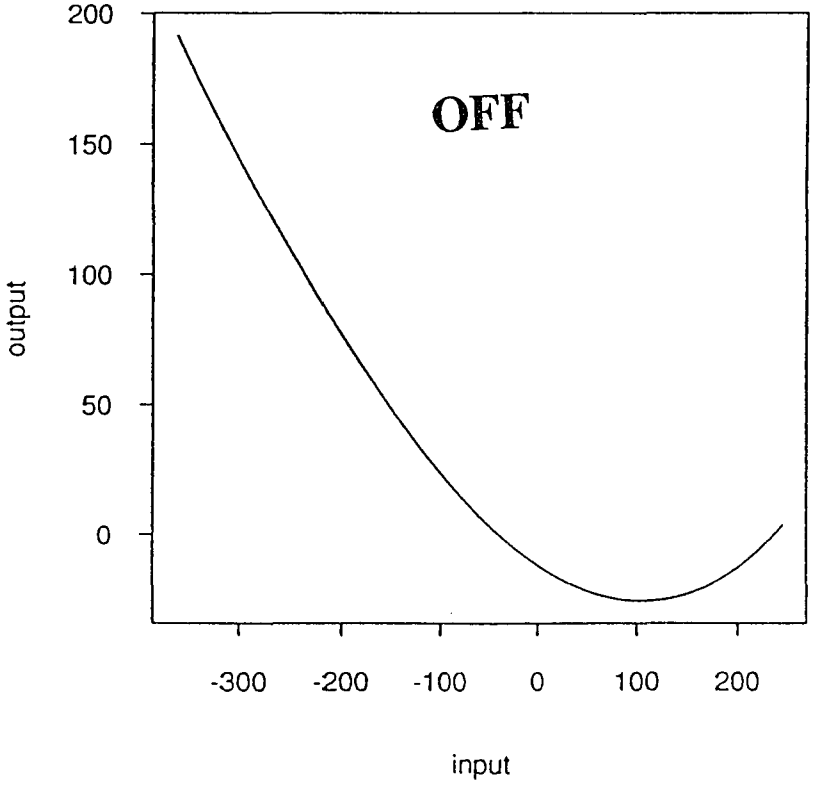
OFF
200
150
100
50
0
output
-300
-200
-100
0
100
200
input

FIG. 38 D)

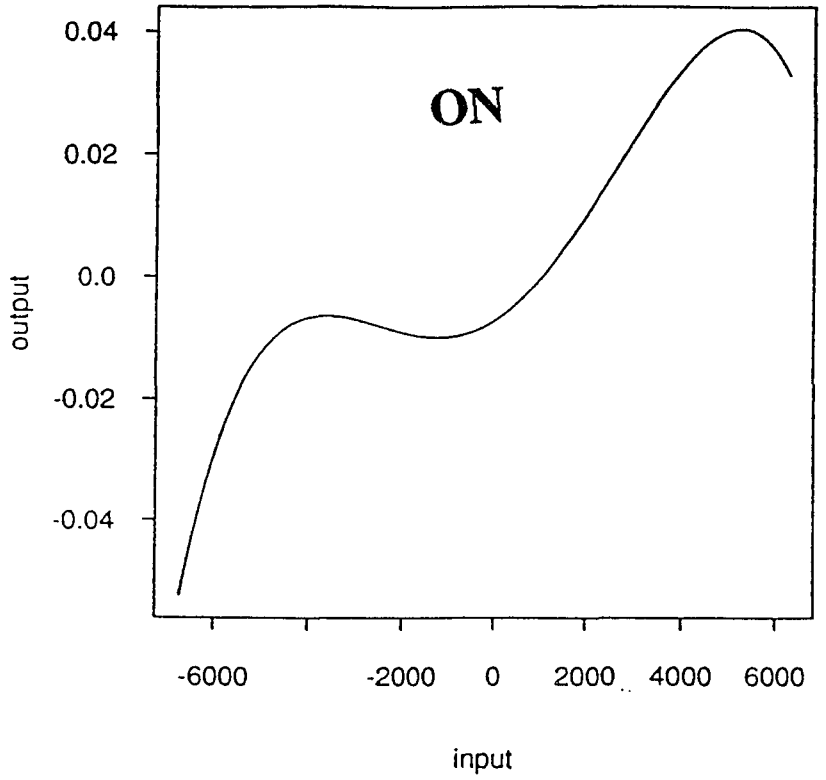
ON
0.04
0.02
0.0
-0.02
-0.04
output
-6000
-2000
0
2000
4000
6000
input

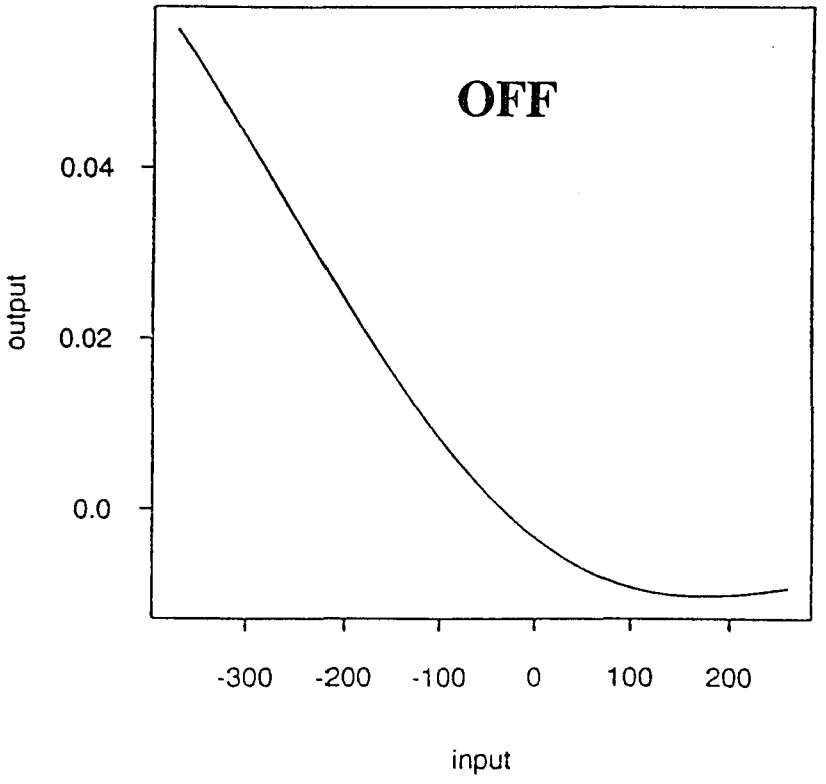
OFF
0.04
0.02
0.0
output
-300
-200
-100
0
100
200
input

FIG. 38 E)

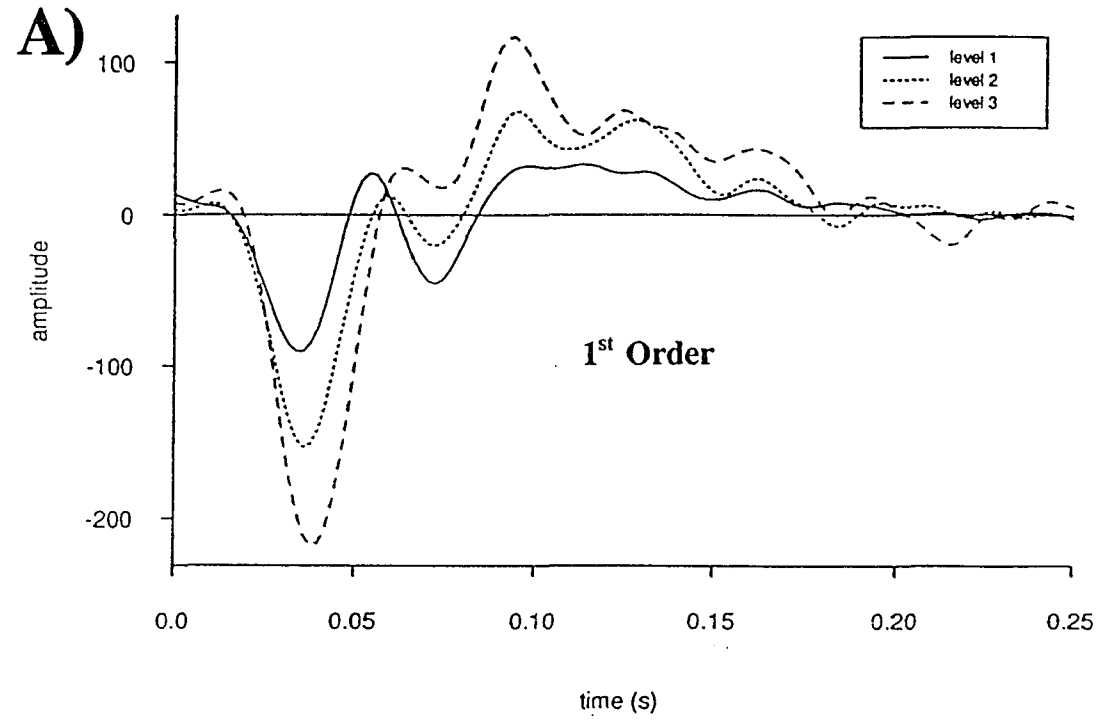

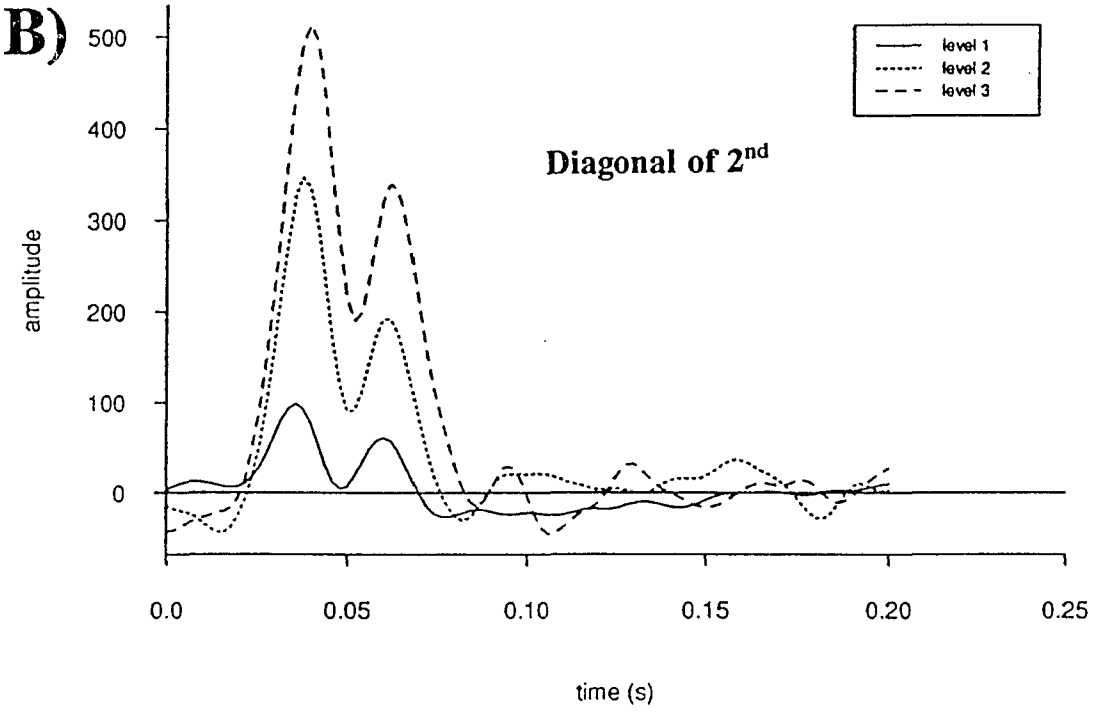

FIG. 39

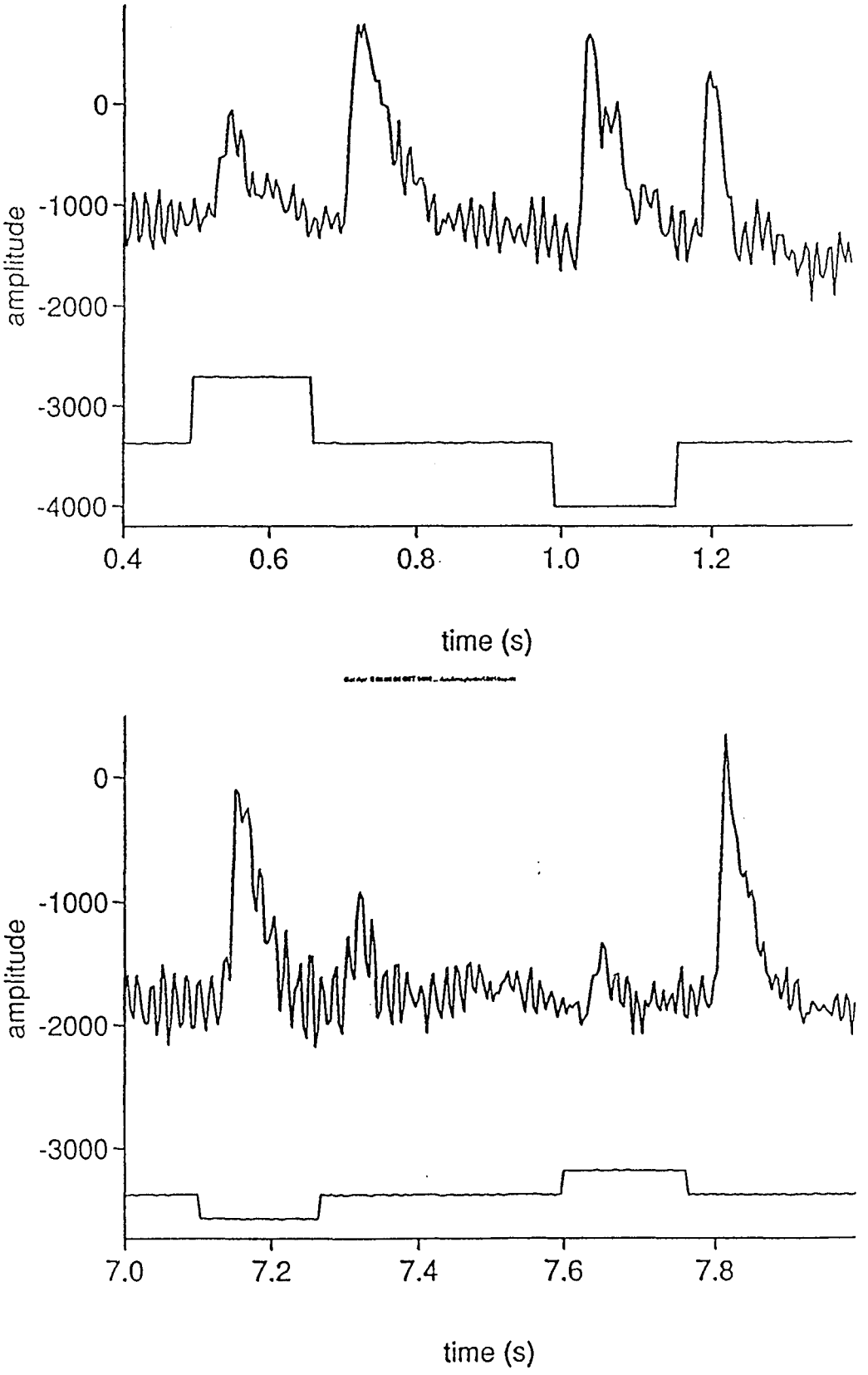
0
-1000
-2000
-3000
-4000
amplitude
0.4
0.6
0.8
1.0
1.2
time (s)
0
-1000
-2000
-3000
amplitude
7.0
7.2
7.4
7.6
7.8
time (s)

FIG. 39 C)

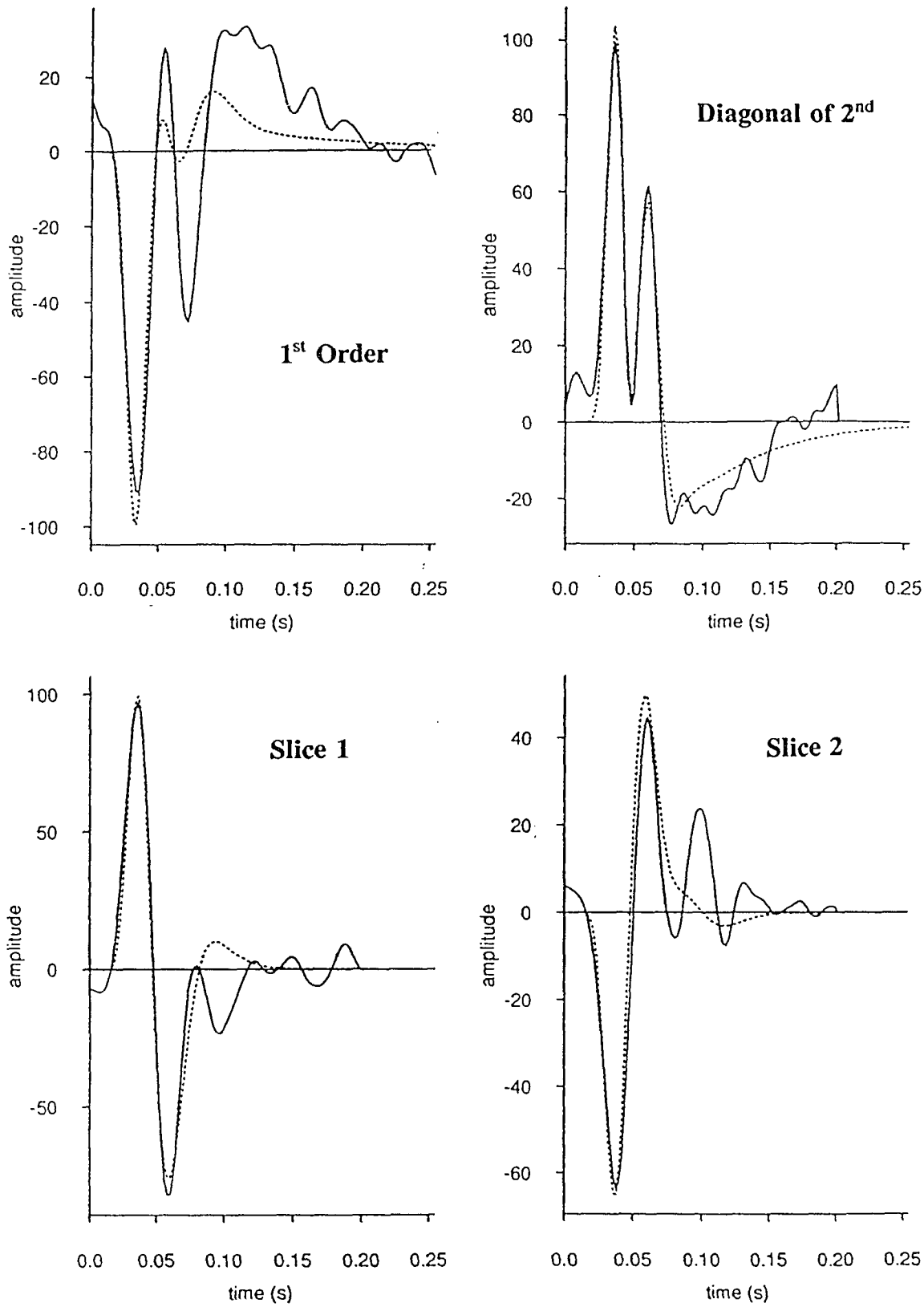
1st Order
amplitude
time (s)
Diagonal of 2nd
amplitude
time (s)
Slice 1
amplitude
time (s)
Slice 2
amplitude
time (s)

FIG. 39 D-i)

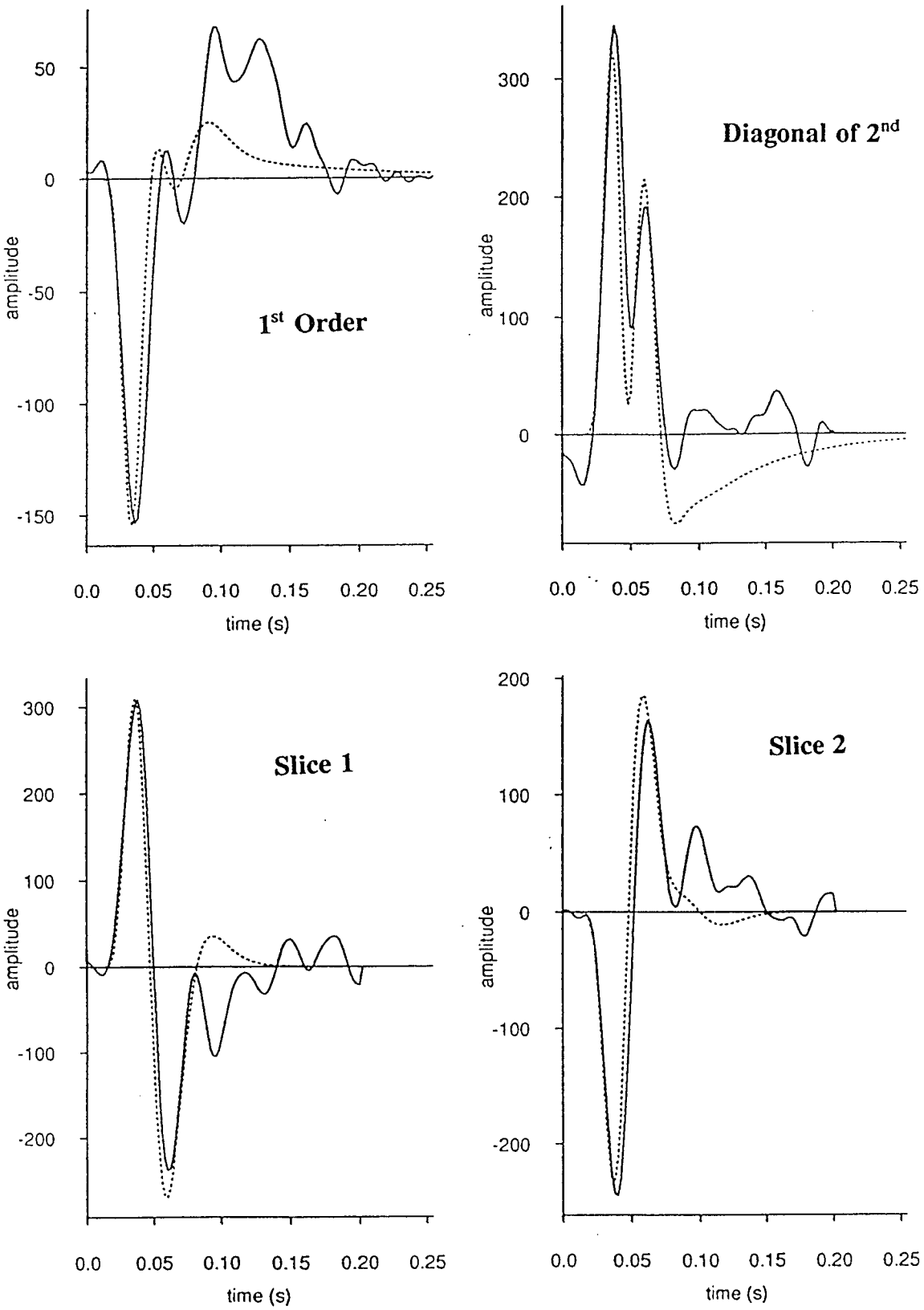
50
0
-50
-100
-150
amplitude
1st Order
0.0
0.05
0.10
0.15
0.20
0.25
time (s)
300
200
100
0
amplitude
Diagonal of 2nd
0.0
0.05
0.10
0.15
0.20
0.25
time (s)
300
200
100
0
-100
-200
amplitude
Slice 1
0.0
0.05
0.10
0.15
0.20
0.25
time (s)
200
100
0
-100
-200
amplitude
Slice 2
0.0
0.05
0.10
0.15
0.20
0.25
time (s)

FIG. 39 D-ii)

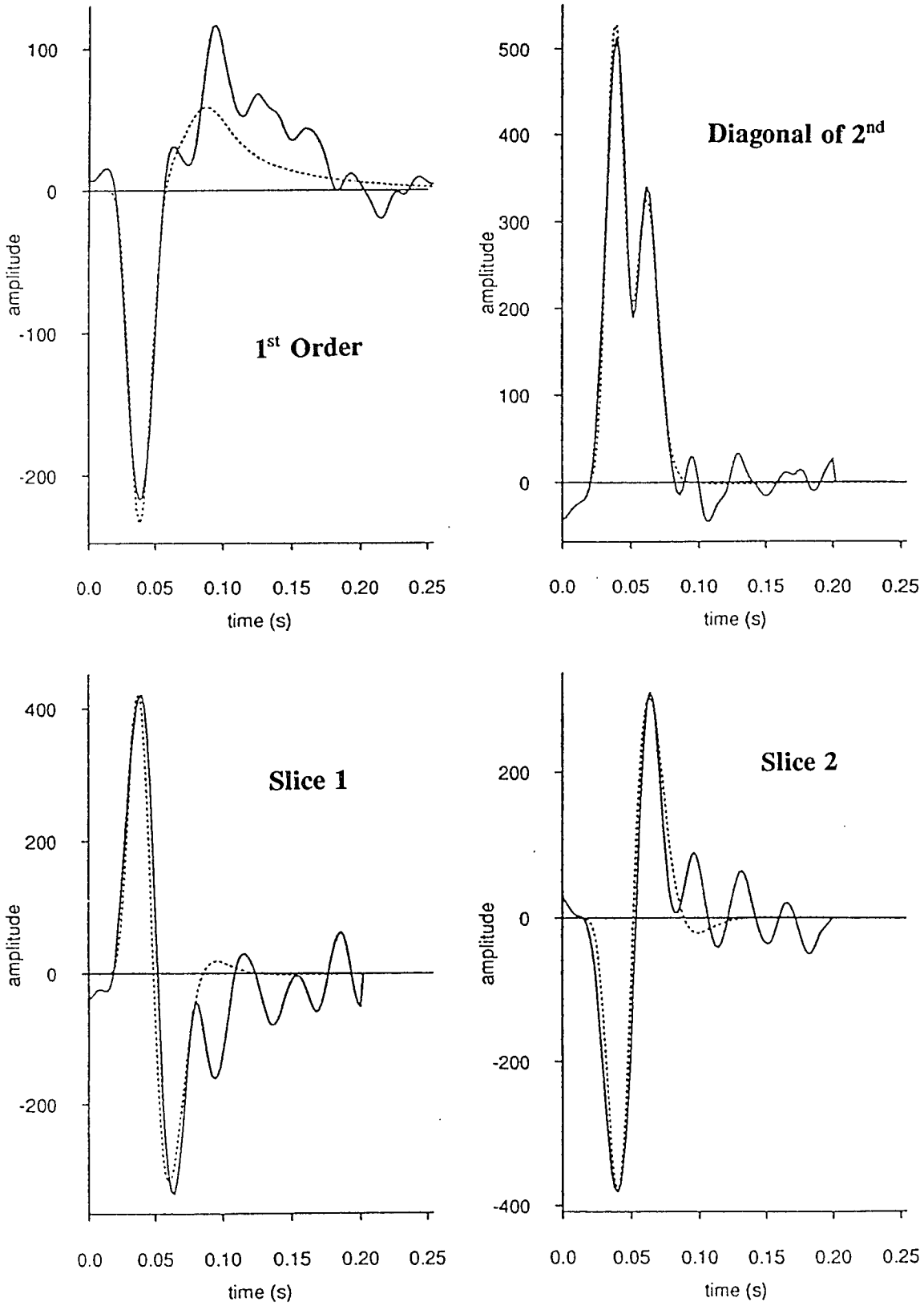
100
0
-100
-200
amplitude
1st Order
0.0 0.05 0.10 0.15 0.20 0.25
time (s)
500
400
300
200
100
0
amplitude
Diagonal of 2nd
0.0 0.05 0.10 0.15 0.20 0.25
time (s)
400
200
0
-200
amplitude
Slice 1
0.0 0.05 0.10 0.15 0.20 0.25
time (s)
200
0
-200
-400
amplitude
Slice 2
0.0 0.05 0.10 0.15 0.20 0.25
time (s)

FIG. 39 D-iii)

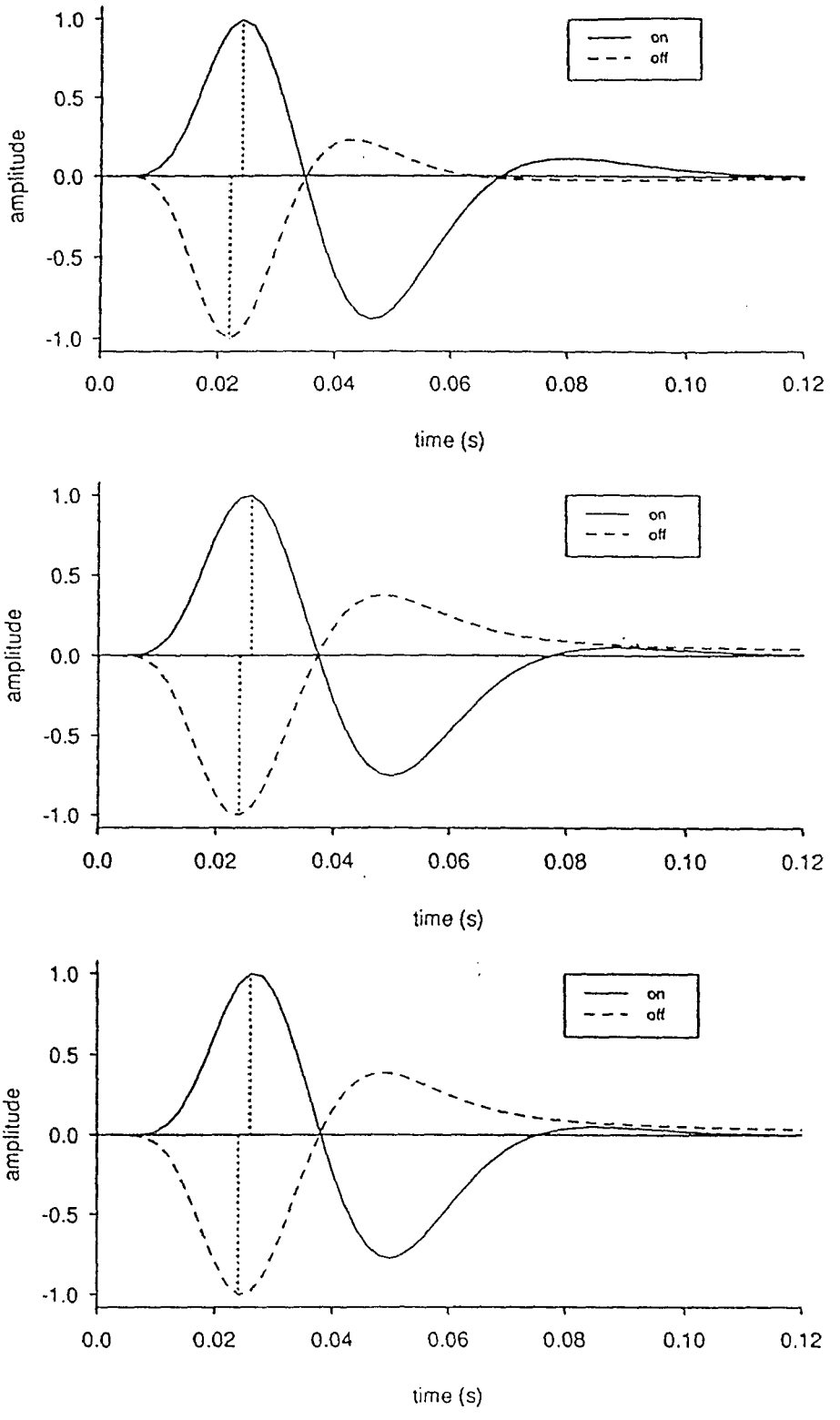
1.0
0.5
0.0
-0.5
-1.0
amplitude
on
off
0.0
0.02
0.04
0.06
0.08
0.10
0.12
time (s)
1.0
0.5
0.0
-0.5
-1.0
amplitude
on
off
0.0
0.02
0.04
0.06
0.08
0.10
0.12
time (s)
1.0
0.5
0.0
-0.5
-1.0
amplitude
on
off
0.0
0.02
0.04
0.06
0.08
0.10
0.12
time (s)

FIG. 39 E)

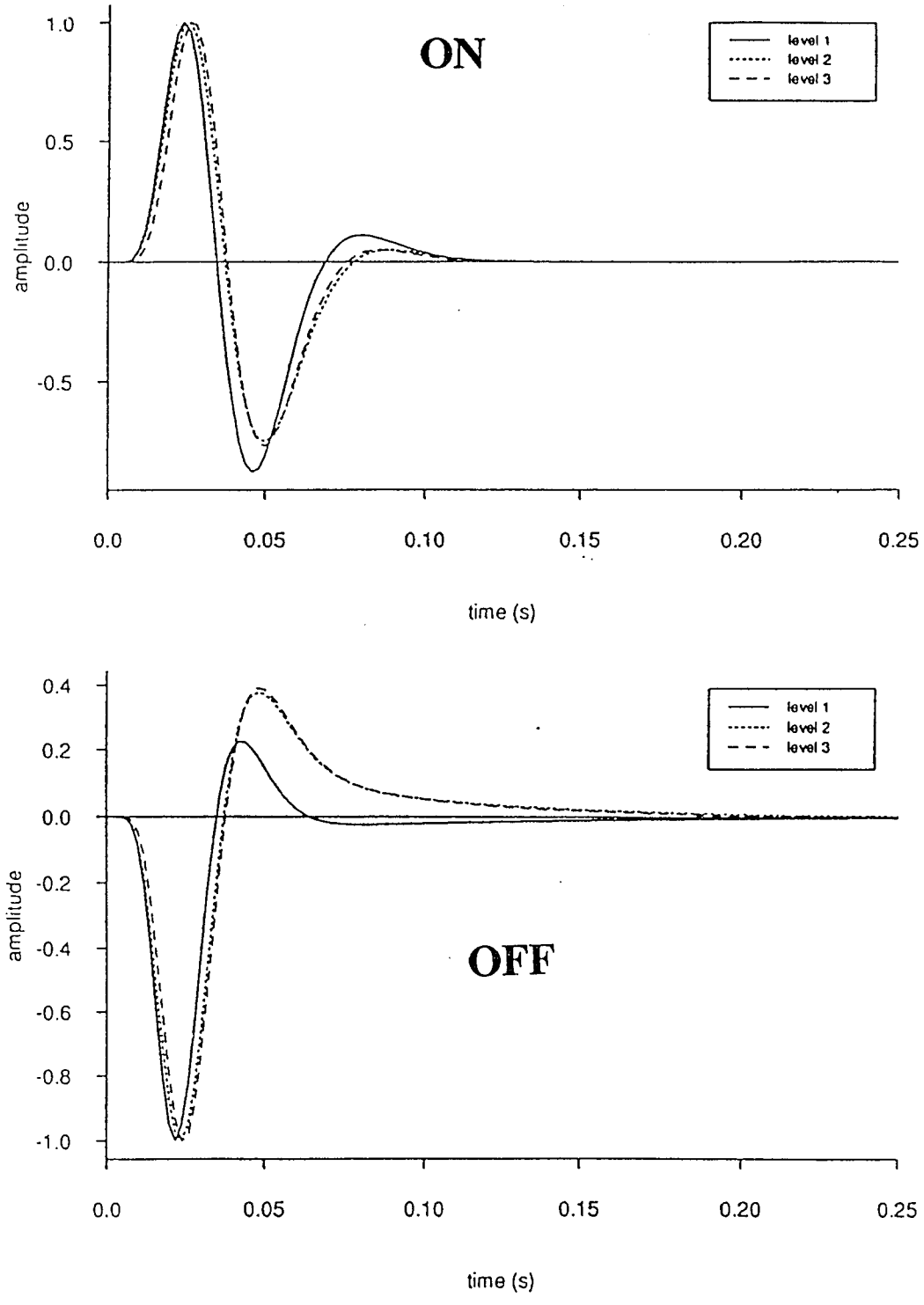
ON
level 1
level 2
level 3
amplitude
1.0
0.5
0.0
-0.5
0.0
0.05
0.10
0.15
0.20
0.25
time (s)
OFF
level 1
level 2
level 3
amplitude
0.4
0.2
0.0
-0.2
-0.4
-0.6
-0.8
-1.0
0.0
0.05
0.10
0.15
0.20
0.25
time (s)

FIG. 39 F)

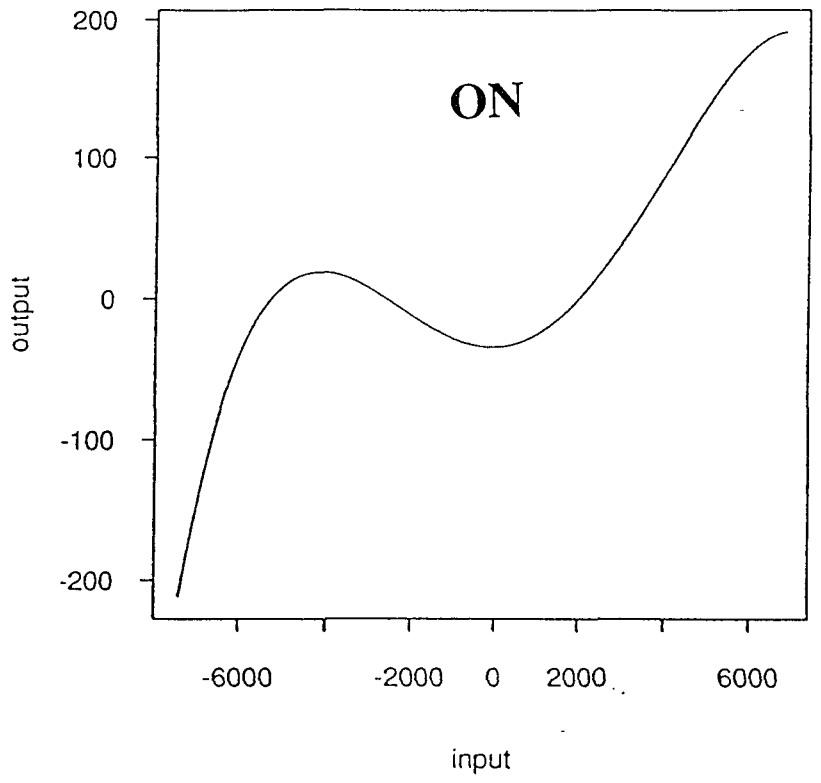
ON
200
100
0
-100
-200
output
-6000
-2000
0
2000
6000
input

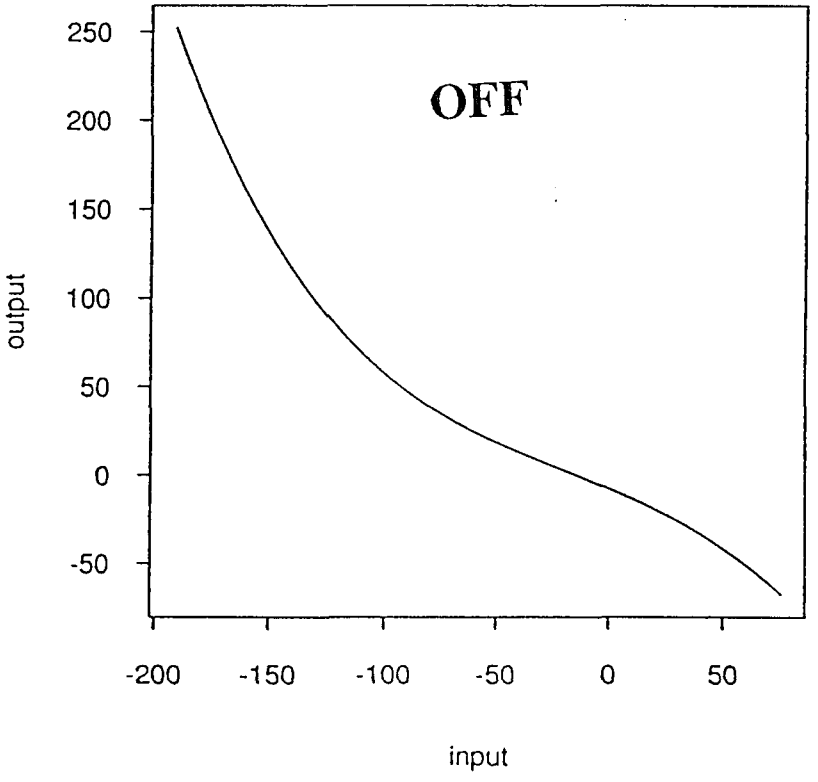
OFF
250
200
150
100
50
0
-50
output
-200
-150
-100
-50
0
50
input

FIG. 39 G-i)

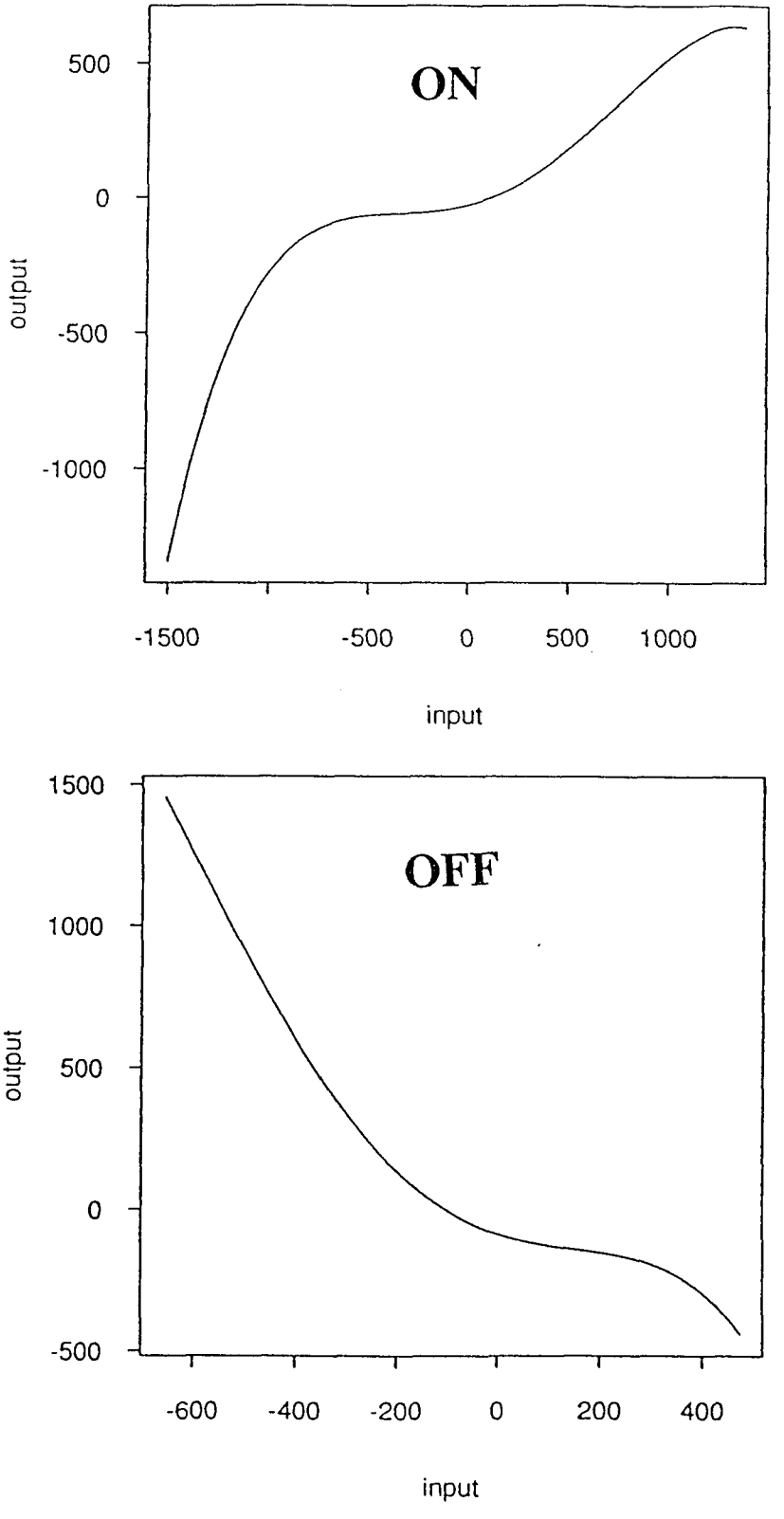
ON
500
0
-500
-1000
output
-1500
-500
0
500
1000
input
OFF
1500
1000
500
0
-500
output
-600
-400
-200
0
200
400
input

FIG. 39 G-ii)

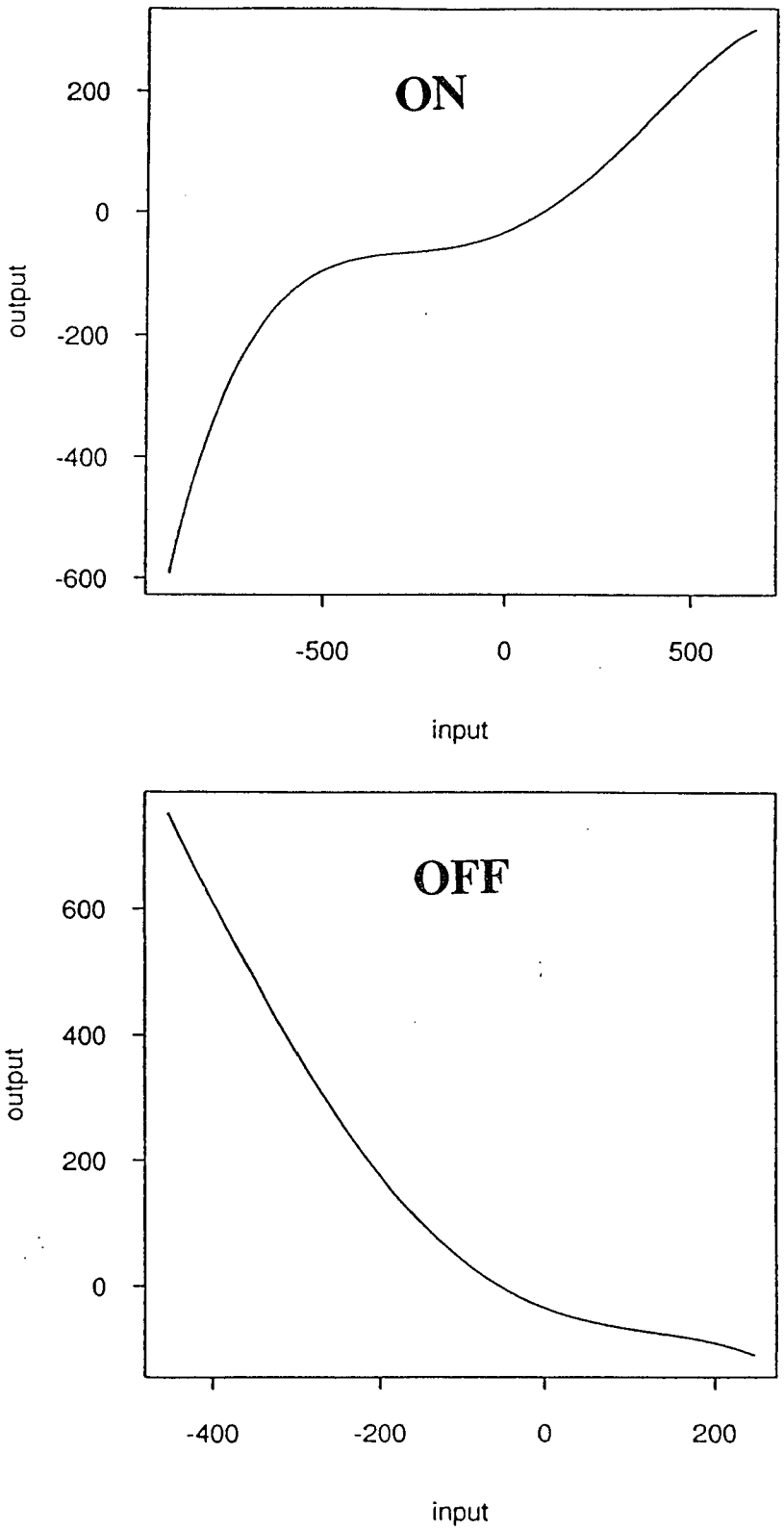
ON
200
0
-200
-400
-600
output
-500
0
500
input
OFF
600
400
200
0
output
-400
-200
0
200
input

FIG. 39 G-iii)

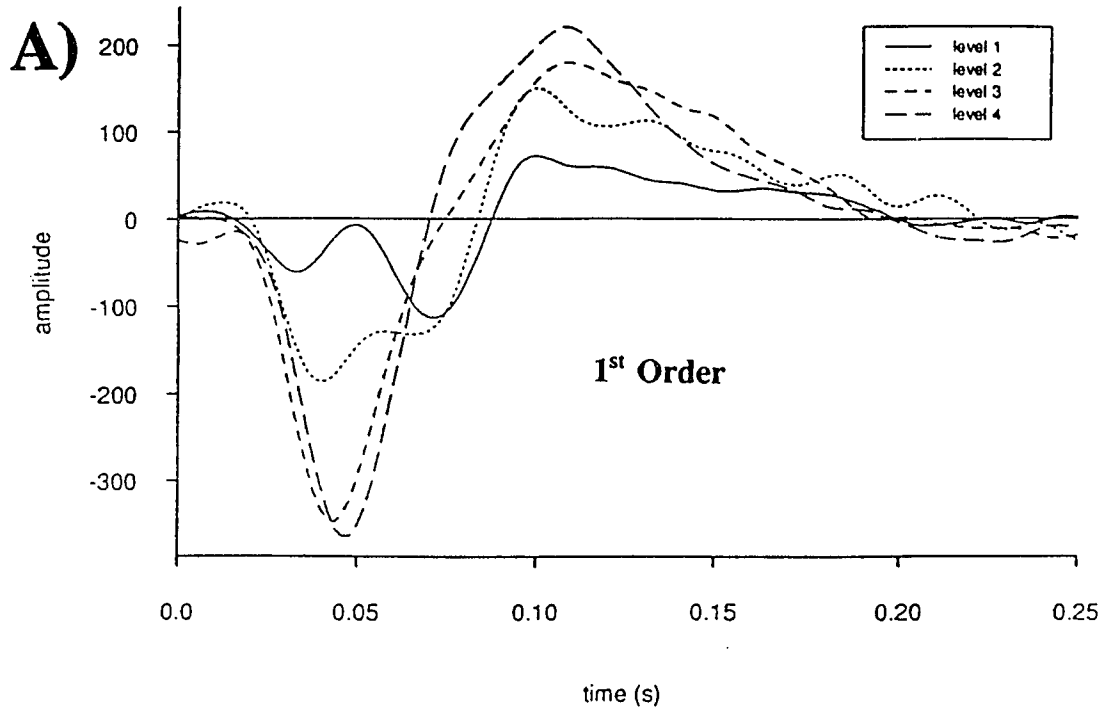
A)
200
100
0
-100
-200
-300
amplitude
level 1
level 2
level 3
level 4
1st Order
0.0
0.05
0.10
0.15
0.20
0.25
time (s)

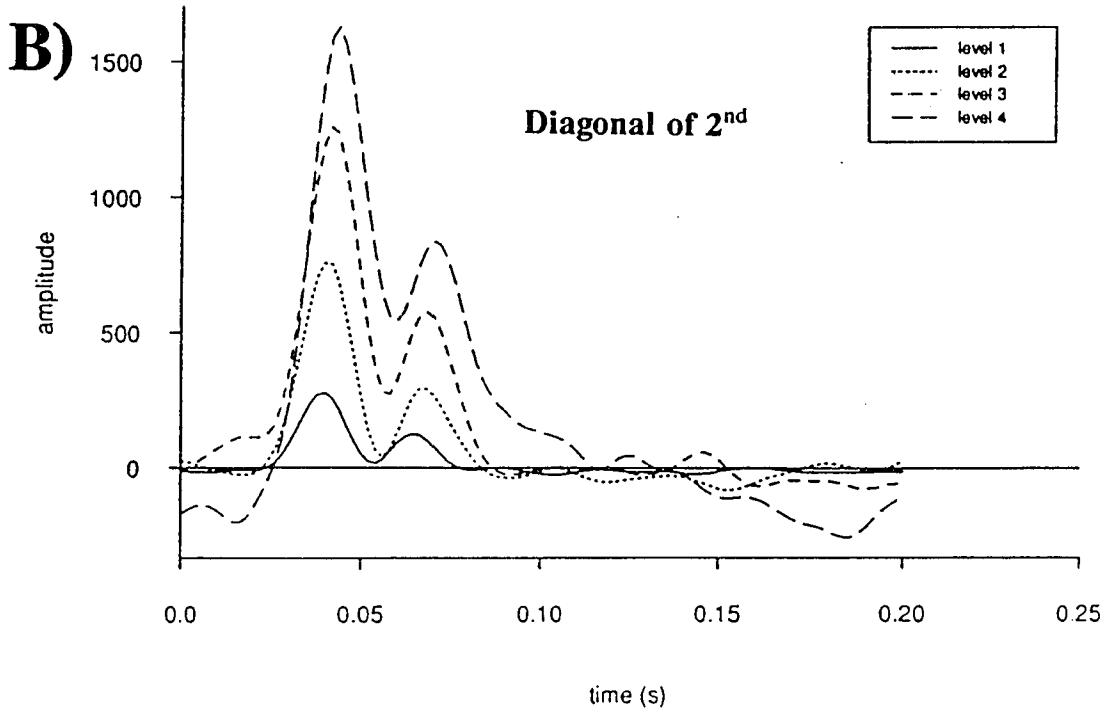
B)
1500
1000
500
0
amplitude
level 1
level 2
level 3
level 4
Diagonal of 2nd
0.0
0.05
0.10
0.15
0.20
0.25
time (s)

FIG. 40

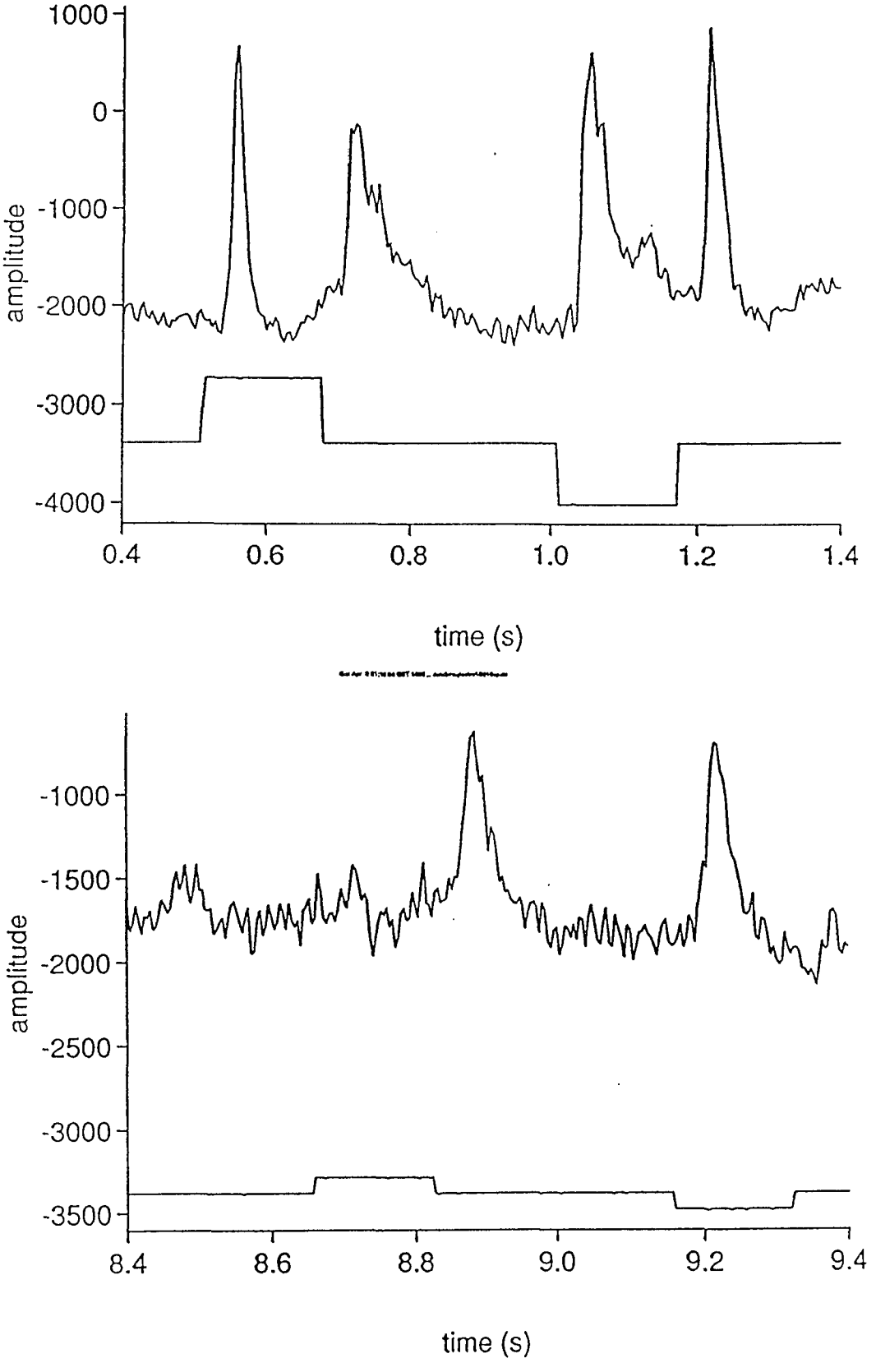
1000
0
-1000
-2000
-3000
-4000
amplitude
0.4
0.6
0.8
1.0
1.2
1.4
time (s)
-1000
-1500
-2000
-2500
-3000
-3500
amplitude
8.4
8.6
8.8
9.0
9.2
9.4
time (s)

FIG. 40 C)

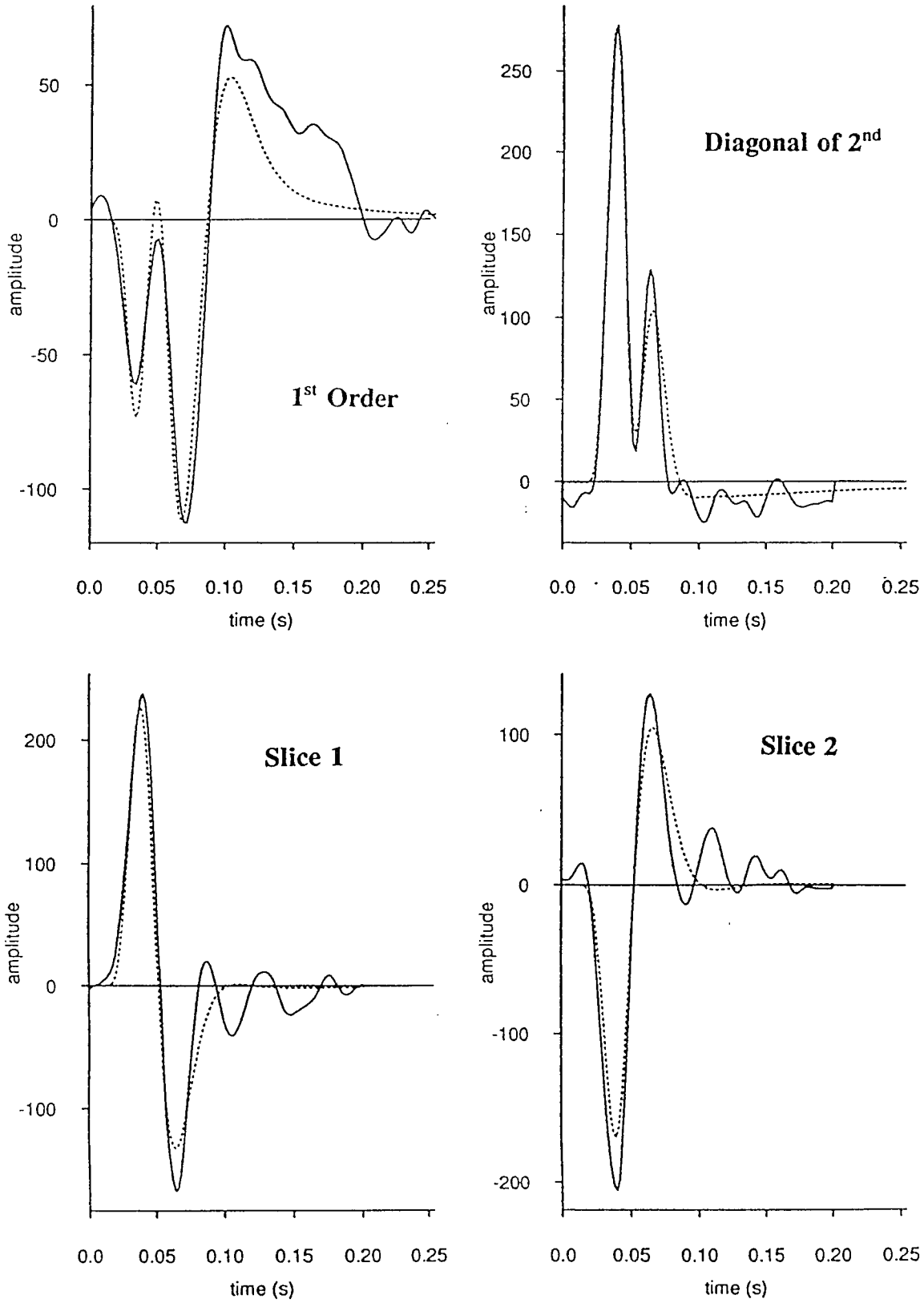
1st Order
Diagonal of 2nd
Slice 1
Slice 2
amplitude
time (s)
50
0
-50
-100
250
200
150
100
50
0
-200
0.0
0.05
0.10
0.15
0.20
0.25

FIG. 40 D-i)

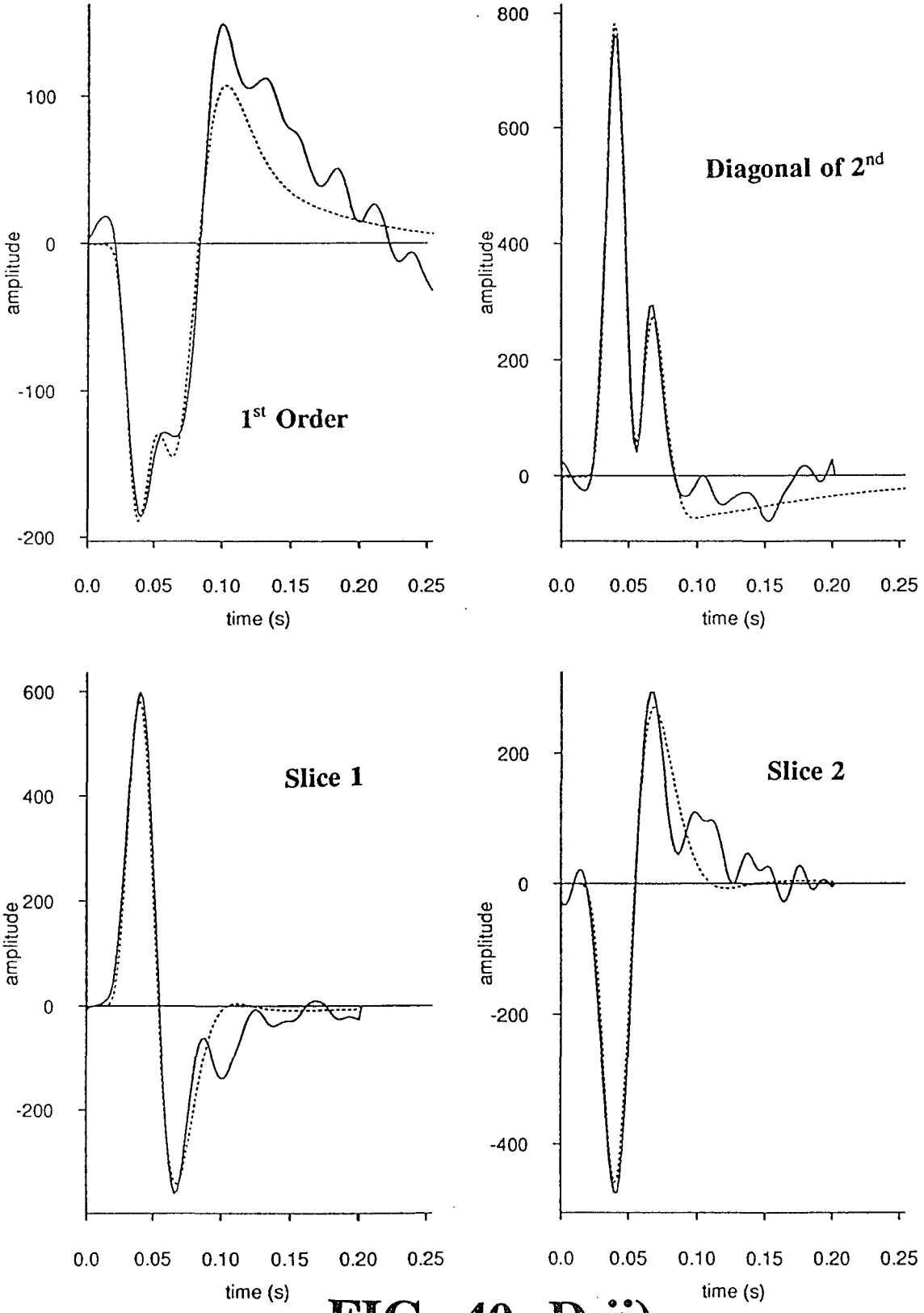
100
0
-100
-200
amplitude
1st Order
0.0
0.05
0.10
0.15
0.20
0.25
time (s)
800
600
400
200
0
amplitude
Diagonal of 2nd
0.0
0.05
0.10
0.15
0.20
0.25
time (s)
600
400
200
0
-200
amplitude
Slice 1
0.0
0.05
0.10
0.15
0.20
0.25
time (s)
200
0
-200
-400
amplitude
Slice 2
0.0
0.05
0.10
0.15
0.20
0.25
time (s)

FIG. 40 D-ii)

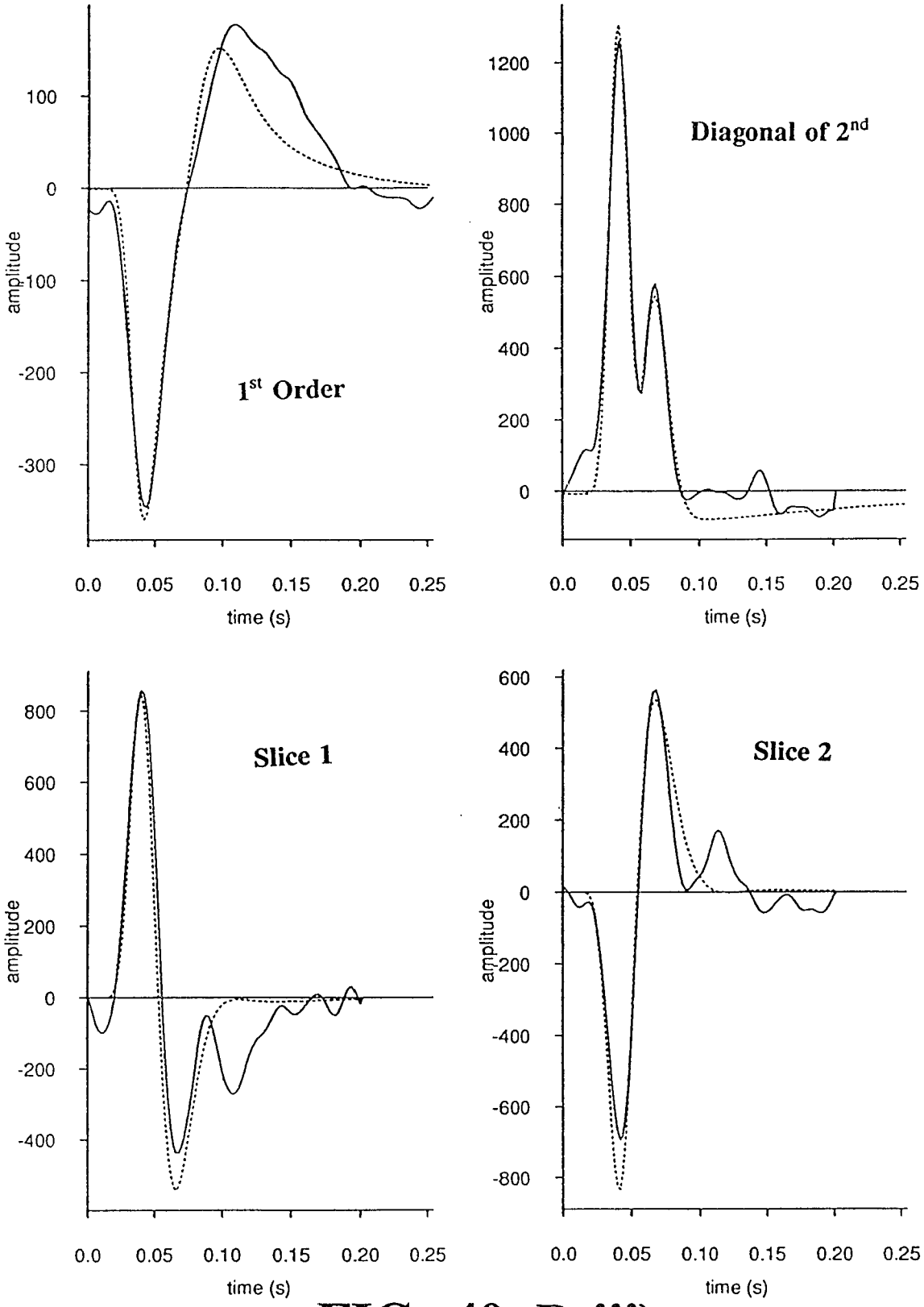
1st Order
Diagonal of 2nd
Slice 1
Slice 2
amplitude
time (s)
100
0
-100
-200
-300
1200
1000
800
600
400
200
0
-400
-600
-800
0.0
0.05
0.10
0.15
0.20
0.25

FIG. 40 D-iii)

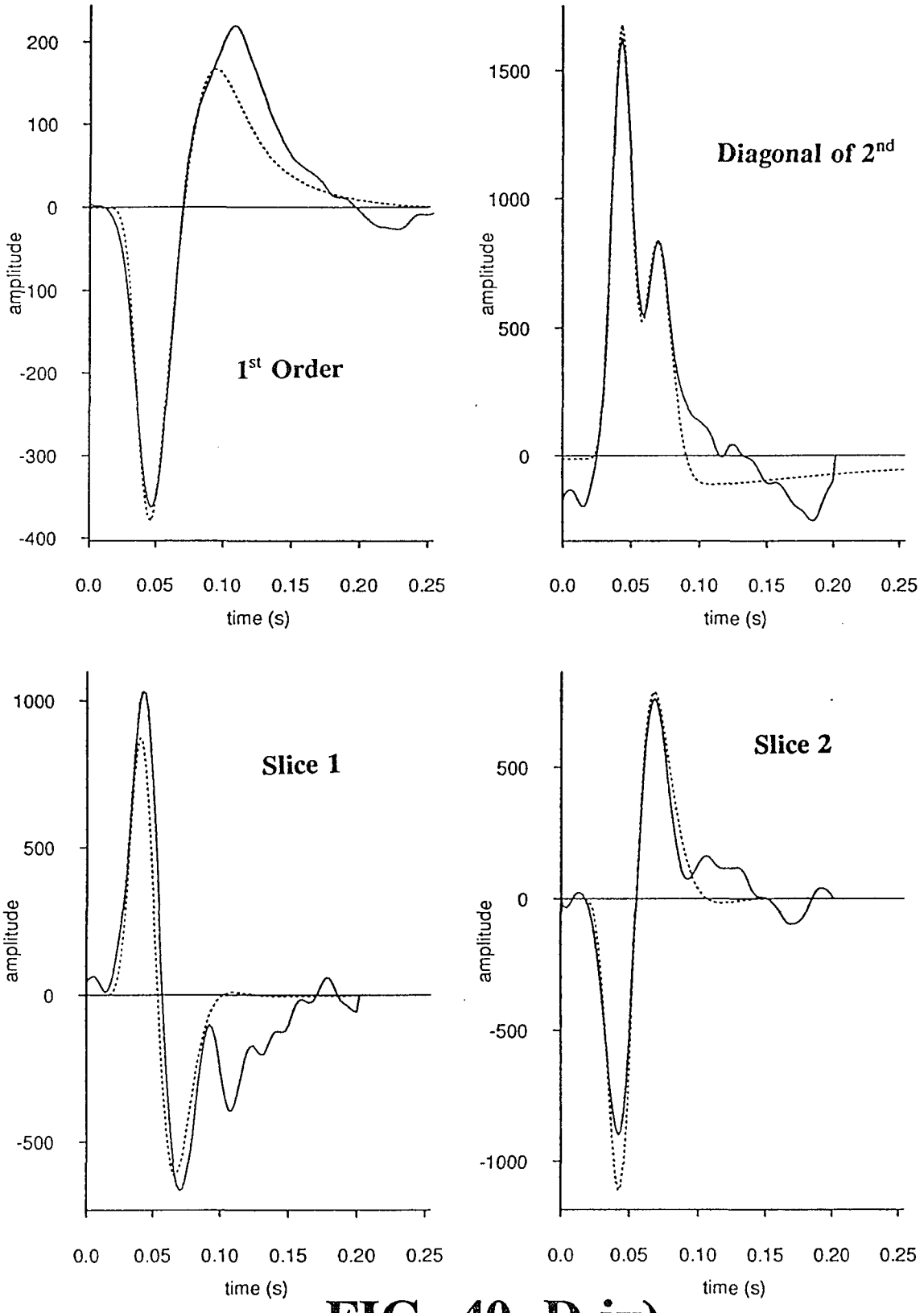
200
100
0
-100
-200
-300
-400
amplitude
1st Order
0.0
0.05
0.10
0.15
0.20
0.25
time (s)
1500
1000
500
0
amplitude
Diagonal of 2nd
0.0
0.05
0.10
0.15
0.20
0.25
time (s)
1000
500
0
-500
amplitude
Slice 1
0.0
0.05
0.10
0.15
0.20
0.25
time (s)
500
0
-500
-1000
amplitude
Slice 2
0.0
0.05
0.10
0.15
0.20
0.25
time (s)

FIG. 40 D-iv)

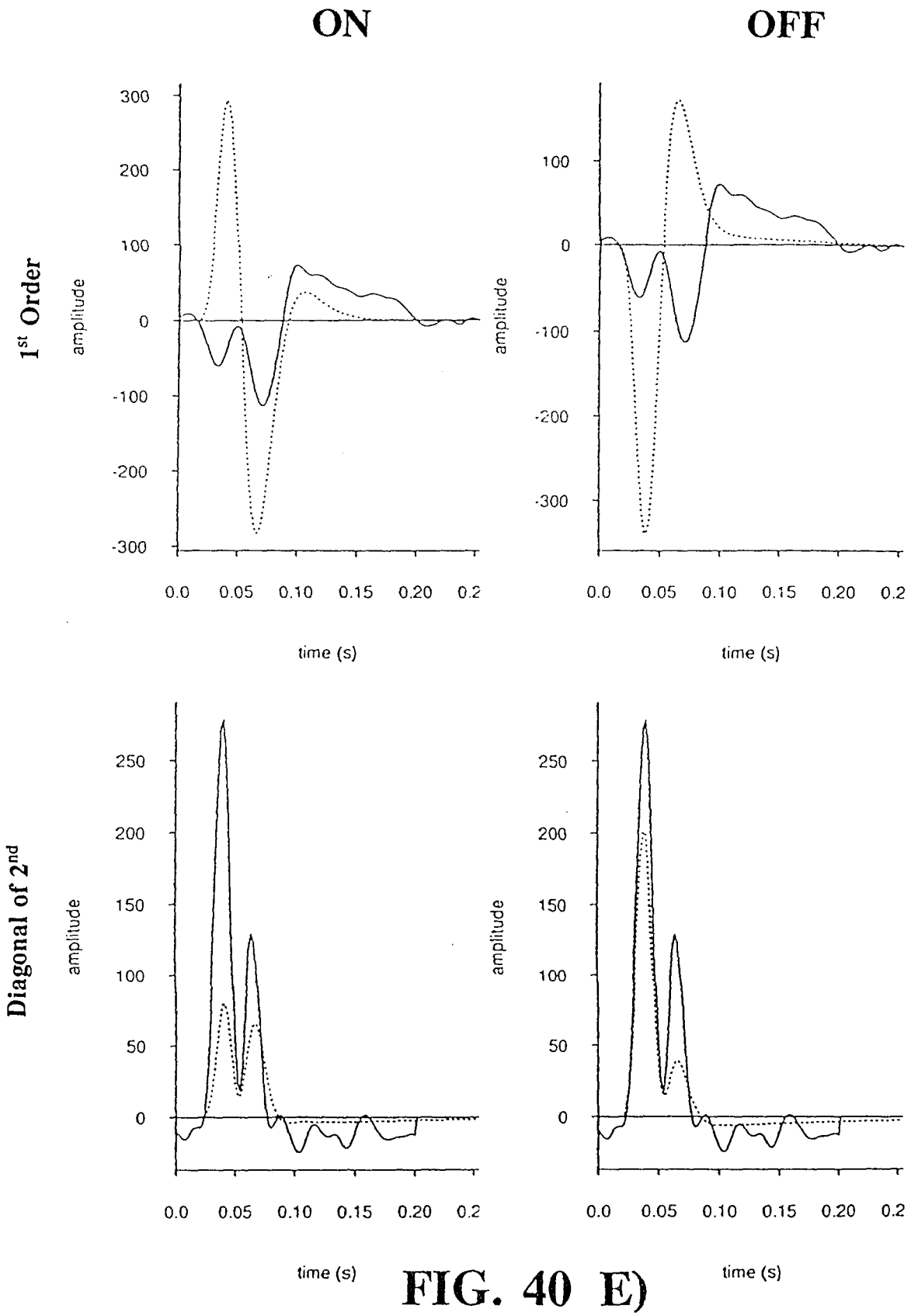
ON
OFF
1st Order
Diagonal of 2nd
amplitude
time (s)
300
200
100
0
-100
-200
-300
250
150
50
0.0
0.05
0.10
0.15
0.20
0.2

FIG. 40 E)

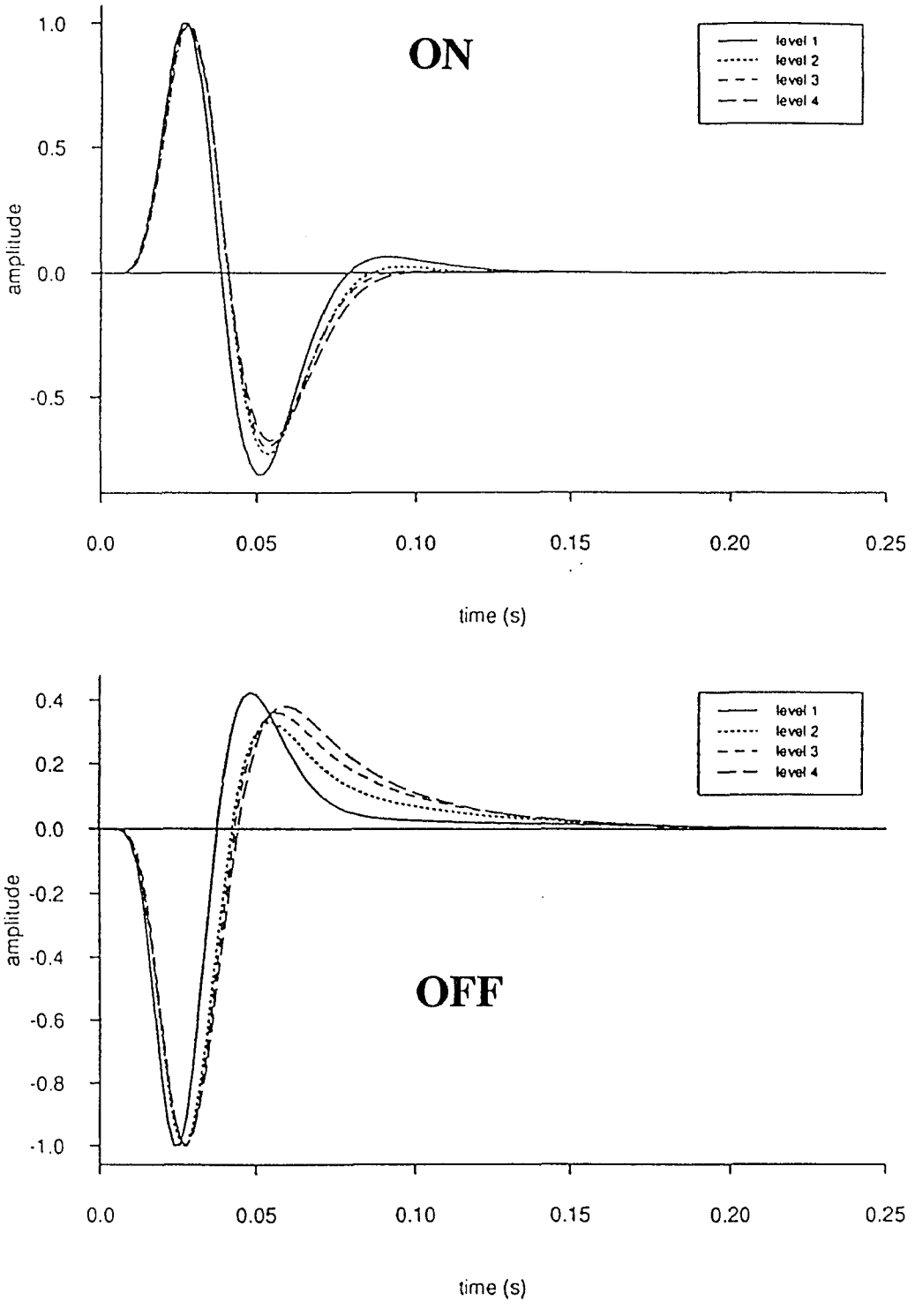
ON
level 1
level 2
level 3
level 4
amplitude
1.0
0.5
0.0
-0.5
0.0
0.05
0.10
0.15
0.20
0.25
time (s)
OFF
level 1
level 2
level 3
level 4
amplitude
0.4
0.2
0.0
-0.2
-0.4
-0.6
-0.8
-1.0
0.0
0.05
0.10
0.15
0.20
0.25
time (s)

FIG. 40 F)

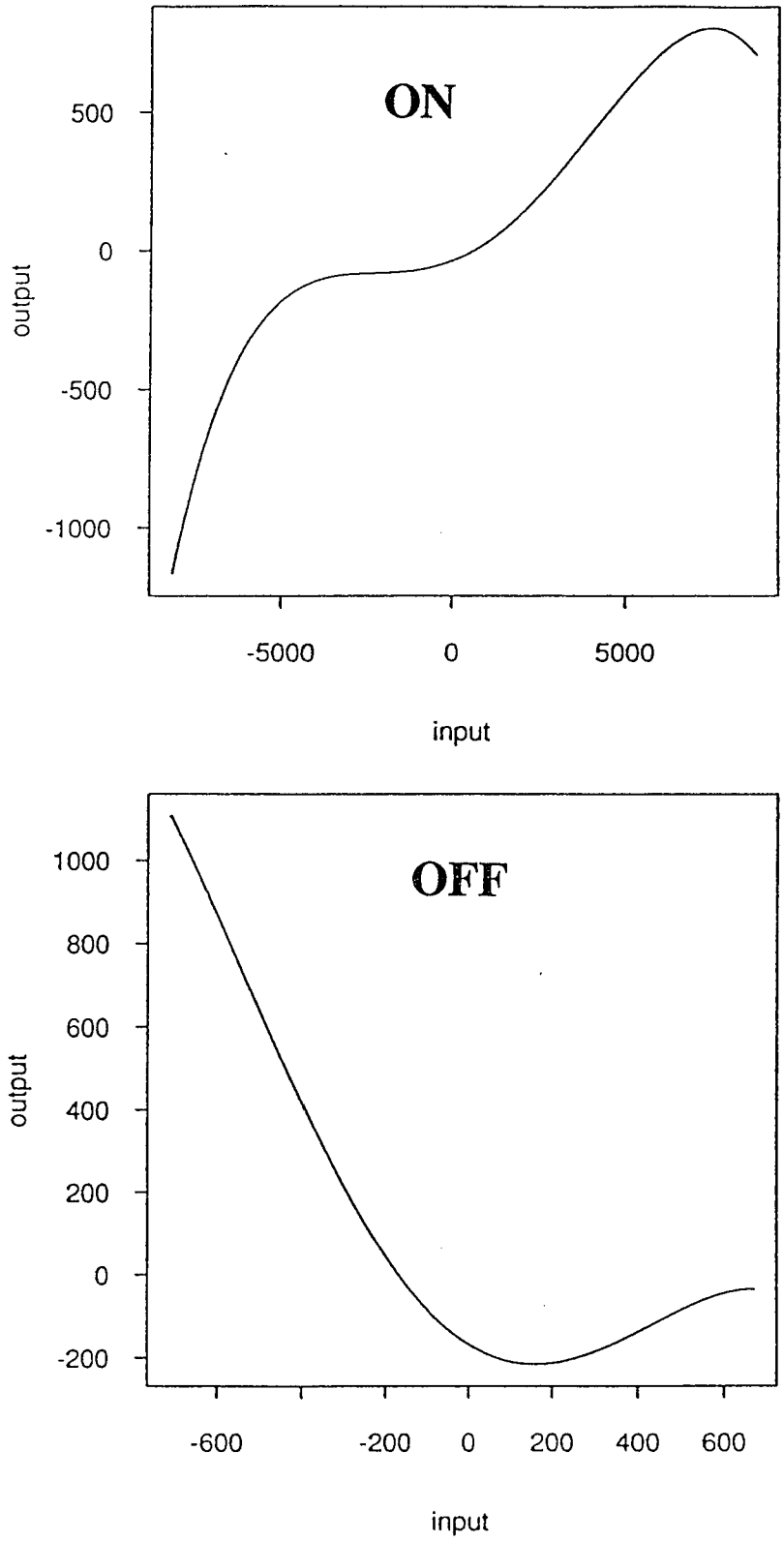
ON
500
0
-500
-1000
output
-5000
0
5000
input
OFF
1000
800
600
400
200
0
-200
output
-600
-200
0
200
400
600
input

FIG. 40 G-i)

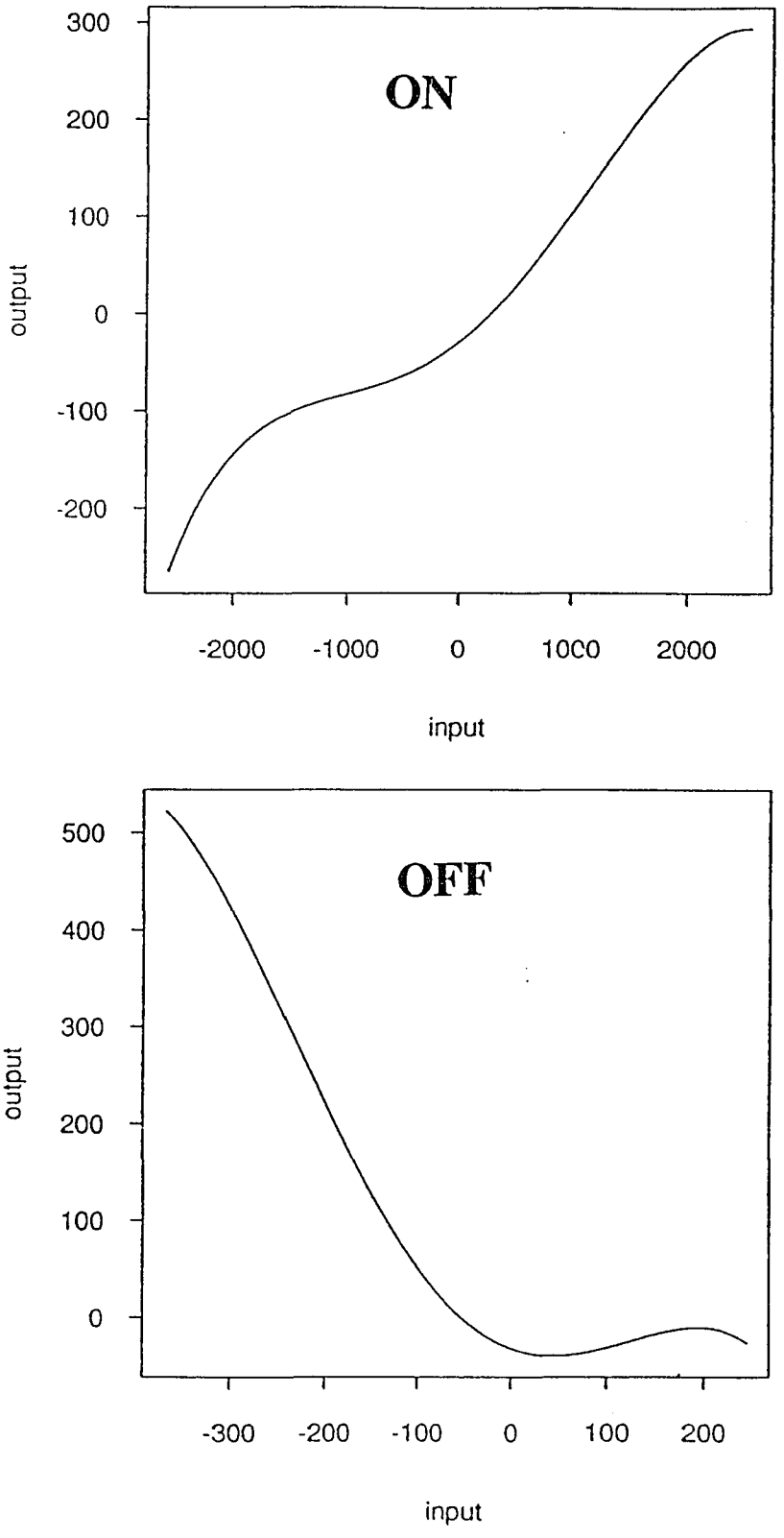
ON
300
200
100
0
-100
-200
output
-2000
-1000
0
1000
2000
input
OFF
500
400
300
200
100
0
output
-300
-200
-100
0
100
200
input

FIG. 40 G-ii)

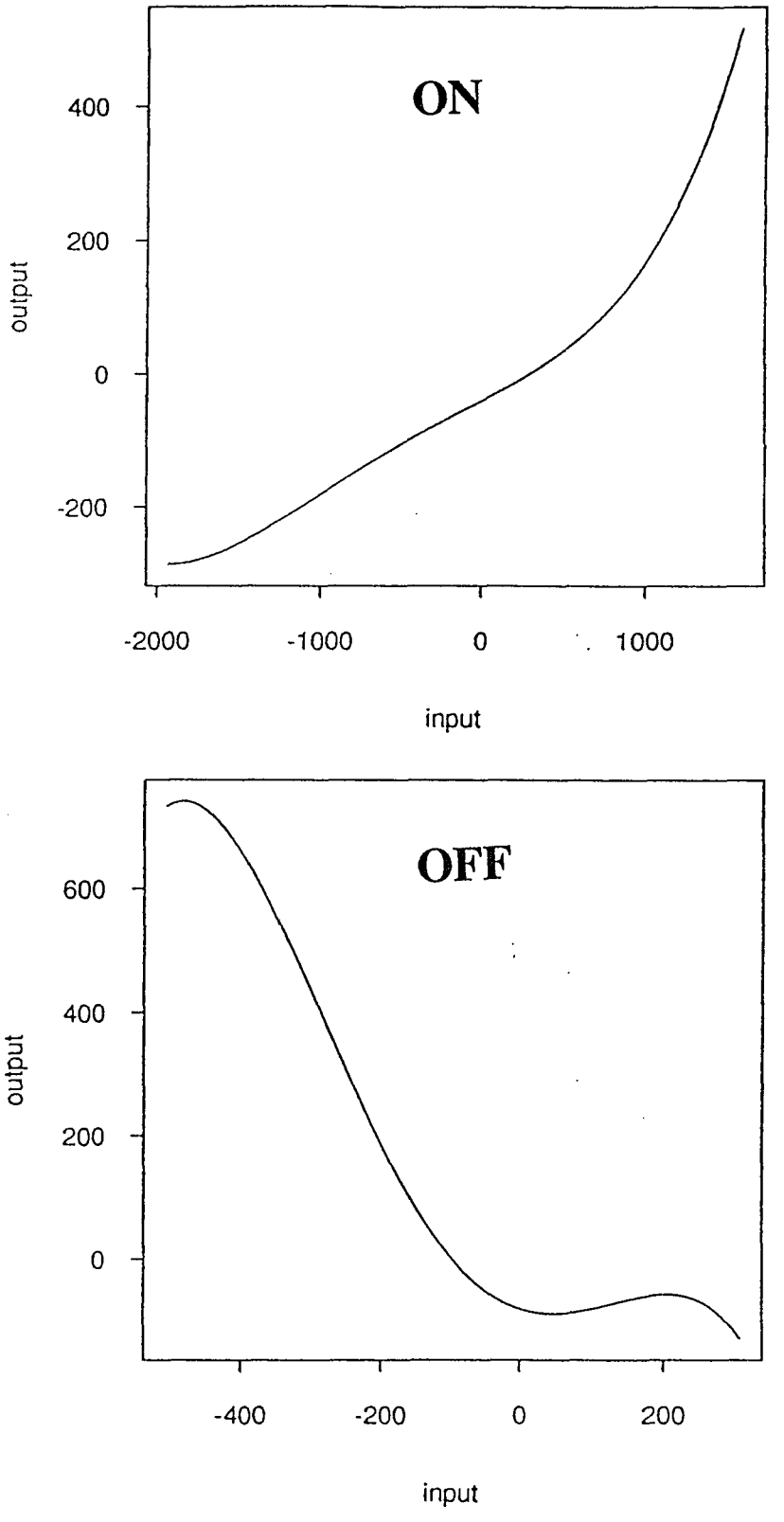
ON
400
200
0
-200
output
-2000
-1000
0
1000
input
OFF
600
400
200
0
output
-400
-200
0
200
input

FIG. 40 G-iii)

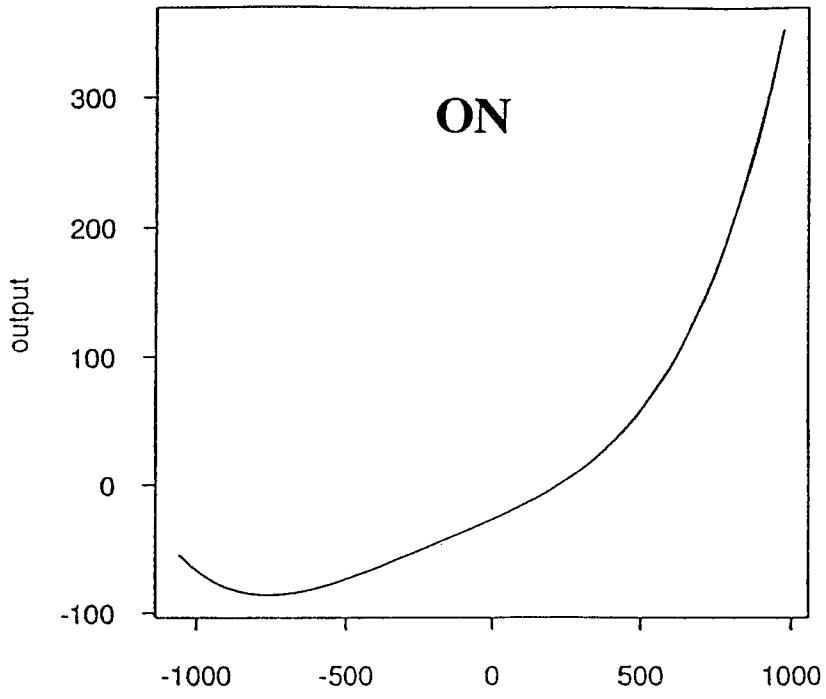
ON
300
200
100
0
-100
output
-1000
-500
0
500
1000
input

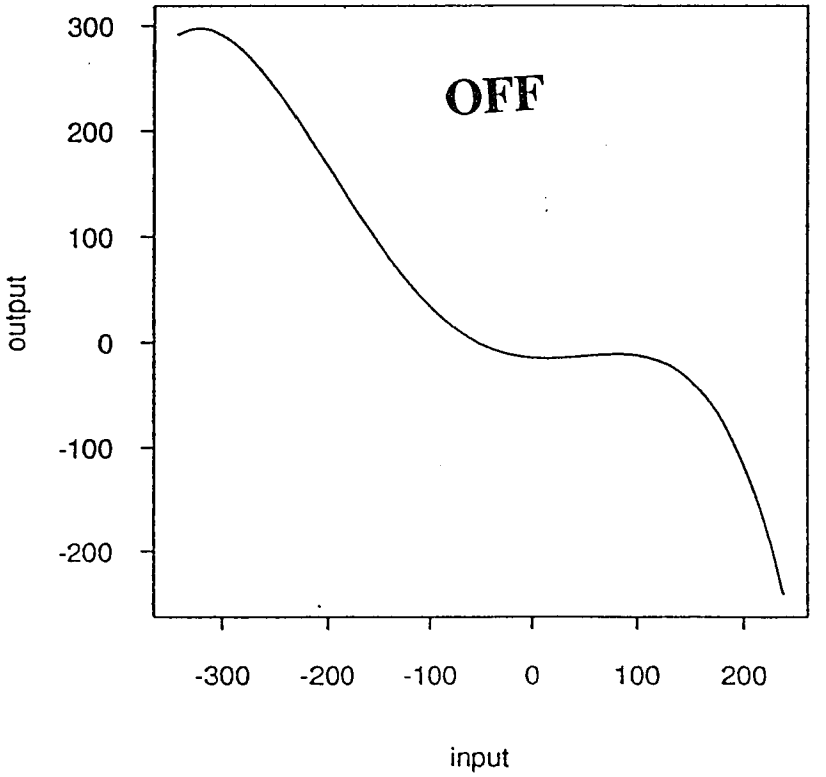
OFF
300
200
100
0
-100
-200
output
-300
-200
-100
0
100
200
input

FIG. 40 G-iv)

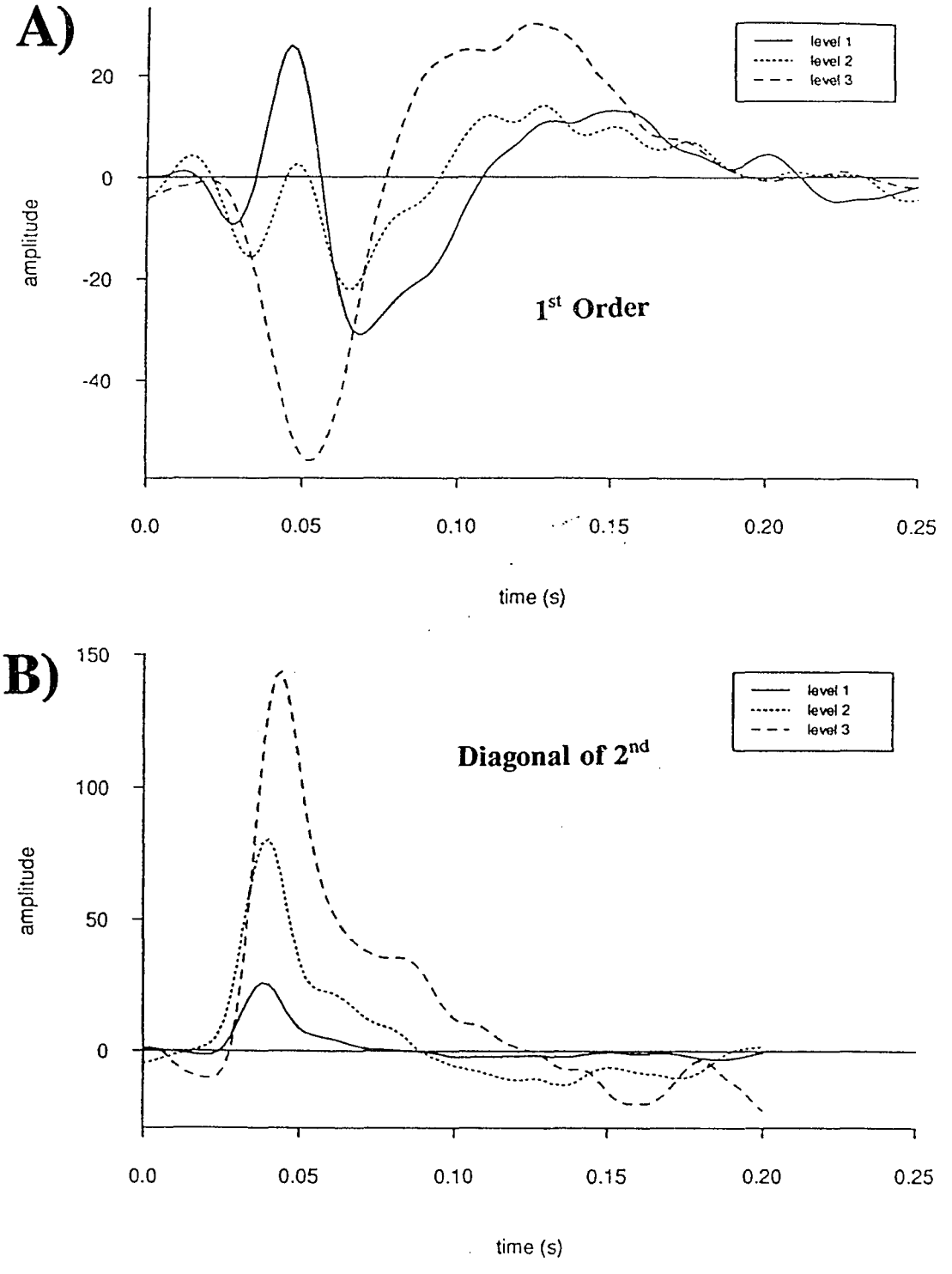

FIG. 41

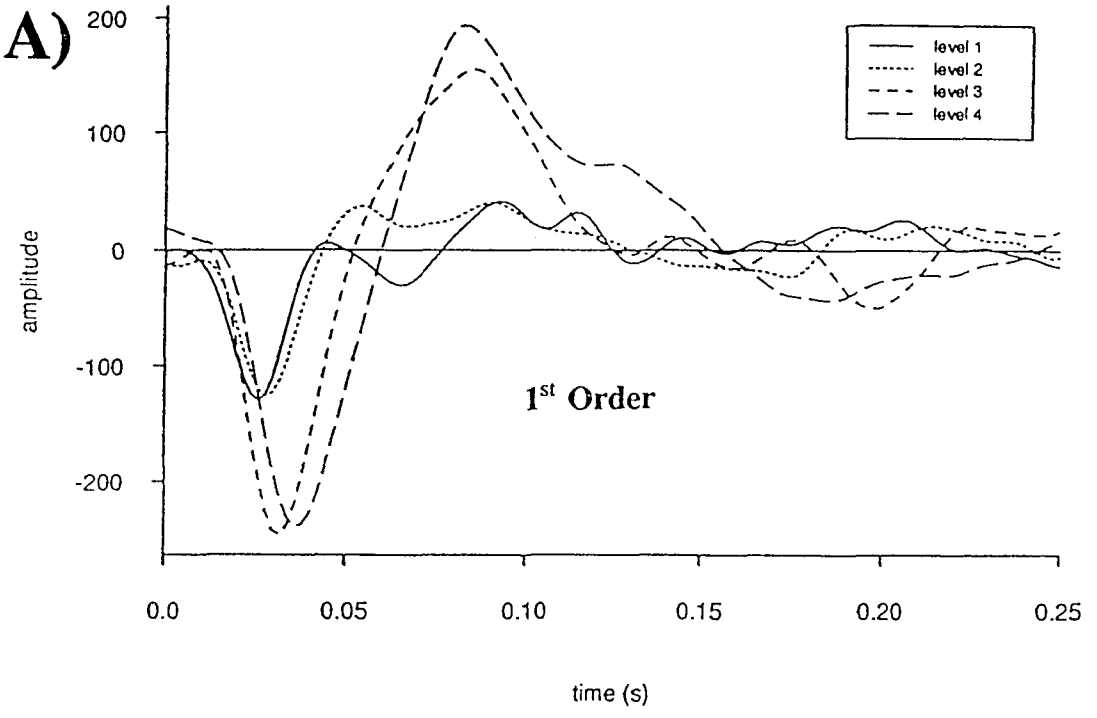

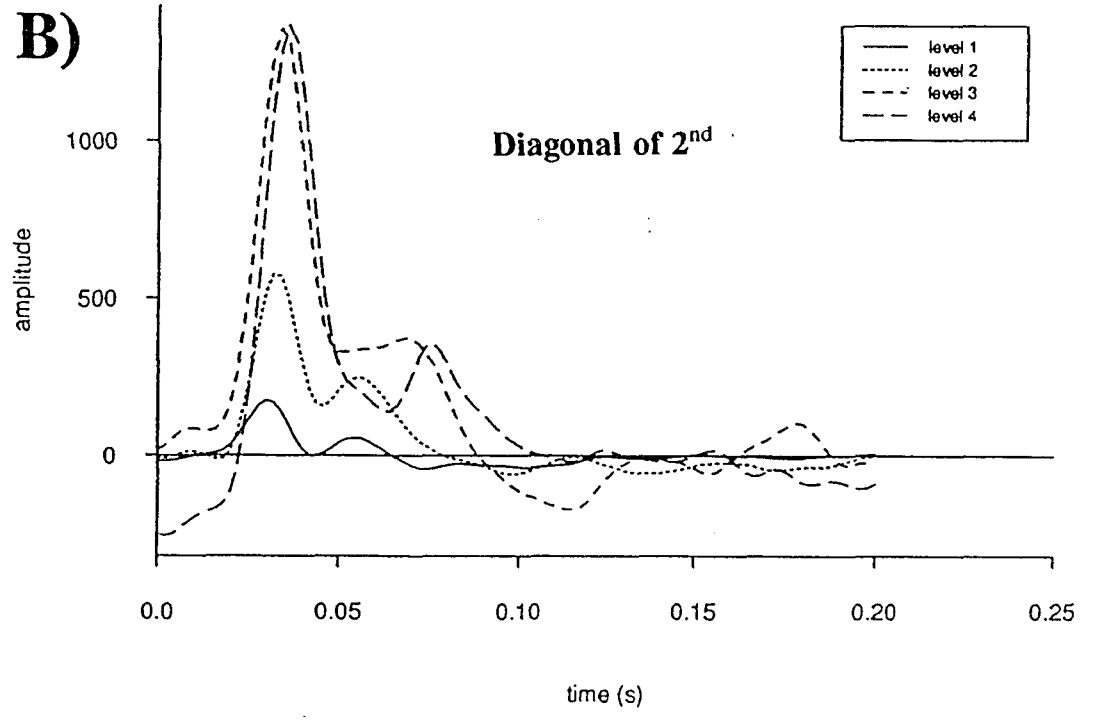

FIG. 42

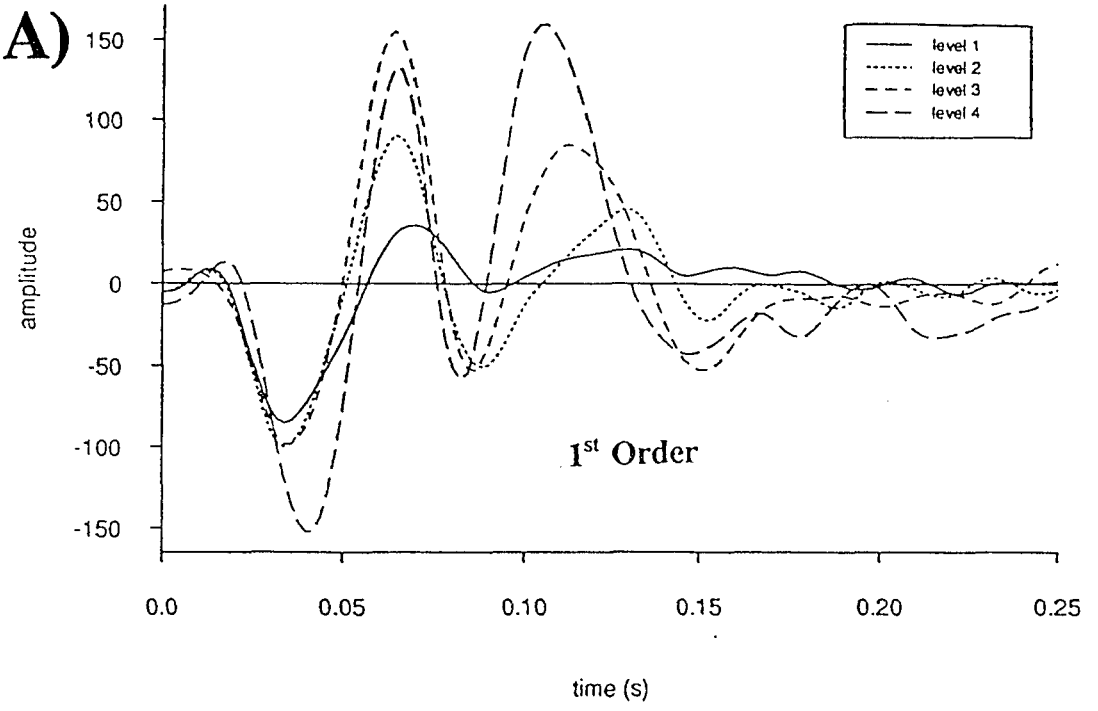

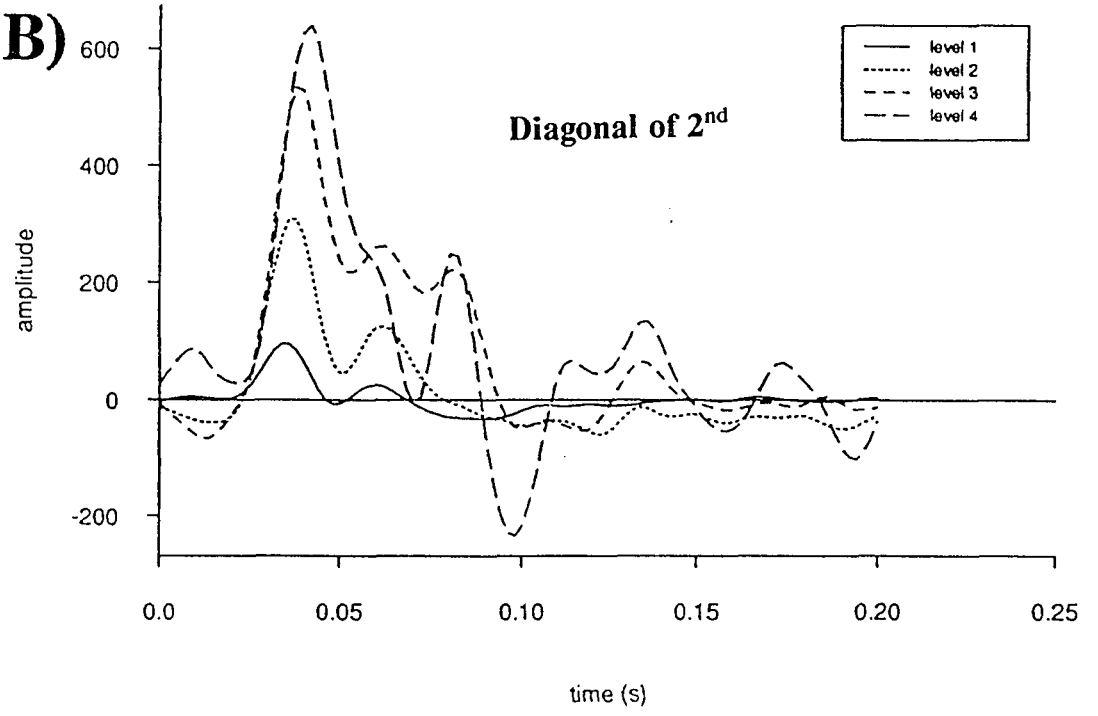

Mon Mar 29 18:44:48 EST 1993 ... /UU3/naylor/n/17020k2.ds

FIG. 43

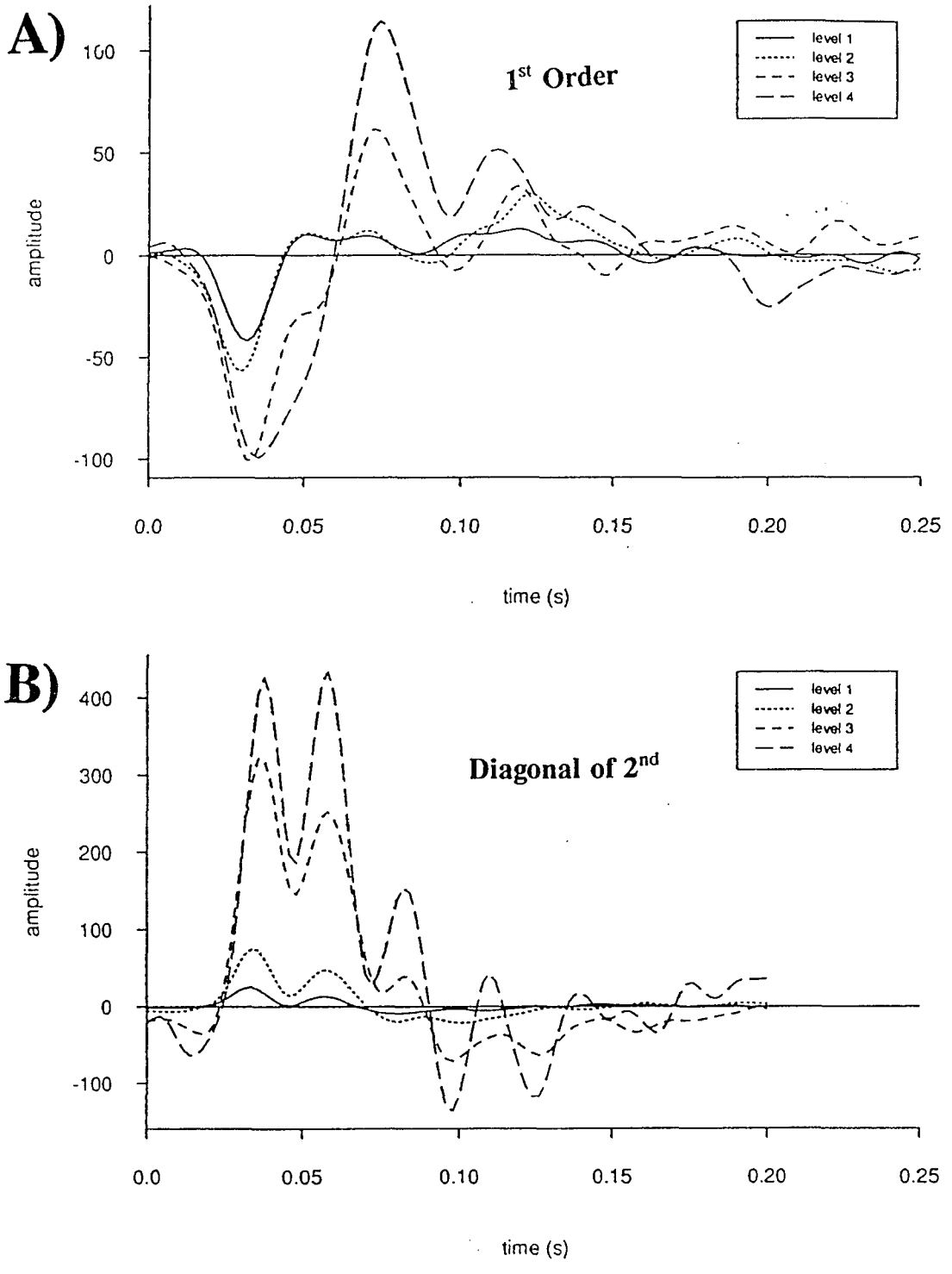

FIG. 44

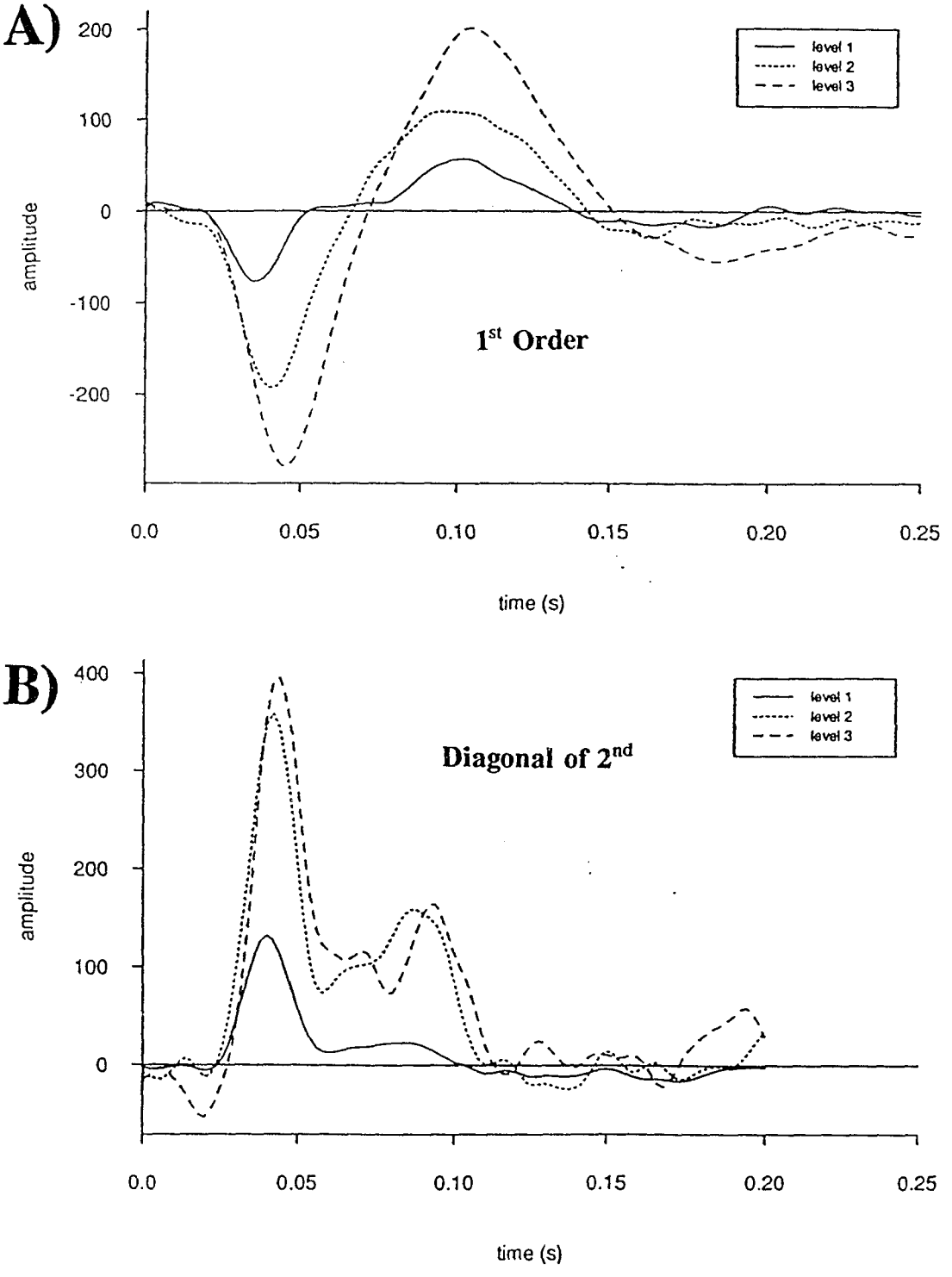

FIG. 45

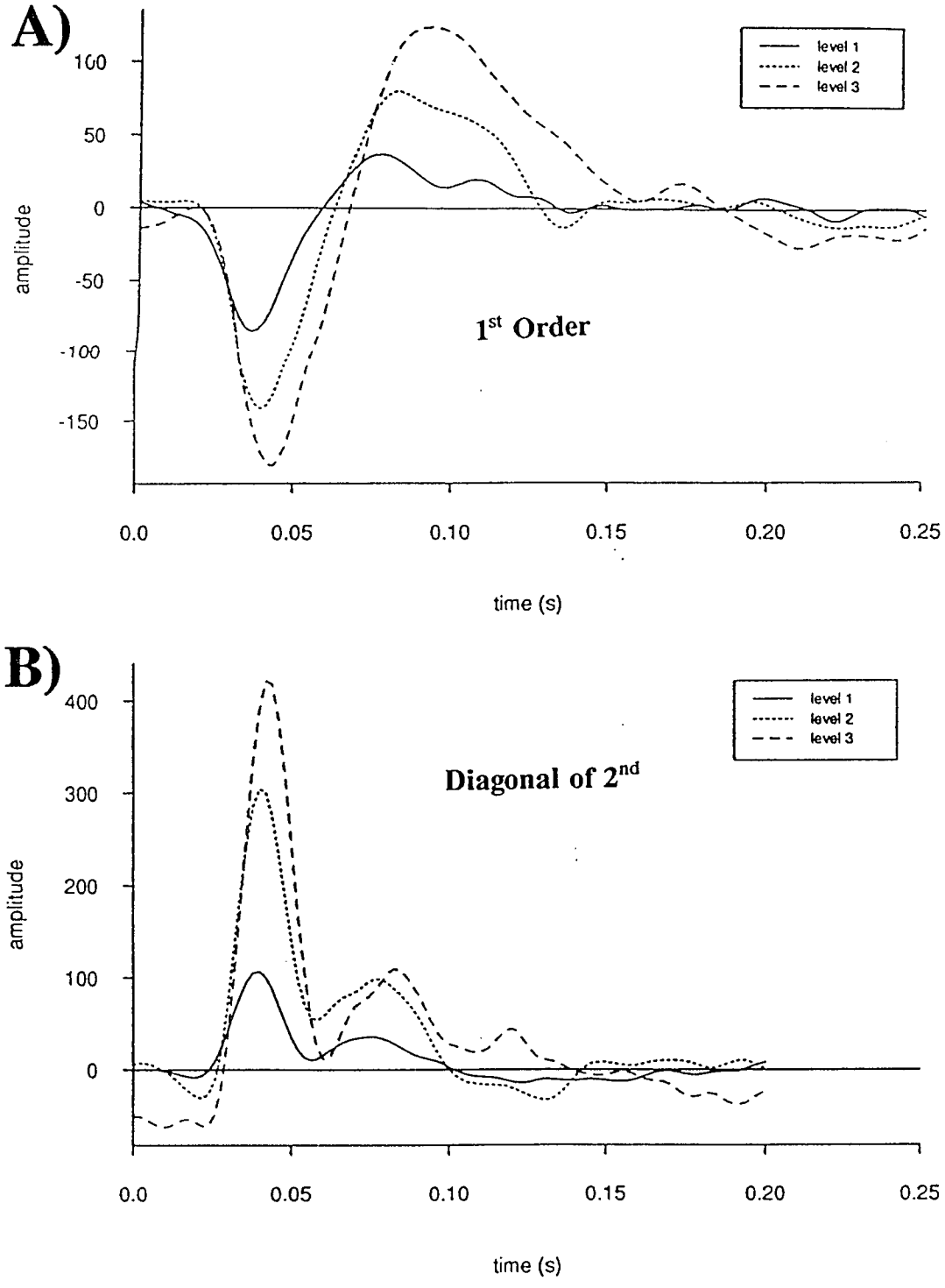

FIG. 46

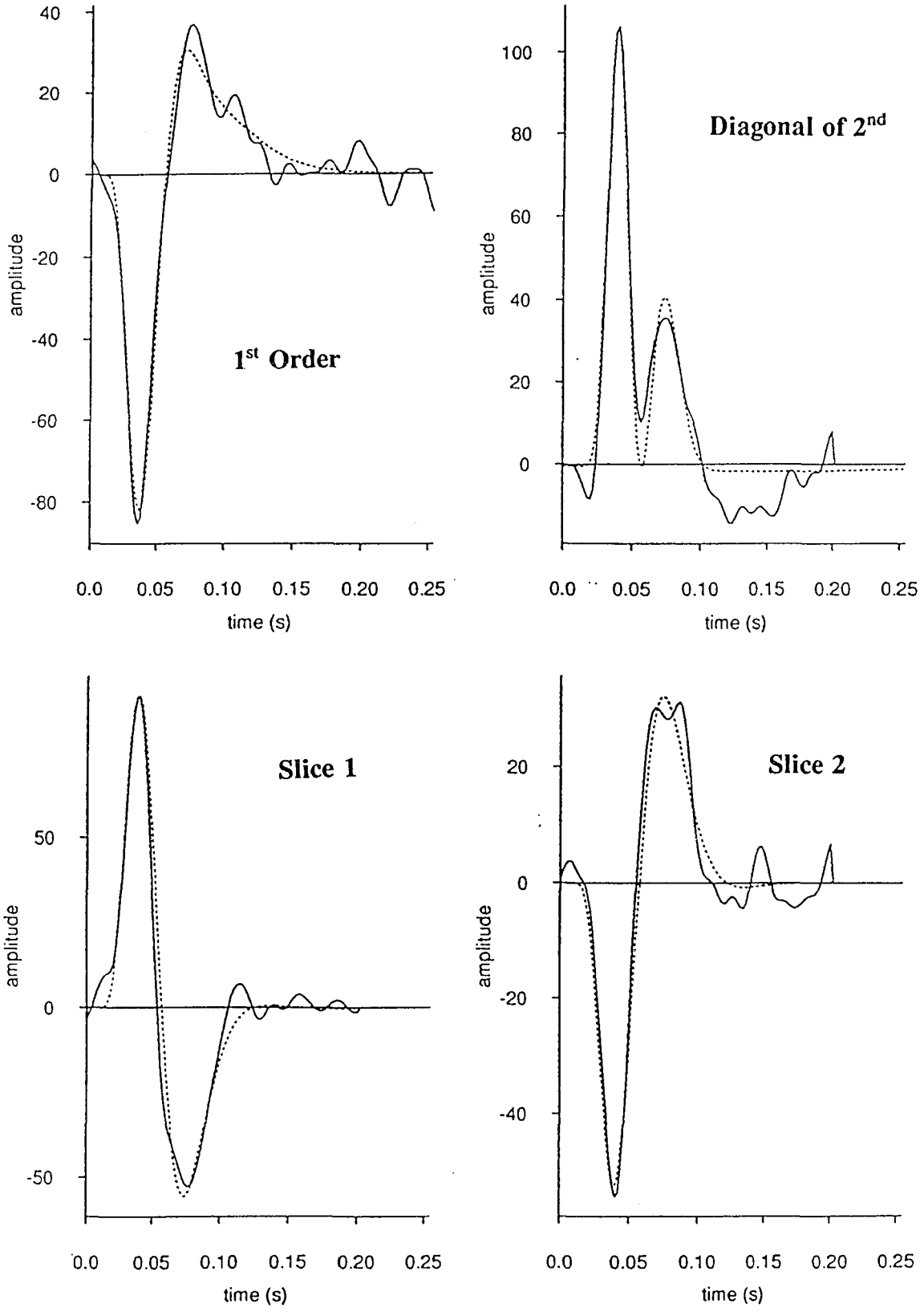
1st Order
amplitude
time (s)
Diagonal of 2nd
amplitude
time (s)
Slice 1
amplitude
time (s)
Slice 2
amplitude
time (s)

FIG. 46 C)

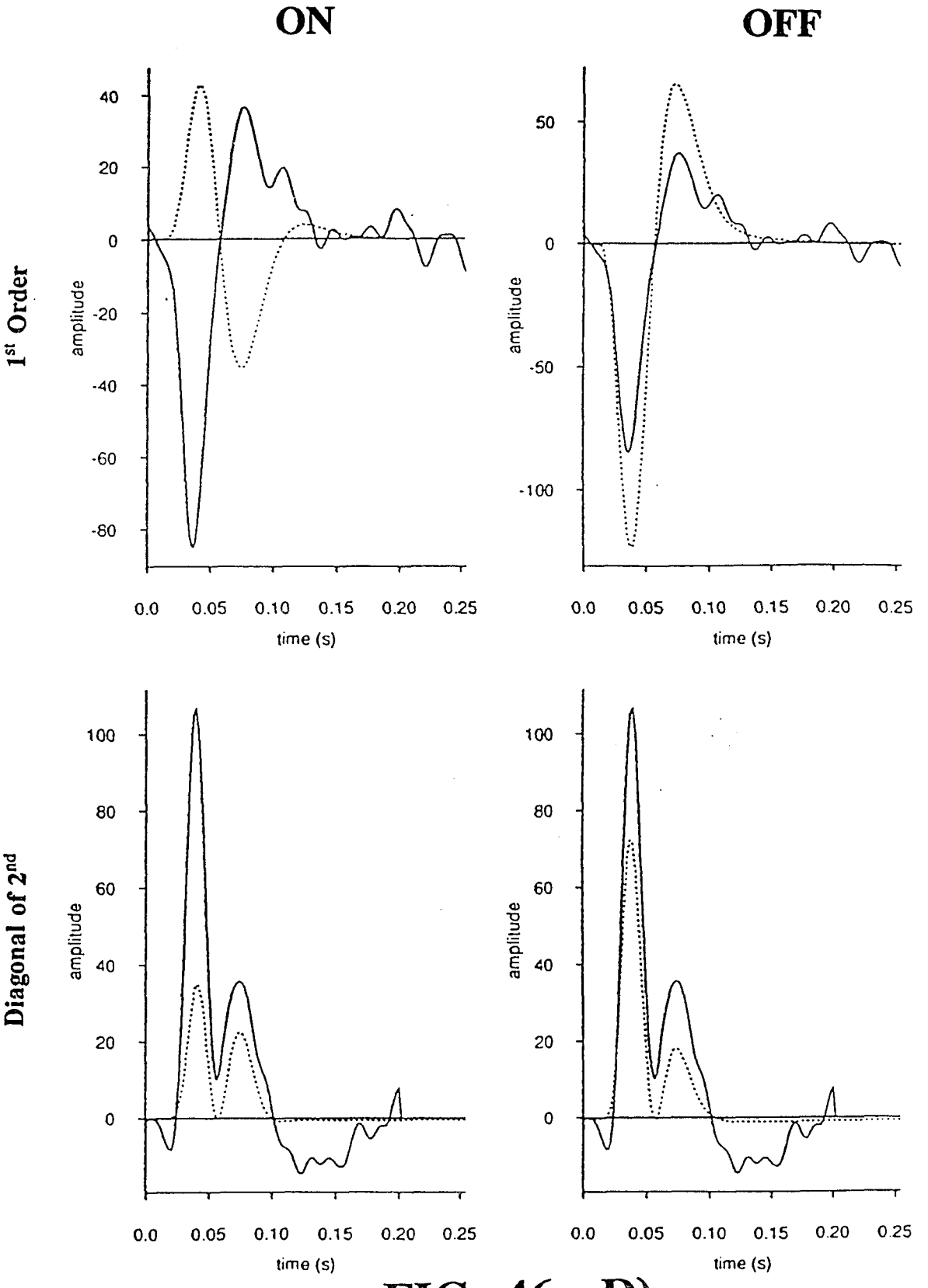
ON
OFF
1st Order
Diagonal of 2nd
amplitude
time (s)
40
20
0
-20
-40
-60
-80
50
-50
-100
100
80
60
0.0
0.05
0.10
0.15
0.20
0.25

FIG. 46 D)

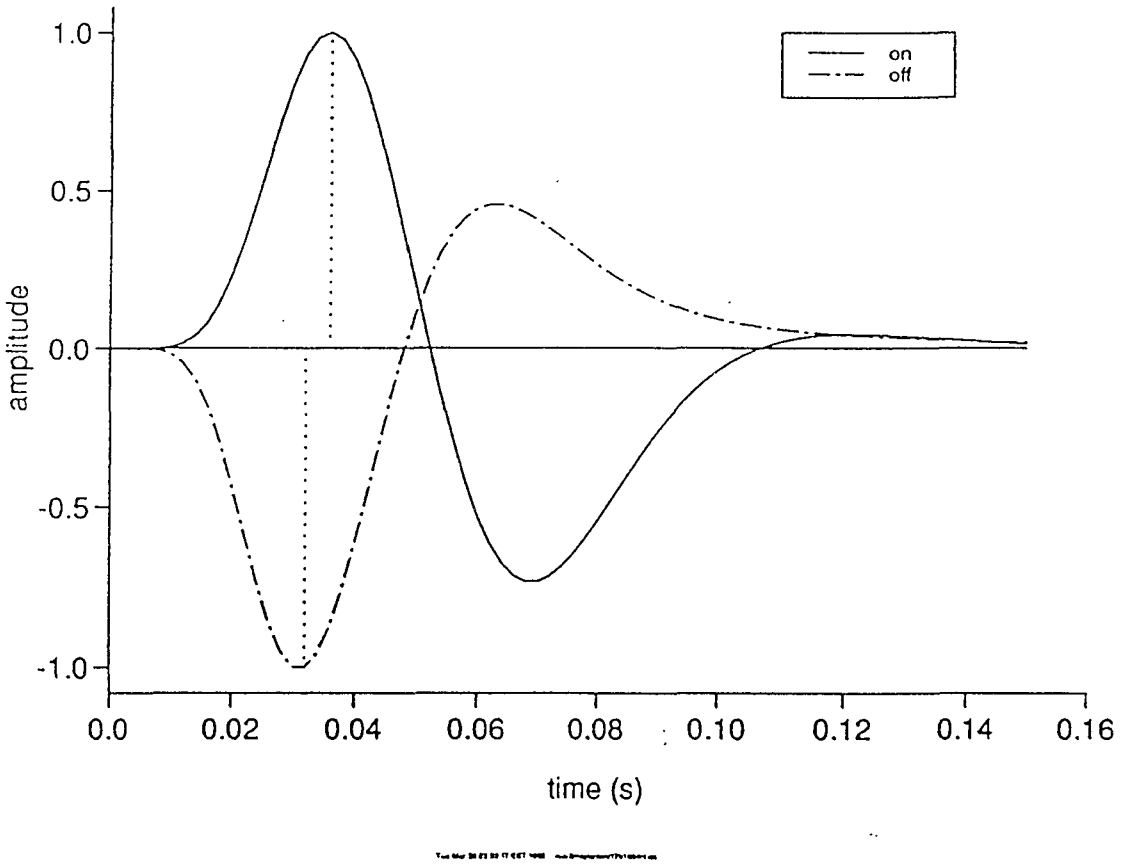
1.0
0.5
0.0
-0.5
-1.0
amplitude
on
off
0.0
0.02
0.04
0.06
0.08
0.10
0.12
0.14
0.16
time (s)

FIG. 46 E)

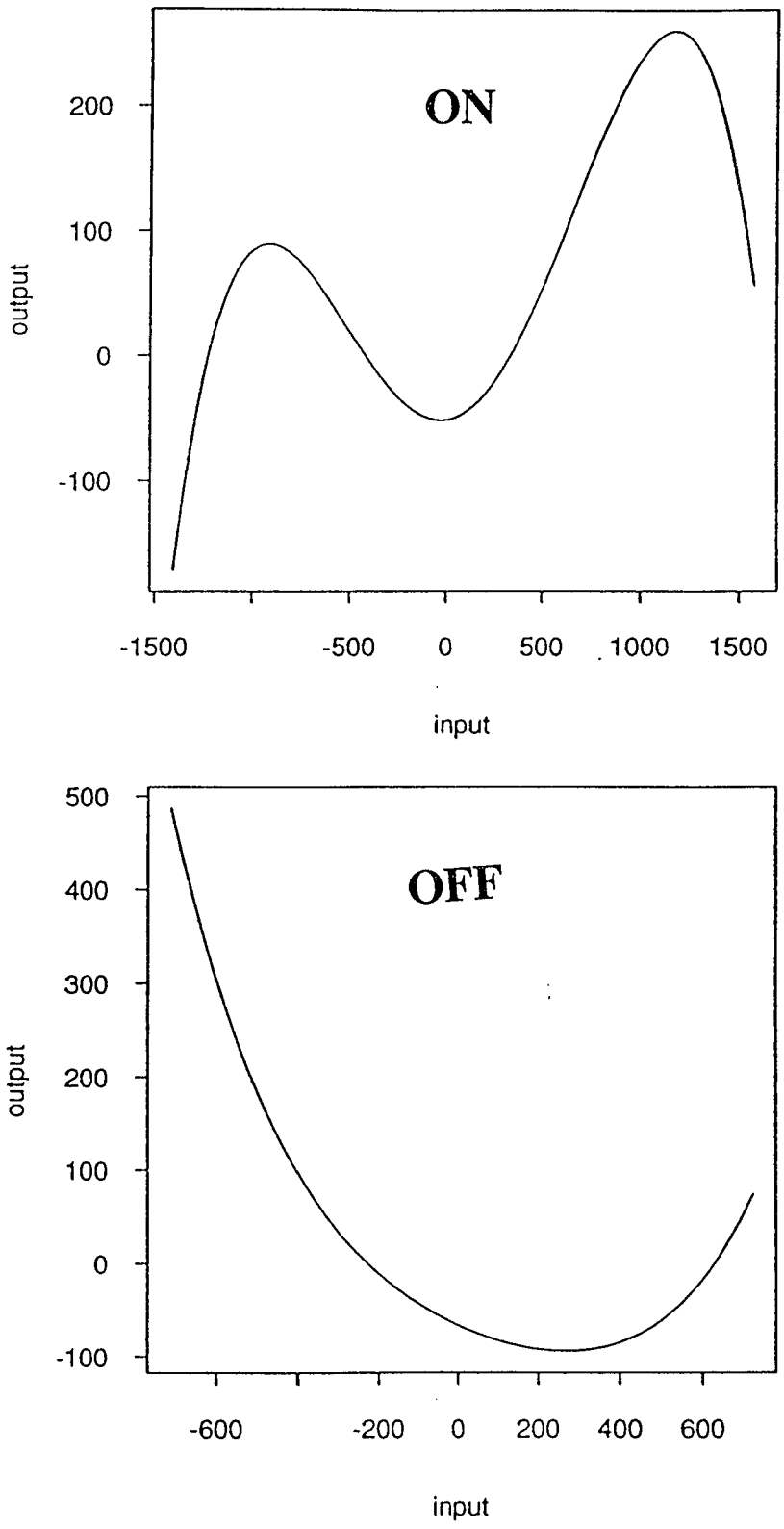
ON
200
100
0
-100
output
-1500
-500
0
500
1000
1500
input
OFF
500
400
300
200
100
0
-100
output
-600
-200
0
200
400
600
input

FIG. 46 F)

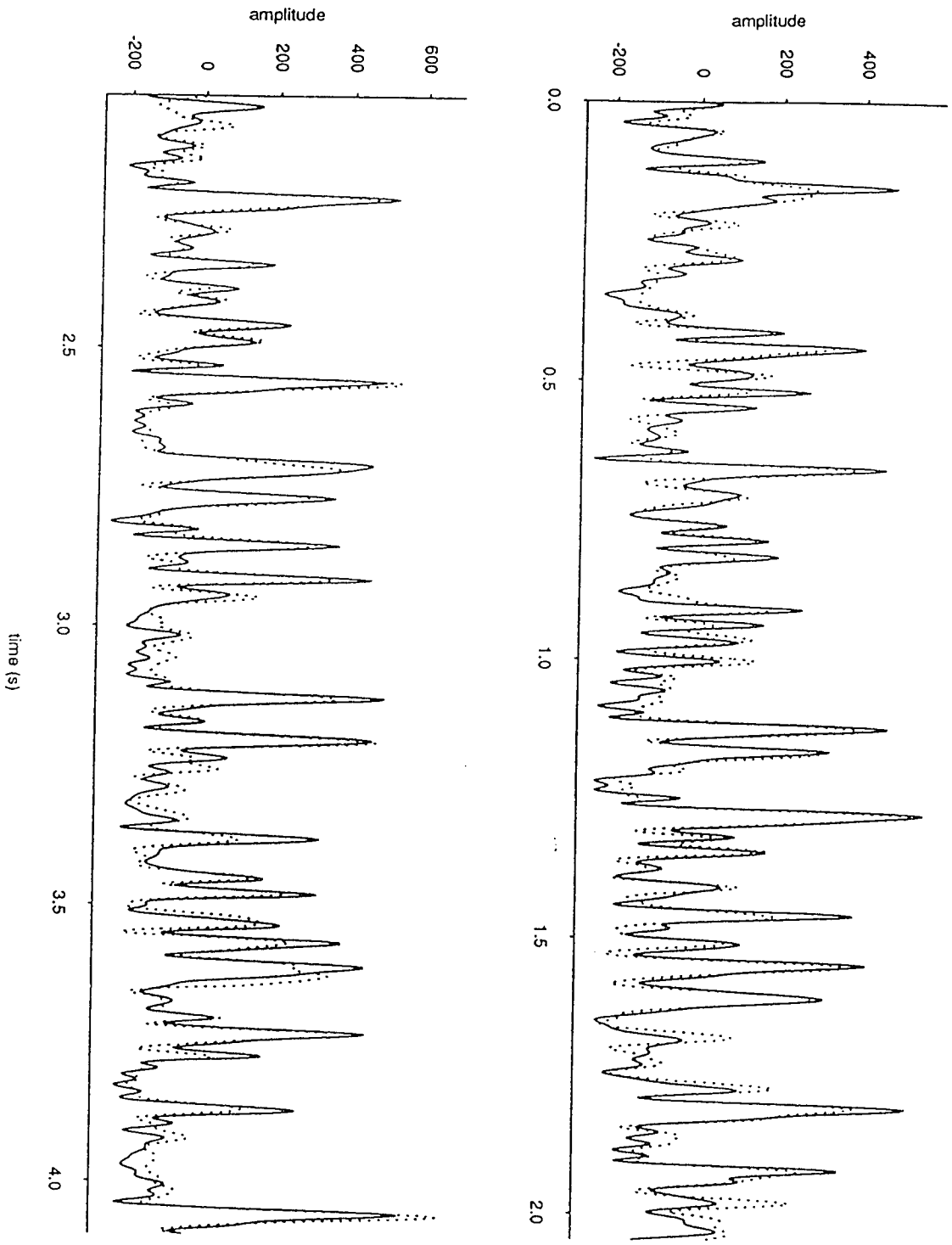
amplitude
-200
0
200
400
600
2.5
3.0
3.5
4.0
time (s)
amplitude
-200
0
200
400
0.0
0.5
1.0
1.5
2.0

FIG. 46 G)

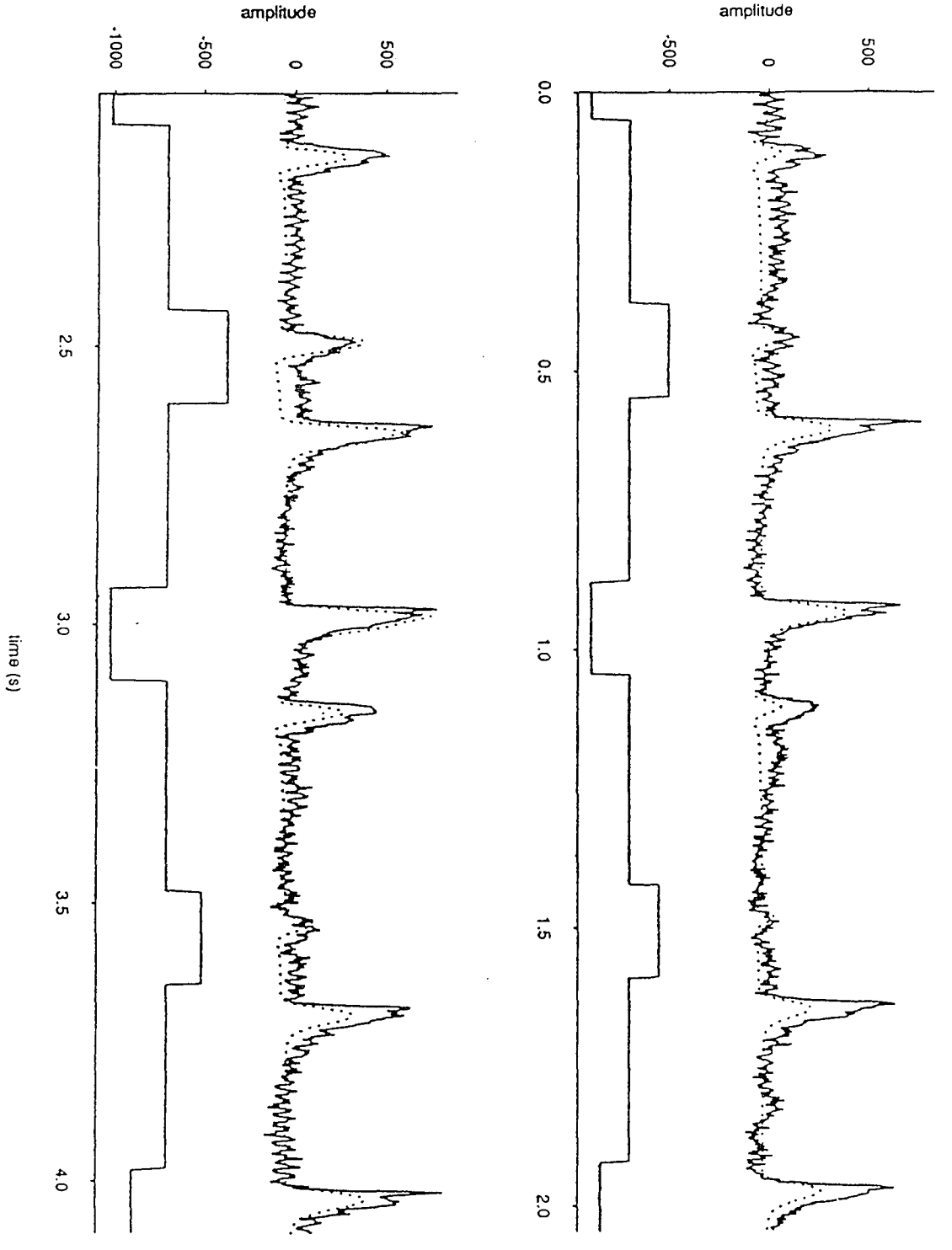
amplitude
-1000
-500
0
500
amplitude
-500
0
500
0.0
0.5
1.0
1.5
2.0
2.5
3.0
3.5
4.0
time (s)

FIG. 46 H)

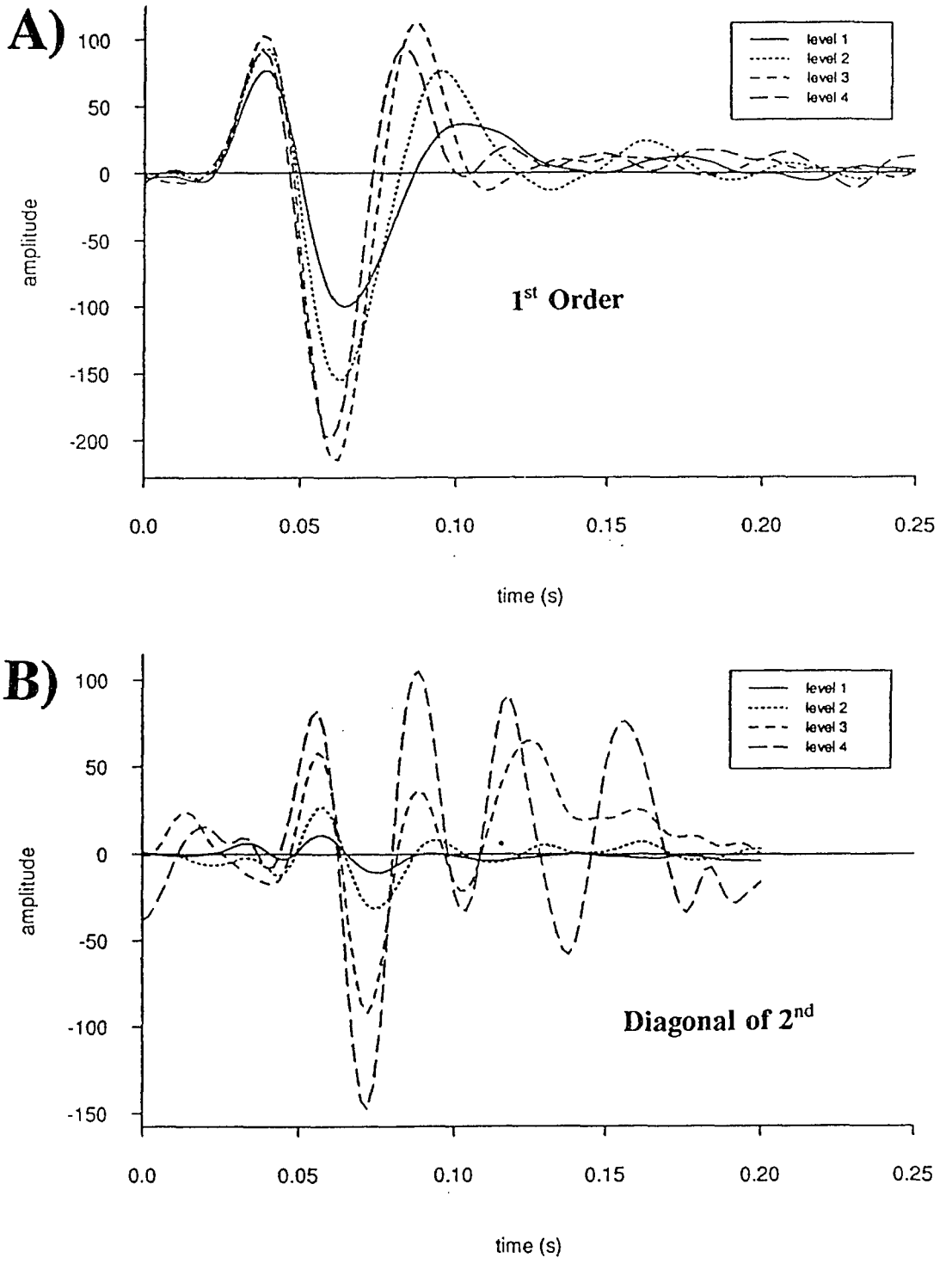

FIG. 47

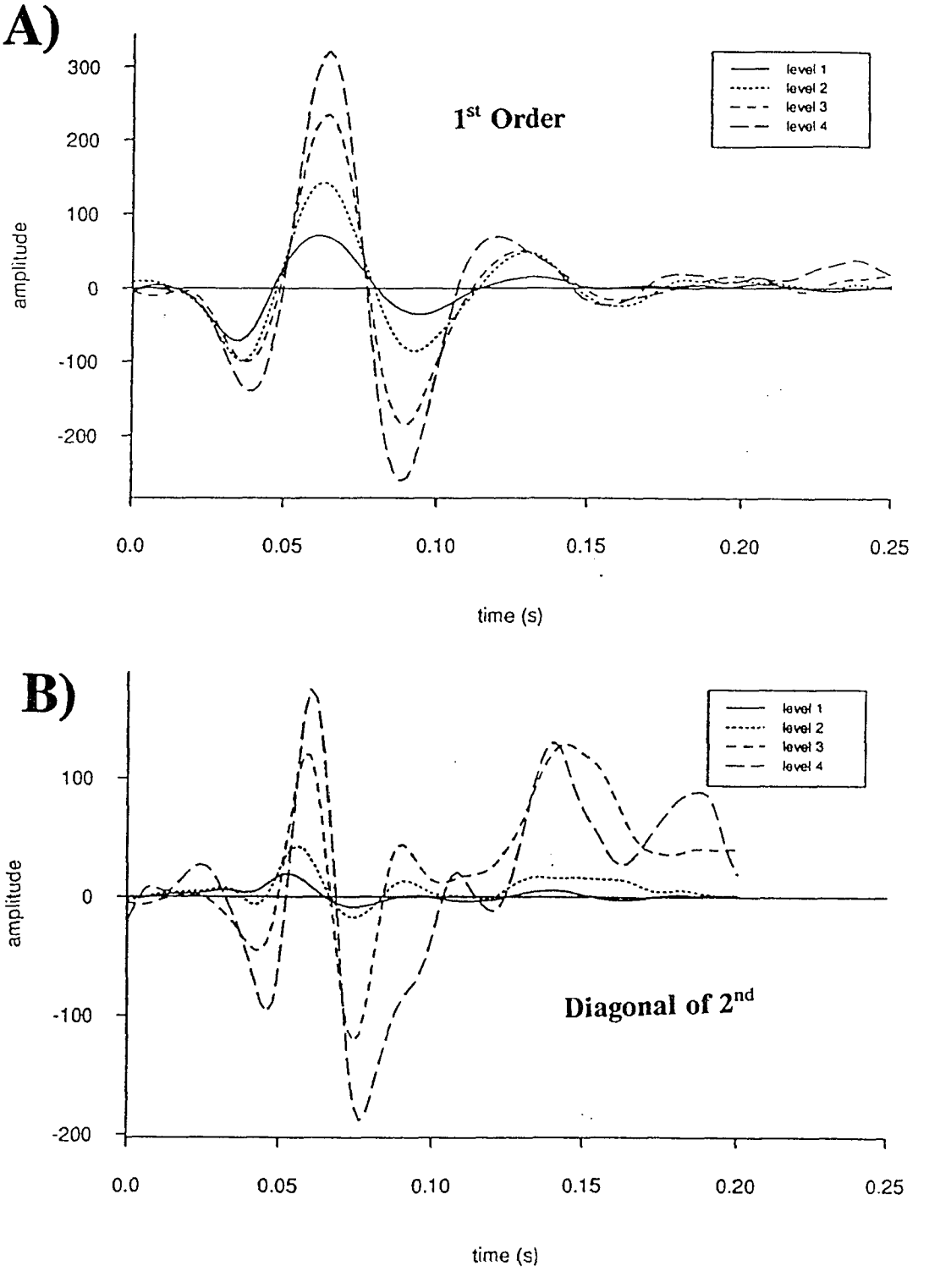

Mon Mar 29 16:05:52 EST 1993 ... /u/u3/naylor/n06031k2.ds

FIG. 48

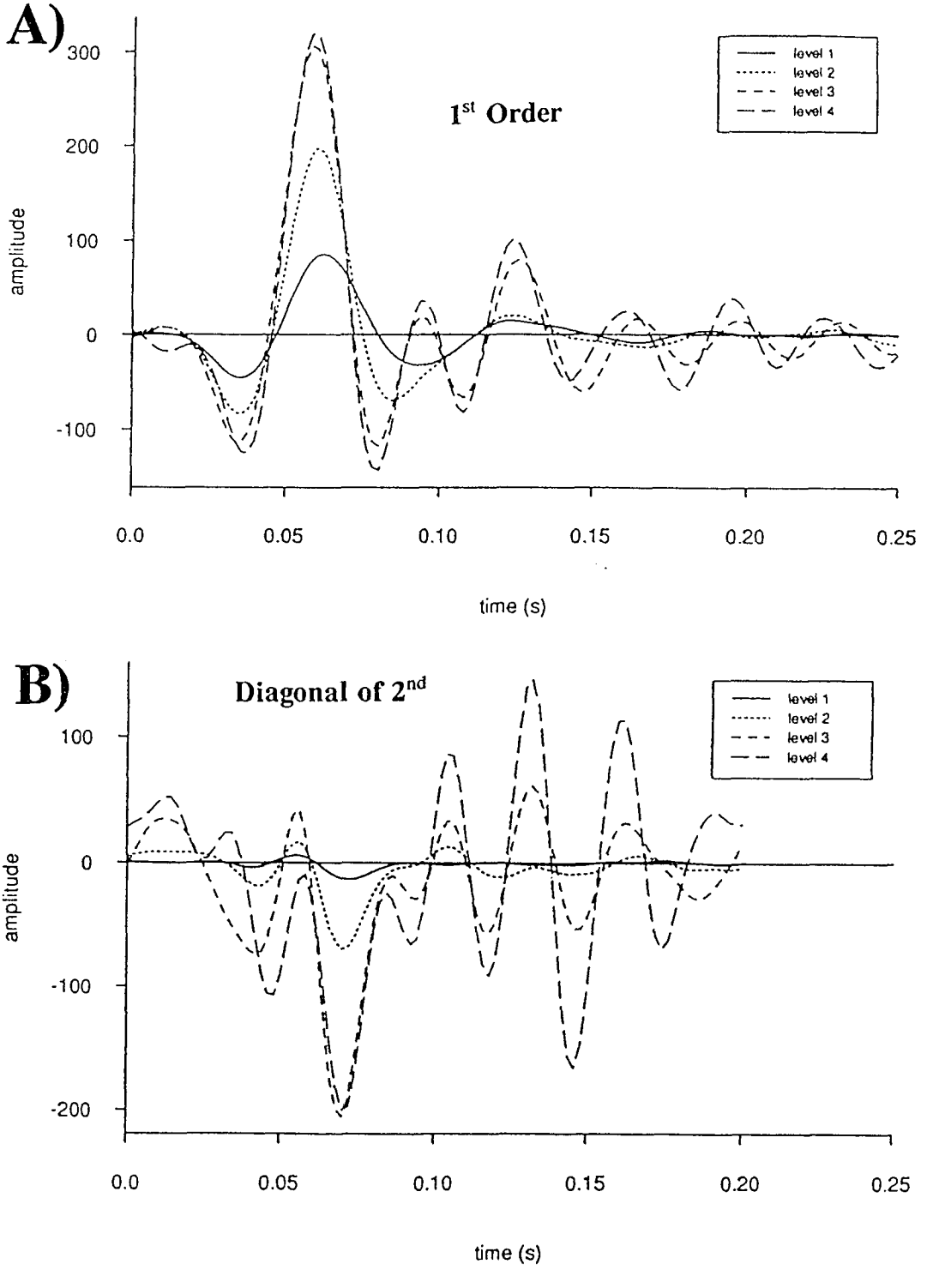

FIG. 49

Mon Mar 29 16:05:43 EST 1993 ... /u/u3/naylook/lrv/04003kd.da

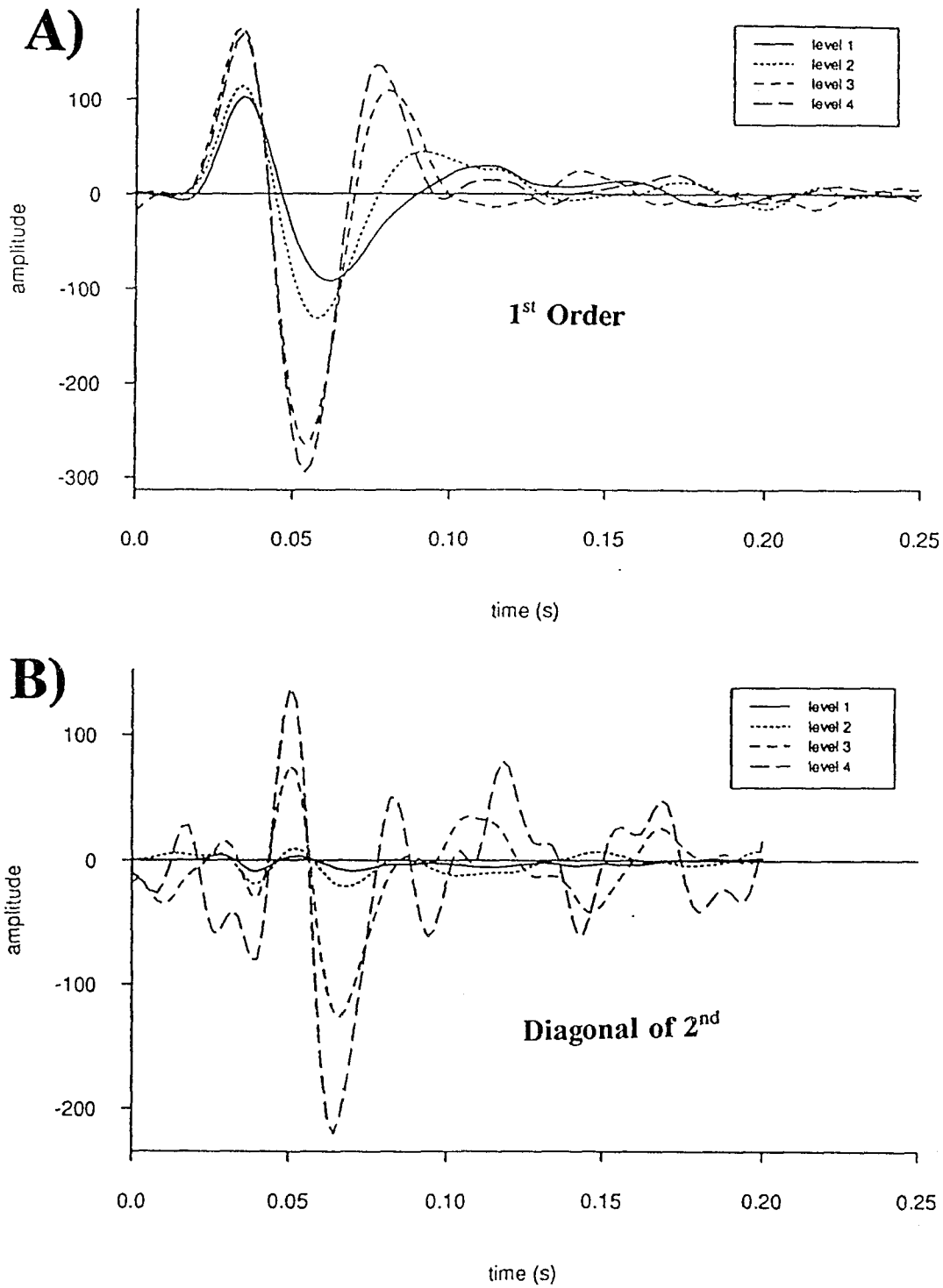
A)
level 1
level 2
level 3
level 4
100
0
-100
-200
-300
amplitude
1st Order
0.0
0.05
0.10
0.15
0.20
0.25
time (s)
B)
level 1
level 2
level 3
level 4
100
0
-100
-200
amplitude
Diagonal of 2nd
0.0
0.05
0.10
0.15
0.20
0.25
time (s)

FIG. 50

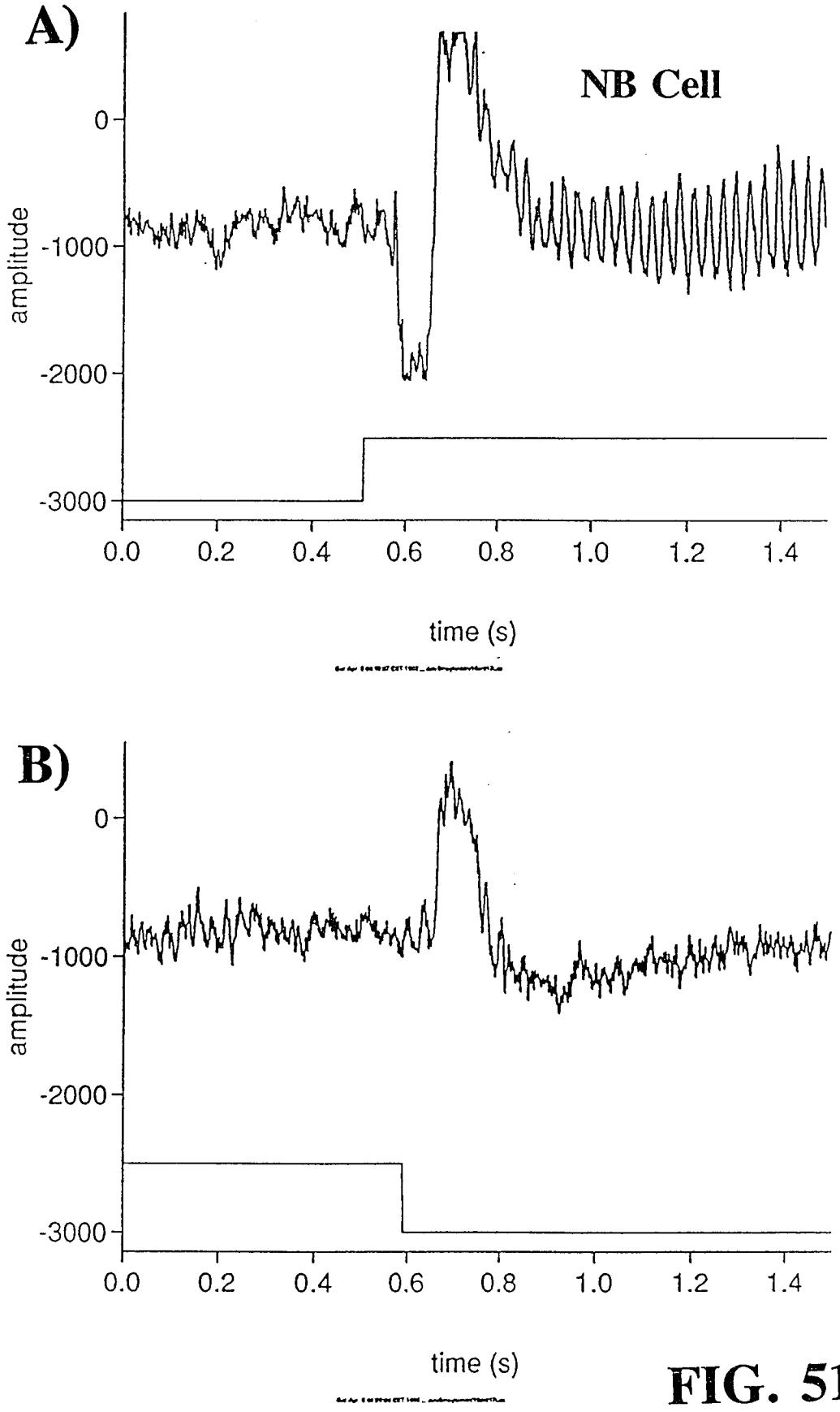
A)
NB Cell
0
-1000
-2000
-3000
amplitude
0.0
0.2
0.4
0.6
0.8
1.0
1.2
1.4
time (s)
B)
0
-1000
-2000
-3000
amplitude
0.0
0.2
0.4
0.6
0.8
1.0
1.2
1.4
time (s)

FIG. 51

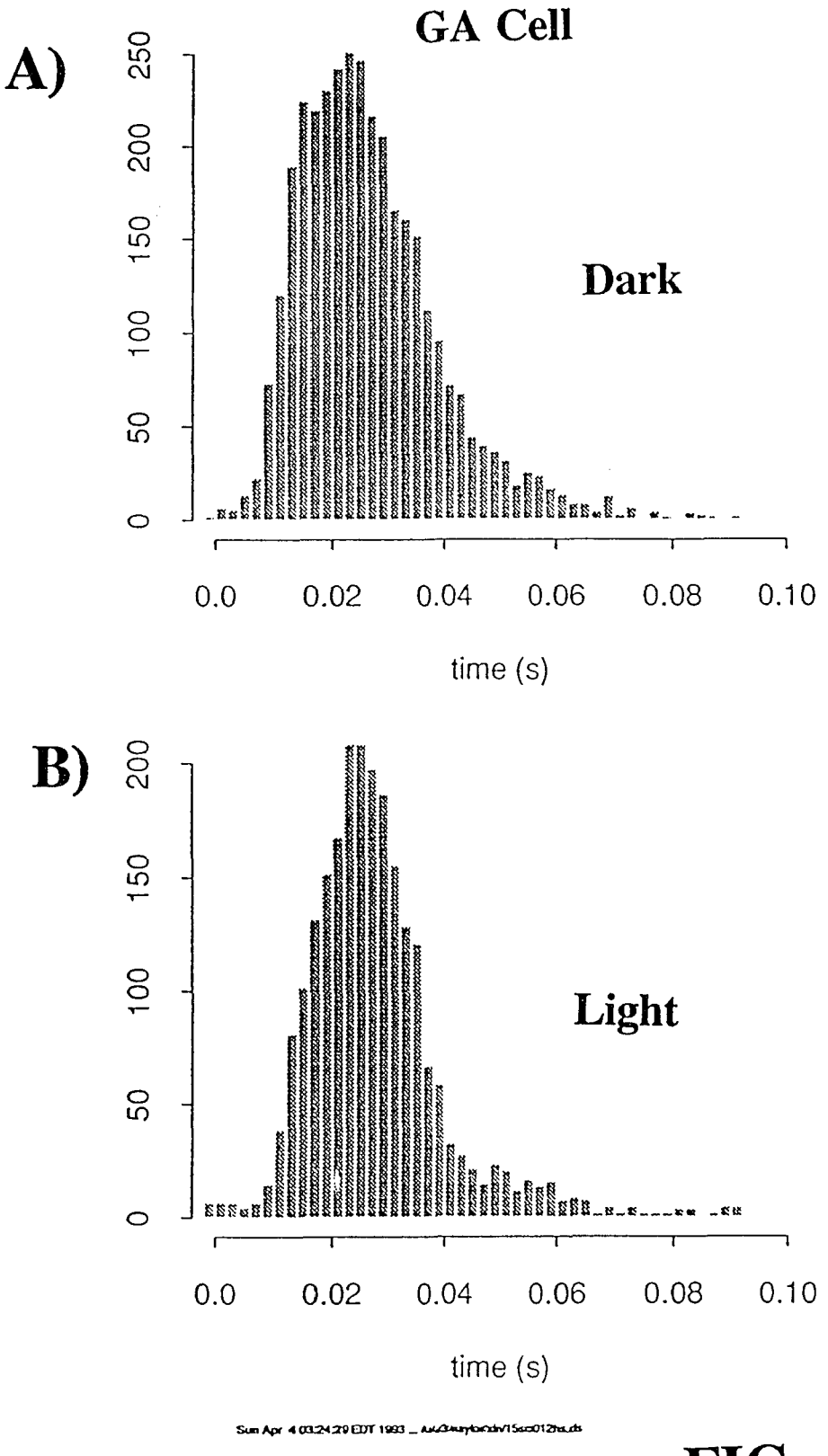
A)
GA Cell
Dark
0
50
100
150
200
250
0.0
0.02
0.04
0.06
0.08
0.10
time (s)
B)
Light
0
50
100
150
200
0.0
0.02
0.04
0.06
0.08
0.10
time (s)

FIG. 52

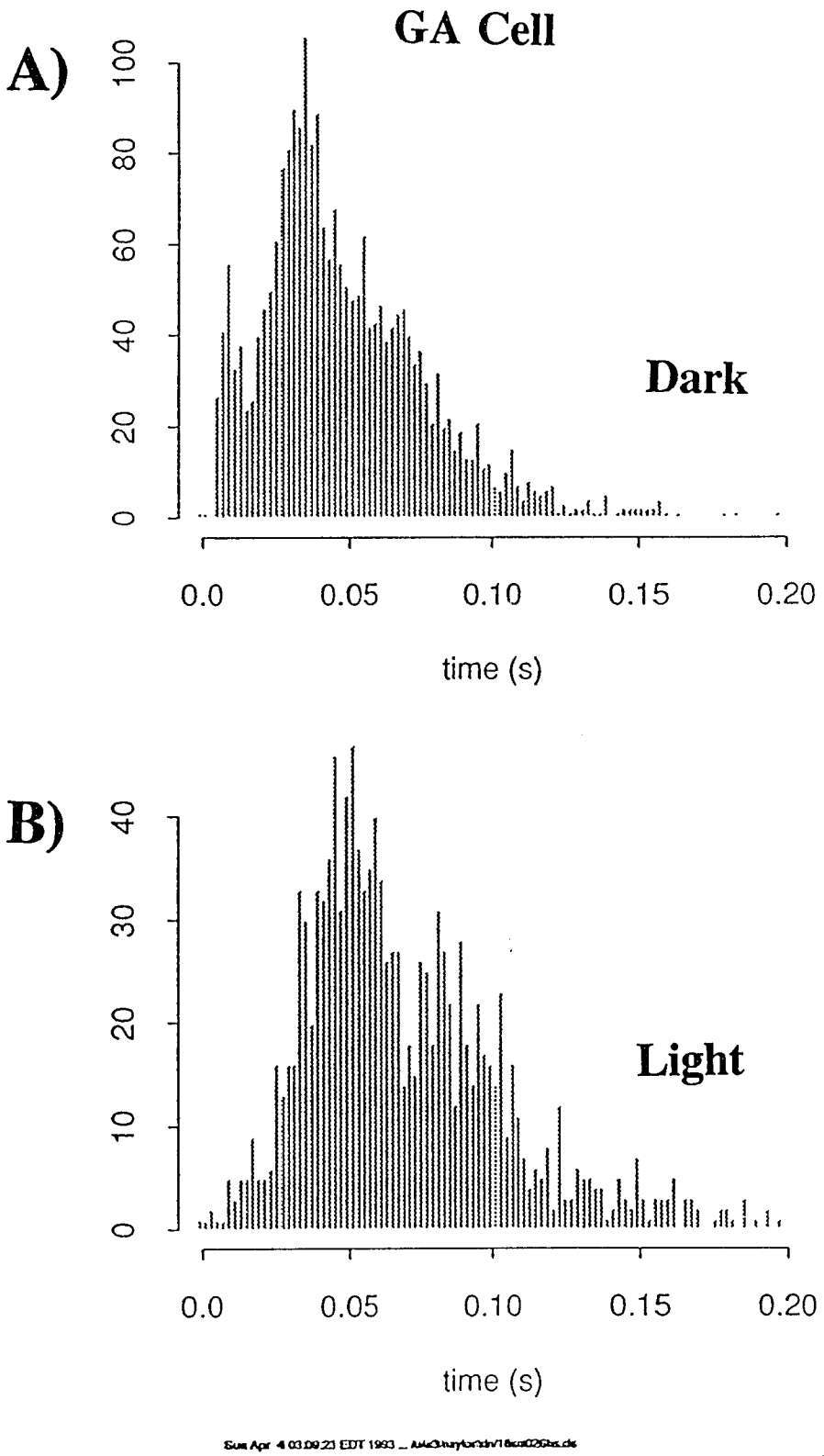
A)
GA Cell
Dark
0
20
40
60
80
100
0.0
0.05
0.10
0.15
0.20
time (s)
B)
Light
0
10
20
30
40
0.0
0.05
0.10
0.15
0.20
time (s)

FIG. 53

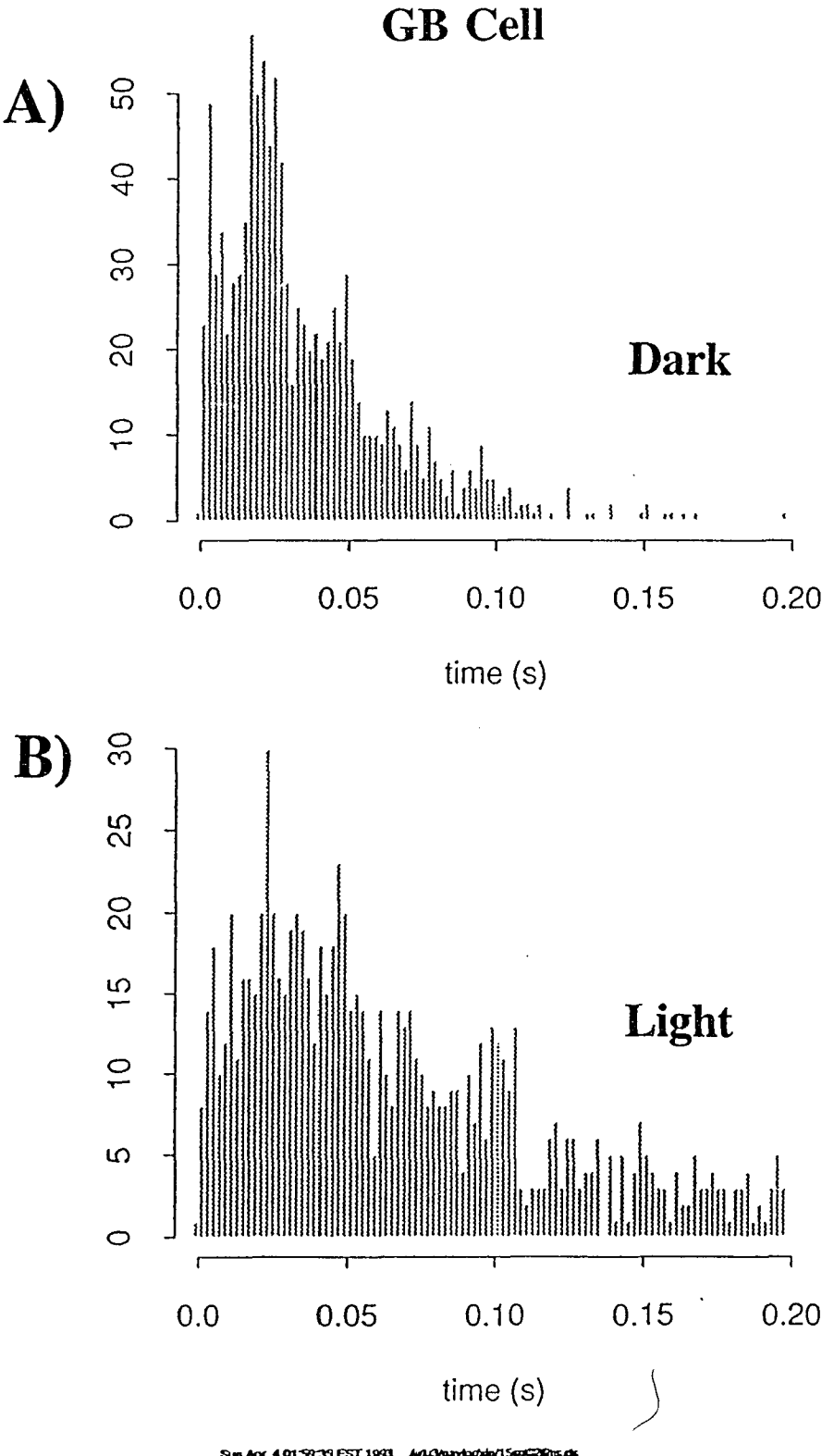
GB Cell
A)
0
10
20
30
40
50
Dark
0.0
0.05
0.10
0.15
0.20
time (s)
B)
0
5
10
15
20
25
30
Light
0.0
0.05
0.10
0.15
0.20
time (s)

FIG. 54

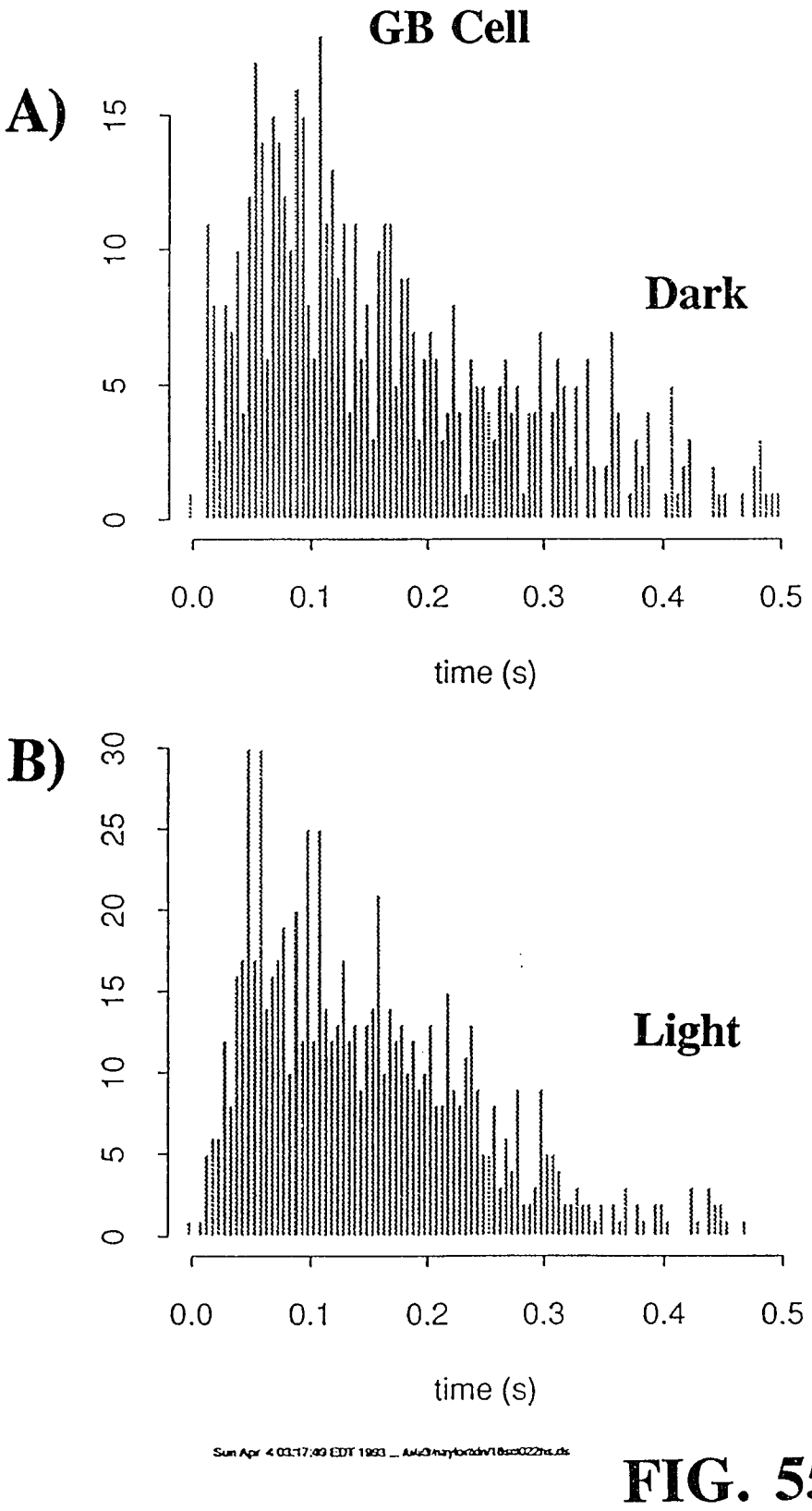
GB Cell
A)
Dark
0
5
10
15
0.0
0.1
0.2
0.3
0.4
0.5
time (s)
B)
Light
0
5
10
15
20
25
30
0.0
0.1
0.2
0.3
0.4
0.5
time (s)

FIG. 55

X. APPENDIX

A. The Mean of a Product of Gaussian Variables

The mean of a product of Gaussians plays an important role in the orthogonality and the kernel estimation of the Weiner functionals. One frequently used result is that for an odd product of independent Gaussian variables of zero mean, ζ_j:

$$E\{\zeta_1\zeta_2\cdot\cdot\zeta_{2m+1}\}=0.$$

Another important result is that for the even product,

$$E\{\zeta_1\zeta_2\cdot\cdot\zeta_{2m}\}=\Sigma\prod E\{\zeta_j\zeta_k\}$$

where the right side of the equation is the sum of the products of the means of all possible distinct pairings of the Gaussian variables (Schetzen, 1980).

The proof of these results involves the use of characterisitc functions. Basically, characteristic functions are Fourier transforms of probability density functions;

$$\Psi(\mathbf{t}^{\rightarrow})=\int_{-\infty}^{\infty}\int_{-\infty}^{\infty}\cdot\cdot\int_{-\infty}^{\infty}\exp(i\mathbf{t}^{\rightarrow\mathbf{T}}\cdot\mathbf{x}^{\rightarrow})f(\mathbf{x}^{\rightarrow})dx_1dx_2\cdot\cdot dx_n \text{ where } \mathbf{t}^{\rightarrow}=(t_1,t_2,..t_n)$$

$\mathbf{t}^{\rightarrow\mathbf{T}}$ is the transpose of $\mathbf{t}^{\rightarrow}$

and $\mathbf{x}^{\rightarrow}=(x_1,x_2,..x_n)$

They are useful because they can be expanded into an infinite series with the n^{th} term involving the n^{th} moment of x.

For example, taking derivatives for the particular case when x and t are single variables,

$\Psi^{(n)}(t) = i^n \int_{-\infty}^{\infty} x^n \exp(itx) f(x) dx$ and

$\Psi^{(n)}(0) = i^n \int_{-\infty}^{\infty} x^n f(x) dx = i^n \alpha_n$ where α_n is the n^{th} moment of x

Therefore, expanding as a Taylor series,

$$\Psi(t) = 1 + \alpha_1 it + \alpha_2 (it)^2/2! + \alpha_3 (it)^3/3! + \cdots$$

From probability theory, if the probability density function of two variables are the same, so are their characteristic functions and vice versa (Cramer, 1949). The basis for the present proof involves aligning the terms of two characteristic functions. Some of the n^{th} moment terms will involve the means of even and odd products of the Gaussian variables, x_j. Consequently, by equating the terms of the two characteristic functions, expressions for the means of products can be derived (Schetzen, 1980).

One of the characteristic functions will be of generic form, making no underlying assumption about the probability density function. The above series is an example for the single variable case. For multiple variables, the Taylor series expansion is

$$\Psi(t_1, t_2, .., t_n) = \sum_{k1=0}^{\infty} \sum_{k2=0}^{\infty} .. \sum_{kn=0}^{\infty} c_{k1k2..kn} t_1^{k1} t_2^{k2} .. t_n^{kn}$$

where

$$c_{k1k2..kn} = \frac{1}{(k1!k2!..kn!)} \frac{\partial^{k1}}{\partial t_1^{k1}} \frac{\partial^{k2}}{\partial t_2^{k2}} \ldots \frac{\partial^{kn}}{\partial t_n^{kn}} \Psi(t_1, t_2, .., t_n) \Big|_{t1=t2=..tn=0}$$

But,

$$\Psi(t_1, t_2, .., t_n) = E\{\exp[i(t_1 x_1 + t_2 x_2 + .. t_n x_n)]\}$$

so that

$$\frac{\partial^{k1}}{\partial t_1^{k1}} \frac{\partial^{k2}}{\partial t_2^{k2}} \ldots \frac{\partial^{kn}}{\partial t_n^{kn}} \Psi(t_1, t_2, .., t_n) \Big|_{t1=t2=..tn=0}$$

$$= E\{x_1^{k1}x_2^{k2}\cdot\cdot x_n^{kn}\}i^{k1}i^{k2}\cdot\cdot i^{kn}$$

Consequently,

$$\Psi(t_1,t_2,..,t_n)=\Sigma_{k1=0}^{\infty}\Sigma_{k2=0}^{\infty}\cdot\cdot\Sigma_{kn=0}^{\infty}\frac{1}{(k1!k2!\cdot\cdot kn!)}E\{x_1^{k1}x_2^{k2}\cdot\cdot x_n^{kn}\}i^{k1}i^{k2}\cdot\cdot i^{kn}t_1^{k1}t_2^{k2}\cdot\cdot t_n^{kn}$$

Note that the term for which $k_1=k_2=\cdot\cdot=k_n=1$ is

$$(**) \qquad E\{x_1x_2\cdot\cdot x_n\}i^n(t_1t_2\cdot\cdot t_n)$$

which has the product mean of Gaussians that is desired.

The characteristic function that has been expicitly derived for Gaussian variables will be compared to this one. In particular, for Gaussian variables with mean zero, the characteristic function would be

$$\Psi(\vec{t})=$$

$$\int_{-\infty}^{\infty}\int_{-\infty}^{\infty}\cdot\cdot\int_{-\infty}^{\infty}\exp(i\vec{t}^{T}\cdot\vec{x})\left[\frac{1}{(2\pi)^{n/2}\sigma_{11}\sigma_{22}\cdot\cdot\sigma_{nn}}\exp(-\tfrac{1}{2}\Sigma_{h=1}^{n}\Sigma_{l=1}^{n}x_hx_l/\sigma^2_{hl})\right]dx_1dx_2\cdot\cdot dx_n$$

where the term in brackets is the probability density function.

Now, allow the matrix $Q(x) = \Sigma_{h=1}^{n}\Sigma_{l=1}^{n}x_hx_l/\sigma_{hl}^2$ to be diagonalized as $D=S^{-1}QS$ so that there are no mixed 2nd moments x_hx_l, and the diagonal terms of D are $(1/\sigma'^2_j)$. This linear operation simplifies the expression of the 2nd moments and will later be reversed.

Now, $\Psi(t)$

$$=\prod_{j=1}^{n}\frac{1}{\sqrt{2\pi\sigma'^2_j}}\int_{-\infty}^{\infty}\exp(it_jx_j-\tfrac{1}{2}x_j^2/\sigma'^2_j)dx_j$$

$$=\prod_{j=1}^{n}\frac{1}{\sqrt{2\pi\sigma'^{2}_{j}}}\sum_{k=0}^{\infty}\frac{(it_j)^k}{k!}\left[\int_{-\infty}^{\infty}x^k\exp(-\tfrac{1}{2}x_j^2/\sigma'^{2}_{j})dx_j\right]$$

note that for odd k the integral in [ ] is over the entire range of a strictly odd function and hence vanishes. Furthermore, note that the operation of differentiating k times with respect to $u=1/\sigma^2$ (Cramer, 1949)

$$\int_{-\infty}^{\infty}\exp(-\tfrac{1}{2}y^2u)dy = \sqrt{2\pi}/u$$

gives

$$\int_{-\infty}^{\infty}y^{2k}\exp(-\tfrac{1}{2}y^2u)dy = \frac{(2k)!\sqrt{2\pi}\,u^{-\frac{1}{2}-k}}{(2^k k!)} = \frac{(2k)!\sqrt{2\pi}\,\sigma^{2(\frac{1}{2}+k)}}{(2^k k!)}$$

so, continuing

$$=\prod_{j=1}^{n}\frac{1}{\sqrt{2\pi\sigma'^{2}_{j}}}\sum_{k=0}^{\infty}\frac{(it_j)^{2k}}{(2k)!}\cdot\left[\int_{-\infty}^{\infty}x^{2k}\exp(-\tfrac{1}{2}x_j^2/\sigma'^{2}_{j})dx_j\right]$$

$$=\prod_{j=1}^{n}\frac{1}{\sqrt{2\pi\sigma'^{2}_{j}}}\sum_{k=0}^{\infty}\frac{(it_j)^{2k}}{(2k)!}\cdot\left[\frac{(2k)!\sqrt{2\pi}\,\sigma'^{2(\frac{1}{2}+k)}_{j}}{(2^k k!)}\right]$$

$$=\prod_{j=1}^{n}\frac{1}{\sqrt{2\pi\sigma'^{2}_{j}}}\sum_{k=0}^{\infty}\frac{(-\frac{1}{2}t_j^2\sigma'^{2}_{j})^k}{k!}\cdot\sqrt{2\pi}\sigma'_j$$

$$=\prod_{j=1}^{n}\exp(-\tfrac{1}{2}t_j^2\sigma'^{2}_{j})$$

$$=\exp(-\tfrac{1}{2}\sum_{j=1}^{n}t_j^2\sigma'^{2}_{j})$$

Now, converting back to Q with the operation SDS^{-1}, the result is

$$\Psi(t_1,t_2,..,t_n) = \exp(-\tfrac{1}{2}\sum_{h=1}^{n}\sum_{l=1}^{n}E\{x_hx_l\}t_ht_l) \text{ using } E\{x_hx_l\}=\sigma_{hl}^2$$

Expanding this exponential as a Taylor series,

$$\Psi(t_1,t_2,..,t_n)$$

$$=\sum_{k=0}^{\infty}(1/k!)(-\tfrac{1}{2})^k\left[\sum_{h=1}^{n}\sum_{l=1}^{n}E\{x_hx_l\}t_ht_l\right]^k$$

$$= 1 + (-\tfrac{1}{2})[\Sigma_{h=1}^{n}\Sigma_{l=1}^{n}E\{x_h x_l\}t_h t_l]$$

$$+ (1/2!)(-\tfrac{1}{2})^2[\Sigma_{i=1}^{n}\Sigma_{j=1}^{n}\Sigma_{h=1}^{n}\Sigma_{l=1}^{n}E\{x_i x_j\}E\{x_h x_l\}t_i t_j t_h t_l] + \ldots$$

By comparing the terms of this Gaussian characteristic function with the appropriate terms of the general characteristic function (**) containing the product $t_1 t_2 \cdots t_n$, the absence of any terms with odd products $t_1 t_2 \cdots t_{2m+1}$ in the former is apparent. Thus,

$$E\{x_1 x_2 \cdots x_{2m+1}\} = 0.$$

For the even products, $t_1 t_2 \cdots t_{2m}$, the k=m series terms of the Gaussian characteristic function are used

$$(1/m!)(-\tfrac{1}{2})^m[\Sigma_{i1=1}^{n}\Sigma_{i2=1}^{n}\cdots\Sigma_{i(2m-1)=1}^{n}E\{x_{i1}x_{i2}\}\cdots E\{x_{i(2m-1)}x_{i2m}\}t_{i1}t_{i2}\cdots t_{i2m}]$$

The terms that are desired have $i1 \neq i2 \neq \cdots \neq i2m$ giving

$$(1/m!)(-\tfrac{1}{2})^m[(t_1 t_2 \cdots t_{2m})\Sigma E\{x_{i1}x_{i2}\}\cdots E\{x_{i(2m-1)}x_{i2m}\}]$$

where the sum is for $i1 \neq i2 \neq \cdots \neq i2m$. Since

(a) $E\{x_i x_j\} = E\{x_j x_i\}$ and (b) $E\{x_i x_j\}E\{x_k x_l\} = E\{x_k x_l\}E\{x_i x_j\}$,

there are many terms that are identical. For consideration of (a) there are m pairs, each of which has 2 possible positions, hence 2^m identical configurations. In (b), there are m! permutations of factoring order for m pairs. Thus, the m^{th} term can be expressed as

$$(2^m m!)\ (1/m!)(-\tfrac{1}{2})^m[(t_1 t_2 \cdots t_{2m})\Sigma\textstyle\prod E\{x_i x_j\}]$$

$$= (-1)^m[(t_1 t_2 \cdots t_{2m})\Sigma\textstyle\prod E\{x_i x_j\}]$$

where the sum is over all distinct ways of forming the product of means. Thus, be equating this term with (**),

$$E\{x_1 x_2 \cdots x_{2m}\} = \Sigma\prod E\{x_i x_j\}$$

As a final note, the number of distinct factorings of pairs for the m^{th} series term can be given as $(2m)!/(2^m m!)$. $(2m)!$ represents the number of ensembles of $2m$ individual elements and the denominator accounts for the pairing considerations as discussed above.

B. Mean Square Error (MSE)

$$\text{MSE} = \frac{\int_0^\infty [y(t) - y_m(t)]^2 dt}{\int_0^\infty [y(t)]^2 dt}$$

where y(t) is the actual response and $y_m(t)$ is the model response.

C. Analytic Forms for L_1-N-L_2 Model

i)

$$y(t) = \sum_{m=0}^{\infty} G_m[h_m(t_0, ..., t_m); x(t'), t' \leq t],$$

where

$$E[x(t)x(t)] = P$$

The first three Wiener functionals are:

$$G_0[h_0; x(t)] = h_0,$$

where

$$h_0 = \overline{y(t)}.$$

$$G_1[h_1; x(t)] = \int_0^{\infty} h_1(t_1)x(t - t_1)dt_1,$$

where

$$h_1(t_1) = (1/P)E[y(t)x(t - t_1)].$$

$$G_2[h_2; x(t)] = \int_0^{\infty} \int h_2(t_1, t_2)x(t - t_1)x(t - t_2)dt_1 dt_2 - P \int_0^{\infty} h_2(t_1, t_1)\, dt_1.$$

where

$$h_2(t_1, t_2) = \frac{1}{2P^2}E[\{y(t) - h_0\}x(t - t_1)x(t - t_2)].$$

ii)

$$h_1(t_1) = \int_0^{\infty} [l_1^{on}(t) + l_1^{off}(t)]l_2(t_1 - t)\, dt \overset{\mathcal{F}}{\Leftrightarrow} [L_1^{on}(\omega) + L_1^{off}(\omega)]L_2(\omega)$$

$$h_2(t_1, t_2) = \int_0^{\infty} [l_1^{on}(t_1 - t)l_1^{on}(t_2 - t) + l_1^{off}(t_1 - t)l_1^{off}(t_2 - t)]l_2(t)\, dt$$

On the diagonal

$$d(t_1) \equiv h_2(t_1, t_1)$$

$$= \int_0^{\infty} [\{l_1^{on}(t_1 - t)\}^2 + \{l_1^{off}(t_1 - t)\}^2]l_2(t)\, dt \overset{\mathcal{F}}{\Leftrightarrow} [Lsqr_1^{on}(\omega) + Lsqr_1^{off}(\omega)]L_2(\omega)$$

iii)

$$L_1^{on}(\omega) \equiv B_1^{on}(\omega)B_2(\omega)$$
$$L_1^{off}(\omega) \equiv B_1^{off}(\omega)B_2(\omega),$$

where

$$B_1^{on}(\omega) = k_1 \frac{(1+i\omega\tau_1)}{(1+i\omega\tau_2)(1+i\omega\tau_3)^n} \text{ with } k_1 > 0;$$
$$B_1^{off}(\omega) = k_2 \frac{(1+i\omega\tau_1')}{(1+i\omega\tau_2')(1+i\omega\tau_3')^n} \text{ with } k_2 < 0;$$
$$B_2(\omega) = \frac{(1+i\omega\tau_1'')}{(1+i\omega\tau_2'')};$$
$$L_2(\omega) = k_3 \frac{(1+i\omega\tau_1''')}{(1+i\omega\tau_2''')(1+i\omega\tau_3''')^n} \text{ with } k_3 > 0;$$

A saturating exponential nonlinearity was of the form:

$$N_i(z_i) = A_i \frac{\exp(z_i/b_i)}{1 + c_i \exp(z_i/b_i)}.$$

i) Equations for Wiener functionals, G_n, and white noise method of calculation of kernels, h_n.

ii) Predicted analytic forms for the 1st order Wiener kernel and the diagonal of the 2nd order kernel.

iii) Analytic representation of L_1^{on}, L_1^{off}, B_1^{on}, B_1^{off}, B_2, L_2, and a form for a saturating nonlinearity that was occasionally used.

XI. BIBLIOGRAPHY

Arkin, M. S. and Miller, R. F. Subtle actions of 2-amino-4-phosphonobutyrate (APB) on the OFF pathway in the mudpuppy retina. Brain Res. 426:142, 1987.

Arkin, M. S. and Miller, R. F. Bipolar origin of synaptic inputs to sustained off-ganglion cells in the mudpuppy retina. J. Neurophysiol. 60(3):1122-1142,1988.

Arkin, M. S. and Miller, R. F. Synaptic inputs and morphology of sustained on-ganglion cells in the mudpuppy retina. J. Neurophysiol. 60(3):1143-1159,1988.

Attwell, D., Borges, S., Wu, S. and Wilson, M. Signal clipping by the rod output synapse. Nature 328:522-524, 1987.

Bai, S. and Slaughter, M. M. Effects of baclofen on transient neurons in the mudpuppy retina: Electrogenic and network actions. J. Neurophys. 61:382-390, 1989.

Barnes, S. and Werblin, F. Gated currents generate single spike activity in amacrine cells of the tiger salamander retina. Proc. Natl. Acad. Sci. USA. 83:1509-1512,1986.

Barnes, S. and Werblin, F. Direct excitatory and lateral inhibitory synaptic inputs to amacrine cells in the tiger salamander retina. Brain Res. 406:233-237, 1987.

Belgum, J., Dvorak, D. and McReynolds, J. Strychnine blocks transient but not sustained inhibition in mudpuppy retinal ganglion cells. J. Physiol.(Lond.) 354:273-286, 1984.

Belgum, J. and Copenhagen, D. Synaptic transfer of rod signals to horizontal and bipolar cells in the retina of the toad (bufo marinus). J. Physiol. 396:225-245,1988.

Bloomfield, S. A. and Dowling, J. E. Roles of aspartate and glutamate in synaptic transmission in rabbit retina. II. Inner plexiform layer. J. Neurophysiol. 53(3):714-725,1985.

Cohen, A. Effects of oscillator frequency on phase-locking in the lamprey central pattern generator. J. Neurosci. Meth. 21:113,1987.

Cramer, H. Mathematical Methods of Statistics. Princeton University Press, Princeton, 1946.

Crick, F. Function of the thalamic reticular complex: The searchlight hypothesis. Proc. Natl. Acad. Sci. USA. 81:4586,1984.

Cunningham, J. R., Dawson, C. and Neal, M. J. Evidence for a cholinergic inhibitory feed-back mechanism in the rabbit retina. J. Physiol. 340:455-468,1983.

Dacheux, R. F., Frumkes, T. E. and Miller, R. F. Pathways and polarities of synaptic interactions in the inner retina of the mudpuppy: I. Synaptic blocking studies. Brain Res. 161:1-12, 1979.

Dacheux, R. F. and Raviola, E. The rod pathway in the rabbit retina: A depolarizing bipolar and amacrine cell. J. Neurosci. 6(2):331-345,1986.

Dixon, D. B. and Copenhagen, D.R. Two types of glutamate receptors differentially excite amacrine cells in the tiger salamander retina. J. Physiol. 449:589-606,1992

Eldred, W. D. and Cheung, K. Immunocytochemical localization of glycine in the retina of the turtle (Pseudemys scripta). Visual Neurosci. 2:331-338,1989.

Eliasof, S. Barnes, S. and Werblin, F. The interaction of ionic currents mediating single spike activity in retinal amacrine cells of the tiger salamander. J. Neurosci. 7(11):3512-3524, 1987.

Fain, G. L. The threshold signal of photoreceptors. *In* Vertebrate Photoreceptors, ed. Barlow, H. B. Academic, London, pp. 305-323,1977 .

Falk, G. and Fatt, P. Physical changes induced by light in the rod outer segment of vertebrates. In Handbook of Sensory Physiology. Photochemistry of Vision, H.J.A. Dartnall,editor. Springer, Berlin. 7(1):200-244,1972.

Famiglietti, E. V. Jr. 'Starburst' amacrine cells and cholinergic neurons: mirror-symmetric On and Off amacrine cells of rabbit retina. Brain Res. 261:138-144,1983.

Freeman, W. J. Measurement of oscillatory responses to electrical stimulation in olfac tory bulb of cat. J. Neurophysiol. 35:780-796,1972.

Freeman, W. J. A model for mutual excitation in a neuron population in olfactory bulb. Trans. IEEE Biomed. Engin. 21:350-358,1974a.

Freeman, W. J. Stability characteristics of positive feedback in a neural population. Trans. IEEE Biomed. Engin. 21:358-364,1974b.

Frumkes, T. E. and Miller, R. F. Pathways and polarities of synaptic interactions in the inner retina of the mudpuppy: II. insight revealed by an analysis of latency and threshold. Brain Res. 161:13-24,1979.

Frumkes, T. E., Miller, R. F. Slaughter, M. and Dacheux, R. F. Physiological and pharmacological basis of GABA and glycine action on neurons of mudpuppy retina. III. Amacrine-mediated inhibitory influences on ganglion cell receptive-field organization: a model. J. Neurophysiol. 45(4):783-804,1981.

Getchell, T. V. and Shepherd, G. M. Short-axon cells in the olfactory bulb: dendrodendritic synaptic interaction. J. Physiol.(London). 251:523-548,1975.

Gottesman, J. and Miller, R. F. Pharmacological properties of N-methyl-D-aspartate receptors on ganglion cells of an amphibian retina. J. Neurophysiol. 68(2):596-604,1992.

Grad, H. Note on N-dimensional Hermite polynomials. Commun. Pure Appl. Math. 2:325-330,1949.

Heidelberger, R. and Matthews, G. Inhibition of calcium influx and calcium current by γ-aminobutyric acid in single synaptic terminals. Proc. Natl. Acad. Sci. USA. 88:7135-7139,1991.

Hosokawa, Y. and Naka, K.-I. Spontaneous membrane fluctuations in catfish type-N cells. Vision Res. 25(4):539-542,1985.

Huba, R. and Hoffmann, H.-D. Transmitter-gated currents of GABAergic amacrine-like cells in chick retinal cultures. Vis. Neurosci. 6:303-314,1991.

Immamura, T., Meecham, W. C., and Siegel, A. Symbolic calculus of the Wiener Process and Wiener-Hermite functionals. J. Math. Phys. 6(5):695-706.

Jager, J. and Wassle, H. Localization of glycine uptake and receptors in the cat retina. Neurosci. Lett. 75:147-151, 1987.

Jardon, B., Yucel, H. and Bonaventure, N. Glutamergic separation of ON and OFF retinal channels: possible modulation by glycine and acetylcholine. Eur. J. Pharmacol. 162:215, 1989.

Jardon, B., Bonaventure, N. and Scherrer E. Possible involvement of cholinergic and glycinergic amacrine cells in the inhibition exerted by the On retinal channel on the Off retinal channel. Eur. J. Pharm. 210:201-207,1992.

Kandel, E. R. and Schwartz, J. H. Principles of Neural Science. Elsevier, New York, 1985.

Kaneko, A. and Tachibana M. GABA mediates the negative feedback from amacrine to bipolar cells. Neurosci. Res. Suppl. 6:s239-s252,1987.

Katz, B. The transmission of impulses from nerve to muscle, and the subcellular unit of synaptic action. Proc. R. Soc. Lond. B 155:455-79,1962.

Katz, B. and Miledi, R. A study of synaptic transmission in the absence of nerve impulses. J. Physiol. (Lond.) 192:407-436,1967.

Kondo, H. and Toyoda, J.-I. GABA and glycine effects on the bipolar cells of the carp retina. Vision Res. 23(11);1259-1264,1983.

Krausz, H. I. and Naka, K.-I. Spatiotemporal testing and modeling of catfish retinal neurons. Biophys. J. 29:13-36,1980.

Kujiraoka, T., Saito, T. and Toyoda, J. Analysis of synaptic inputs to on-off amacrine cells of the carp retina. J. Gen. Physiol. 92:475-487,1988.

Lee, Y. W. and Schetzen, M. Measurement of the Wiener kernels of a nonlinear system by cross-correlation. Int. J. Control. 2:237-254,1965.

Liley, A. W. The effects of presynaptic polarization on the spontaneous activity at the mammalian neuromuscular junction. J. Physiol. 134:427-43,1956.

Lin, D. M., Blazynski, C., Redburn, D. and Massey, S. Acetylcholine release from the rabbit retina mediated by kainate receptors. J. Neurosci. 11(1):111-122, 1991.

Lin, D. M. and Massey, S. C. Acetylcholine release from the rabbit retina mediated by NMDA receptors. J. Neurosci. 11(1):123-133, 1991.

Llinas, R., Steinberg, I. Z. and Walton, K. Presynaptic calcium currents in squid synapse. Biophys. J. 33:289-322,1981a.

Llinas, R., Steinberg, I. Z. and Walton, K. Relationship between presynaptic calcium current and postsynaptic potential in squid giant synapse. Biophys. J. 33:323-352,1981b.

Llinas, R. The intrinsic electrophysiological properties of mammalian neurons: Insights into central nervous system function. Science. 242:1654-1664, 1988.

Lukasiewicz, P. D. and McReynolds, J. S. Synaptic transmission at N-methyl-D-aspartate receptors in the proximal retina of the mudpuppy. J. Physiol. 367:99-115,1985.

Lukasiewicz, P. D., Werblin, F. The spatial distribution of excitatory and inhibitory inputs to ganglion cell dendrites in the tiger salamander retina. J. Neurosci. 10(1):210-221,1990.

Maguire, G., Lukasiewicz, P. and Werblin, F. Amacrine cell interactions underlying the response to change in the tiger salamander retina. J. Neurosci. 9(2):726-735, 1989a.

Maguire, G., Maple, B., Lukasiewicz, P. and Werblin, F. γ-aminobutyrate type B receptor modulation of L-type calcium channel current at bipolar cell terminals in the retina of the tiger salamander. Proc. Natl. Acad. Sci. USA. 86:10144-10147,1989b.

Markram, H. and Segal, M. The inositol 1,4,5-trisphosphate pathway mediates cholinergic potentiation of rat hippocampal neuronal responses to NMDA. J. Physiol. 447:513-533,1992.

Marc, R. E. and Lam, D. M.-K. Glycinergic pathways in the goldfish retina. J. Neurosci. 1(2):152-165,1981.

Marc, R. E., Liu, W.-L. S. and Muller, J. F. Gap junctions in the inner plexiform layer of the goldfish retina. Vision Res. 28(1):9-24,1988.

Marmarelis, P. Z. and Marmarelis, V. Z. Analysis of Physiological Systems: The White-Noise Approach. Plenum Press, New York, 1978.

Masland, R. H., Mills, J. and Cassidy, C. The function of acetylcholine in the rabbit retina. Proc. R. Soc. Lond. B. 223:121-139, 1984.

Masland, R. H. and Cassidy C. The resting release of acetylcholine by a retinal neuron. Proc. R. Soc. Lond. B. 232:227-238,1987.

Massey, S. C. and Redburn, D. A. The cholinergic amacrine cells of rabbit retina receive on and off input: and analysis of [^{3}H]-ACh release using 2-amino-4-phosphonobutyric acid (APB) and chloride free medium. Vision Res. 23(12):1615-1620,1983.

Massey S. C. and Miller, R. F. Excitatory amino acid receptors of rod- and cone-driven horizontal cells in the rabbit retina. J. Neurophysiol. 57:645-659, 1987.

Massey, S. C. and Miller, R. F. N-methyl-D-aspartate receptors of ganglion cells in rabbit retina. J. Neurophysiol. 63(1):16-30, 1990.

Massey, S. C., Blankenship, K. and Mills, S. L. Cholinergic amacrine cells in the rabbit retina accumulate muscimol. Visual Neurosci. 6:113-117,1991.

Matsumoto, N. Responses of the amacrine cell to optic nerve stimulation in the frog retina. Vision Res. 15:509-514, 1975.

Mayer, M., Westbrook, G. and Guthrie, P. Voltage-dependent block by Mg^{2+} of NMDA responses in spinal cord neurones. Nature Lond. 309:261-263, 1984.

Miller, R. F. and Dacheux, R. F. Synaptic organization and ionic basis of on and off channels in mudpuppy retina. I. Intracellular analysis of chloride-sensitive

electrogenic properties of receptors, horizontal cells, bipolar cells, and amacrine cells. J. Gen. Physiol. 67:639-659,1976.

Miller, R. F., Dacheux, R. F. and Frumkes, T. E. Amacrine cells in necturus retina: evidence for independent γ-aminobutyric acid- and glycine-releasing neurons. Science. 198:748-750,1977.

Miller, R. F., Frumkes, T. E., Slaughter, M. and Dacheux, R. F. Physiological and pharmacological basis of GABA and glycine action on neurons of mudpuppy retina. I. Receptors, horizontal cells, bipolars, and G-cells. J. Neurophysiol. 45(4):743-763,1981.

Miller, R. F., Frumkes, T. E., Slaughter, M. and Dacheux, R. F. Physiological and pharmacological basis of GABA and glycine action on neurons of mudpuppy retina. II. Amacrine and ganglion cells. J. Neurophysiol. 45(4):764-782,1981.

Miller, R. F. and Bloomfield, S. A. Electroanatomy of a unique amacrine cell in the rabbit retina. Proc. Natl. Acad. Sci. USA. 80:3069-3073, 1983.

Miller, R. F. and Slaughter, M. Excitatory amino acid receptors of the retina: diversity of subtypes and conductance mechanisms. Trends Neurosci. 9:211,1986.

Miller, R. F. Are single retinal neurons both excitatory and inhibitory? Nature. 336:517-518,1989.

Miller, R. J. and Oliva A. A. Excitatory amino acids provide the stimulus. Curr. Biology. 2(4):174-176, 1992.

Mittman, S., Taylor, W. R. and Copenhagen, D. R. Concomitant activation of two types of glutamate receptor mediates excitation of salamander retinal ganglion cells. J. Physiol. 428:175-197,1990.

Moore, L. E., Yoshi, K., and Christensen, B. N. Transfer impedances between different regions of branched excitable cells. J. Neurophysiol. 59:689-705, 1988.

Muller, J. F. and Marc, R. E. GABA-ergic and glycinergic pathways in the inner plexiform layer of the goldfish retina. J. Comp. Neurol. 291:281-304,1990.

Muller, J. F., Ammermuller, J., Normann, R. A. and Kolb, H. Synaptic inputs to physiologically defined turtle retinal ganglion cells. Visual Neurosci. 7:409-429,1991.

Naka, K.-I., Marmarelis, P. Z., and Chan, R. Y. Morphological and functional identifications of catfish retinal neurons. III. Funtional identification. J. Neurophysiol. 38:92-131, 1975.

Naka, K.-I. Functional organization of catfish retina. J. Neurophysiol. 40:26-43,1977.

Naka, K.-I. A class of catfish amacrine cells responds preferentially to objects which move vertically. Vision Res.
20:961-965,1980.

Naka, K.-I. and Christensen, B. N. Direct electrical connections between transient amacrine cells in the catfish retina. Science 214:462-464,1981.

Neal, M., Cunningham, J., James, T., Joseph, M. and Collins, J. The effect of 2-amino-4-phosphonobutyrate(APB) on acetylcholine release from the rabbit retina: Evidence for ON-channel input to cholinergic amacrine cells, Neurosci. Lett. 26:301, 1981

Neal, M. J., Cunningham, J. R. and Shah, M. A. Excitatory amino acid receptors and transmitter release in the retina. Neurochem. Int. 14(4):407-412, 1989.

Negishi, K. and Teranishi, T. Close tip-to-tip contacts between dendrites of transient amacrine cells in carp retina. Neurosci. Lett. 115:1-6,1990.

Negishi, K., Teranishi, T., Sugawara, K. and Wagner, H.-J. Dendritic contacts between neighboring homologous amacrine cells in carp retina. Neurosci. Res. Suppl. 15:s145-s155,1991.

Nowak, L., Bregestovski, P., Ascher, P., Herbet, A. and Prochiantz, A. Magnesium gates glutamate-activated channels in mouse central neurones. Nature Lond. 307:462-465, 1984.

O'Dell, T. J. and Christensen, B. N. A voltage-clamp study of isolated stingray horizontal cell non-NMDA excitatory amino acid receptors. J. Neurophysiol. 61(1):162-172,1989a.

O'Dell, T. J. and Christensen, B. N. Horizontal cells isolated from catfish retina contain two types of excitatory amino acid receptors. J. Neurophysiol. 61(6):1097-1109,1989b.

O'Malley, D. M., Sandell, J. H. and Masland, R. H. Co-release of acetylcholine and GABA by the starburst amacrine cells. J. Neurosci. 12(4):1394-1408,1992.

Ogura, H. Orthogonal functionals of the poisson process. IEEE Trans. Inf. Theory,IT-18(4):473-481,1972.

Oppenheim, A. V., Willsky, A. S. and Young, I. T. Signals and Systems. Prentice-Hall, Englewood Cliffs, New Jersey, 1983.

Pourcho, R. G. and Goebel, D. J. Visualization of endogenous glycine in cat retina: an immunocytochemical study with Fab fragments. J. Neurosci. 7:1189-1197, 1987.

Raviola, E. and Dacheux, R. Excitatory dyad synapse in rabbit retina. Proc. Natl. Acad. Sci. USA. 84:7324-7328,1987.

Sakai, H. M. and Naka, K.-I. Novel pathway connecting the outer and inner vertebrate retina. Nature. 315:570-571,1985.

Sakai, H. M., Naka, K.-I. and Dowling, J. E. Ganglion cell dendrites are presynaptic in catfish retina. Nature 319:495-497,1986a.

Sakai, H. M. and Naka, K.-I. Synaptic organization of the cone horizontal cells in the cafish retina. J. Comp.Neurol. 245:107-115,1986b.

Sakai, H. M. and Naka, K.-I. Signal transmission in the catfish retina. IV. Transmission to ganglion cells. J. Neurophysiol. 58:1307-1328,1987a.

Sakai, H. M. and Naka, K.-I. Signal transmission in the catfish retina. V.Sensitivity and circuit.J. Neurophysiol. 58:1329-1350,1987b.

Sakai, H. M. and Naka, K.-I. Dissection of the neuron network in the catfish inner retina. I. Transmission to ganglion cells.J. Neurophysiol.60:1549-1567,1988a.

Sakai, H. M. and Naka, K.-I. Dissection of the neuron network in the catfish inner retina. II. Interactions between ganglion cells.J. Neurophysiol.60:1568-1583,1988b.

Sakai, H. M. and Naka, K.-I. Neuron network in catfish retina:1986-1987. In Progress in Retinal Research. N. Osborne and G. Chader,editors. Pergamon Press, London. 7:140-208,1988c.

Sakai, H. M. and Naka, K.-I. Dissection of the neuron network in the catfish inner retina. IV. Bidirectional interactions between amacrine and ganglion cells.J. Neurophysiol.63:105-119,1990a.

Sakai, H. M. and Naka, K.-I. Dissection of the neuron network in the catfish inner retina.V.Interactions between NA and NB amacrine cells.J. Neurophysiol.63:120-130,1990b.

Sakai, H. M. and Naka, K.-I. Response dynamics and receptive-field organization of catfish amacrine cells. J. Neurophysiol.67(2):430-442,1992.

Sakuranaga, M. and Naka, K.-I. Signal transmission in the catfish retina.I. Transmission in the outer retina.J. Neurophysiol. 53:373-389,1985a.

Sakuranaga, M. and Naka, K.-I. Signal transmission in the catfish retina.II. Transmission to type-N cell.J. Neurophysiol. 53:390-410,1985b.

Sakuranaga, M. and Naka, K.-I. Signal transmission in the catfish retina.III. Transmission to type C-cell.J. Neurophysiol. 53:411-428,1985c.

Sakuranaga, M., Sato, N., Hida, E. and Naka, K.-I. Nonlinear analysis: Mathematical theory and biological applications. Critical Reviews in Biomedical Engineering,CRC Press,Boca Raton,Florida, 14:127-184,1986.

Schetzen, M. The Volterra and Wiener Theories of Nonlinear Systems. John Wiley and Sons, New York, 1980.

Shapley, R. M. and Victor, J. D. The effect of contrast on the transfer properties of cat retinal ganglion cells. J. Physiol. 285:275-298,1978.

Shapley, R. M. and Victor, J. D. The contrast gain control of the cat retina. Vision Res. 19:431-434,1979a.

Shapley, R. M. and Victor, J. D. Nonlinear spatial summation and the contrast gain control of cat retinal ganglion cells.J. Physiol. 290:141-161,1979b.

Shapley, R. M. and Victor, J. D. The effect of contrast on the non-linear response of the Y cell. J. Physiol. 302:535-547,1980.

Shapley, R. M. and Victor, J. D. How the contrast gain control modifies the frequency responses of cat retinal ganglion cells. J. Physiol. 318:161-179,1981.

Shapley, R. M., and Enroth-Cugell, C. Visual adaptation and retinal gain controls. In Progress in Retinal Research. N. Osborne and G Chader,editors. Pergamon Press, London. 3:263-346,1984.

Shepherd, G. M. Synaptic organization of the mammalian olfactory bulb. Physiol. Rev. 52:864-917,1972.

Slaughter, M. M. and Miller, R. F. The role of excitatory amino acid transmitters in the mudpuppy retina: an analysis with kainic acid and N-methyl aspartate. J. Neurosci. 3:1701-1711, 1983.

Slaughter, M. M. and Miller, R. F. Characterization of an extended glutatmate receptor of the ON bipolar neuron in the vertebrate retina. J. Neurosci. 5:224-233, 1985.

Slaughter, M. M. and Bai, S. Differential effects of baclofen on sustained and transient cells in the mudpuppy retina. J. Neurophys. 61:374-381, 1989.

Suzuki, S., Tachibana, M. and Kaneko A. Effects of glycine and GABA on isolated bipolar cells of the mouse retina. J. Physiol. 421:645-662,1990.

Tachibana, M. and Kaneko, A. Retinal bipolar cells receive negative feedback input from GABAergic amacrine cells. Vis. Neurosci. 1:297-305,1988.

Teranishi, T., Negishi, K. and Kato, S. Dye coupling between amacrine cells in carp retina. Neurosci. Lett. 52:73-78,1984.

Toyoda, J.-I., Kondo, H. and Fujimoto, M. Effect of some putative transmitters on amacrine cells and on spreading depression potential. Neurosci. Res. Suppl. 6:s227-s238,1987.

Tranchina, D., Gordon, J. and Shapley, R. Spatial and temporal properties of luminosity horizontal cells in the turtle retina. J. Gen. Physiol. 82:573-598, 1983.

Tranchina, D., Sneyd, J. and Cadenas, I. D. Light adaptation in turtle cones.Testing and analysis of a model for phototransduction. Biophys. J. 60:217-237,1991.

Traub, R. D., Miles, R. and Wong, R. K. S. Model of the origin of rhythmic population oscillations in the hippocampal slice.
Science 243:1319-1325, 1989.

Vaney, D. I., Collin S. and Young, H. Dendritic relationships between cholinergic amacrine cells and direction-selective retinal ganglion cells. In Neurobiology of the Inner Retina. R. Weiler and N. Osborne, editors. Springer Verlag, Berlin, 31:157-168, 1989.

Victor, J. D. and Shapley, R. M. Receptive field mechanisms of cat X and Y retinal ganglion cells. J. Gen. Physiol. 74:275-298,1979a.

Victor, J. D. and Shapley, R. M. The nonlinear pathway of Y ganglion cells in the cat retina. J. Gen. Physiol. 74:671-689,1979b.

Victor, J. D. The dynamics of the cat retinal X cell centre. J. Physiol. 386:219-246,1987.

Victor, J. D. The dynamics of the cat retinal Y cell subunit. J Physiol. 405:289-320,1988.

Werblin, F. S. Response to retinal cells to moving spots: Intracellular recording in Necturus maculosus. J. Neurophysiol. 33:342, 1970.

Werblin, F. S. and Copenhagen, D. R. Control of retinal sensitivity III. Lateral interactions at the inner plexiform layer. J. Gen. Physiol. 63:88-110,1974.

Werblin, F. Maguire, G., Lukasiewicz, P. Eliasof, S. and Wu, S. M. Neural interactions mediating the detection of motion in the retina of the tiger salamander. 1:317-329,1988.

Werblin, F. Synaptic connections, receptive fields, and patterns of activity in the tiger salamander retina. Invest. Opth. Vis. Sci. 32:459-483,1991.

Wiener, N. Nonlinear Problems in Random Theory. MIT Press, Cambridge, Massachusetts, 1958.

Wiener, N. Cybernetics. MIT, Cambridge, 1961.

Yang, C.-Y. and Yazulla, S. Light microscopic localization of putative glycinergic neurons in the larval tiger salamander retina by immunocytochemical and autoradiographical methods. J. Comp. Neurol. 272:343-357,1988.

Yazulla, S., Studholme, K. and Wu, J-Y. GABAergic input to the synaptic terminals of mb_1 bipolar cells in the goldfish retina. Brain Res. 411:400-405,1987.

Yoshi, K., Moore, L. E., and Christensen, B. N. Effect of subthreshold voltage-dependent conductances on the transfer function of branched excitable cells and the conduction of synaptic potentials. J. Neurophysiol. 59:706-716, 1988.